NAVAL SHIP RESEARCH AND DEVELOPMENT CENTER
Bethesda, Md. 20034

# HYDRODYNAMIC DESIGN PRINCIPLES OF PUMPS AND DUCTING FOR WATERJET PROPULSION

by
George F. Wislicenus



APPROVED FOR PUBLIC RELEASE: DISTRIBUTION UNLIMITED

SYSTEMS DEVELOPMENT DEPARTMENT
RESEARCH AND DEVELOPMENT REPORT

June 1973

Report 3990

Report 3990
HYDRODYNAMIC DESIGN PRINCIPLES OF PUMPS AND DUCTING FOR WATERJET PROPULSION

The Naval Ship Research and Development Center is a U. S. Navy center for laboratory effort directed at achieving improved sea and air vehicles. It was formed in March 1967 by merging the David Taylor Model Basin at Carderock, Maryland with the Marine Engineering Laboratory at Annapolis, Maryland.

Naval Ship Research and Development Center
Bethesda, Md. 20034

## MAJOR NSRDC ORGANIZATIONAL COMPONENTS

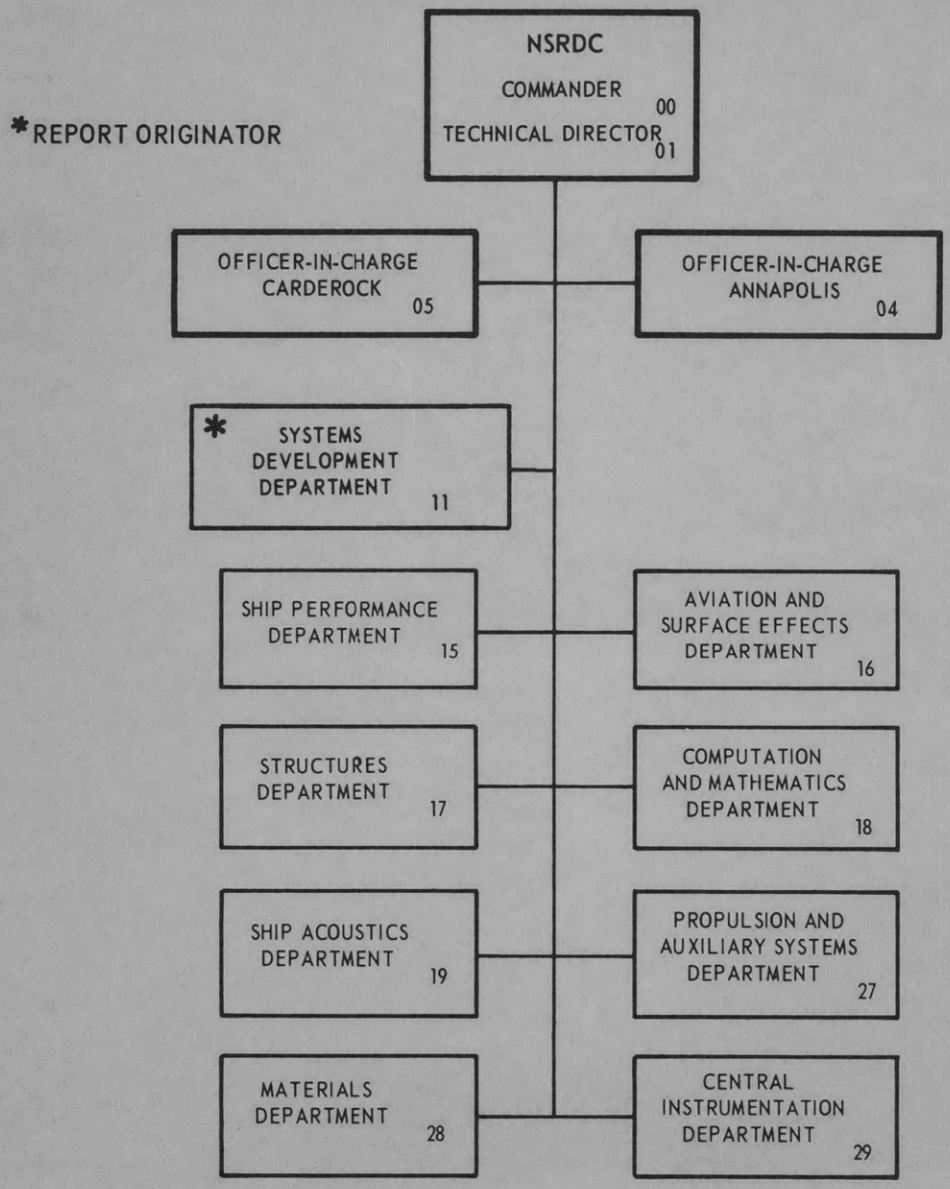


NDW-NSRDC 3960/43b (Rev. 3-72)
GPO 928-108

DEPARTMENT OF THE NAVY
NAVAL SHIP RESEARCH AND DEVELOPMENT CENTER
BETHESDA, MD. 20034

# HYDRODYNAMIC DESIGN PRINCIPLES OF PUMPS AND DUCTING FOR WATERJET PROPULSION

by
George F. Wislicenus




June 1973 Report 3990

# PREFACE

The principal objective of this report is to make the viewpoint of a pump designer known to developers of waterjet propulsion devices. Therefore no attempt has been made to cover the *entire* field of waterjet propulsion design. Furthermore, only aspects of preliminary design have been considered because it is in this stage of development that irreparable mistakes can be made.

What contribution can the pump design engineer make to significant improvements in waterjet propulsion? To answer this question, it is necessary to lay the foundations for significant departures from conventional pump design and arrangement. These foundations are obviously the principles of centrifugal pump design at a sufficiently fundamental level to permit rational departures from conventional practices.

For many years, competently designed and well-executed centrifugal pumps have approached and even exceeded efficiencies of 90 percent in a favorable range of operating conditions (specific speeds). Major advances over such values can hardly be expected. However, even the most elementary analysis of waterjet propulsion, as presented here, for example, in Chapter 2, reveals quickly that the efficiency problem of waterjet propulsion lies outside of the pump proper. It is primarily related to duct and intake losses which unfavorably influence the overall hydrodynamic operating conditions of the propulsion plant.

Thus the task of the pump designer is twofold: (1) he must rationally relate the operating characteristics of his pump to the operating characteristics of the propulsion plant and (2) he must find or choose a form or arrangement of the pump that minimizes the hydrodynamic losses and weight penalties connected with other parts of the pump system. In other words, the pump designer must give the designer of the entire propulsion plant the greatest possible freedom to find and use the most favorable overall arrangement. This requires departures not only from common pump arrangements but also from the conventional arrangements of the driving gas turbine.

It is perfectly reasonable to look to the commercial pump field for acceptable solutions of the pump design problem because that field offers the most extensive reservoir of practical pump experience and, in many cases, the highest efficiencies. However, the critical importance of the size and weight of the propulsion pump and plant makes it mandatory to pay equal attention to the field of rocket pumps because size and weight are at least as important there as in the propulsion field.

As mentioned before, this report is concerned primarily with the *preliminary* design of the propulsion pump and plant. As a consequence, relatively little attention is paid to final refinements or to great accuracy of the numerical results obtained. The principal aim has been to arrive at one or several truly promising arrangements as quickly as possible. To achieve this, one must, for example, first select the velocity increase ratio of the propulsor on the basis of hydrodynamic considerations only, although the importance of weight considerations for this selection is well recognized. Weight can be considered only after the general arrangement has been chosen. This is not too serious if such weight considerations later lead to a different (higher) velocity increase ratio so long as this change does not affect the general arrangement fundamentally.

In view of the limited objective of the report the reader should become aware of other aspects of the broader field of waterjet propulsion. The reader is referred to the extensive list of references contained in the comprehensive discussion of this field by Brandau.[1] This makes it unnecessary to add such a list to the present report except for the three sources used directly.[1-3]

In closing this preface, the writer expresses his appreciation for the assistance, comments, and constructive criticisms received from his friends at the Naval Ship Research and Development Center (NSRDC). The writer hopes that despite its shortcomings, this report will serve some useful purpose in connection with the future development of waterjet propulsion plants.

Tucson, Arizona, June 1972.

---

[1]Brandau, J., "Performance of Waterjet Propulsion Systems–A Survey of the State of the Art," J. Hydronautics (Apr 1968).

[2]Wislicenus, G.F., "Fluid Mechanics of Turbomachinery," Dover Publications, Inc., New York (1965).

[3]Wislicenus, G.F., "Hydrodynamics and Propulsion of Submerged Bodies," J. American Rocket Society, pp. 1140–1148 (Dec 1960).

## TABLE OF CONTENTS

## LIST OF FIGURES

## LIST OF TABLES

## NOTATION

| Symbol | Description | Dimensions |
|---|---|---|
| $L$ | Quantity having dimension of length | L |
| $M$ | Quantity having dimension of mass | M |
| $T$ | Quantity having dimension of time | T |
| $F$ | Quantity having dimension of force | F |
| $A$ | Area | $L^2$ |
| $A_1$ | Intake area (see Figure 1.2) | $L^2$ |
| $A_j$ | Jet cross-section area | $L^2$ |
| $A_m$ | Flow section area normal to the meridional flow (see pg. 24) | $L^2$ |
| $A_{th}$ | "Throat" area of volute or diffusor | $L^2$ |
| $a$ | Major axis of an ellipse (elliptic cross section) | L |
| $b$ | Minor axis of an ellipse | L |
| $b$ | Width of a passage, impeller | L |
| $b_0$ | Impeller width at outer periphery | L |
| $C_1$ | Coefficient in Equation (3.1.23) (3.24) | |
| $C_L$ | Lift coefficient | |
| $C_{L_1}$ | Lift coefficient referred to the inlet velocity of a vane system | |
| $C_{L_\infty}$ | Lift coefficient referred to the vectorial mean $w_\infty$ or $V_\infty$ of the (relative) inlet and discharge velocities of a vane system | |
| $C_p$ | Local (vane) surface pressure coefficient, usually the free-stream static pressure ($p_0$) minus the local surface pressure ($p$) divided by the prevailing velocity pressure $C_p = (p_0 - p)/(\rho V_0^2/2)$ | |
| $C_T$ | Intake drag coefficient referred to intake area ($A_1$); $\Delta T = C_T A_1 \rho V_0^2/2$ | |
| $D$ | Diameter or any representative linear dimension of a machine | L |
| $D_{th}$ | Distance of center of "throat" area from axis of rotation multiplied by two | L |
| $\Delta D$ | Difference or change in diameter | L |
| $g$ | Gravitational acceleration | $LT^{-2}$ |
| $g_0$ | Standard gravitational acceleration at sea level on earth | $LT^{-2}$ |
| $H$ | Total (static plus velocity) head; net pump work per unit of weight of fluid | $FLF^{-1} = L$ |
| $H_j$ | Jet velocity head increase $(V_j^2 - V_0^2)/2g_0$ (Equation (2.5)) | L |
| $H_r$ | Runner head; total work per unit weight of fluid exchanged between the runner and the fluid | L |

| Symbol | Description | Dimensions |
|---|---|---|
| $H_{sv}$ | Total (static plus velocity) inlet head of a pump over the vapor pressure of the fluid | L |
| $HP$ | Horsepower | $LFT^{-1} = ML^2T^{-3}$ |
| $h$ | Static head; static pressure divided by the weight per unit volume of the fluid | L |
| $\Delta h_i$ | Elevation of pump inlet above free water surface | L |
| $\Delta h_j$ | Elevation of the jet above free water surface | L |
| $h_a$ | Atmospheric pressure divided by the weight per unit volume of the fluid | L |
| $h_L$, $h_{\text{loss}}$ | Head loss, duct head loss | L |
| $h_{sv}$ | Static inlet head of a pump over the vapor pressure of the fluid | L |
| $h_v$ | Vapor pressure divided by the weight per unit volume of the fluid | L |
| $K$ | Duct head loss coefficient | |
| $K_T$ | Corrected intake drag coefficient $K_t = C_T/a_1$ $\Delta T = K_T\, a_1 A_1 \rho\, V_0{}^2/2$ | |
| $\ell$ | Length, chord length of a vane | L |
| $M$ | Moment or torque | $FL = ML^2\, T^{-2}$ |
| $N$ | Number; number of vanes<br>number of stages<br>number of pumps in parallel | |
| $n$ | Number of revolutions per unit of time (usually second) | $T^{-1}$ |
| $n$ | Linear coordinates normal to the meridional stream lines | L |
| $n_s$ | Basic specific speed | |
| $n_\sigma$ | Stress specific speed (Equation (3.28)) | |
| $P$ | Power | $FLT^{-1} = ML^2\, T^{-3}$ |
| $P_i$ | Ideal power | $FLT^{-1} = ML^2\, T^{-3}$ |
| $P_{HP}$ | Power expressed in horsepower | $FLT^{-1} = ML^2\, T^{-3}$ |
| $p$ | Pressure | $FL^{-2} = ML^{-1}\, T^{-2}$ |
| $p_v$ | Vapor pressure | $FL^{-2} = ML^{-1}\, T^{-2}$ |
| $Q$ | Rate of volume flow | $L^3\, T^{-1}$ |
| $R$ | Range or distance of travel (usually in nautical miles) | L |

| Symbol | Description | Dimensions |
|---|---|---|
| $r$ | Radius, distance from axis of rotation | L |
| $S$ | Suction specific speed (Equation (3.22)) | |
| $T$ | Thrust | $F = MLT^{-2}$ |
| $\Delta T$ | External intake or propulsor drag | $F = MLT^{-2}$ |
| $t$ | Circumferential spacing of vanes | L |
| $t_0$ | Circumferential spacing of vanes at the outer periphery | L |
| $U$ | Peripheral velocity of the solid parts of a turbomachine | $LT^{-1}$ |
| $V$ | "Absolute" fluid velocity in a turbomachine; velocity relative to the (moving) craft | $LT^{-1}$ |
| $V_d$ | Average fluid velocity in the ducts | $LT^{-1}$ |
| $V_j$ | Jet velocity relative to the moving craft | $LT^{-1}$ |
| $V_k$ | Velocity (or speed) of the craft in knots | $LT^{-1}$ |
| $V_0$ | Velocity (or speed) of the craft, and undisturbed water velocity relative to the moving craft | $LT^{-1}$ |
| $\Delta V$ | $= V_j - V_0$ = velocity increase through the propulsor = jet velocity relative to the ocean | $LT^{-1}$ |
| $W$ | Weight, specifically weight of the craft (in pounds) | $F = MLT^{-2}$ |
| $W_a$ | Part of pump weight proportional to number of stages | $F = MLT^{-2}$ |
| $W_b$ | Part of pump weight (inlet and discharge) independent of number of stage and speed of rotation | $F = MLT^{-2}$ |
| $W_f$ | Fuel weight (in pounds) | $F = MLT^{-2}$ |
| $W_{f_1}$ | Fuel weight consumed per hour | $FT^{-1} = MLT^{-3}$ |
| $W_{pp}$ | Weight of power and propulsion plant (in pounds) | $F = MLT^{-2}$ |
| $W_{pw}$ | Water weight in pump(s) and duct(s) above free water surface | $F = MLT^{-2}$ |
| $w$ | Fluid velocity relative to a rotating vane system | $LT^{-1}$ |
| $w_\infty$ | Vectorial mean between the incoming and the discharging velocities of a vane system | $LT^{-1}$ |
| $a_1$ | Intake area correction factor (Equation (2.2) and Figure 1.2) | |
| $\Delta$ | Denotes a difference or change, e.g., $\Delta D$, $\Delta V$ | |
| $\eta$ | Efficiency | |
| $\eta_h$ | "Hydraulic efficiency" $H/H_r$ | |

| Symbol | Description | Dimensions |
|---|---|---|
| $\eta_j$ | Ideal jet efficiency, $1/(1 + \Delta V/2V_0)$ | |
| $\eta_j$ | Ideal jet efficiency corrected for jet elevation only (Equation (2.4)) | |
| $\eta_{j_1}$ | Jet efficiency corrected for duct head loss only (Equation (2.7)) | |
| $\eta_{j_2}$ | Jet efficiency corrected for duct head loss and external intake or propulsor drag only (Equations (2.8), (2.10), (2.12)) | |
| $\eta_{j_3}$ | Jet efficiency corrected for duct head loss and jet elevation only (Equation (2.14)) | |
| $\eta_{j_4}$ | Jet efficiency corrected for duct head loss, jet elevation, and intake or propulsor drag (Equation (2.15)) | |
| $\sigma$ | Stress in a solid part | $FL^{-2} = ML^{-1}\ T^{-2}$ |
| $\sigma_H$ | Thoma cavitation parameter $H_{sv}/H$ | |
| $\sigma_p$ | Cavitation number $(p_0 - p_v)/(\rho V_0{}^2/2)$ | |
| $\sigma_0$ | Cavitation number of a local surface irregularity (roughness) alone | |
| $\sigma_R$ | Resulting cavitation number from effects of average boundary curvature and boundary roughness | |
| $\rho$ | Mass per unit volume | $ML^{-3}$ |
| $\rho_s$ | Mass per unit volume of the structural parts of the machine | $ML^{-3}$ |
| $\tau$ | Shear stress | $FL^{-2} = ML^{-1}\ T^{-2}$ |
| $\psi$ | Head coefficient of a pump rotor; i.e.: $H = \psi\ U^2/2g_0$ | |
| $\omega$ | Angular velocity (radian/sec) | $T^{-1}$ |

Subscripts

| | |
|---|---|
| 1 | Unity (one), first station along a series of stations (e.g., intake, inlet), or first operating condition considered |
| 1 | Minimum speed of travel at which maximum speed of rotation and power is required (e.g., "hump condition") |
| 2 | A second station along a series of stations (discharge), or second operating condition considered |
| *a, b* | Division of pump weight according to dependency |
| *c* | Cruising conditions (40 knots) |
| *av* | Average |

| Subscript | Description |
|---|---|
| *h* | Hub diameter of a pump rotor |
| *i* | Inlet of a pump rotor or runner |
| *j* | Propulsion jet |
| *m* | Meridional component of fluid velocity |
| 0 | Reference value of any type, and outside of a pump rotor or stator |
| *th* | "Throat" area of volute or vane diffusor |
| *u* | Peripheral component of fluid velocity or any other vector |

## ABSTRACT

The purpose of this report on the special form of hydrodynamic propulsion known as waterjet propulsion is to make the viewpoint of a pump designer known to the developers of waterjet devices. More specifically, it is concerned with the contribution that the pump designer can make in order to give the designer of the entire propulsion plant the greatest possible freedom to find and use the most favorable overall arrangement. There is no attempt to cover the entire field of waterjet propulsion. Moreover, only aspects of preliminary design are considered because it is in this stage of development that irreparable mistakes can be made.

The report assumes that the reader is familiar with the general characteristics of hydrofoil and captured air-cushion craft to which this type of propulsion mainly applies. Following an outline of the principal problems involved in the propulsion of high-speed surface craft, the design principles of hydrodynamic (centrifugal and axial-flow) pumps are described and later applied to the design of waterjet propulsion pumps. The intake and duct problem is then described and designs are illustrated for a few typical overall arrangements. The report concludes with an example of propulsion pump and duct design for a particular set of specifications. This example can serve as the foundation for additional preliminary design studies.

## ADMINISTRATIVE INFORMATION

This work was authorized under the Hydrofoil Development Program Office of the Naval Ship Research and Development Center (NSRDC) in support of the Naval Ship Systems Command (NAVSHIPS) Advanced Hydrofoil Systems Project. Funding was provided under Subproject S4606, Task 1722. The report by Mr. Wislicenus was written under Contract 00014-70-C-0019. Technical review and manuscript preparation were done at NSRDC.

# CHAPTER 1. INTRODUCTION

This report deals with a special form of hydrodynamic propulsion called waterjet propulsion.

All forms of hydrodynamic propulsion generate the propelling force, or thrust $T$, by discharging a stream of water from the "propulsor" at a higher velocity $V_j$ than the velocity of the stream entering the propulsor. In the simplest case, this velocity of the entering stream, $V_0$, is oppositely equal to the forward velocity of the propelled craft. The propelling force so generated is obviously:

$$T = \rho Q \ (V_j - V_0) \tag{1.1}$$

where $Q$ is the rate of volume flow passing through the propulsor and $\rho$ is the mass per unit of volume of the fluid.

The most widely used form of hydrodynamic propulsor is, of course, the standard marine propeller. If well designed and operated under favorable conditions, it represents the most efficient form of hydrodynamic propulsor. Therefore the use of other types of propulsors must be justified.

The original reason for considering departures from the standard propeller was the limitation imposed on propeller speed by cavitation. Since the propeller blades advance through the water along helical paths, the resultant blade velocity reltative to the water is necessarily higher than the forward velocity of the propeller and of the propelled vehicle. If the same hydrodynamic qualities are assumed for the propelled vehicle and for the propeller blades, the propeller blades will cavitate at a lower *forward* velocity than the propelled vehicle.

This cavitation problem of open propellers was solved by ducting the flow toward the propelling rotor, leading to what is now known as the "pumpjet." The pumpjet has fulfilled expectations and has essentially solved the propulsor cavitation problem in this field. It is shown in Figure 1 as applied to a submerged body of revolution (a torpedo). The flow approaching the rotor is retarded in a diffusor; this not only reduces the velocity of the approaching flow but also increases its static pressure according to the Bernoulli equation. This principle was successfully applied and may be considered as firmly established. It permits propulsion by means of rotating propulsors which will not cavitate before the propelled body itself is subject to cavitation.

A second reason for departing from the propeller in the open stream is illustrated by some recently developed water surface craft such as hydrofoil or captured air-cushion craft. In both cases the capability of very high speeds is achieved by minimizing the surface area of the craft *below* the free water surface. For hydrodynamic propulsion, the minimum of such an area is that connected with the water intake to the propulsion unit. The propulsor and its driver may be located above the free water level, thus eliminating hydrodynamic drag on the exterior surface of the propulsion plant. This type of hydrodynamic jet propulsion is called waterjet propulsion and is shown diagrammatically in Figure 2 in connection with a hydrofoil craft. To minimize the surface-piercing parts which generate considerable wave drag, the interiors of the hydrofoil support struts are used for the passage of water from the submerged intake to the propulsion pump. With captured air-cushion craft, the side skirts of the cushion would be used for this purpose.

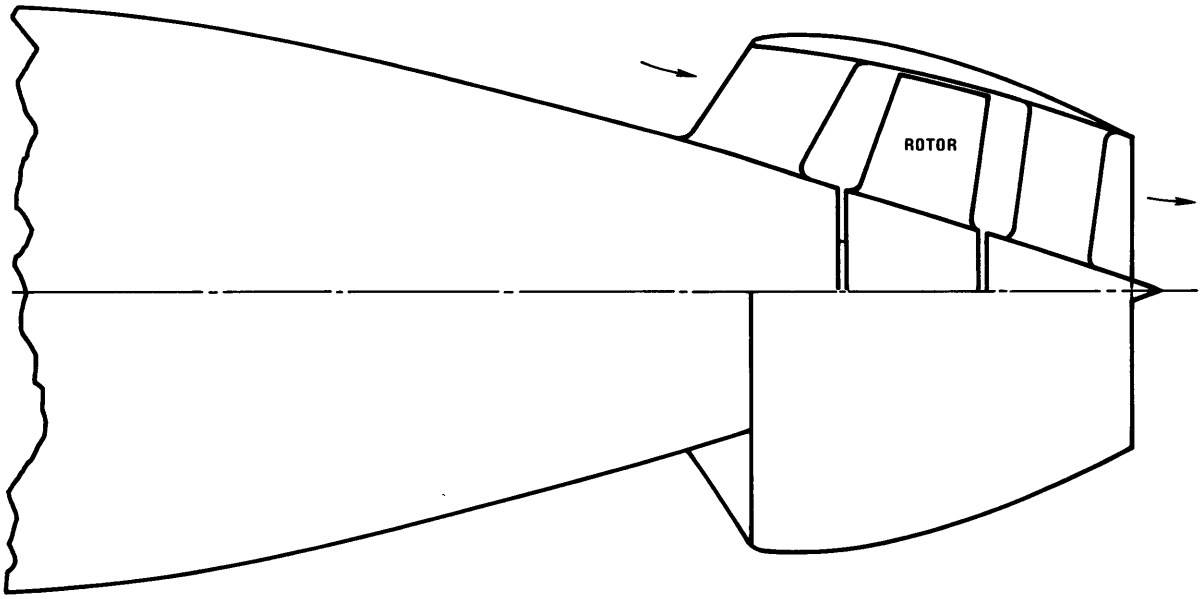


Figure 1 – Pumpjet on the Aft End of a Submerged Body of Revolution

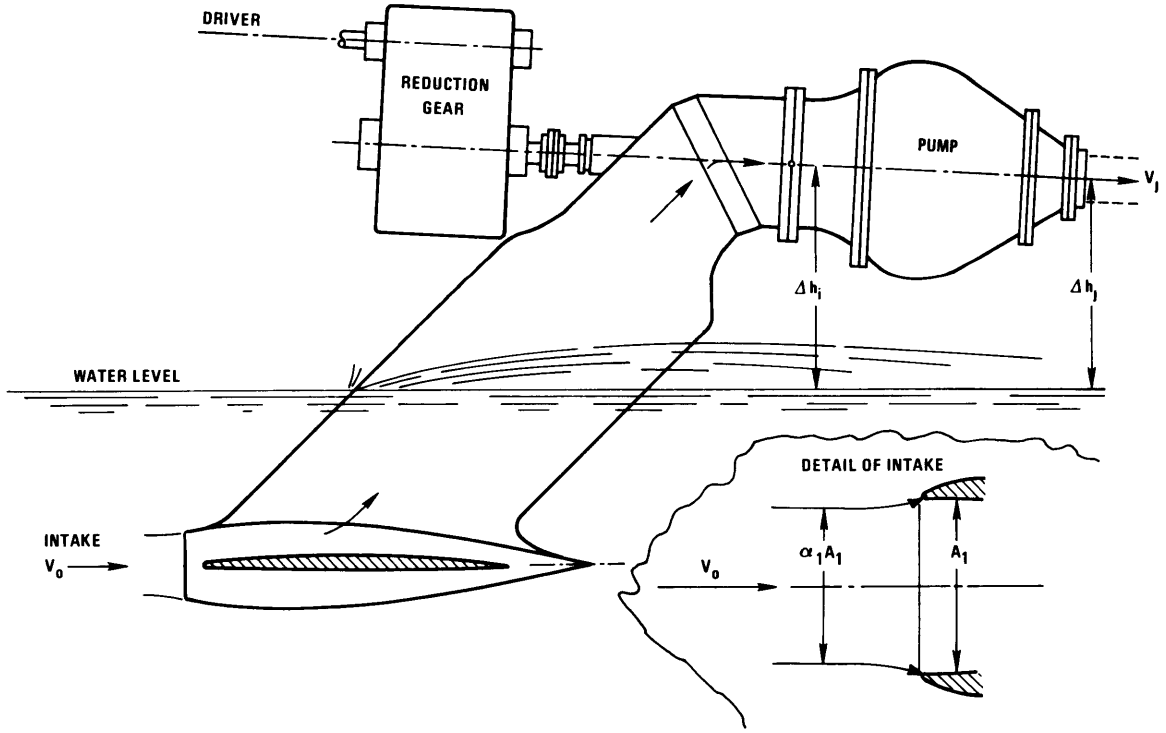


Figure 2 – Waterjet Propulsion Unit

Even if the drag penalty of an enlarged, submerged nacelle carrying a (supercavitating or ventilated) propeller or a pumpjet is accepted, there are still problems related to the size and—even more particularly—to the *reliability* of a submerged, mechanical angle drive. This problem of reliability may well have been the decisive factor in the selection of above-surface propulsors for hydrofoil and captured air-cushion craft.

Waterjet propulsion units (Figure 2) share with the pumpjet (Figure 1) the possibility of retarding the incoming propulsion stream before it reaches the propulsion pump. In fact, with the propulsion pump above the free water surface, such retardation is a practical necessity in order to provide the pump with the required inlet pressure. Thus in contrast to a conventional propeller in an open stream, both pumpjet and waterjet propulsion devices make the rotating propulsor somewhat independent of the design speed of travel. Obviously there is the additional necessity of ducting the propulsion stream if the propulsor is located above the free water surface.

Generally an attempt is made to minimize the elevation of a waterjet propulsion unit above the free water surface. Since it does not contribute to propulsion, the elevation $\Delta h_j$ of the propelling jet above the water surface constitutes an energy loss. The pump inlet elevation $\Delta h_i$ reduces the pump inlet pressure and is therefore harmful with respect to pump cavitation. Nevertheless, practical considerations of sea state usually lead to greater elevations $\Delta h_i$ and $\Delta h_j$ in comparison with the size of the propulsor than shown in Figure 2.

The present report is primarily intended to describe the design of waterjet propulsion *pumps*. It assumes that the reader is familiar with the general characteristics of hydrofoil and captured air-cushion craft to which this type of propulsion principally applies.

Chapter 2 outlines the principal *problems* connected with the propulsion of "high-speed" water surface craft, i.e., surface craft that operate at substantially higher *Froude numbers* than do conventional surface ships.

Chapter 3 briefly describes the design principles of hydrodynamic (centrifugal and axial-flow) pumps in general and then applies these principles to the design of waterjet propulsion pumps.

Chapter 4 outlines the intake and duct problem of propulsion pumps and describes the inlet and discharge duct design for a few typical overall arrangements.

Chapter 5 presents an example of propulsion pump and duct design.

# CHAPTER 2. GENERAL PROBLEMS OF WATERJET PROPULSION

## 2.1 PROPULSOR OPERATING CONDITIONS AS FUNCTIONS OF THE SPEED OF TRAVEL

The principal operating conditions of the rotating propulsor are the speed of rotation $n$, the thrust force developed by the propulsor $T$, the rate of volume flow through the propulsor $Q$, and the total inlet head to the propulsion pump above the vapor pressure of the water $H_{sv}$.

The simplest relation between these operating conditions and the speed of travel would exist if (1) all velocities in the propulsor could be changed proportionally to the speed of travel and (2) all head values and all forces would change proportionally to the square of the speed of travel. These conditions are called the conditions of similarity of flow.

In the absence of cavitation and at the high Reynolds numbers of full-scale operation, the drag and therefore the *required* propulsor thrust of a completely submerged body changes closely with the square of the speed of travel, and thus one part of the conditions of similarity of flow is satisfied. Under similar flow conditions, the speed of rotation $n$ and the rate of volume flow $Q$ of the propulsion pump would change proportionally to the speed of travel.

However, the inlet head (above vapor pressure) of the propulsion pump is:

$$H_{sv} = h_a - h_v + h + (1 - K)\ \frac{V_0^2}{2g_0} \tag{2.1}$$

where $h_a$ is the atmospheric pressure in feet of sea water,
$h_v$ is the vapor pressure in the same units,
$h$ is the depth of immersion in feet,
$V_0$ is the velocity of travel,
$K$ is a head-loss coefficient, and
$g_0$ = 32.2 ft/sec$^2$.

It is seen that only the last term changes with the speed of travel squared, whereas all other terms are independent of $V_0$. Thus $H_{sv}$ does not satisfy the conditions of similarity. This departure from the similarity relation applies, of course, not only to *submerged* bodies but to all waterborne vehicles because Equation (2.1) is quite general, except that the depth of immersion $h$ may be negative if the inlet to the propulsion pump is above the water surface as shown in Figure 2, where $h = -\Delta h_i$.

It is well known that the drag of *surface* vessels generally does *not* increase with the square of the speed of travel but follows a different and usually quite complicated law. Thus surface vessels do not follow the simple condition of similarity which apply to the propulsor, i.e., the hydrodynamic propulsor of a surface vessel does not operate under similar flow conditions at different speeds of travel. This departure of the

drag from the conditions of similarity of flow is particularly pronounced for surface vehicles to which waterjet propulsion primarily applies (hydrofoil and captured air-cushion craft). Figure 3 shows a typical curve for drag versus speed of travel for this type of vehicle. The "hump" in this drag curve is related to the change in the mode of travel from that of a displacement craft to the intended form of operation on the foils or on the air cushion in a "planing" fashion. The "hump drag" may well be higher than the full-speed drag, thus constituting a very dramatic departure from the similarity relation. At hump speed, the required speed of rotation of the propulsor may have to be as high or higher than at full speed of travel. This may constitute a severe cavitation problem since according to Equation (2.1), the pump inlet head $H_{sv}$ is substantially lower at the (lower) hump speed than at full speed.

Another result of the departure from similarity represented by the "hump" is concerned with the submerged *intake opening* to the propulsor inlet duct (see Figure 2). To obtain a good so-called "ram efficiency," i.e., a good recovery of the kinetic energy of the incoming stream ($V_0^2/2g_0$), it is essential that the intake area ($A_1$) be carefully related to the intake approach velocity $V_0$ and the rate of volume flow $Q$ according to the condition of continuity:

$$Q = a_1 A_1 V_0 \tag{2.2}$$

where the correction factor $a_1$ cannot vary between very wide limits. However at the "hump" $V_0$ is usually less than one-half of its value at full speed whereas $Q$ must have about the same value at both speed conditions in order to overcome the high hump drag. This means that the intake area $A_1$ has to be adjustable since it must be greater at hump conditions than at full speed of travel. A variable intake naturally poses a considerable problem of mechanical reliability since the hydrodynamic quality of the intake is of vital importance and must not be compromised.

Figure 3 also shows two parabolas, i.e., curves of constant drag coefficients; one runs through the high-speed part of the drag curve and the other touches the low-speed part of the curve. Any parabola of this type is associated with a set of similar flow conditions in the propulsion pump. (There is no *general* reason why the lower parabola should either contact or intersect the drag curve at the high-speed point.)

For the same speed of travel, the drag indicated by these two parabolas differs by a multiple of about six. This is mainly a qualitative statement, but it does indicate the general magnitude of this departure from the similarity relations.

It will be shown in Chapter 3 that the hump condition, or any other low-speed-of-travel condition that falls substantially above the parabola through the full-speed-condition, will determine the cavitation characteristics of the propulsion pump. The maximum speed of rotation and maximum power are often *specified* for a speed of travel substantially below that at the hump so that a high vehicle acceleration is available at conditions near zero speed of travel (an obvious military requirement). Chapter 3 will show that this specification cannot be met without sacrifices in the quality of hydrodynamic design and performance.

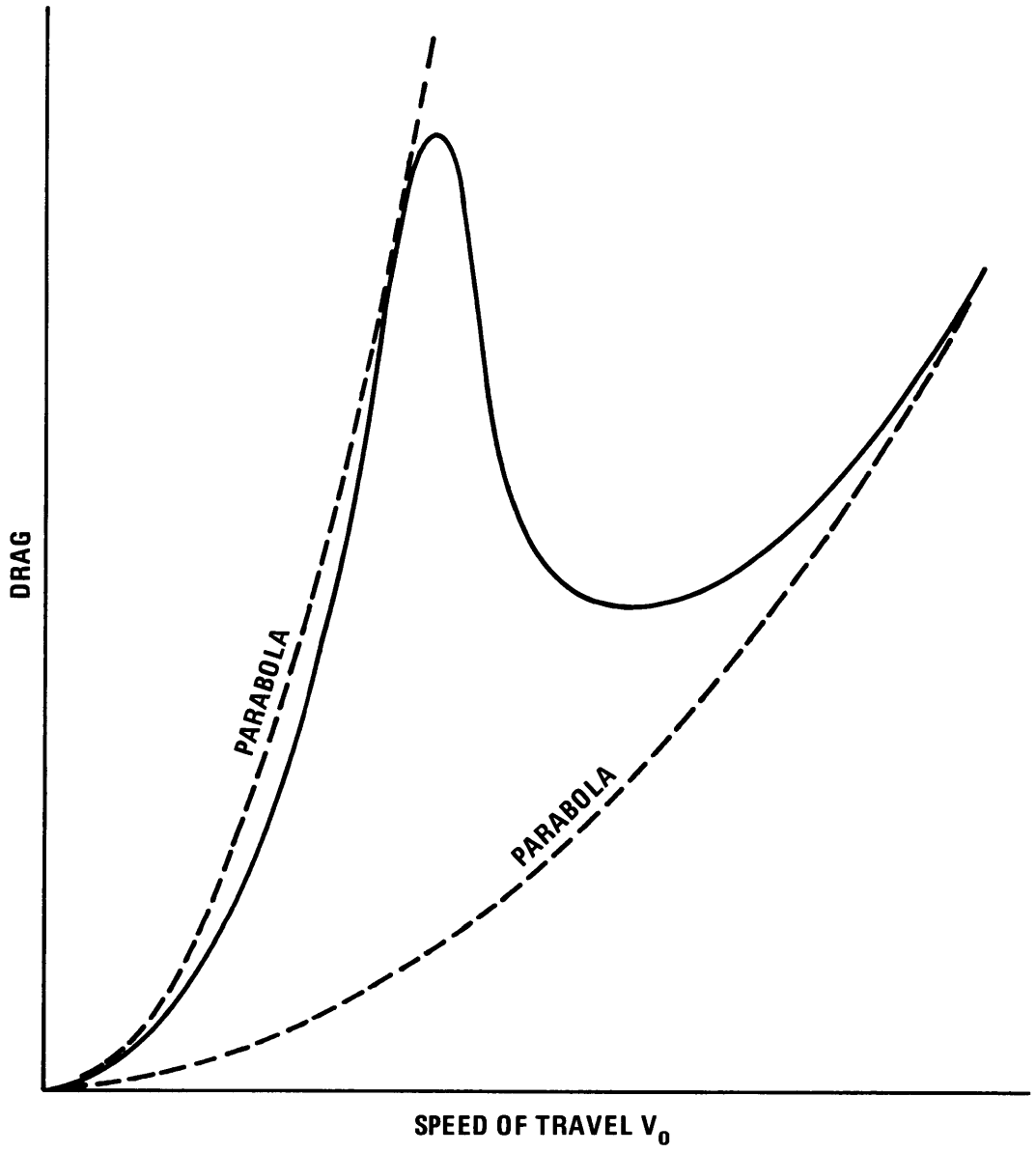


Figure 3 – Typical Drag-Speed Relation

## 2.2 THE EFFICIENCY OF HYDRODYNAMIC PROPULSION

If the inlet velocity $V_0$ to a hydrodynamic propulsor is oppositely equal to the speed of travel, then according to Equation (1.1), the discharge or jet velocity $V_j$ must necessarily be higher than the speed of travel, i.e., a stream of the velocity $\Delta V = V_j - V_0$ is left in the (ideally) stationary body of fluid behind the moving craft. Thus an energy loss per unit of time (i.e., a loss in power) $\rho Q\, \Delta V^2/2$ is necessarily associated with hydrodynamic propulsion.

The useful work per unit of time (power) is obviously:

$$T \cdot V_0 = \rho Q\, \Delta V \cdot V_0 \tag{1.1a}$$

and the so-called "ideal jet efficiency" which expresses the loss in kinetic energy left behind the craft is:

$$\eta_j = \frac{\rho Q\, \Delta V \cdot V_0}{\rho Q\, \Delta V \cdot V_0 + \rho Q\ \Delta V^2/2} = \frac{1}{1 + \dfrac{\Delta V}{2V_0}} \tag{2.3}$$

It is of interest to observe that the same expression is obtained by dividing the useful work by the increase in kinetic energy from inlet to discharge:

$$\eta_j = \frac{\rho Q\, \Delta V \cdot V_0}{\rho Q\, [(V_0 + \Delta V)^2 - V_0^2]/2} = \frac{\Delta V \cdot V_0}{\Delta V \cdot V_0 + \Delta V^2/2} \tag{2.3a}$$

when divided by $\Delta V \cdot V_0$, this reduces to exactly the same expression as Equation (2.3).

Division by just the increase in kinetic energy of the propulsion stream obviously implies that the sum of the remaining terms in the Bernoulli equation ($p/\rho g_0 + z$, where $z = -h$ as defined before) has the same value at inlet as at discharge. This is true for any submergence $h$ below the free water surface, so Equation (2.3) is valid even if inlet and discharge have different depths of submergence. It is not true if the jet has an elevation $\Delta h_j$ above the *free* water surface (see Figure 2). In this case:

$$\eta_j = \frac{\Delta V \cdot V_0}{\Delta V \cdot V_0 + \dfrac{\Delta V^2}{2} + g_0\, \Delta h_j} = \frac{1}{1 + \dfrac{\Delta V}{2V_0} + \dfrac{g_0\, \Delta h_j}{\Delta V \cdot V_0}} \tag{2.4}$$

which is obviously lower than the efficiency expressed by Equation (2.3) since it takes into account the work lost by lifting the propulsion stream to the elevation $\Delta h_j$ above the free water surface. Other considerations of the efficiency of propulsion will first be made without taking this increase in elevation into account, i.e., by ignoring Equation (2.4). Equation (2.4) will be considered later in combination with other relations to be derived.

Equation (2.3) indicates that the ideal jet efficiency $\eta_j$ will increase with diminishing ratio of velocity increase $\Delta V/V_0$ and will approach unity as $\Delta V/V_0$ approaches zero. According to the principle of hydrodynamic propulsion expressed by Equation (1.1), diminishing $\Delta V/V_0 = (V_j - V_0)/V_0$ means an increasing rate of flow $Q$ and a decreasing jet head of the propulsion pump $H_j$ which, in agreement with the second derivation of Equation (2.3), is:

$$H_j = [(V_0 + \Delta V)^2 - V_0^2]/2g_0 = \frac{V_0 \Delta V}{g_0} + \frac{\Delta V^2}{2g_0}$$

$$H_j = \frac{V_0^2}{2g_0}\left[2\frac{\Delta V}{V_0} + \left(\frac{\Delta V}{V_0}\right)^2\right] \tag{2.5}$$

Obviously, the greater the mass flow, the less this mass must be accelerated to produce a certain propulsive force $T$, or the lower the energy that will be required per unit mass or per unit weight (the latter ratio is the "head" $H_j$ of the propulsor in foot pounds per pound = feet). This reasoning can and has been pursued in the field of open propellers where values of $\Delta V/V_0$ as low as 1/10 (or less) are possible. Equation (2.5) shows that in this case the propeller head is as low or lower than $0.21\ V_0^2/2g_0$.

However, the designer of ducted propulsors such as those shown in Figures 1 and 2 cannot ignore the existence of certain head losses in the ducts. It will be assumed here that these duct losses are proportional to the velocity head of the oncoming stream ($V_0^2/2g_0$). If the loss of head in the duct were as low as $0.1\ V_0^2/2g_0$, the aforementioned velocity increase ratio $\Delta V/V_0 = 0.10$ would be associated with a useful pump head of the same magnitude as the duct-loss head. This obviously reduces the efficiency due to duct losses alone to something in the vicinity of 65 percent. In this case, the high ideal jet efficiency related to $\Delta V/V_0 = 0.10$ (about 95 percent) would be of no practical value.

It should be mentioned here that the idea of considering the duct losses as proportional to the velocity head of the *oncoming* stream ($V_0^2/2g_0$) has been questioned. Brandau[1] gives (among many valuable considerations) a brief survey of various suggestions made by several investigators, and recommends a somewhat different approach than used here.

One alternate approach is that of Joseph Levy who uses the jet velocity head $V_j^2/2g_0$ to describe the duct losses. It has already been mentioned that the inlet duct, which propably accounts for most of the duct losses, is subjected to velocities that are proportional to $V_0$ and not to $V_j$. However it should be considered that $V_j = V_0 + \Delta V = V_0\ (1 + \Delta V/V_0)$. Thus $V_0$ and $V_j$ are proportional to each other for similar

propulsion *system* characteristics; i.e., for $\Delta V/V_0$ = constant. Thus there does not appear to be a fundamental difference between the use of $V_j$ or $V_0$ as reference velocity for the duct losses. However, it will be seen later that the optimum value of $\Delta V/V_0$ for fixed loss coefficients is somewhat different when $V_j$ rather than $V_0$ is used as the reference velocity.

If the duct loss is accepted as

$$h_{\text{loss}} = K\, V_0^2/2g_0 \tag{2.6}$$

the "jet efficiency" corrected for this duct head loss (but otherwise derived like the ideal jet efficiency) is:

$$\eta_{j_1} = \frac{V_0 \cdot \Delta V}{V_0 \Delta V + \frac{\Delta V^2}{2} + K\,\frac{V_0^2}{2}} = \frac{1}{1 + \frac{\Delta V}{2V_0} + K\,\frac{V_0}{2\Delta V}} \tag{2.7}$$

The results of this equation are plotted in Figure 4.

A second influence of real-flow effects is concerned with the drag of submerged bodies; e.g., the intake structure to the propulsor duct. It is important to consider here only those parts of the submerged or semisubmerged structure that would *not* exist in the absence of this particular propulsor.

The net propulsive force in this case is obviously $T - \Delta T$, where $T$ is the propulsor force as previously used and $\Delta T$ is the external drag of the propulsor. For a propulsor above the free water surface (where the drag is in air and may therefore be disregarded compared with the drag in water), the only additional drag due to the propulsor is the drag of the intake nacelle (see Figure 2) or "scoop" and the added drag resulting from the fact that the surface-piercing elements (hydrofoil-supporting struts or side skirts of a captured air-cushion vehicle) may be somewhat larger than required without the presence of hydrodynamic propulsor flow through these elements. The nearly unavoidable lack of axial symmetry of the intake also involves an *induced* drag; the surface wave drag must also be included in $\Delta T$.

Taking this external drag increase into account leads to the expression for the "real" jet efficiency $\eta_{j_2}$:

$$\eta_{j_2} = \frac{1}{1 + \frac{\Delta V}{2V_0} + K\,\frac{V_0}{2\Delta V}}\,\frac{T - \Delta T}{T} = \frac{1}{1 + \frac{\Delta V}{2V_0} + K\,\frac{V_0}{2\Delta V}}\left(1 - \frac{\Delta T}{T}\right) \tag{2.8}$$

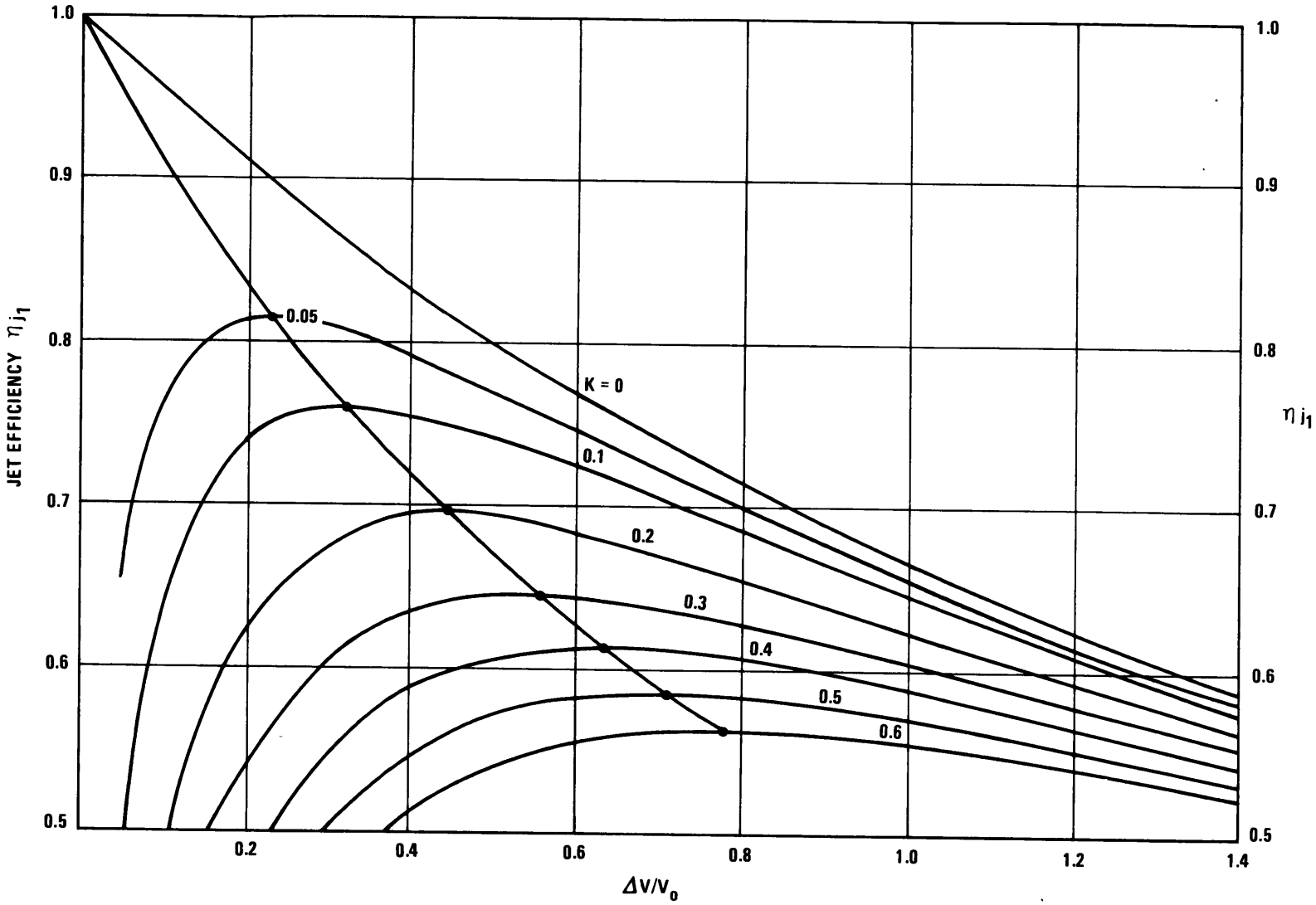


Figure 4 – Jet Efficiency as a Function of Increase in Through-Flow Velocity $\Delta V = V_j - V_0$ and the Duct-Loss Coefficient $K = 2g_0\, h_{loss}/V_0^2$

Assume that

$$\Delta T = C_T \frac{\rho V_0^2}{2} A_1 \text{ and } \rho Q \Delta V = \rho a_1 A_1 V_0 \Delta V$$

($A_1$ is the submerged intake area of the duct and $a_1$ is defined by Figure 2). Hence:

$$\frac{\Delta T}{T} = C_T \frac{\rho V_0^2 A_1}{2 \rho a_1 A_1 V_0 \Delta V} = \frac{C_T}{a_1} \frac{V_0}{2 \Delta V} \tag{2.9}$$

Therefore, according to Equations (2.8) and (2.7):

$$\eta_{j_2} = \eta_{j_1} \left(1 - \frac{\Delta T}{T}\right) = \eta_{j_1} \left(1 - \frac{C_T}{a_1} \frac{V_0}{2 \Delta V}\right) \tag{2.10}$$

Consider that $a_1 < 1$ as the incoming flow is slightly retarded before reaching the intake area $A_1$ ("pre-diffusion;" see Figure 2). Now estimate the drag coefficient $C_T/a_1$. (This is the drag coefficient referred to the cross section $a_1 A_1$ of the incoming stream which has the undisturbed velocity $V_0$, i.e., the cross section of the stream before it comes under the influence of the intake structure.) By introducing the coefficient $K_T = C_T/a_1$, one may write propulsor drag as

$$\Delta T = K_T a_1 A_1 \rho V_0^2/2 \tag{2.11}$$

and the jet efficiency including duct head loss ($K V_0^2/2g_0$) and propulsor or propulsor intake drag ($\Delta T = K_T a_1 A_1 \rho V_0^2/2$) as

$$\eta_{j_2} = \frac{1 - K_T V_0/2 \Delta V}{1 + \Delta V/2 V_0 + K V_0/2 \Delta V} \tag{2.12}$$

It is important to remember that the propulsor or propulsor-intake drag $\Delta T$ does *not* include the momentum of the incoming propulsion stream $\rho Q_v V_0$ which was taken into account in deriving the "ideal" jet efficiency (Equation (2.3)) and the "real" jet efficiency (Equation (2.7)).

Furthermore it is important to remember that neither Equation (2.12) nor any of the preceding equations takes account of the energy losses in the propulsion pump. This means that all jet efficiencies quoted here become propulsive efficiencies in an overall sense only when multiplied by the hydrodynamic efficiency of the propulsion pump; this efficiency may be expected to be close to 90 percent, assuming competent design.

Figure 4 shows the jet efficiencies $\eta_{j_1}$ corrected only for the *duct* losses (Equation (2.7)). Its outstanding characteristic is that this efficiency approaches zero rather than unity for $\Delta V/V_0 \to 0$, even for small duct losses. This is in agreement with the foregoing physical considerations. The optimum value of the velocity-increase ratio through the propulsor system ($\Delta V/V_0$) rises rather rapidly with increasing duct-loss coefficient $K$. It may be in the vicinity of one-half rather than zero as derived from the *ideal* jet efficiency ($\eta_j$ in Equation (2.3)).

The importance of duct losses is immediately evident from this evaluation of Equation (2.7) since any duct-loss coefficient ($K$) sets an upper limit for the effective jet efficiency actually obtainable. Consider that a 90-deg elbow of the best design (with turning vanes) involves a loss of about 15 percent. The arrangement shown in Figure 2 indicates two changes in direction of the duct flow by not less than about 45 deg, and the necessarily retarded flow in the inlet duct (see Chapter 3) involves greater duct head losses than a flow of constant (or accelerated) velocity. It is evident from Figure 4 then that an arrangement such as shown in Figure 2 necessarily involves serious losses in efficiency. In particular, propulsor arrangements which do *not* transport the mechanical work to or below the free water surface must be expected to be substantially less efficient than more or less conventional subsurface propulsion systems, for example, that shown in Figure 1.

The situation becomes even worse when the hydrodynamic drag of the submerged part of the propulsion system is considered; see Equations (2.8) through (2.12). Figure 5 shows the evaluation of these equations. Solid, broken, and dash-and-dot curves distinguish between *external* drag coefficients $K_T = 0$, 0.1, and 0.2. Curves for duct-loss coefficients $K = 0.2$ and 0.5 have been omitted to avoid confusing interference between curves (note the overlapping of the curves for $K = 0.4$, $K_T = 0.2$ and for $K = 0.6$, $K_T = 0.1$). It is evident from this figure that the combination of internal duct losses $K$ and external drag $K_T$ rapidly brings the jet efficiency (corrected for such losses) down to the undesirable range between 60 and 50 percent (recall that these values must be multiplied by the efficiency of the propulsion pump).

The curves for very low duct loss factors ($K = 0$ and 0.05) apply, of course, primarily to completely submerged propulsors of the type shown diagrammatically in Figure 6 and involve the problem of mechanical transfer of power to a nacelle below the free water surface. It is seen from Figure 6 that the gearing leads to a larger nacelle diameter than would otherwise be required. In this case, the external drag $K_T$ becomes more important than the internal duct losses (which may be quite small as expressed by small values of $K$).

Along with other propulsion systems for high-speed surface vehicles, this submerged propulsor shares the need for efficient diffusion of the incoming stream and for an additional inlet area for low-speed, high-thrust operation.

According to Figure 5, the "jet efficiency" which can be expected from a submerged propulsor is in the neighborhood of 0.7 for a value of $K$ no greater than 0.05 and $K_T = 0.1$. If a value of 0.2 is assumed for $K_T$ because of the large nacelle diameter, then with $K = 0.05$, the jet efficiency is 0.62. Compare this with the jet efficiencies of propulsors above the water surface (Figure 2) where the duct-loss coefficient $K$

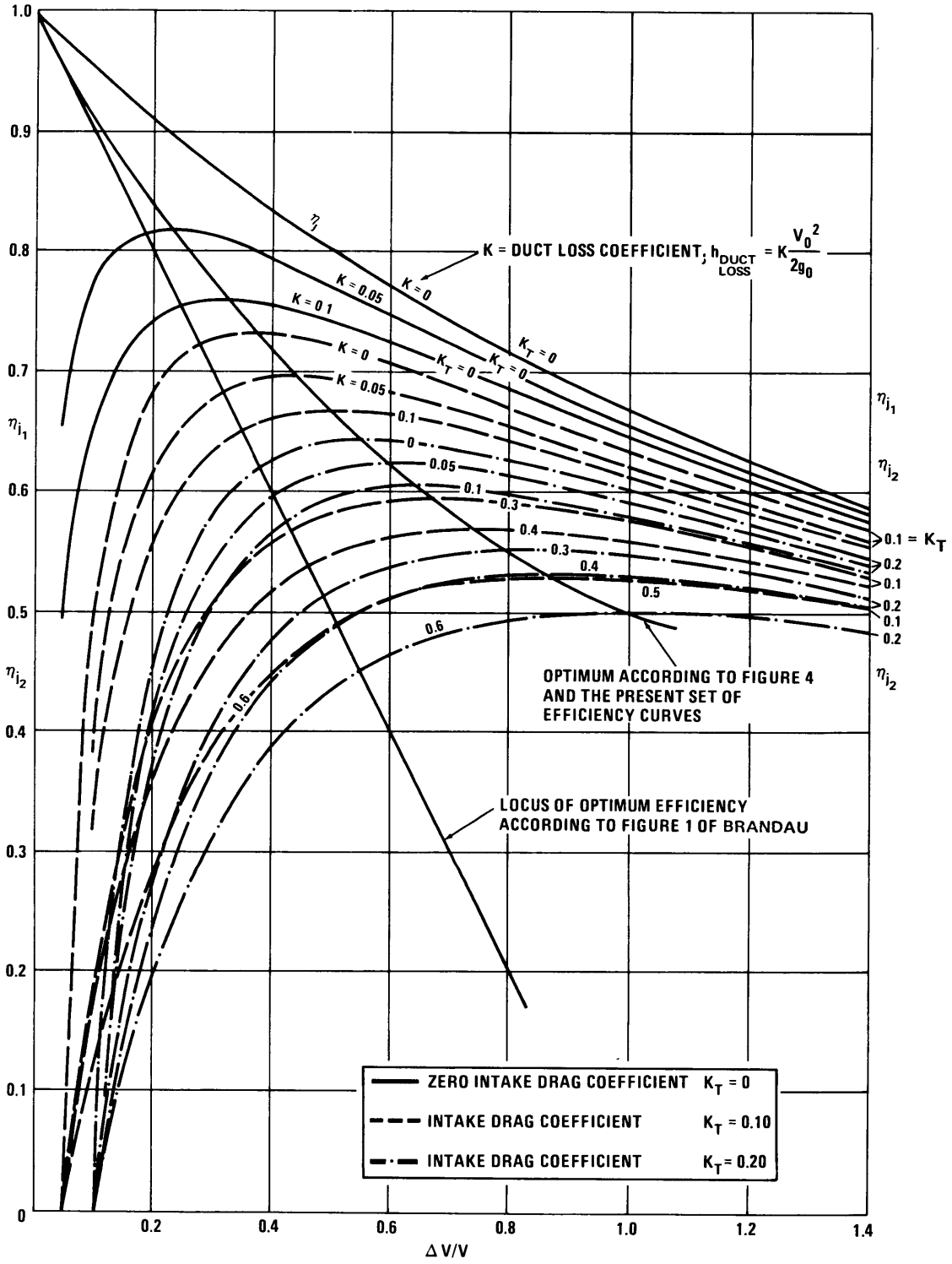


Figure 5 – Jet Efficiency Corrected for Duct Losses and for Intake Parasite Drag

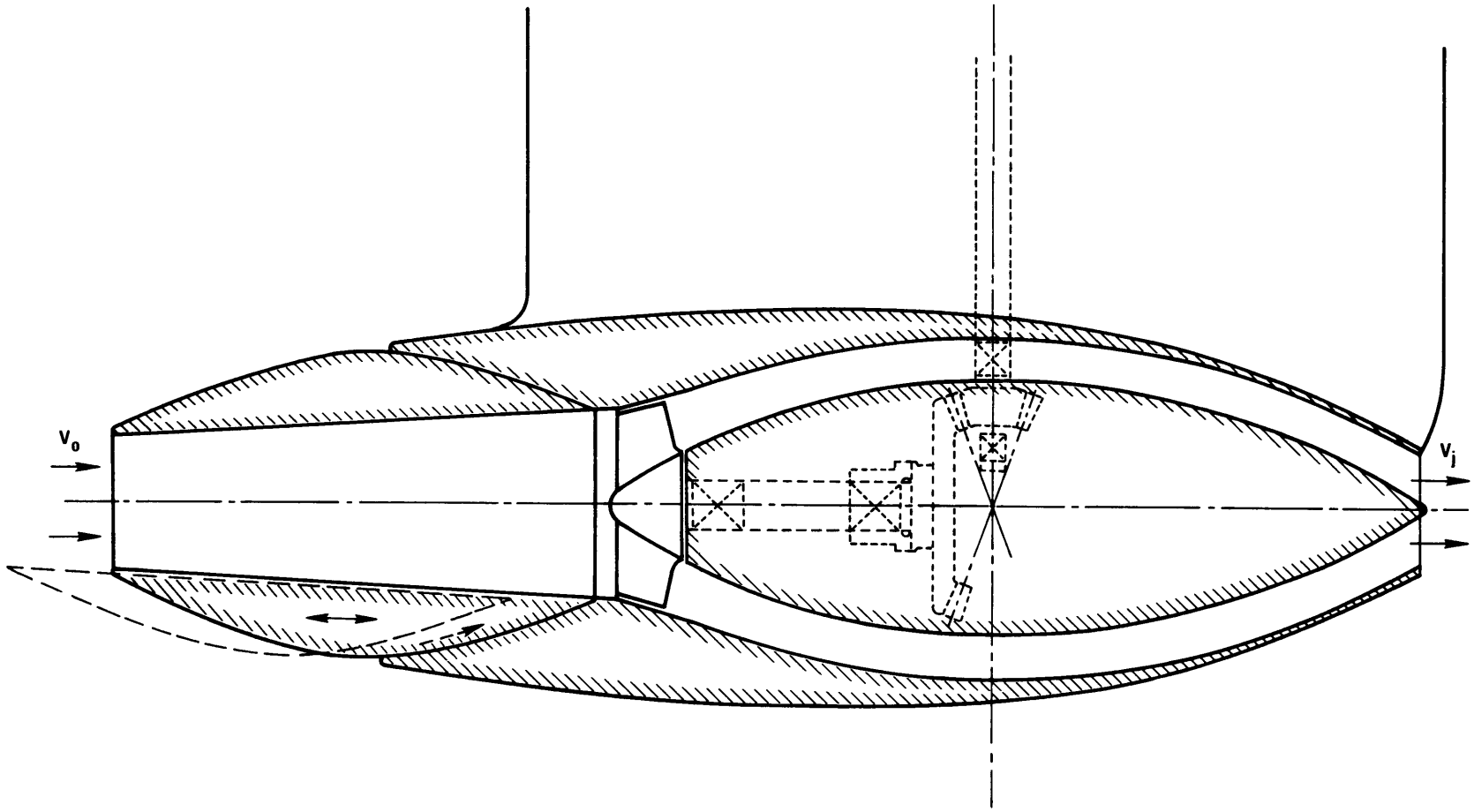


Figure 6 – Completely Submerged Propulsor

is likely to be not less than 0.4 unless a much more efficient duct arrangement can be found than shown in Figure 2. With $K = 0.4$ and no intake drag ($K_T = 0$), Figure 4 indicates a jet efficiency $\eta_{j_1} = 0.61$. With the same $K$ value and $K_T = 0.1$, Figure 5 shows a jet efficiency $\eta_{j_2} = 0.57$. Therefore, in order for above-surface propulsors to compete with submerged propulsors, it would be necessary to reduce their duct-loss coefficient $K$ to something around 0.2. This can be achieved only by major advances in the general arrangement and detail of the ducting.

Figures 4 and 5 show a curve through the maximum values of the efficiency curves presented. It has been mentioned that the location of this optimum along the $\Delta V/V_0$ scale depends on the choice of the variable (a velocity head) by which the head and thrust losses are made dimensionless; i.e., reduced to coefficients like $K$ and $K_T$. It has already been stated that the present choice of $V_0^2/2g_0$ or $\rho V_0^2/2$ is not the only choice possible. Figure 1 in Brandau[1] shows an alternate jet efficiency plot. Its locus of optimum efficiency is a straight line through $\Delta V/V_0 = 0$, $\eta_j = 1$ and $\Delta V/V_0 = 1$, $\eta_j = 0$. This line is also shown in Figure 5 to indicate that the optimum value of $\Delta V/V_0$ is lower under different assumptions than under the present assumption that hydrodynamic losses outside of the propulsion pump are proportional to $V_0^2/2g_0$ and $\rho V_0^2/2$.

The previously mentioned justification for the present choice is that most duct losses occur in the inlet duct and that this part of the duct losses may well be assumed to be proportional to the velocity head or pressure of the velocity of travel $V_0$. The inlet duct cannot be shortened below the limits dictated by the location of the pump relative to the intake and by the required retardation of the flow from the intake to the pump. On the other hand, the discharge duct length can and must be minimized as shown in Figure 2 in order to keep the duct-loss coefficient $K$ as low as possible.

One additional effect on jet efficiency was introduced at the beginning of this section, namely, the additional loss from the elevation $\Delta h_j$ of the jet above the free water surface (see Figure 2). Its discussion was postponed because its importance diminishes with increasing speed of travel, yet it requires attention in, say, the 50-knot range of speed.

Equation (2.4) may be written in the form:

$$\eta_j = \frac{1}{1 + \frac{\Delta V}{2V_0} + \frac{2g_0\,\Delta h_j}{V_0^2}\,\frac{V_0}{2\Delta V}} \tag{2.13}$$

which has exactly the same form as Equation (2.7) except that $2g_0\,\Delta h_j/V_0^2$ replaces the duct-loss coefficient $K$. Proceeding exactly as in the derivation of Equations (2.4) and (2.7), i.e., dividing the useful work per unit of mass flow by the same work plus the losses per unit of mass flow, one arrives at the following:

$$\eta_{j_3} = \frac{V_0 \Delta V}{V_0 \Delta V + \frac{\Delta V^2}{2} + K \frac{V_0^2}{2} + g_0 \Delta h_j} = \frac{1}{1 + \frac{\Delta V}{2 V_0} + \left( K + \frac{2 g_0 \Delta h_j}{V_0^2} \right) \frac{V_0}{2 \Delta V}} \tag{2.14}$$

which again has the same form as Equation (2.7) except that the *sum* of the duct-loss and the jet-elevation coefficients ($K + 2g_0 \Delta h_j / V_0^2$) takes the place of the duct-loss coefficient $K$ alone. This means that one can use Figures 4 and 5 to evaluate the effect of jet elevation on jet efficiency by using the sum $K + 2g_0 \Delta h_j / V_0^2$ in place of the duct-loss coefficient $K$. In so doing, Figure 4 represents $\eta_{j_3}$ (above), and (analogously with Equation (2.12)) and Figure 5 represents:

$$\eta_{j_4} = \frac{1 - K_T V_0 / 2 \Delta V}{1 + \frac{\Delta V}{2 V_0} + \left( K + \frac{2 g_0 \Delta h_j}{V_0^2} \right) \frac{V_0}{2 \Delta V}} \tag{2.15}$$

Neither, of course, includes the losses expressed by the pump efficiency.

Figure 7 gives the jet elevation coefficient $2g_0 \Delta h_j / V_0^2$ as a function of the speed of travel in knots and the jet elevation $\Delta h_j$ in feet. It is evident that only values of $2g_0 \Delta h_j / V_0^2$ above 0.05 are of major significance; according to Figures 4 and 5 a step in $K$ of one-half a tenth makes quite a difference in jet efficiency, and particularly in the optimum value of $\Delta V / V_0$. Jet elevations $\Delta h_j$ of less than 10 feet are important at speeds below 60 knots. The jet elevation would have to be over 20 ft before it would be significant at speeds of 100 knots or more.

In summary, the potential capability of waterjet propulsion with the propulsor and its jet above the free water surface hinges primarily on the head losses in the ducts. Presently used arrangements and details are not very promising. Not a great deal of improvement can be expected from the propulsion pump alone inasmuch as the efficiency of a competent and well-executed design is already in the neighborhood of 90 percent. What is needed is to approach the duct-loss problem by an imaginative general arrangement and to design details which offer some hope for significant advances. Some approaches to the solution of this problem will be outlined in Chapter 4. Nevertheless, any solutions of this problem must be compared with propulsors at/or below the free water surface. In other words, the problem of carrying the propulsion stream to a pump above the water surface must be critically compared with the problem of carrying the propulsion power to a propulsor at or below the free water surface.

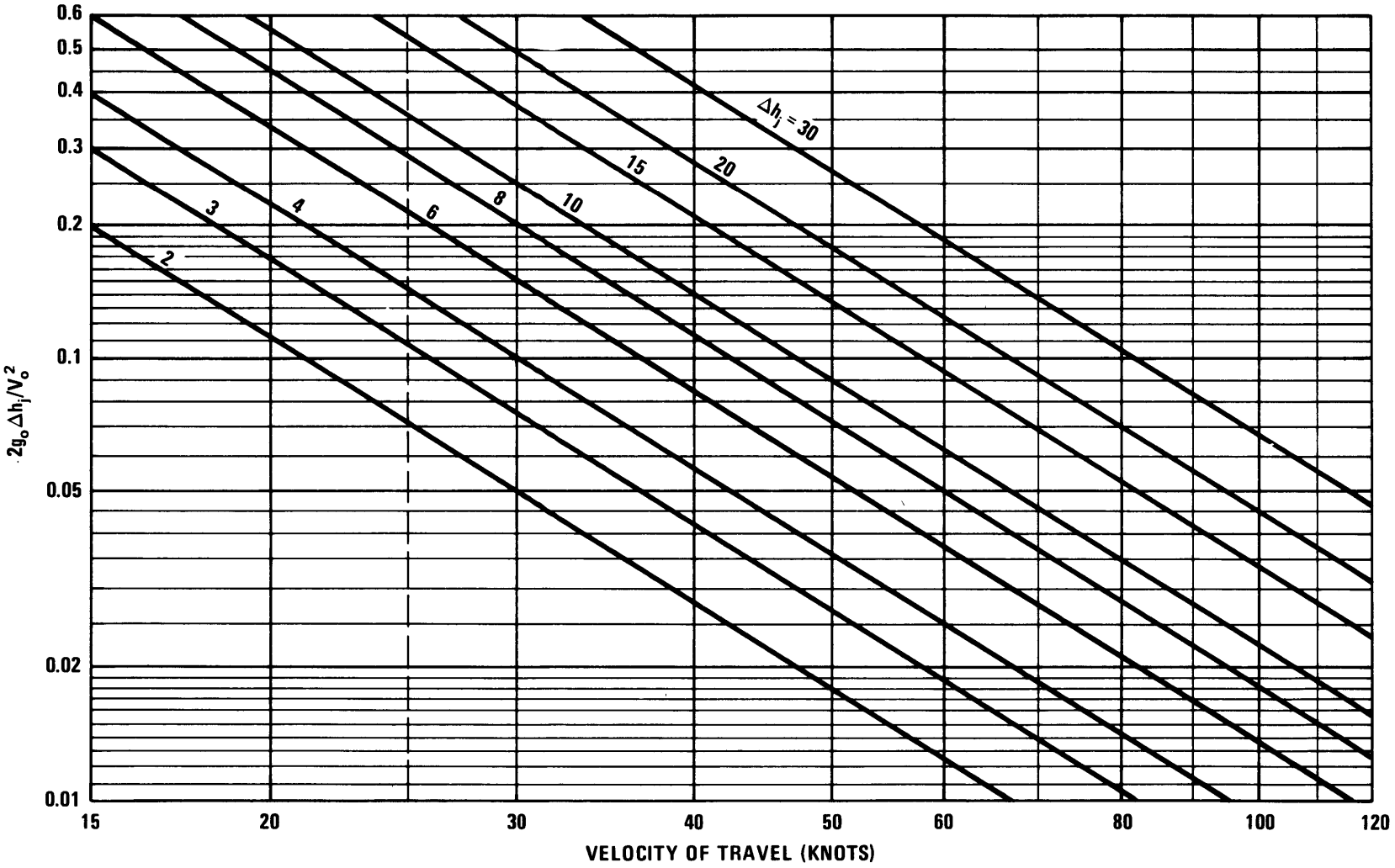


Figure 7 – Effect of Jet Elevation $\Delta h_j$ on Jet Efficiency (Equation (2.14)

## 2.3 SOME WEIGHT CONSIDERATIONS ON THE PROPULSION PLANT

It has become standard to consider the propulsion plant of modern, high-speed, "dynamic" surface craft from the point of view of aircraft practice. This means that the weight of the propulsion plant is considered a matter of major significance. This general contention deserves some quantitative examination. No accurate calculations are intended for this section. Approximate answers are sufficient for this line of inquiry and are the best that can be achieved by simple, and thereby reliable, considerations.

A lift-to-drag ratio of 14 is probably the best that can be expected at present from hydrofoil craft. For simplicity of reasoning, this value is assumed throughout this section. Thus the ideal power required to propel the craft without any losses in the propulsion system is:

$$P_i = \frac{W}{14} \cdot V_0 \tag{2.16}$$

where $W$ is the gross weight of the craft (in pounds) including its propulsion plant, fuel, and payload and $P_i$ is the ideal power in foot pounds per second.

The assumption of a constant lift-to-drag ratio of 14 (Equation (2.16)) is of course meaningful only if applied to the design cruise-speed condition of various vehicles. Even this assumption can be justified only for the purpose of obtaining the most simple basis for the approximate considerations presented in this section. The assumption of a constant lift-to-drag ratio is definitely *not* applicable to various speeds of one vehicle; this should be clear from the drag versus speed curve in Figure 3. *The possibility of an approximately constant lift-to-drag ratio at design conditions is the primary reason for departing from the conventional forms of displacement vessel design.*

If a propulsion pump efficiency of 90 percent is assumed, the curves in Figures 4 and 5 suggest a value of 0.55 for the hydrodynamic efficiency of propulsion. (This means that the value for this factor is assumed to lie somewhere between 0.45 and 0.65.)

Therefore the actual power $P$ required for propulsion is approximately:

$$P = \frac{W}{0.55 \times 14} \cdot V_0 = \frac{W \cdot V_0}{7.70} \tag{2.17}$$

This may be converted into more conventional units, e.g., $P_{HP}$ for the power in horsepower, $W_t$ for the weight in long tons, and $V_k$ for the speed in knots. Now $P = 550\ P_{HP}$, $W = 2240\ W_t$, and $V_0 = V_k \times 1.69$. Then

$$550\ P_{HP} = \frac{2240\ W_t \cdot V_k \cdot 1.69}{7.70}$$

or

$$P_{HP} = 0.894\ W_t \text{ x } V_k \tag{2.18}$$

Assume (optimistically) a specific fuel consumption (SFC) of 0.5 lb per horsepower hour. Thus the fuel consumption *per hour* will be:

$$W_{f_1} = 0.5 \cdot P_{HP} = 0.894\ W_t\ V_k \text{ x } 0.5 \tag{2.19}$$

Assume a total range (total distance of travel) of $R$ nautical miles. Then the total fuel consumption *in pounds* will be:

$$W_f = W_{f_1} \cdot \frac{R}{V_k} = 0.447\ W_t \text{ x } R \tag{2.20}$$

and, by conversion to the same units for $W_f$ and $W_t$,

$$W_f = \frac{0.447}{2{,}240}\ W \text{ x } R = \frac{WR}{5000}$$

where $W$ is the vehicle weight in pounds. Hence:

$$\frac{W_f}{W} = \frac{R}{5000} \tag{2.21}$$

or the traveling range in nautical miles will be:

$$R = 5000\ \frac{W_f}{W} \tag{2.22}$$

It thus appears that the fuel to gross-weight ratio would be $W_f/W = 2/5$ for a traveling distance of 2000 nm. This clearly implies an aircraft type of structure for a hydrofoil or air-cushion vehicle. (It would not imply this for a displacement tanker, but its drag versus speed characteristics would prohibit high speeds.)

Accordingly, for an aircraft type of propulsion plant, one might assume (optimistically) a propulsion plant weight of 2 lb/hp since the weight of water in the ducts above the free water surface must be counted as propulsor weight. According to Equation (2.18) then, this means that the weight of the propulsion plant $W_{pp}$ (in pounds) would be

$$W_{pp} = 2P_{HP} = 1.788\ W_t V_k$$

Converted to the same units of weight (pounds or tons):

$$W_{pp} = \frac{1.788}{2{,}240}\ W\ V_k$$

or

$$\frac{W_{pp}}{W} = \frac{V_k}{1253} \tag{2.23}$$

Hence the ratio of propulsion plant to vehicle weight for 60 knots is:

$$\frac{W_{pp}}{W} = \frac{1}{20.9} \tag{2.24}$$

and the same ratio for 100 knots is:

$$\frac{W_{pp}}{W} = \frac{1}{12.53} \tag{2.25}$$

According to Equation (2.21), $W_f/W$ (the ratio of fuel weight to gross weight) is 2/5 for a range of 2000 nm. It follows that the ratio of propulsion plant weight $W_{pp}$ to fuel weight $W_f$ for the same distance of travel is

$$\frac{W_{pp}}{W_f} = \frac{W_{pp}}{W}\,\frac{W}{W_f} = \frac{1}{20.9} \times \frac{5}{2} = \frac{1}{8.36} \tag{2.26}$$

for 60 knots and

$$\frac{W_{pp}}{W_f} = \frac{1}{12.53} \times \frac{5}{2} = \frac{1}{5.01} \tag{2.27}$$

for 100 knots.

Since $W_f$ is inversely proportional to the efficiency, a 1-percent change in efficiency would have about the same effect on weight as an 8-percent change in propulsion plant weight at 60 knots and 5 percent at 100 knots (assuming that with regard to weight, the propulsion plant is designed according to aircraft practice).

The foregoing assumption of a propulsion plant weight of 2 lb/hp is, of course, of major significance regarding the last results obtained and it therefore demands further scrutiny. A general study of this value is outside the scope of this section. However an estimate of the weight of *water* that should be included in the weight of the propulsion plant is of interest and can be obtained in a fairly simple manner.

Let the volume of the duct be $A \cdot L_d$. (Here the cross-sectional area, $A = Q/V_d$; $V_d$ is the average meridional velocity of flow in duct and pump, and $L_d$ is the duct length *above the free water* surface, including the pump.) For a vehicle weight-to-drag ratio of 14, the net thrust is:

$$\frac{W}{14} = \rho Q \Delta V \tag{2.28}$$

or

$$Q = \frac{W}{14 \rho \Delta V}$$

The volume of the duct and pump is

$$\text{Vol.} = \frac{Q}{V_d} L_d = \frac{W}{14 \rho \Delta V} \times \frac{L_d}{V_d} \tag{2.29}$$

and the weight of water in the duct and pump is

$$W_{pw} = \text{Vol.}\, g_0 \rho = W \frac{g_0 L_d}{14 V_d \Delta V}$$

or

$$\frac{W_{pw}}{W} = \frac{g_0 L_d}{14 V_d \Delta V} = \frac{g_0 L_d}{V_0^2} \times \frac{V_0}{V_d} \frac{V_0}{\Delta V} \times \frac{1}{14} \tag{2.30}$$

This means that the ratio of duct water weight to vehicle weight is inversely proportional to the square of a Froude number $V_0/\sqrt{g_0 L_d}$ referred to the duct length $L_d$ above the free water surface. It is also inversely proportional to the velocity ratios $V_d/V_0$ and $\Delta V/V_0$ and to the lift-to-drag ratio (which was assumed to be 14). The Froude number referred to the duct length is not proportional to the Froude number of the entire vehicle since the pump elevations $\Delta h_i$ and $\Delta h_j$ and thereby $L_d$ are *not* expected to increase proportionally with the linear dimensions of the vehicle.

To check whether the foregoing assumption of a total power-plant weight of 2 lb/hp is reasonable relative to the weight of the water in the pump and ducts, consider a definite example:

Let $L_d$ = 30 ft, $V_0$ = 80 knots = 135 ft/sec, $\Delta V/V_0$ = 0.65, and $V_0/V_d$ = 2. Then (according to Equation (2.30)):

$$\frac{W_{pw}}{W} = \frac{32.2 \times 30 \times 2}{18{,}230 \times 0.65 \times 14} = \frac{1.164}{100} \tag{2.31}$$

i.e., slightly over 1 percent of the total weight of the vehicle.

For a propulsion plant weight of 2 lb/hp and propulsion efficiency of 0.55, the ratio of propulsion plant weight to vehicle weight is (according to Equation (2.23))

$$\frac{W_{pp}}{W} = \frac{V_k}{1253} = \frac{80}{1253} = \frac{1}{15.66}$$

and therefore

$$\frac{W_{pw}}{W_{pp}} = \frac{W_{pw}}{W}\,\frac{W}{W_{pp}} = \frac{1.164 \times 15.66}{100} = 0.1824 \qquad (2.32)$$

Assuming that the *pump weight plus duct weight* $W_{pd} = 0.4\ W_{pp}$, the ratio of water weight to pump and duct weight is:

$$\frac{W_{pw}}{W_{pd}} = \frac{W_{pw}}{W_{pp}}\,\frac{W_{pp}}{W_{pd}} = \frac{0.1824}{0.4} = 0.456 \qquad (2,33)$$

Short of an actual design study, there is no way to check this figure. However, the previous assumption of 2 lb/hp for the total propulsion plant has not lead to any contradictory results, and it may therefore be accepted as a sufficient approximation for the purposes of this section.

Most considerations presented in this section obviously serve only for general orientation. Nevertheless, at least one definite conclusion can be drawn from the results obtained:

For a cruising range from one to several thousand nautical miles, the fuel weight is a fairly large multiple of the propulsion plant weight (5 to 8 for the examples given). Therefore a sacrifice in overall efficiency is generally not justified in order to reduce the weight of the propulsion plant unless the percentage change in weight is greater by at least one order of magnitude than the percentage change in efficiency and fuel consumption. For example, the use of aircraft practice rather than stationary machinery practice reduces the weight considerably without necessarily involving any significant sacrifice in efficiency. Thus the adoption of aircraft practice is definitely justified and, in fact, necessary for the propulsion plants of the high-speed surface craft considered here.

# CHAPTER 3. DESIGN OF THE PROPULSION PUMP

## 3.1 GENERAL FEATURES

### 3.1.1 Foundations of Hydrodynamic Pump Design

The most important principles for the design of *any* hydrodynamic pump, i.e., centrifugal or axial flow (or "propeller") pumps should be presented prior to a discussion of the design of pumps for a particular application, e.g., the propulsion of marine vehicles. Accordingly, the foundations of the design of such pumps will be reviewed very briefly even though they are probably known to most readers. A discussion of the most important hydrodynamic limitation in the design of such pumps (cavitation), will then be presented, and followed by an outline of the general design process with due consideration for that limitation.

The theoretical foundation for the design of turbomachinery is given by the condition of continuity, by the Euler equation for the change of angular momentum in the vane systems of the machine, and by the basic similarity considerations of the flow in turbomachinery. These three items will be discussed in this order.

For practically incompressible fluids like water, the condition of continuity states that at any particular time, the volume rate of flow $Q$ has only one value throughout the machine, i.e.,

$$Q = A_m \, V_{m_{av}} = \text{constant} \tag{3.1}$$

for all cross sections $A_m$ of the same machine at the same time. In this equation, $V_{m_{av}}$ is the average value over the cross section $A_m$ of the "meridional" fluid velocity, i.e., the velocity component lying in radial planes parallel to and containing the axis of rotation and $A_m$ is any flow cross section which is everywhere normal to the local meridional velocity component $V_m$. For a uniform direction of $V_m$ along any circle coaxial to the machine, $A_m$ is a surface of revolution that is also coaxial to the machine (*AA* and *BB* in Figure 8). Evidently

$$A_m = \int_a^b 2\pi r \, dn \tag{3.2}$$

In Figure 8, where the limits $a$ and $b$ refer to the two surfaces of revolution $AB$ which form the inner and outer boundaries of the space of revolution containing the flow.

Equation (3.1) can obviously be written in the form:

$$A_{m_1} \, V_{m_{av_1}} = A_{m_2} \, V_{m_{av_2}} \tag{3.3}$$

If the local velocity $V_m$ is used instead of $V_{m_{av}}$, the condition of continuity appears in the form:

$$dQ = 2\pi r \, dn \, V_m \cdot \text{constant} \tag{3.4}$$

i.e., constant along any "meridional streamline" $CD$ in Figure 8.

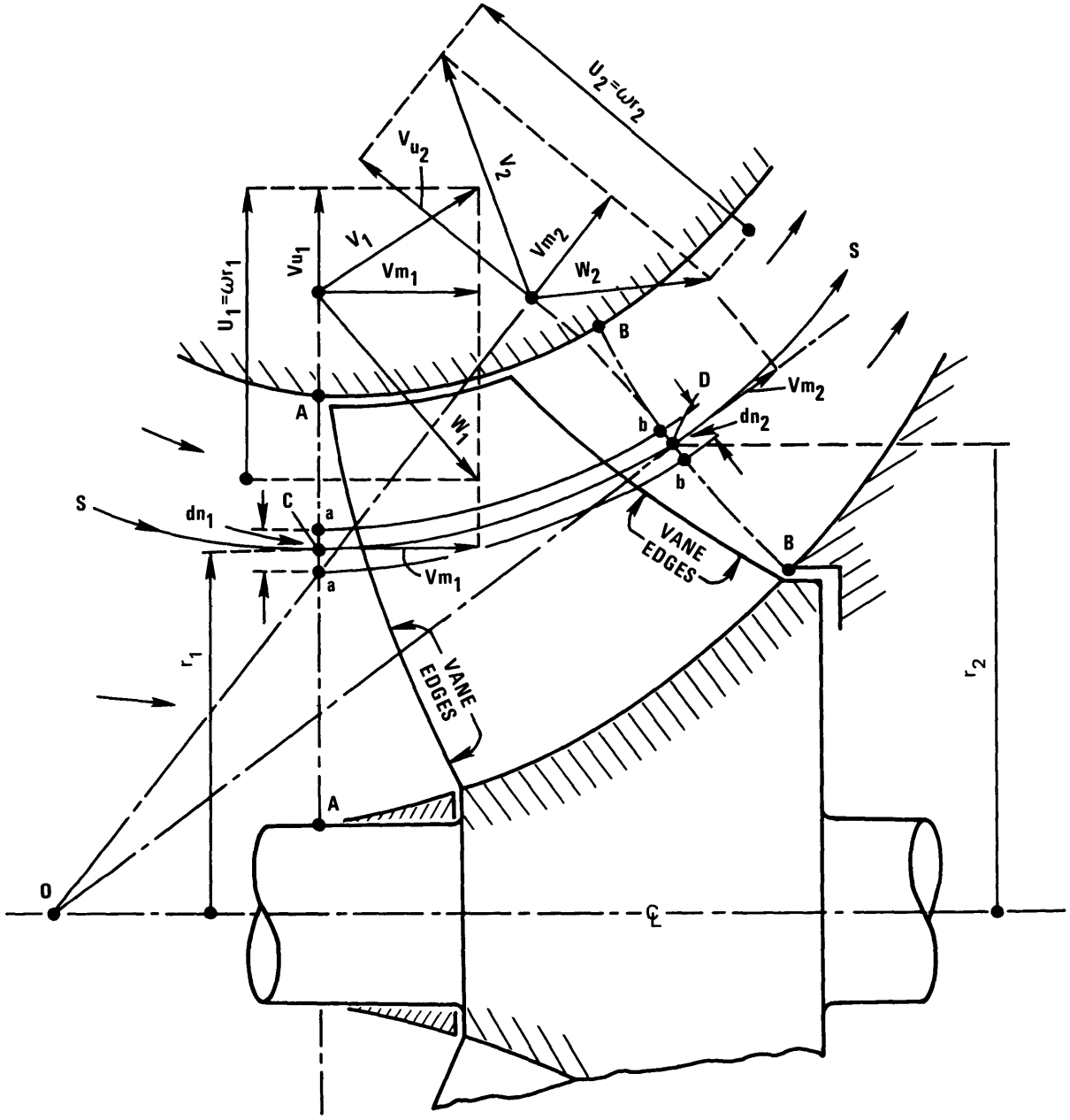


Figure 8 – Runner Profile and Notations for the Derivation of the Euler Turbomachinery Equation

When the elementary steps $dQ$ and $dn$ are replaced by finite steps $\Delta Q$ and $\Delta n$, Equation (3.4) can be used for the construction of the meridional streamlines or stream surfaces. This makes the finite parts $\Delta Q$ of the total capacity constant through the portion of the machine considered, i.e., $\Delta Q = Q/m$, where $m$ is a constant integer.

In Equation (3.4), $V_m$ is assumed to be constant along circles coaxial to the machine, not only in direction but also in magnitude; this is called the assumption of "axial symmetry."

With the meridional velocity component $V_m$ determined or approximated by the condition of continuity, the remaining circumferential fluid velocity component $V_u$ is determined by the circumferential forces, or the torque, applied by the vanes (or other means) to the fluid in the machine. This relation is the Euler turbomachinery momentum equation.

Refer to Figure 8 and consider an elementary part $dQ$ of the flow moving along the stream surface $CD$. Evidently the condition of continuity demands that

$$dQ = 2\pi r_1 \, dn_1 \, V_{m_1} = 2\pi r_2 \, dn_2 \, V_{m_2} \tag{3.5}$$

If a certain torque (moment) $dM$ is applied by the vanes to the fluid between $C$ and $D$, this torque will change the moment of momentum (or "angular momentum") of the flow according to the relation:

$$dM = \rho \cdot dQ \, (V_{u_2} \cdot r_2 - V_{u_1} \cdot r_1) \tag{3.6}$$

where $\rho$ is the fluid mass per unit volume. This is the Euler turbomachinery momentum equation for the elemental stream $dQ$.

Assume that the torque $dM$ is applied to the stream by a vane system which turns about the axis of the system at an angular velocity $\omega$. The mechanical work per unit of time or the "power" interchanged between the turning vane system, the "runner" (or "impeller"), and the fluid is:

$$\omega \, dM = \rho \, dQ \, (V_{u_2} \, U_2 - V_{u_1} \, U_1) \tag{3.7}$$

where ($U_2 = r_2 \times \omega$) and ($U_1 = r_1 \times \omega$) are the peripheral velocities of the runner vanes at distances $r_2$ and $r_1$ from the axis of rotation.

Division of both sides of Equation (3.7) by the elementary weight flow $g_0 \rho \, dQ$ along the stream surface $CD$ leads to

$$\frac{\omega \times dM}{g_0 \rho \, dQ} = H_r = \frac{V_{u_2} \, U_2 - V_{u_1} \, U_1}{g_0} \tag{3.8}$$

where $H_r$ is the work per pound of fluid exchanged between the runner and the fluid; this is called the "runner head" of the machine. In the case of a pump, the torque exerted on the fluid by the runner has the same direction as the angular velocity $\omega$, so that this work is transmitted from the runner to the fluid. The

dimension of $H_r$ is foot pounds per second divided by pound per second, which is foot pounds per pound or "feet" (although the cancellation of pounds is somewhat problematic). If this work could be converted into static pressure without any loss, $H_r$ would represent this pressure increase in terms of the height of a column of the liquid pumped or the height to which the fluid could be lifted by this pumping action.

If the conversion into pressure were to take place at an efficiency $\eta_h$, then the actual height or "net head" $H$ to which the pump can lift the fluid (without further losses such as pipe friction losses) is

$$H = \eta_h H_r = \eta_h \frac{V_{u_2} U_2 - V_{u_1} U_1}{g_0} \tag{3.9}$$

Here $\eta_h$ is called the "hydraulic efficiency;" it is somewhat higher than the overall efficiency $\eta$ of the pump because it expresses only hydrodynamic losses and not parasitic torque changes which are included in the definition of the overall efficiency $\eta$.

The Euler turbomachinery head equation (Equation (3.8) or (3.9)) has been derived for one elementary part of the flow through the machine. In most cases, one would want this head or energy input to the fluid to be uniform across the entire stream that passes through the machine. This means that the runner head $H_r$ must be the same along all coaxial stream surfaces that pass through the runner, and (according to Equation (3.8)) the same must be true for $V_{u_2} U_2 - V_{u_1} U_1$. This constitutes a design requirement for the runner vane system.

For a development of a cylindrical section at the runner inlet (Point C) and a conical section at the discharge (Point D), Figure 8 shows the velocity vector diagrams which should be drawn in space tangentially to the stream surface of revolution that describes the meridional flow. The first approximation of the required vane shape would be to make the ends of this particular vane section parallel to the relative velocities $w_1$ and $w_2$. This is a poor approximation for pumps at the discharge vane edge but it is fairly good at the inlet, provided an allowance is made for vane thickness so that the flow cross section between the vanes satisfies the condition of continuity with respect to the relative velocity $w$.

An additional correction is needed at the discharge of pump vane systems as illustrated in Figure 9. If it is assumed that $w_2^*$ satisfies the condition of continuity at the discharge cross section between the vanes, then the real peripheral component $V_{u_2}$ of the absolute flow at discharge is less than $V_{u_2}^*$, corresponding in the diagram to $w_2^*$ (both velocities marked by * are fictitious). Surprisingly, a fair approximation of the real flow $V_2$ can be obtained by assuming that $V_{u_2}/V_{u_2}^* = 0.8$, so long as the vane length $\ell$ is substantially larger than the circumferential vane spacing $t_0$ at the discharge diameter. This approximation applies also to the development of a conical section that approximates the meridional stream surface in the discharge region of the vanes.

Other approximations are available for wider vane spacing ($\ell / t_0 < 1$); however, these do not fall within the scope of this presentation.

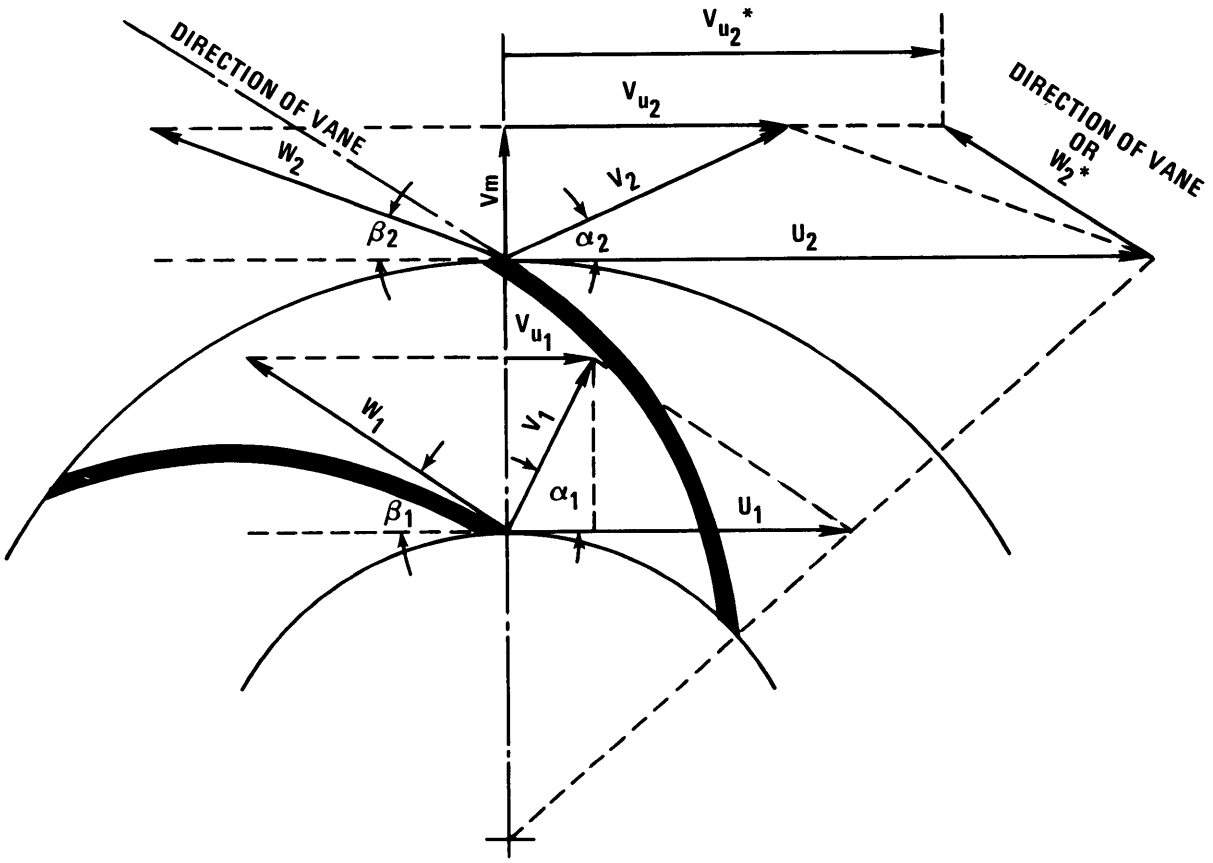


Figure 9 – Velocity Diagrams of a Radial-Flow Pump Runner

A final item concerns basic similarity relations for turbomachinery. In general, fluid mechanics, similarity relations are truly significant only if the flow *departs* from a frictionless, incompressible flow or if it involves the influence of gravity (or another acceleration of the system as a whole). Without such departures from ideal flow, the similarity statement is nearly trivial since the flow will be similar for geometrically similar flow boundaries and similar approaching flow relative to these boundaries, for example, the same angle of attack on geometrically similar airfoils. In the field of turbomachinery, however, very significant similarity relations are in order under the most simple ideal flow conditions because there are two independent velocities, the velocities of flow $V$ and the circumferential velocities of solid parts of the machine $U$. Since flow velocities as well as circumferential velocities form essential parts of the velocity vector diagrams (as shown, for example, in Figure 8), it is apparent that similarity of flow in turbomachinery is possible only if fluid velocities $V$ and circumferential velocities $U$ have the same ratio to each other at geometrical points similarly located in similar machines. (Similarity of velocity vector diagrams at similarly located points may be regarded as a definition of "similarity of flow.")

Evidently

$$V = \text{constant x } \frac{Q}{D^2} \text{ , and } U = \text{constant } n \text{ x } D \tag{3.10}$$

where $D$ is any representative linear dimension of the machine (say, an impeller diameter) and $n$ is the number of revolutions per second of the rotating solid parts, the impellers.

Hence the aforementioned "kinematic condition of similarity of flow in turbomachines" may be expressed by the "flow coefficient:"

$$\frac{V}{U} = \text{constant or } \frac{Q}{n D^3} = \text{constant} \tag{3.11}$$

With respect to $V/U$, "constant" means the same at similar locations in similar machines; with respect to $Q/nD^3$ it means the same for similar machines. $V/U$ = constant applied only to similarly located points in these machines. For an incompressible fluid like water, $Q$ and $Q/nD^3$ are constant throughout any one machine at any one time.

The flow conditions considered are "ideal" to the extent that inertia forces dominate, i.e., all pressure differences $\Delta p$ are proportional to $\rho V^2$ or to $\rho U^2$. This means that

$$\frac{g_0 H}{U^2} = \text{constant and } \frac{g_0 H}{V^2} = \text{constant} \tag{3.12}$$

at similarly located points in similar machines under similar flow conditions. The ratio $g_0 H/U^2$ or $2g_0 H/U^2$ is called the "head coefficient." Expressed in terms of the operating conditions $Q$, $n$, and $H$ and the characteristic dimension $D$, the above relations assume the form:

$$\frac{g_0 H}{n^2 D^2} = \text{constant and } \frac{g_0 H D^4}{Q^2} = \text{constant} \tag{3.13}$$

which applies to the *entire* machines compared.

Figure 10 compares the head, efficiency, and power as a function of the rate of volume flow (or "capacity") for two different speeds of rotation. According to Equations (3.11) and (3.13), the head $H$ increases proportionally to the square of the speed of rotation $n$ whereas the capacity $Q$ increases linearly with $n$ for similar flow conditions. Thus similar flow conditions are connected in an $H$ versus $Q$ diagram by the parabolas shown in Figure 10. Applying the preceding equations, (3.11) and (3.13), to the conditions in this figure, one finds that with $D_1 = D_2$:

$$\frac{Q_1}{Q_2} = \frac{n_1}{n_2} \text{ and } \frac{H_1}{H_2} = \frac{n_1^2}{n_2^2} \tag{3.14}$$

The validity of the similarity relations leading to Equations (3.11), (3.13), and (3.14) can be proven by plotting the head versus capacity characteristics in dimensionless form. This was done in Figure 11 for an axial-flow pump. The inlet pressure was kept sufficiently high to avoid any appreciable cavitation, and the impeller diameter was 15 in. Thus, with water as the test fluid, there were no appreciable effects of viscosity. It is evident from Figure 11 that under these conditions, the similarity relations expressed by Equations (3.11), (3.12), and (3.13) hold within the rather high accuracy of the tests performed.

It should be evident from Equations (3.11) and (3.13) that under similar flow conditions, similar pumps of different sizes $D$ and operating at different speeds of rotation $n$ cover a very wide–indeed infinite–range of actual operating conditions. It is thus reasonable to ask which range of operating conditions $n$, $Q$, and $H$ can be covered by geometrically similar pumps of different sizes operating at different speeds or rotation. This question can be answered by eliminating from Equations (3.11) and (3.13) the linear dimension $D$. This gives a similarity relation of the operating conditions $n$, $Q$, and $H$ which is independent of the absolute dimensions $D$ of the machine. Evidently

$$\left(\frac{Q}{n D^3}\right) : \left(\frac{g_0 H}{n^2 D^2}\right)^{3/2} = \frac{n^2 Q}{(g_0 H)^{3/2}} = \text{constant}$$

It is customary (for no particular reason) to use the one-half power of this expression although any other power would serve as well. The one-half power is called the "(basic) specific speed" of the machine:

$$n_s = \frac{n Q^{1/2}}{(g_0 H)^{3/4}} \tag{3.15}$$

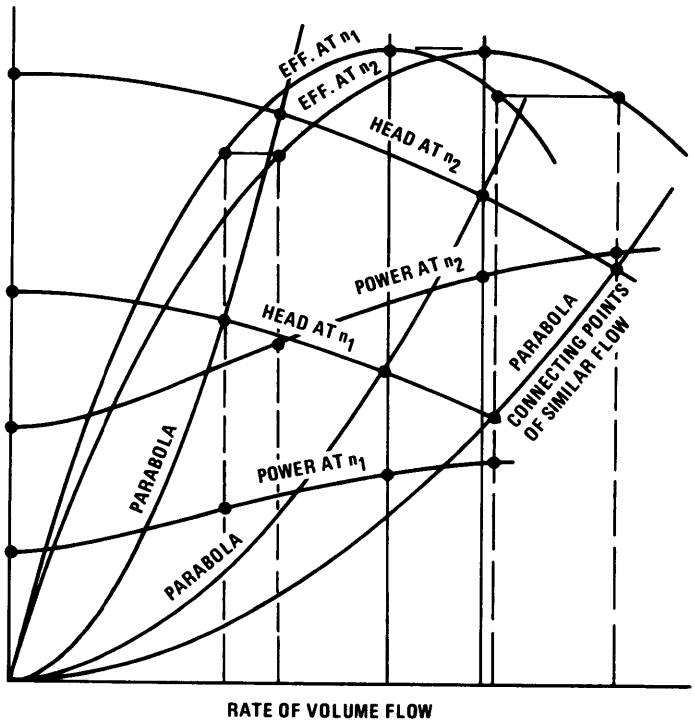


Figure 10 – Characteristic Curves of a Centrifugal Pump at Two Different Speeds of Rotation $n_1$ and $n_2$

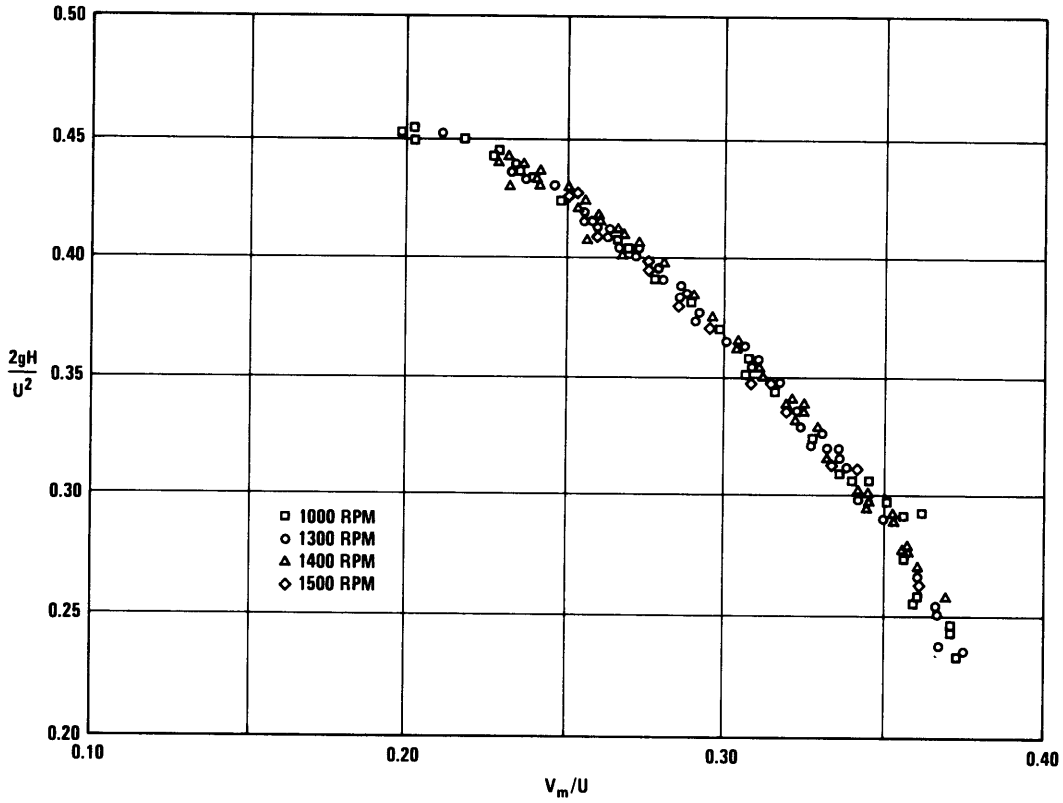


Figure 11 – Dimensionless Head-Capacity Curve of an Axial-Flow Pump

It can be defined by the statement that *any constant value of the specific speed describes that combination of operating conditions n, Q, and H which can be satisfied by similar flow conditions in geometrically similar machines* as far as their waterways are concerned.

It may, or may not, be evident, from the above definition of the specific speed but it is nevertheless true that the specific speed must be related to certain design and form characteristic of the machine concerned. By using the dimensions defined by Figure 12 and the obvious relations

$$Q = V_{m_i} \frac{D_i^2 \pi}{4} \left(1 - \frac{D_h^2}{D_i^2}\right) \quad \text{and} \quad U_0 = \pi D_0 n$$

it is easy to find

$$n_s = \frac{n\, Q^{1/2}}{(g_0 H)^{3/4}} = \frac{1}{2^{1/4}\, \pi^{1/2}} \left[\frac{U_0^2}{2 g_0 H}\right]^{3/4} \left[\frac{V_{m_i}}{U_i}\right]^{1/2} \left[\frac{D_i}{D_0}\right]^{3/2} \left[1 - \frac{D_h^2}{D_i^2}\right]^{1/2} \tag{3.16}$$

*For axial-flow machines*, obviously $D_i = D_0$ and $U_i = U_0$. Thus:

$$n_s = \frac{n\, Q^{1/2}}{(g_0 H)^{3/4}} = \frac{1}{2^{1/4}\, \pi^{1/2}} \left[\frac{U_0^2}{2 g_0 H}\right]^{3/4} \left[\frac{V_{m_i}}{U_0}\right]^{1/2} \left[1 - \frac{D_h^2}{D_i^2}\right]^{1/2} \tag{3.17}$$

There are other relations that can be established between the form of the machine and the specific speed.

Any relation between the specific speed and the design of centrifugal and axial-flow pumps as expressed by Equations (3.16) and (3.17) is obviously meaningful only if the specific speed is calculated for a point at or near the point of best efficiency (see Figure 10) which should be the design point of the machine.

Figure 13 shows a series of single-stage centrifugal and axial-flow pump impellers of different specific speeds derived from Equation (3.16) under the assumption that $V_{m_i}/U_i$ = constant and $U_{0_{min}}^2/2g_0H$ = constant. Evidently $U_0^2/2g_0H = (U_{0_{min}}^2/2g_0H) \times (D_0/D_{0_{min}})^2$. Figure 14 shows impeller profiles derived under the same assumptions for axial-flow runners by using Equation (3.17). (The values for $n_{s1}$ and $n_{s4}$ were calculated with the root head coefficient $2g_0H/U_h^2 = 1$ and 4, respectively; the second value applies mainly to turbines.) Evidently a design choice has to be made between radial and axial-flow machines inasmuch as the design forms shown in Figures 13 and 14 cover somewhat the same range of specific speeds.

It is thus evident that the entire field of centrifugal and axial-flow pumps can be represented as (probably) a multivalued function of the specific speed. The specific speed can be calculated before anything is known about the design of the machine concerned, thus locating the design problem within a vast field of

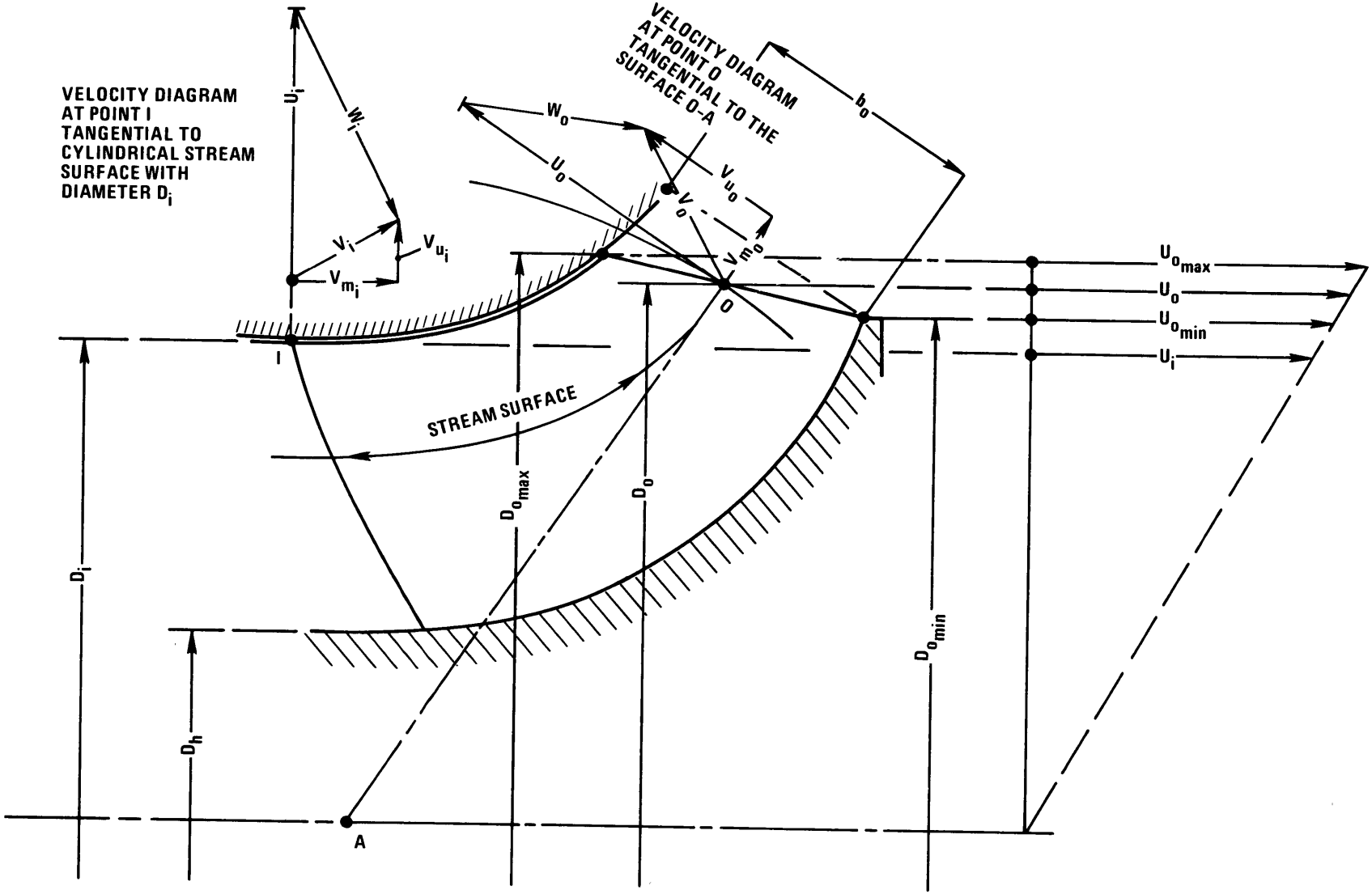


Figure 12 – Mixed Flow Runner Profile and Defining Notations

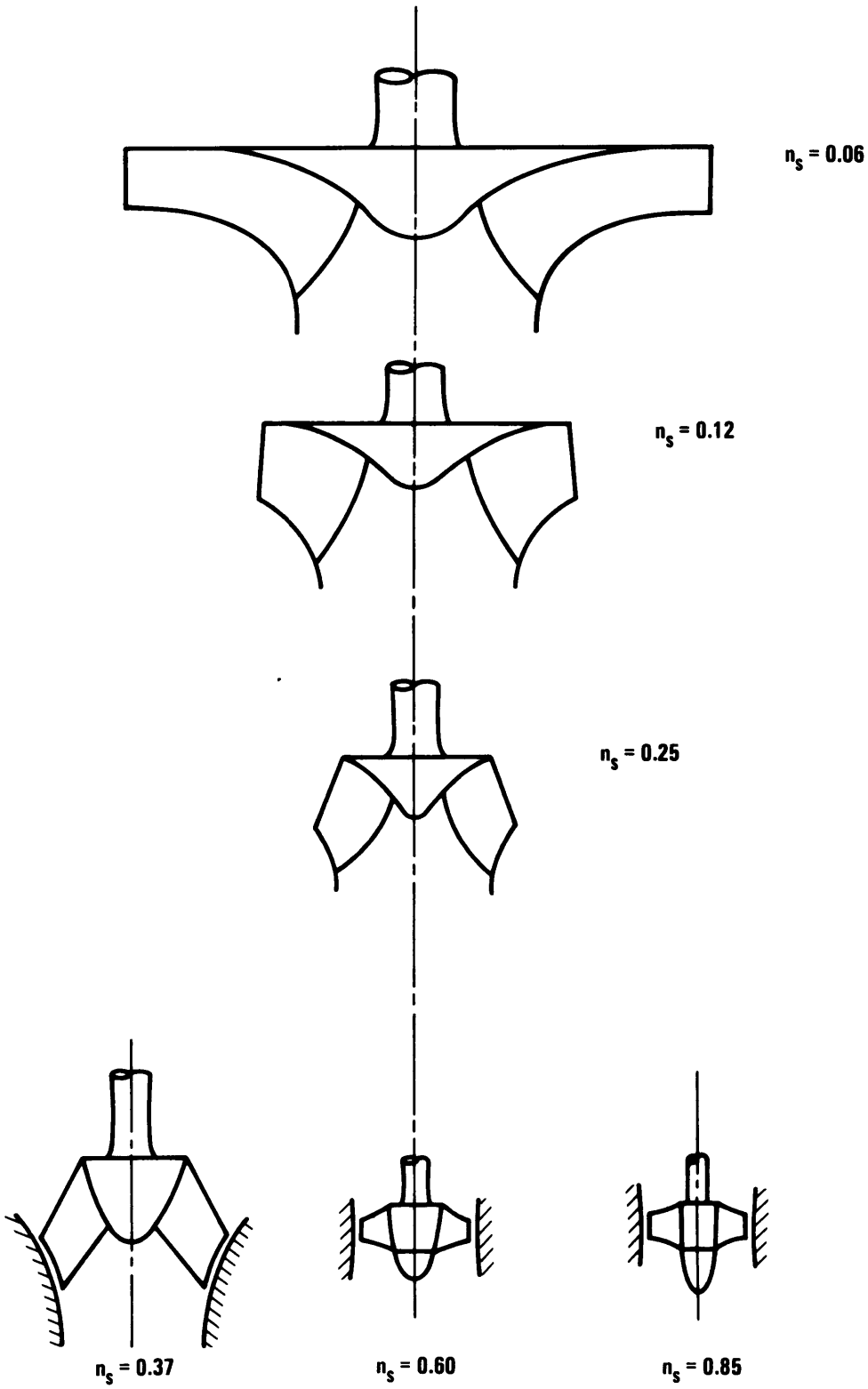


Figure 13 – Pump Impeller Profiles as a Function of the Basic Specific Speed

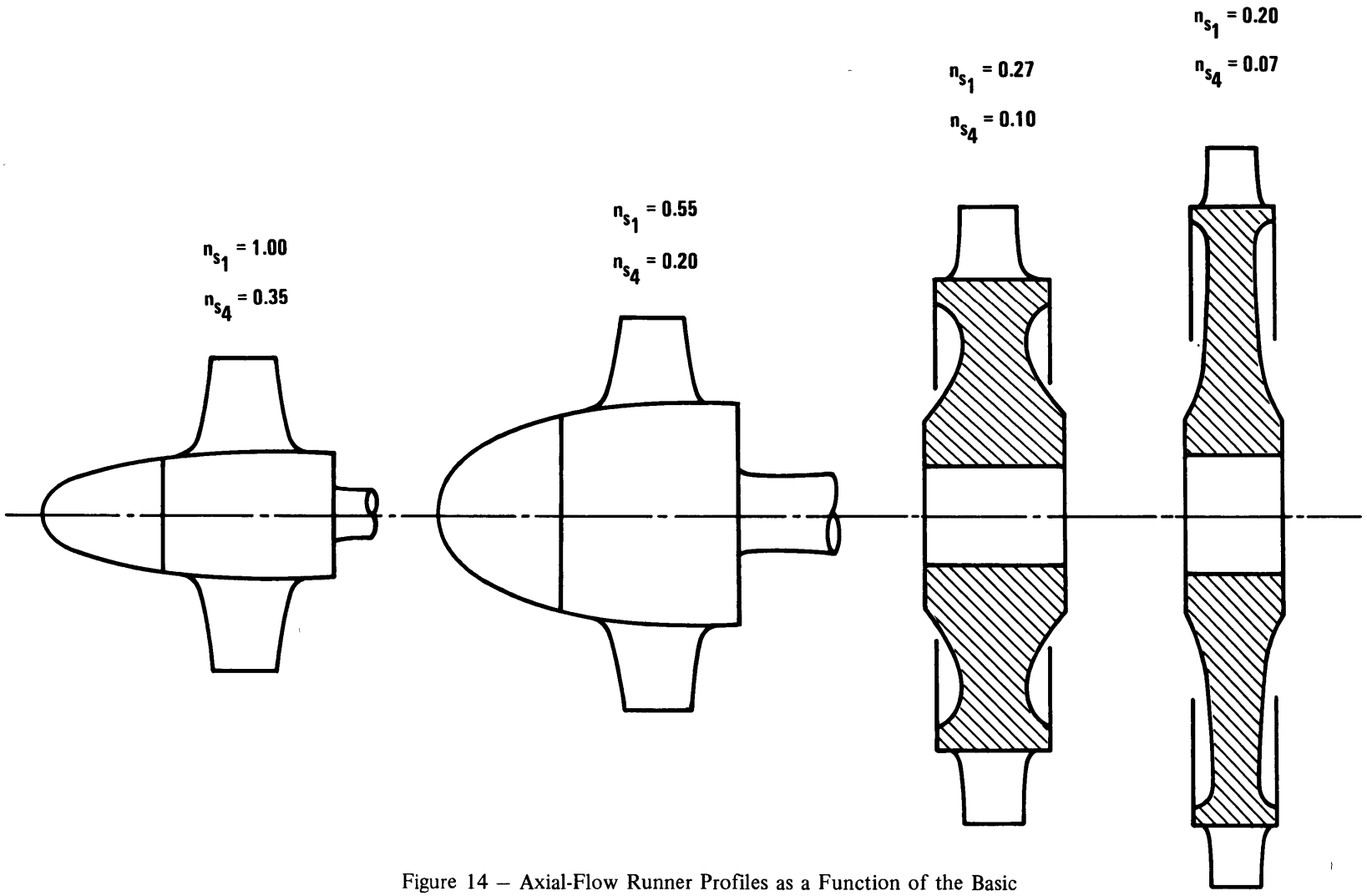


Figure 14 – Axial-Flow Runner Profiles as a Function of the Basic Specific Speed

($\eta_{s_1}$ for $2g_0H/U_h^3 = 1$, $\eta_{s_4}$ for $2g_0H/U_h^2 = 4$)

design possibilities. For example, if the specific speed should be very much lower than the lowest value indicated in Figure 13, then the use of several stages in series might be indicated so that the head per stage is reduced by dividing by the number of stages. Thus the specific speed of each stage is increased by the 3/4 power of the number of stages, thereby avoiding the loss in efficiency connected with very low specific speeds per stage.

The upper limits of the specific speed are more stringent. It is evident from Figures 13 and 14 that the size of a pump (and thereby the weight and cost of a pump and of its driver) decreases rapidly with increasing specific speed. It can be shown by some simple similarity considerations that the weight of a torque-producing, torque-demanding, or torque-transmitting machine is roughly proportional to the torque. The torque is, of course, inversely proportional to the speed of rotation. Thus doubling the specific speed for the same $Q$ and $H$ may be expected to cut in half the weight of the rotating machinery operating at that speed. Therefore there is a very strong incentive to always select the highest specific speed possible under given circumstances. The upper limits of the specific speed are therefore of great practical importance. Before turning to this question, it is necessary to consider briefly the units of the variables used in the specific speed.

It should be evident that the expressions for specific speed, $(nQ^{1/2}/(g_0H)^{3/4})$, flow coefficient $(Q/nD^3)$, and head coefficient $(g_0H/n^2D^2$ or $g_0HD^4/Q^2)$ are dimensionless. The dimensionless form of these expressions are used in this report to make it more universal and to avoid possible confusion with those that use other systems of units. If the same units of force, length, and time are used in all of the factors of these dimensionless ratios, they will have the same value regardless of which system of units is chosen (i.e., metric or English system).

Unfortunately, in the United States, it is not customary to use the dimensionless expression for specific speed. Rather it has been customary to express the rotational speed $n$ in revolutions per minute (rpm), flow rate $Q$ in gallons per minute (gpm), and head $H$ in feet and to completely omit the acceleration of gravity $(g_0)$. The relationship between the dimensionless form of specific speed and the form customarily used in the United States is given below:

$$\frac{\text{Specific Speed (U.S. Practice)}}{\text{Specific Speed (Dimensionless)}} = 17170 \quad \frac{(\text{gallons})^{1/2}}{(\text{minutes})^{3/2}\,(\text{feet})^{3/4}} \tag{3.18}$$

In this report, the dimensionless form of specific speed will be used. In some cases the corresponding dimensional value (U.S. practice) is given in parentheses.

It may be of interest that the maximum specific speed of propeller pumps is about unity in the dimensionless form used here (Equation (3.15)). Other values of the dimensionless specific speed are given in Figures 13 and 14; the dimensional values of $n_s$ are indicated in parentheses. Pump efficiencies begin to fall off below $n_s = 0.1$ and loss about 8 percent in efficiency (compared with specific speeds above 0.1) at $n_s = 0.05$.

### 3.1.2 Upper Limits of the Specific Speed Set by Cavitation

There are various reasons for an upper limit in the specific speed, e.g., stresses in the solid parts of the machine or speed limits of the driver. By far the most important reason for such limits, however, is cavitation.

Cavitation is the vaporization of the flowing liquid under the influence of local pressure reductions caused by the dynamic action of the liquid. It must be clearly distinguished from the damaging effects of cavitation on the solid walls, which should be called "cavitation damage."

Whenever cavitation takes place inside the machine, vapor pressure is present at that particular location in the machine. The difference between the total head on the suction side of the machine and the vapor pressure expressed as a head value ($h_v$) is therefore a head difference existing in the machine. It follows the same laws as any other head difference in the machine, in particular the same laws as the head $H$ of the machine. This *total suction head above the vapor pressure*, also called "net positive suction head" (NPSH), will be designated by the symbol $H_{sv}$.

The oldest and most simple way to make $H_{sv}$ dimensionless is to divide it by the total head $H$ of the machine. The resulting ratio is called the "Thoma parameter:"

$$\sigma_H = \frac{H_{sv}}{H} \tag{3.19}$$

Obviously it should be constant for similar flow and cavitation conditions in similar machines. Like $H_{sv}$ (or NPSH), it has a definite physical meaning only if vapor pressure (i.e., cavitation) is present somewhere in the machine.

The existence of cavitation can be established in various ways. The best, but perhaps most difficult, way is by visual observation. Visual observation is difficult because it requires a special test machine or test setup. It is best because it locates the point of cavitation and is accurate relative to the first onset or "inception" of cavitation. If by such observation a certain "critical" value of $H_{sv}$—and thereby of $\sigma_H$—has been established (for example, the value at cavitation inception), then the value may be expected to follow the same laws as the pump head $H$. Such a critical value of $\sigma_H$ should therefore be constant under similar flow conditions in similar machines (i.e., for $Q/nD^3$ = constant) irrespective of the absolute speed $n$ or absolute size $D$ of the machine.

The existence of cavitation can also be established by observing the effect of cavitation on the operation of the machine. Acoustic observations are accurate relative to the inception of cavitation, but they require special apparatus and experience. The most commonly used method is to measure the hydrodynamic performance of the machine as a function of $H_{sv}$ or of $\sigma_H$. If the head or power or efficiency changes at constant speed, constant capacity, and diminishing $H_{sv}$, the reason can only be cavitation since the absolute pressure level can affect the performance only by cavitation so long as the fluid is practically incompressible.

It is customary to specify the percentage by which the head or efficiency is allowed to change before the corresponding $H_{sv}$ or $\sigma_H$ value is considered "critical" with respect to cavitation. The percentage change specified for head or efficiency ranges from about 0.3 percent for rather exacting conditions to 1 percent or even more (the Hydraulic Institute standards suggest 3 percent). However, even the lowest percentage change that can be reliably measured does not mean that there is really no cavitation at slightly higher values of $H_{sv}$ than the critical value so determined. Thus if an absolute absence of cavitation is required, it is necessary to refer to a more exacting method for determining the presence or absence of cavitation, e.g., the visual method of observation already mentioned. The avoidance of cavitation damage at very high velocities of flow involves this problem.

It is apparent that any "critical" value of $H_{sv}$ or $\sigma_H$ must be related to the requirements of no cavitation that apply to the conditions of operation concerned. Commercially valid conditions may not apply to the special conditions of hydrodynamic performance of naval propulsors.

The existence of a "critical" value of $H_{sv}$ or of $\sigma_H$ gives numerical values to $H_{sv}$ or $\sigma_H$. It has been stated that $H_{sv}$ and $\sigma_H$ follow the same laws that apply to the pump head $H$. Thus the similarity relations that apply to $H$ also apply to $H_{sv}$. In particular, there is a "*suction specific speed*"

$$S = \frac{n\,Q^{1/2}}{(g_0 H_{sv})^{3/4}} = \frac{1}{2^{1/4}\pi^{1/2}} \left(\frac{U_0^2}{2g_0 H_{sv}}\right)^{3/4} \left(\frac{D_i}{D_0}\right)^{3/2} \left(\frac{V_{m_i}}{U_i}\right)^{1/2} \left(1 - \frac{D_h^2}{D_i^2}\right)^{1/2} \tag{3.20}$$

This expression may not be as useful for predicting cavitation as the corresponding expression for the basic specific speed $n_s$. It is known that the suction specific speed is particularly concerned with the low-pressure side of the runner. It is therefore more useful to write the suction specific speed in the form

$$S = \frac{n\,Q^{1/2}}{(g_0 H_{sv})^{3/4}} = \frac{1}{2^{1/4}\pi^{1/2}} \left(\frac{V_i^2}{2g_0 H_{sv}}\right)^{3/4} \left(\frac{V_{m_i}}{V_i}\right)^{3/2} \left(\frac{U_i}{V_{m_i}}\right)\left(1 - \frac{D_h^2}{D_i^2}\right) \tag{3.21}$$

Evidently this can be simplified to the form

$$S = \frac{n\,Q^{1/2}}{(g_0 H_{sv})^{3/4}} = \frac{1}{2^{1/4}\pi^{1/2}} \left[\frac{V_{m_i}^2}{2g_0 H_{sv}}\right]^{3/4} \left(\frac{U_i}{V_{m_i}}\right)\left(1 - \frac{D_h^2}{D_i^2}\right)^{1/2} \tag{3.22}$$

Another very useful form of the suction specific speed is:

$$S = \frac{1}{2^{1/4}\pi^{1/2}} \cdot \left[\frac{w_i^2}{2g_0 H_{sv}}\right]^{3/4} \frac{(V_{m_i}/U_i)^{1/2}}{\left[1 - 2\frac{V_{u_i}}{U_i} + \frac{V_{u_i}^2}{U_i^2} + \frac{V_{m_i}^2}{U_i^2}\right]^{3/4}} \left(1 - \frac{D_h^2}{D_i^2}\right)^{1/2} \tag{3.23}$$

Equations (3.20), (3.22), and (3.23) are evaluated in Figure 15 for $V_{u_i} = 0$ (zero "prerotation").

Equation (3.23) is derived from Equation (3.22) by means of the relation

$$H_{sv} = C_1 \frac{V_i^2}{2g_0} + \sigma_p \frac{w_i^2}{2g_0} \tag{3.24}$$

where $C_1$ is a constant (slightly greater than 1.0) used to account for nonuniformities in the "absolute" inlet velocity and $w_i$ is the relative velocity at the inlet.

Here $\sigma_p$ is introduced as the cavitation parameter of any object exposed to the velocity $w_i$:

$$\sigma_p = \frac{p_i - p_v}{\frac{\rho w_i^2}{2}} \tag{3.25}$$

It describes the pressure drop below the inlet static pressure $p_i$ due to the flow at the velocity $w_i$. Figure 16 illustrates this situation. It is practically impossible to operate free from cavitation for values of $\sigma_p$ below about 0.20 because the range of the angles of attack that permit cavitation-free operation is one-half a degree (or less), i.e., so small that it is practically useless. Furthermore the precision of vane shape required is so great as to be practically unachievable. Finally, available design theories are not sufficient to predict the flow within such a degree of accuracy. Considering commercial design and manufacturing practices, it is doubtful whether truly cavitation-free operation can be achieved at $\sigma_p$ values less than about 0.4. According to Figure 15, this leads to a maximum suction specific speed of about 0.40, or 7000 $gal^{1/2}/min^{3/2}$ $ft^{3/4}$ in dimensional form, assuming the most favorable case of zero hub diameter ($D_h/D_i = 0$). Even $\sigma_p = 0.4$ is very optimistic and demands the very best manufacturing and design techniques available. Truly cavitation-free operation is not required commercially, but it may be required at high fluid velocities for prolonged times because of cavitation damage.

The effect of *surface roughness* on local cavitation may be as important as that of accuracy of shape and angle of attack. Figure 17 gives results by Holl regarding the cavitation number $\sigma_0$ of a sharp-edged roughness as a function of the height of the roughness $h$ divided by the local boundary layer thickness $\delta$. In the Holl investigation, the roughness was placed on a flat plate with a cavitation number of zero. It is seen

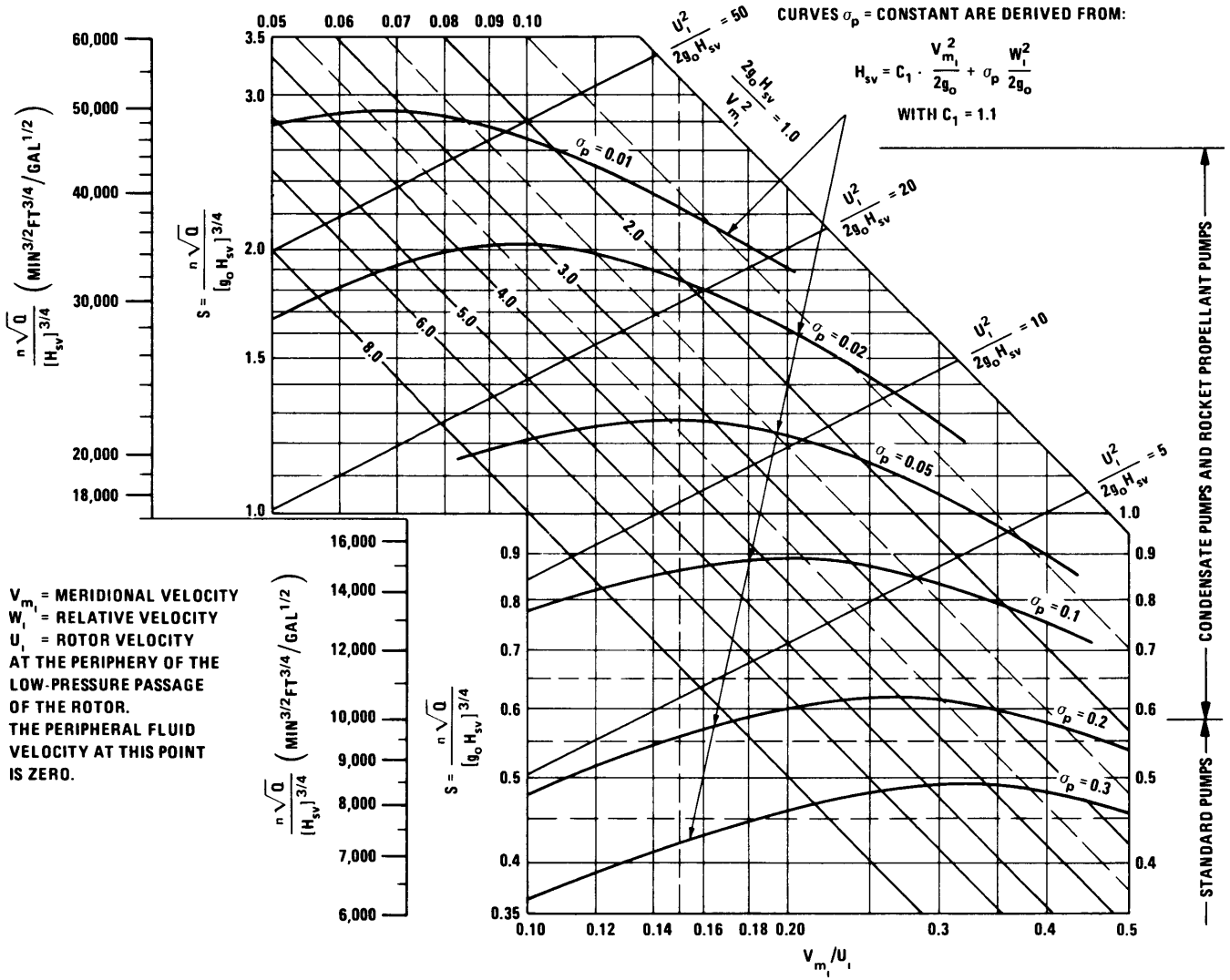


Figure 15 – Relation between Cavitation Parameters of Turbomachinery

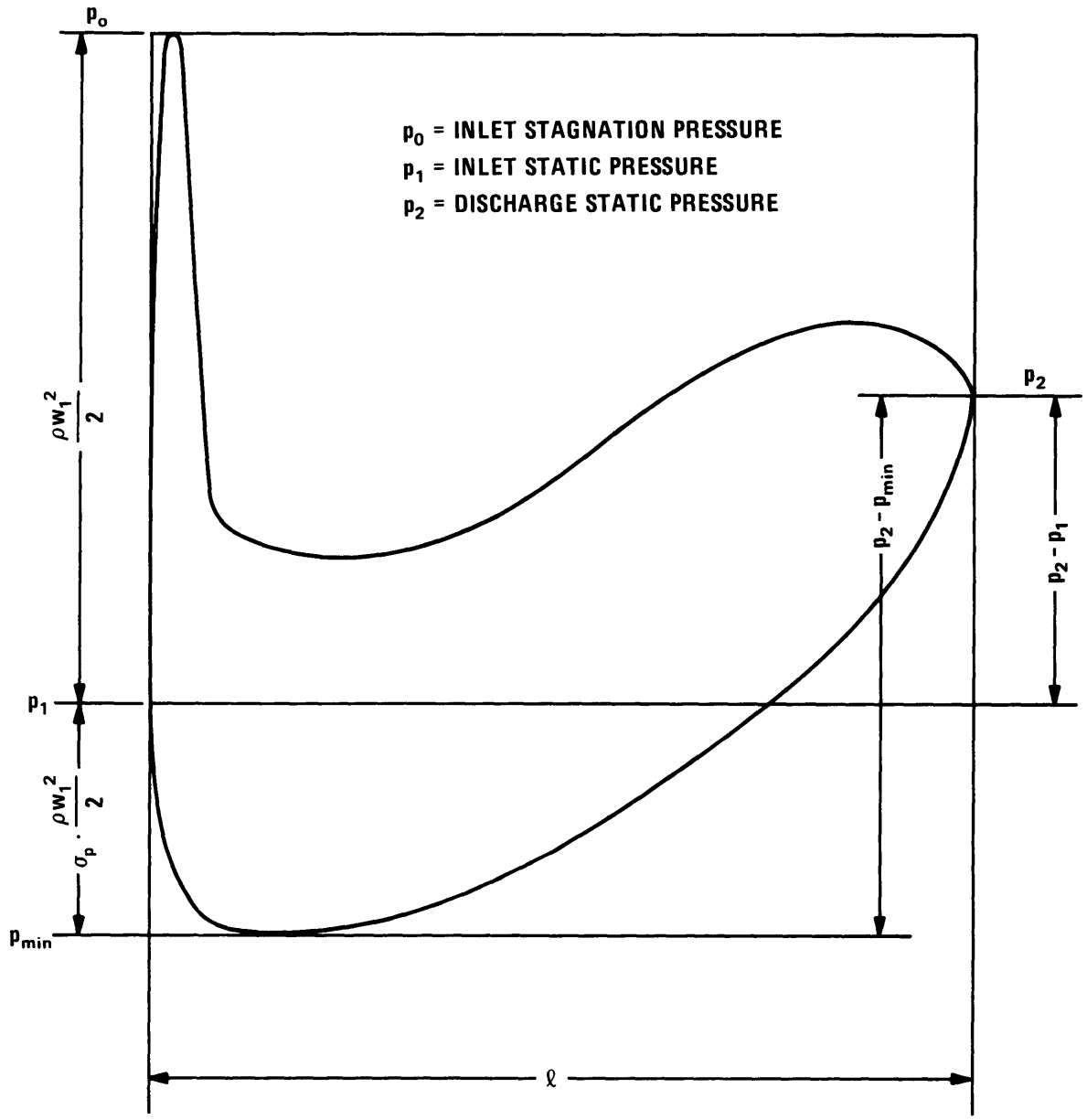


Figure 16 – Typical Vane Pressure Distribution of a Pump Vane System
(Axial Flow)

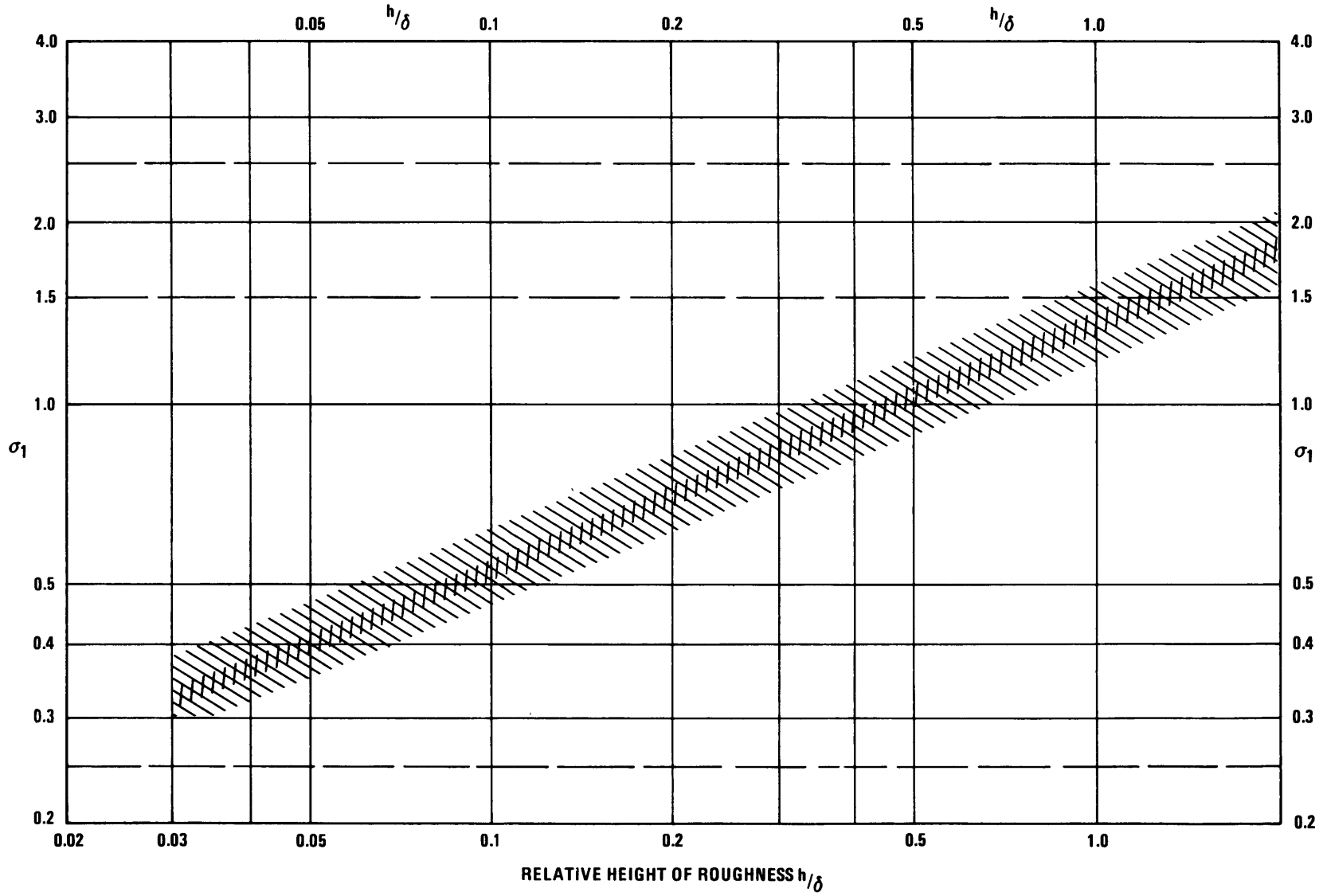


Figure 17 – Approximate Cavitation Numbers of Sharp-Edged Surface Irregularities

that a roughness only one-twentieth as high as the thickness of the local boundary layer can have a cavitation number $\sigma_0 = 0.40$. If such a roughness is placed on a curved contour at a place where its pressure reduction is $p - p_{min} = C_p \rho V^2/2$ without any roughness, then the resulting cavitation number of the curved contour with roughness (referred to free-stream conditions) is:

$$\sigma_R = C_p + (1 + C_p) \sigma_0 \tag{3.26}$$

For example, if the smooth contour pressure coefficient were $C_p = 0.3$ and the cavitation number of the roughness alone were $\sigma_0 = 0.4$, then the curved contour with roughness would have a cavitation number $\sigma_R = 0.3 + 1.3 \times 0.4 = 0.82$, i.e., 2.7 times that of the contour without roughness. Since the boundary layer thickness $\delta$ near the leading edge of a vane may be quite small, even a very small roughness can have such an effect.

The most important conclusion is that truly cavitation-free operation requires the use of very conservative suction specific speeds, say, lower than 0.4 (or 7000 $gal^{1/2}/min^{3/2}$ $ft^{3/4}$ in dimensional form), i.e., considerably lower than the commercial standards of the Hydraulic Institute. Of course truly cavitation-free operation is not always required. The most important case where it *is* required is operation at very high absolute fluid velocities (substantially higher than in commercial practice) since *cavitation damage* is known to increase very rapidly with the velocity of flow. It has been estimated to increase as fast or faster than the sixth power of the velocity of flow. An increase in this velocity by a factor of only 1.5 (for example) will increase the rate of cavitation damage by a factor of more than ten. Thus even a small amount of cavitation (acceptable at lower velocities) may lead to intolerable cavitation damage at increased velocities.

The situation is quite different at either very low fluid velocities, for example, as used with commercial condensate pumps, or for very short operation with cavitation, as in the case of pumps for liquid rockets. In such cases suction specific speeds as high as 2 (34,000 $gal^{1/2}/min^{3/2}$ $ft^{3/4}$ in dimensional form) can be used reliably, provided very special designs are used at the inlet to the first stage ("inducers"). Figure 15 shows that very low flow coefficients $V_{m_i}/U_i$ are essential at very high suction specific speeds. With these go very low cavitation parameters $\sigma_p$, indicating clearly that cavitation-free operation is not expected. To achieve such low $\sigma_p$ values without a complete breakdown of operation, it is necessary to use very thin and sharp leading vane edges, very slight curvature of the leading portions of the vanes, and yet somewhat larger cross-sectional areas between the vanes (at the inlet) than prescribed by the condition of continuity with respect to the relative velocity of the flow approaching the vane system. This inducer design practice differs substantially from that for pumps with more conservative suction specific speeds and involves certain sacrifices in efficiency. *It may prevent truly cavitation-free operation even at very low suction specific speeds.* This problem will be discussed further in Section 3.3 because it is of particular importance for propulsion pumps.

A few words are necessary with respect to the operation of several pumps in parallel, in particular the effect of the widely used "double-suction" arrangement on the cavitation performance of the unit (see Figure 18).

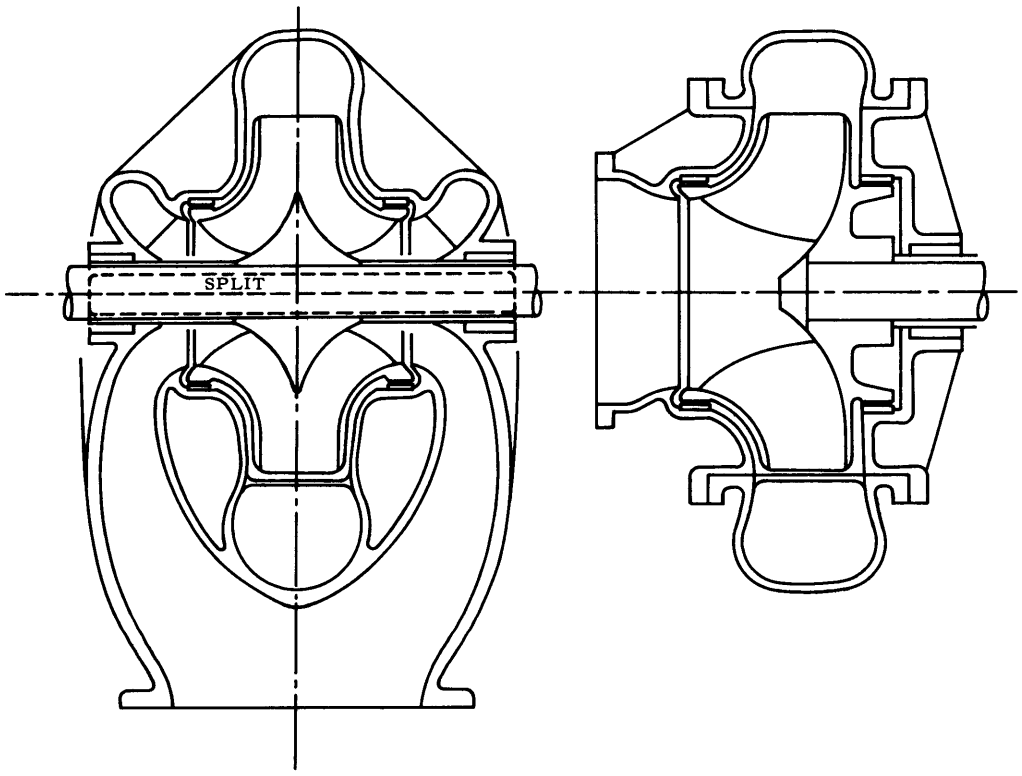


Figure 18 – Comparison of a Single-Suction, Horizontally Split Pump and a Single-Suction, Vertically Split Pump

So far as its cavitation performance is concerned, a double-suction pump should be regarded as two single-suction centrifugal pumps arranged back-to-back on the same shaft. Equations (3.20) through (3.23) as well as Figure 15 (derived therefrom) apply to single-suction pumps and therefore to each half of a double-suction pump. However, there is no reason why the suction specific speed as given by the left sides of these equations

$$S = \frac{n\, Q^{1/2}}{(g_0 H_{sv})^{3/4}} \tag{3.27}$$

cannot be applied to an entire double-suction pump. If so, this suction specific speed will be higher by a factor of $\sqrt{2}$ than the suction specific speed calculated according to Figure 15 for only one side of a double-suction pump. Similarly, if $N$ single-suction pumps are operated *in parallel*, the suction specific speed of the aggregate of the $N$ pumps would be $\sqrt{N}$ times higher than the suction specific speed of each individual impeller inlet. This possibility will be discussed further in connection with propulsion pumps.

Finally, attention must be paid to the physical limitations of similarity consideration on cavitation on which this entire Section 3.1.2 has been based. These similarity relations are based on the "classical assumption" that cavitation takes place *instantaneously* whenever and wherever the equilibrium vapor pressure corresponding to the bulk temperature of the liquid is reached. Since the classical assumption is by no means self-evident, it is really amazing how well the similarity considerations based on it are usually satisfied. Vaporization must be explained physically by the presence of certain weak spots in the liquid, called "nuclei," and the universal availability of such nuclei is not generally assured. Furthermore the gas content of the liquid must be expected to have an effect on the inception of vaporization. Indeed, careful laboratory experiments have shown departures from the classical assumption, but such departures are relatively rare in practical pump operation. Certain departures from the similarity relations based on the classical assumption have recently been observed and are probably explainable by the gas content of the liquid. Control of the gas content of the test liquid in relation to the liquid encountered in the field would be highly desirable, e.g., the partial pressure of the gas could be treated like any other pressure in the system. However, some other departures from the classical assumption cannot be ruled out. The effect of surface roughness has already been mentioned; in comparisons of model test results with prototype performance, the similarity of such roughness is certainly important within the limits of practical feasibility.

### 3.1.3 Principles of the Design Process for Hydrodynamic Pumps

On the basis of Sections 3.1.1 and 3.1.2, the design process for hydrodynamic pumps may be outlined as follows:

1. In any event, the rate of volume flow $Q$, the total pump head $H$, and the total suction (inlet) head above the vapor pressure $H_{sv}$ or NPSH are given.

If the speed of rotation $n$ is also given, calculate the basic specific speed ($n_s = nQ^{1/2}/(g_0H)^{3/4}$) and the suction specific speed ($S = nQ^{1/2}/(g_0H_{sv})^{3/4}$).

If the speed of rotation $n$ is *not* given, assume the value of the *suction* specific speed according to the general operating requirements of the unit and from it determine the speed of rotation $n$. This also determines the *basic* specific speed.

Commercial limits of the suction specific speed ($S = 0.5 = 8000$ gal$^{1/2}$/min$^{3/2}$ ft$^{3/4}$ in dimensional form) permit prolonged operation at commercially customary fluid velocities.

Lower limits than $S = 0.5$ are required for prolonged operation at velocities that are substantially higher than commercially customary fluid velocities.

Substantially higher limits of $S$, say, $S = 2$ (34,400 gal$^{1/2}$/min$^{3/2}$ ft$^{3/4}$) are permissible if operation under these conditions is required only for short duration (comparable to rocket pump operation) or if the relative fluid velocities in the pump are quite low.

2. An additional limitation of the speed of rotation (or fluid velocity) is set by the mechanical stresses in the machine. It can be expressed by the "stress specific speed:"

$$n_\sigma = \frac{n\,Q^{1/2}}{(\sigma/\rho)^{3/4}} = \frac{1}{2^{1/4}\,\pi^{1/2}} \left[\frac{\rho U^2}{2\sigma}\right]^{3/4} \left[\frac{D_i}{D_0}\right]^{3/2} \left(\frac{V_{m_i}}{U_i}\right)^{1/2} \left(1 - \frac{D_h^2}{D_i^2}\right)^{1/2} \tag{3.28}$$

The centrifugal-stress coefficient $\rho_s U_0^2/2\,\sigma_c$ may be as high as 4 for machines with radial blade elements and a mechanically very favorable hub construction and hub-to-tip diameter ratio. For centrifugal pumps of medium specific speeds and backward-bent vanes, the upper limit of $\rho_s U_0^2/2\,\sigma_c$ lies between 1 and 2.

3. With the suction specific speed and basic specific speed determined according to the foregoing (Items 1 and 2, certain *design choices* must be made. The basic specific speed suggests the choice between radial-flow, mixed-flow, and axial-flow pumps for single-stage pumps. However, a choice of the number of stages must be made, particularly in the domain of low basic specific speeds. Below $n_s = 0.1$ (1720 gal$^{1/2}$/min$^{3/2}$ ft$^{3/4}$), increasing sacrifices in efficiency are unavoidable for single-stage units. Multistage units avoid this because the resulting reduction in the head per stage leads to an increased basic specific speed per stage. A related choice must be made, for example, between a single-stage, radial-flow pump and a multistage, axial-flow pump with about the same outside runner diameter as the inlet diameter $D_i$ of the radial-flow unit (see Figure 19). The radial-flow pump has fewer vanes and larger waterway; this is particularly advantageous for small units but might involve the danger of pulsations of the discharge pressure. Axial-flow pumps have a much simpler and stronger casing, but their useful operating (capacity) *range* is narrower at constant speed of rotation.

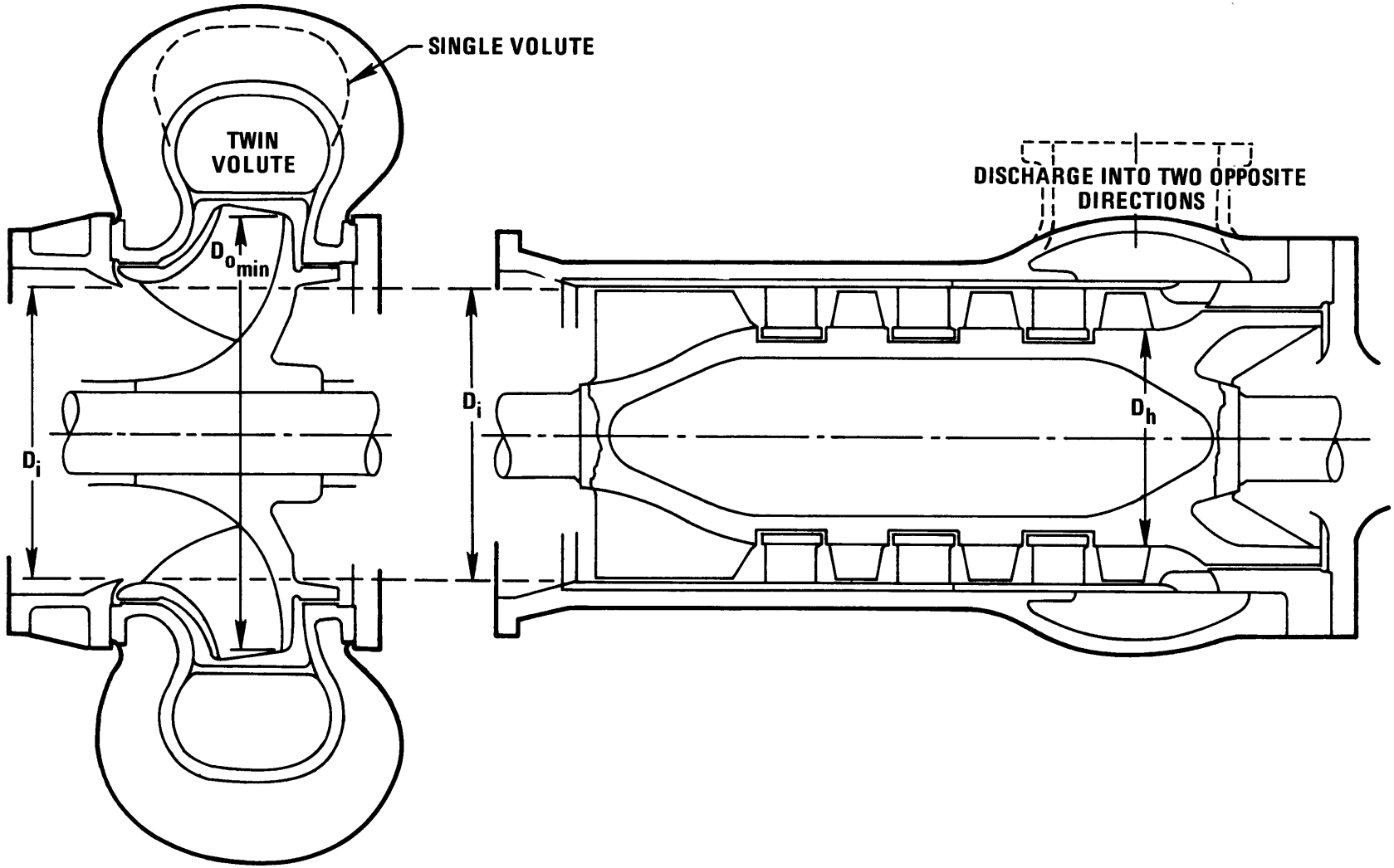


Figure 19 – Comparison of a Single-Stage Radial-Flow Pump and a Multistage, Axial-Flow Pump

Furthermore, a design choice must be made between single- and double-suction pumps as shown in Figure 18. Single-suction pumps are simpler, but double-suction pumps have a higher suction specific speed (and thereby a higher speed of rotation) referred to the *total* capacity. The same choise also applies to (more than two) pumps *in parallel* (see Section 3.5).

Finally, a choice has to be made between the "horizontally split" and "vertically split" casing design (outlined in the chapter on centrifugal pumps in Marks' Mechanical Engineers Handbook). However, this choice involves mechanical construction rather than overall arrangement and hydrodynamic design.

4. With the basic specific speed and suction specific speed *per stage* and *per parallel stream* determined according to Items 1, 2, and 3, Equations (3.16), (3.17), and (3.20) through (3.23) determine the most essential design variables of the runner, and thereby also those of the waterways next to the runner. A "design choice" must still be made regarding the absolute rotation of the fluid on one side of the runner, usually the low-pressure side. After this choice has been made, the flow coefficient $V_{m_i}/U_i$ and the head coefficient $2g_0H/U_0^2$ determine the velocity vector diagrams at any desired point of the inlet and discharge vane edges of the impeller. It follows from the Euler equation (3.9) that

$$\frac{2g_0H}{U_2^2} = 2\eta_h \left( \frac{V_{u_2}}{U_2} - \frac{V_{u_1}}{U_1} \frac{r_1^2}{r_2^2} \right) \tag{3.29}$$

with the notations defined as in Figure 8. This equation, together with the flow coefficient $V_{m_1}/U_1$, the "prerotation" ratio $V_{u_1}/U_1$, and the condition of continuity in the simplified form $V_{m_2}/V_{m_1} = A_{m_1}/A_{m_2}$, permits the construction of the velocity vector diagrams for any pair of Points C and D in Figure 8.

The velocity vector diagrams, particularly the relative velocities $w_1$ and $w_2$, determine the shape (direction) of the runner vane ends as was outlined in Section 3.1.1. This information and the diameter ratios appearing in the specific speed equations ((3.16), (3.17), and (3.20) through (3.23)) determine the runner shape so far as this elementary outline of turbomachinery theory permits. The completion of the design consists of combining these bits of information into a geometrically and mechanically consistent overall structure.

The stationary vanes or passages adjacent to the runner are determined by the absolute velocities $V_1$ and $V_2$ and by smooth connections between the runner profile and the inlet and discharge openings of the casing or other stages of the machine.

There is only one additional relation to be mentioned, namely, separation or "stall" of the vanes in hydrodynamic pumps. The complete treatment of this subject exceeds any reasonable scope of the present remarks. However, there is a very simple *limitation of the velocity diagrams* in turbomachines resulting from considerations of operation or "stall" which deserves mention. The flow relative to the vane systems is usually *retarded* in pumps (or compressors) because one is concerned with the conversion of kinetic energy into static pressure. The degree of retardation is limited; a practical limit is 0.6 for the ratio of the discharging to the entering relative velocity for rotating systems and for the ratio the discharging to the entering

absolute velocity for stationary systems. This limit is particularly important in the case of pump runners of high suction specific speeds. The low flow coefficient required at the runner inlet (see Section 3.1.2 and Figure 15) leads to a rather high inlet relative velocity since a low $V_{m_i}$ requires a relatively large inlet diameter. For a given discharge velocity diagram, a high inlet relative velocity can easily lead to unacceptable retardation of the relative flow. Figure 20 illustrates the effect of this consideration on the profiles of single-suction pump runners; the profiles shown to the left are similar to those given in Figure 13. If the profiles shown for a moderate suction specific speed are assumed to be close to an optimum, it should be evident that very high suction specific speeds can easily lead to sacrifices in efficiency.

Even if the retardation ratio $w_2/w_1$ or $V_2/V_1$ is kept above the limit of 0.6, mentioned above, it is still necessary to properly select the vane length-to-spacing ratio ($\ell/t$) in order to avoid overloading the vanes. Cavitation limits of this ratio can be estimated by comparing the average vane pressure difference $\Delta p$ to the total inlet pressure $\rho_f g_0 H_{sv}$. A very crude but simple approximation (applicable primarily to axial-flow pumps) would be

$$H_{sv} \cdot \ell > H \cdot t \text{ or } \frac{H_{sv}}{H} > \frac{t}{\ell} \tag{3.30}$$

This relation is not valid for large overlap and radial-flow runners.

However, the preceding consideration is not concerned with "stall." To safeguard against "stall," the vane *lift coefficient*

$$C_L = 2 \frac{V_{u_2}}{w_\infty} \frac{t_0}{\ell} \left(1 - \frac{r_1}{r_2} \frac{V_{u_1}}{V_{u_2}}\right) \tag{3.31}$$

must not exceed certain limits (see Figure 8 for definition of notations). Here $w_\infty$ is the vectorial mean of the velocity of flow relative to the vanes and $t_0$ is the circumferential vane spacing at the outer periphery.

$C_L$ should not be much larger than 1 for vane systems with retarded flow, whereas it might be approximately 1.5 when flow is not retarded and perhaps as high as 2 with accelerated flow.

For given $C_L$ and velocity vector diagrams, Equation (3.31) permits the calculation of the "solidity of the vane system" $\ell/t_0$.

## 3.2 DETERMINATION OF OPERATING CONDITIONS AND SPECIFIC SPEED FOR A PROPULSION PUMP

The variables to be satisfied by a marine propulsion unit are primarily a certain thrust $T$ and the speed or speeds of travel $V_0$ at which this thrust is to be developed.

The thrust $T$ is that for one propulsion unit, i.e., a propulsor connected with one intake. Evidently

$$T = \rho Q \Delta V \tag{3.32}$$

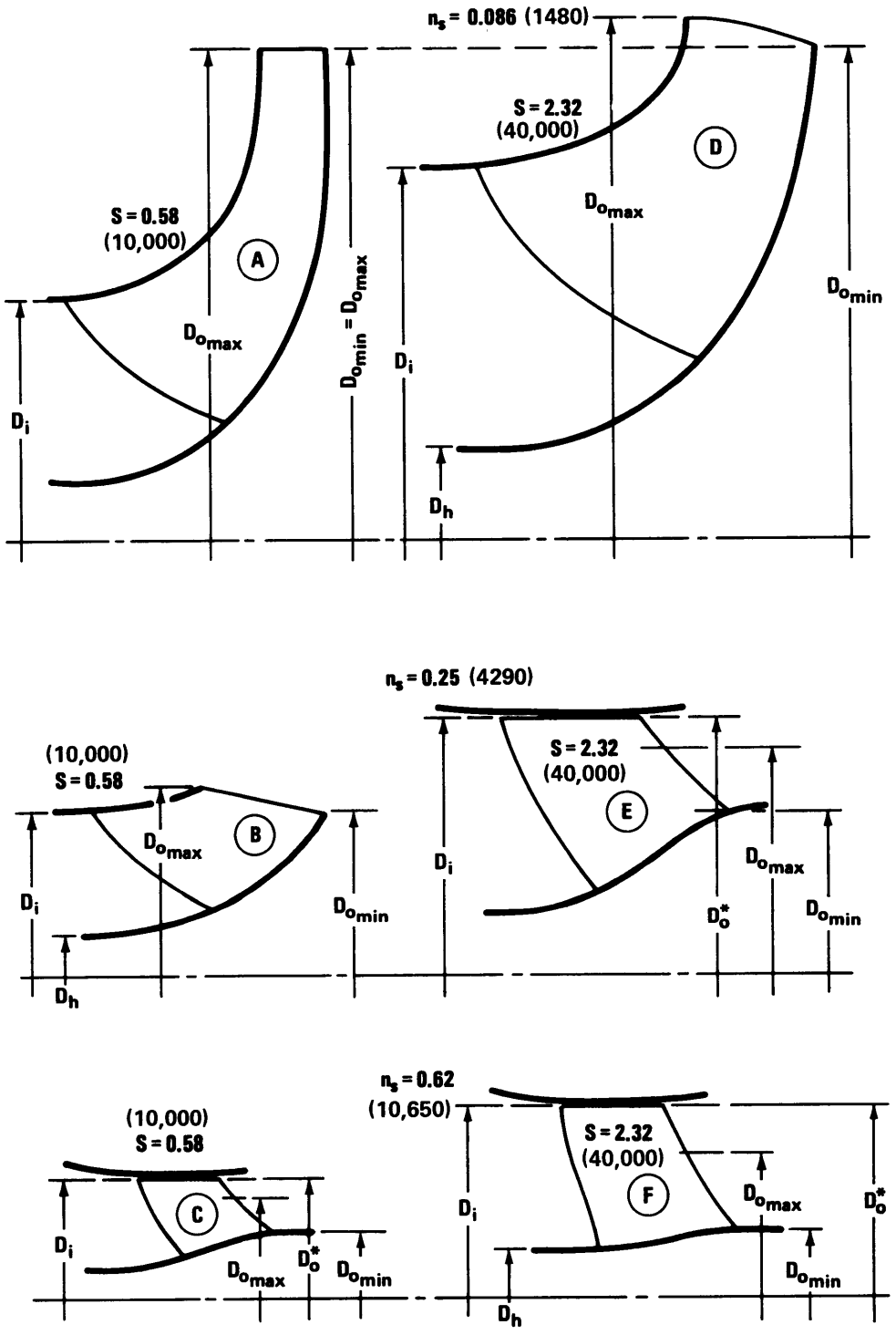


Figure 20 – Runner Profiles as Functions of $n_s$ and $S$

where $\Delta V$ is the velocity increase through the unit, i.e., $\Delta V = V_j - V_0$. Here $V_0$ is the *relative approach velocity of flow*, corresponding to velocity of travel, and $V_j$ is the jet velocity relative to the craft. ($V_j$ and $V_0$ are assumed to have the same direction relative to the craft.)

The rate of volume flow $Q$ is given directly by Equation (3.32), assuming that $\Delta V/V_0$ is given by considerations of propulsive efficiency presented in Chapter 2.

The required pump head is

$$H = \frac{V_j^2 - V_0^2}{2g_0} + K \frac{V_0^2}{2g_0} + \Delta h_j \tag{3.33}$$

where $K$ is the inlet and duct-loss coefficient introduced in Chapter 2. $\Delta h_j$ is the elevation of the propelling jet above the free water surface. It is zero for any submergence of the jet below the free water surface.

With $V_j = V_0 + \Delta V$ and $V_j^2 = V_0^2 + 2V_0\Delta V + \Delta V^2$, Equation (3.33) assumes the form:

$$H = \frac{V_0^2}{2g_0}\left[2\frac{\Delta V}{V_0} + \frac{\Delta V^2}{V_0^2} + K + \frac{2g_0\,\Delta h_j}{V_0^2}\right] \tag{3.33a}$$

Obviously, $\Delta h_j$ is to be minimized, inasmuch as it constitutes an energy loss.

The total pump *inlet* head above the vapor pressure is

$$H_{sv} = \frac{V_0^2}{2g_0} - K\frac{V_0^2}{2g_0} + (h_a - h_v) - \Delta h_i$$

where $h_a$ is the atmospheric pressure and $h_v$ is the vapor pressure; both are expressed as a "head" in feet of water. $\Delta h_i$ the elevation of the *pump inlet* above the free water surface; it is negative for a pump inlet below the free water surface.

Designating $(h_a - h_v)$ by $h_{sv}$, one may write

$$H_{sv} = (1 - K)\frac{V_0^2}{2g_0} + (h_{sv} - \Delta h_i)$$

$$= \frac{V_0^2}{2g_0}\left[1 - K + \frac{2g_0}{V_0^2}(h_{sv} - \Delta h_i)\right] \tag{3.34}$$

Considering also Equation (3.33a), the Thoma cavitation parameter is:

$$\sigma_H = \frac{H_{sv}}{H} = \frac{1 - K + \dfrac{2g_0}{V_0^2}(h_{sv} - \Delta h_i)}{2\dfrac{\Delta V}{V_0} + \left(\dfrac{\Delta V}{V_0}\right)^2 + K + \dfrac{2g_0\,\Delta h_j}{V_0^2}} \tag{3.35}$$

If an allowable suction specific speed $S$ is determined on the basis of the considerations presented in Section 3.1.2, it is now possible to calculate the basic specific speed by the relation:

$$n_s = S \cdot \sigma_H^{3/4} \tag{3.36}$$

With the specific speed so determined, the design of the propulsion pump is essentially established and depends only on certain "design choices" as discussed in Section 3.1.3.

Since, according to Equation (3.33a), the pump head $H$ depends on the ratio $\Delta V/V_0$, the foregoing determination of the specific speed can apply only to operating conditions for which $\Delta V/V_0$ can be selected on a rational basis. This is true only for the *cruising* condition because the real propulsive efficiency (as defined in Section 2.2) is of determining importance only for that condition. Therefore, the foregoing considerations, including the determination of the basic specific speed, apply only to the cruising condition.

## 3.3 SPECIFIC SPEED OF THE PROPULSION PUMP IN RELATION TO THE DIVERSITY OF OPERATION REQUIRED

It was pointed out in Chapter 2 that the thrust requirements for high-speed surface craft generally depart very strongly from the similarity conditions which require that drag must increase as the square of the speed. Rather there is a so-called "hump" of the drag at about one-half to one-third of the cruising speed (see Figure 21). The hump speed is the speed at which the craft changes from displacement-craft behavior to that of the intended behavior at cruising speed, i.e., foilborne or bubbleborne. Thus there is a high-thrust condition to be met at a speed that is substantially less (by a factor of 1/2 to 1/3) than the cruising condition.

Two facts require consideration. First, the total inlet head above the vapor pressure ($H_{sv}$ or NPSH) will decrease according to Equation (3.34) *partly* according to the square of the velocity of travel. The other part of $H_{sv}$, i.e. $(h_{sv} - h_j)$, is approximately constant; this happens to be about equal to the dynamic part $(1 - K)\ V_0^2/2g_0$ at a reduced speed of 25 knots and is therefore substantially less than $(1 - K)\ V_0^2/2g_0$ at speeds twice or three times higher than the reduced speed. Evidently $H_{sv}$ depends heavily on $(1 - K)$ $V_0^2/2g_0$ and will decrease substantially with decreasing speed of travel $V_0$. Thus it is the *reduced* speed of travel at which the pump performance will be limited by cavitation.

Second, the thrust of the propulsor will increase with diminishing speed of travel at constant speed of rotation (or constant power) of the propulsor. This (second) consideration will be explored first under the simple assumption that $Q_{\text{hump}} = Q_{\text{cruise}}$ and $H_{\text{hump}} = H_{\text{cruise}}$. It should be understood that this assumption can be correct only if the propulsor has a variable discharge (nozzle) area.

Equation (3.33) can be written in the form:

$$2g_0\ (H - \Delta h_j) = V_0^2 \left[ 2\ \frac{\Delta V}{V_0} + \left( \frac{\Delta V}{V_0} \right)^2 + K \right] \tag{3.37}$$

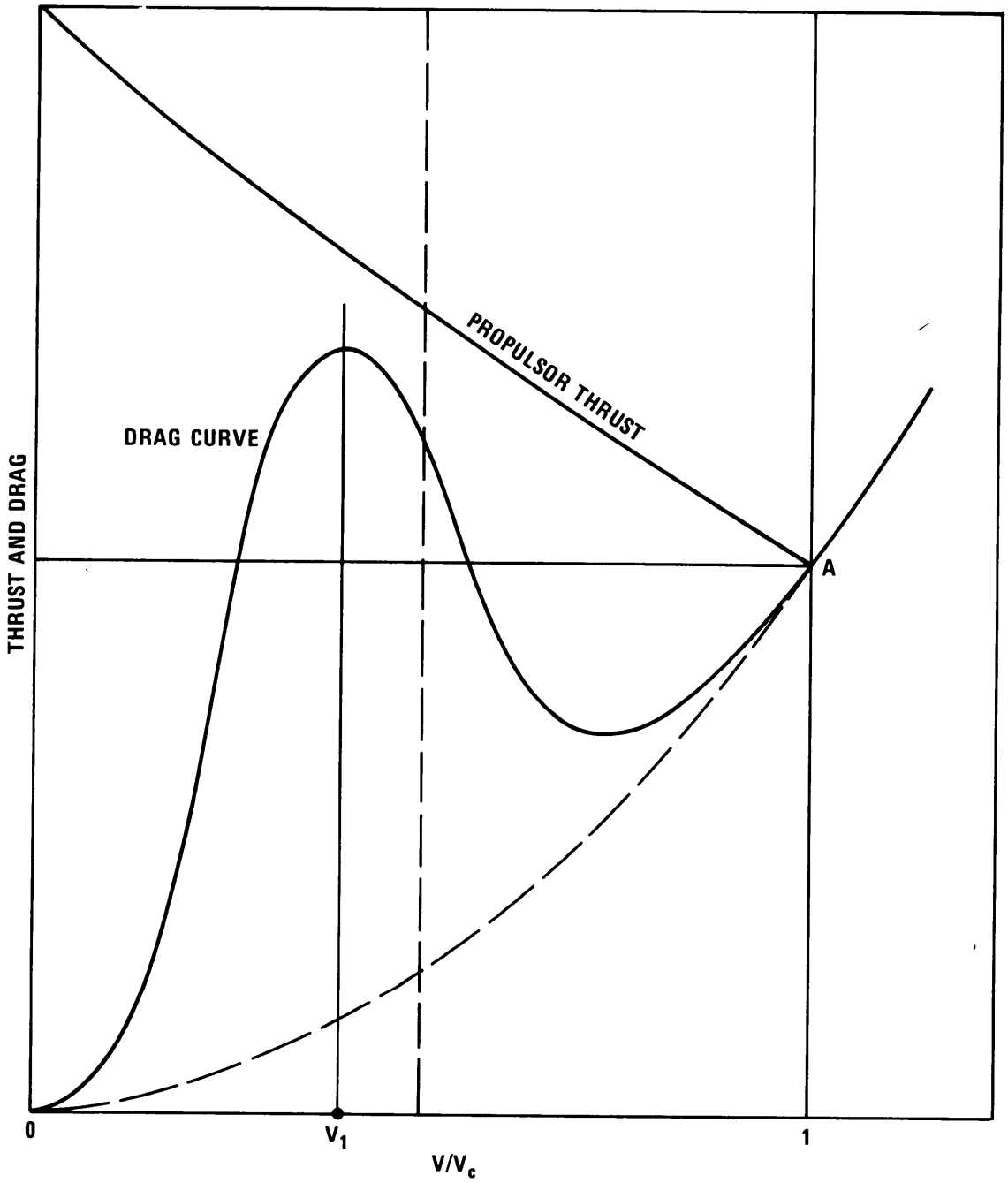


Figure 21 – Drag and Thrust as a Function of Speed of Travel $V$ in Relation to Cruise Speed $V_c$

The "hump," or reduced speed condition, is designated by subscript 1 and the cruising condition by subscript $c$. If, as stated before, it is assumed that $H_1 = H_c$, then

$$\frac{2\left(\frac{\Delta V}{V_c}\right)_1 + \left(\frac{\Delta V}{V_0}\right)_1^2 + K_1}{2\left(\frac{\Delta V}{V_0}\right)_c + \left(\frac{\Delta V}{V_0}\right)_c^2 + K_c} = \frac{V_c^2}{V_1^2} \tag{3.38}$$

This equation can be solved for $\Delta V_1/\Delta V_c$ which is the ratio of thrust increase $T_1/T_c$ under the assumption that $Q_1 = Q_c$. Figure 22 shows the results of this calculation. One of the curves in Figure 22 may then be superposed onto the thrust versus speed-of-travel curve for the propulsion plant and vehicle considered. Figure 21 shows this superposition and indicates that in order to permit acceleration of the craft under thrust-hump conditions, the thrust curve of the propulsor must pass above the hump of the thrust-demand curve. This requirement determines a minimum speed at Point A where the propulsor thrust curve intersects the thrust-demand curve of the craft. If this speed of travel $V_A$ is higher than the given cruise speed ($V_A > V_c$), then the cruise condition requires less pump speed and power than the hump condition. If the cruise speed is higher than $V_A$, then the cruise condition requires more pump speed and power than the hump condition. In the following it will be assumed that by an appropriate selection of the cruise speed in relation to the thrust-demand curve, $V_c$ equals $V_A$ with an adequate thrust margin at the hump.

It is important to remember that the propulsor thrust curves in Figures 21 and 22 were derived under this assumption that $Q_1 = Q_c$ and $H_1 = H_c$ and that this requires an adjustable discharge opening. Section 3.6 analyzes the case of a fixed discharge nozzle opening by a series of successive approximations. The results of these calculations indicate that for a constant discharge opening the thrust increase from cruise to reduced speed conditions is about 10 percent less than indicated in Figure 22 for an adjustable discharge opening. This must be considered when applying these curves.

The foregoing considerations establish the relation between the "hump speed" and the cruising speed $V_c$ as indicated in Figure 21. Of course, $V_1$ *may be any other minimum speed of travel required at full speed of rotation.* The next step is obviously to determine the low-speed total inlet head $H_{sv_1}$ in relation to the inlet head at cruising speed $H_{sv_c}$ because this will permit the determination (or selection) of the suction specific speeds at both low speed and cruising conditions.

According to Equation (3.34)

$$H_{sv} = (1 - K)\frac{V_0^2}{2g_0} + (h_{sv} - \Delta h_i) \tag{3.34}$$

Hence the ratio of the total inlet head above vapor pressure at low speed (subscript 1) and at cruising (subscript $c$) conditions is

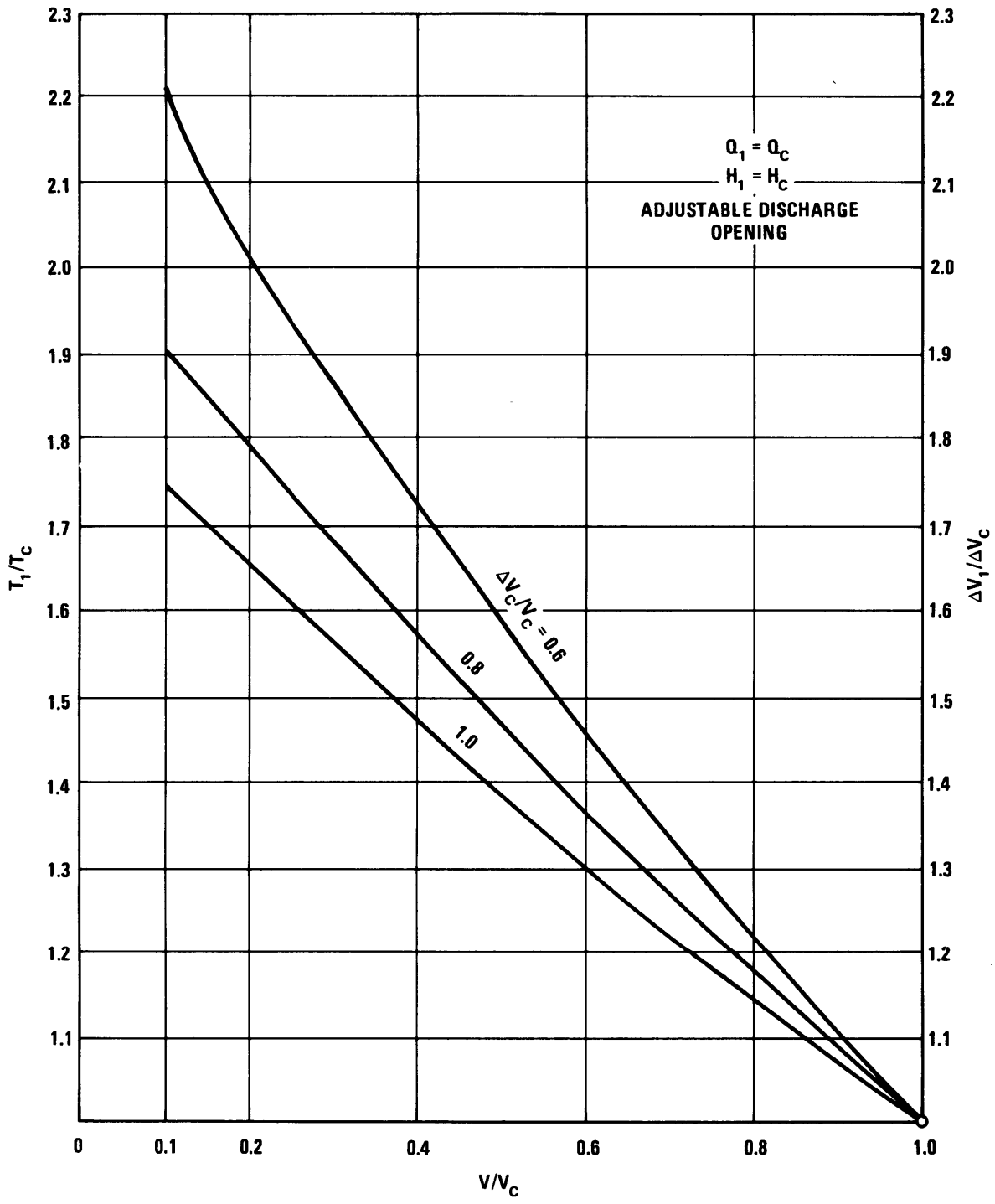


Figure 22 – Propulsor Thrust as a Function of Speed of Travel

$$\frac{H_{sv_1}}{H_{sv_c}} = \frac{(1-K)\ \dfrac{V_1^2}{2g_0} + (h_{sv} - \Delta h_i)}{(1-K)\ \dfrac{V_c^2}{2g_0} + (h_{sv} - \Delta h_i)} \tag{3.39}$$

or

$$\frac{H_{sv_1}}{H_{sv_c}} = \frac{V_1^2}{V_c^2}\ \frac{\left[1 + \dfrac{2g_0(h_{sv} - \Delta h_i)}{(1-K)\ V_1^2}\right]}{\left[1 + \dfrac{2g_0(h_{sv} - \Delta h_i)}{(1-K)\ V_c^2}\right]} \tag{3.40}$$

Figure 23 shows the evaluation of this equation for 50, 60, and 100 knots under the assumption that $(h_{sv} - \Delta h_i) = 25$ ft. Also shown is the increase in suction specific speed with diminishing speed of travel. Evidently

$$\frac{S_1}{S_c} = \left[\frac{H_{sv_c}}{H_{sv_1}}\right]^{3/4} \tag{3.41}$$

The $S_1/S_c$ curves in Figure 23 are based on the earlier assumption that $Q_1 = Q_c$ and $H_1 = H_c$. For a fixed discharge opening, $S$ will rise slightly less than the curves show, but the difference is usually less than 5 percent.

With the curves in Figure 23, it is now possible to complete the procedure of finding the specific speed of a propulsion pump outlined in Section 3.2. Recall that this procedure required an estimate of the suction specific speed at cruising speed and this was not easy to make because it is the low-speed condition and not the cruising condition that is critical with respect to cavitation. The S-ratio curves in Figure 23 answer this problem because some knowledge of the rise in suction specific speed with decreasing speed of travel permits a rational estimate of the suction specific speed under cruise conditions.

It should be noted that here the low speed of travel $V_1$ is only indirectly related to the "hump speed." Basically, $V_1$ is simply *the lowest speed of travel at which the propulsor is expected to operate at maximum speed of rotation*, or at the same speed of rotation used under cruise conditions. There is a strong temptation to specify that $V_1$, so defined, must be very low in order to accelerate the craft from stand-still to cruise speed within a minimum length of time. The curves in Figure 23 show the effect of such a specification on the design of the propulsion plant. For example, assume that the full speed of rotation is specified as applicable down to one-tenth of the cruise speed of travel. The S-ratio curves show that this will call for an

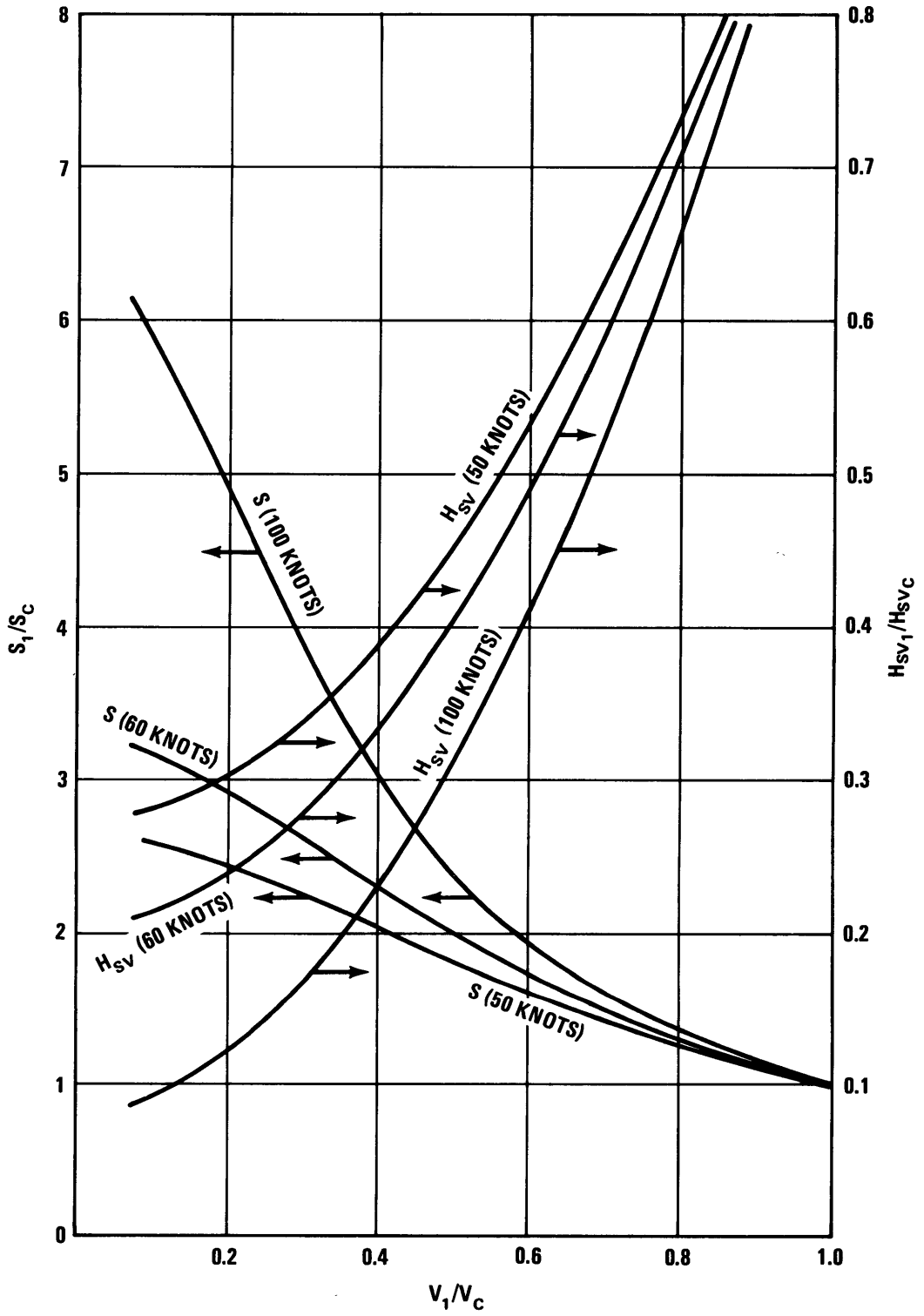


Figure 23 – Total Inlet Head (NPSH) and Suction Specific Speed as a Function of Speed of Travel at Constant Speed of Rotation

increase in suction specific speed by a factor between 2.5 and 6, depending on the cruise speed of travel. Since the *maximum* suction specific speed is limited by cavitation and design considerations, the suction specific speed at cruise conditions must be quite low for this specification. According to Equation (3.36), it is evident that a low $S$ value will lead to a correspondingly low value of the basic specific speed $n_s$ because $\sigma_H$ is fixed by given operating conditions and the general location (height) of the propulsion pump (see Equation (3.35)). A low value of $n_s$ is known to lead to an increase in the size and weight of the propulsion pump and its directly coupled driver (low-speed turbine or gear box). This disadvantage of a low specific speed will always exist regardless of the measures taken to increase the speed of rotation (e.g., the use of several pump inlets *in parallel*; see Section 3.5) because such measures can be applied to high as well as to low specific speeds. To illustrate this fact, consider a definite example:

Assume that according to Section 2.2 (Figure 5) the propulsor velocity ratio $\Delta V/V_0 = 0.7$, has been selected and that the duct and intake loss coefficient has been estimated as $K = 0.4$. It should be noted that these selections (or estimates) are quite independent of the specific speed of the pump, which was not considered in Section 2.2. Furthermore, assume that the velocity-independent head values are $h_{sv} - \Delta h_i = 25$ ft and $\Delta h_j = 7$ ft. (It will be found that moderate and reasonable variations in $h_{sv} - \Delta h_i$ and in $\Delta h_j$ have very little effect on the results obtained.) Finally, assume that the cruise speed $V_c$ is 60 knots or 101.4 ft/sec. Hence $V_c^2/2g_0 = 160$ ft.

According to Equation (3.35)

$$\sigma_H = \frac{H_{sv}}{H} = \frac{1 - 0.4 + \dfrac{25}{160}}{1.4 + 0.49 + 0.4 + \dfrac{7}{160}} = 0.324$$

This value obviously applies to the cruise condition.

If at this point, a definite suction specific speed *is assumed* for the cruise condition, the specific speed can immediately be calculated according to Equation (3.36). For example, if a fairly conservative suction specific speed of 0.407 (7000 $gal^{1/2}/min^{3/2}$ $ft^{3/4}$ in dimensional form) is assumed, Equation (3.36) yields:

$$n_s = 0.407 \times 0.324^{3/4} = 0.1745$$

or 3000 $gal^{1/2}/min^{3/2}$ $ft^{3/4}$ in dimensional form. This is a very reasonable value for a propulsion pump, and calls for a radial to mixed-flow impeller (see Figure 13).

However, the above assumption for the cruise suction specific speed was somewhat arbitrary and requires further justification on the basis of the low-speed condition. At this point one must assume a speed reduction ratio $V_1/V_c$. Two assumptions will be considered: $V_1/V_c = 0.4$ (which is reasonable for the hump speed of a hydrofoil craft) and $V_1/V_c = 0.1$.

For $V_1/V_c = 0.4$, the 60-knot curve in Figure 23 gives $S_1/S_c = 2.3$. For the assumed cruise suction specific speed of 0.407 (7000 $gal^{1/2}/min^{3/2}$ $ft^{3/4}$ in dimensional form), the suction specific speed at the

low speed $V_1 = 0.4\ V_c$ would be $S_1 = 0.936$ (16,000 $gal^{1/2}/min^{3/2}\ ft^{3/4}$ in dimensional form) which is high but may be considered as acceptable for an impeller that is still fairly standard although especially designed. However, if full speed of rotation were specified down to $V_1 = 0.10\ V_c$, the ratio of rise in suction specific speed would be $S_1/S_s = 3.15$, bringing the suction specific speed at low speed of travel to a value of $S_1 = 1.282$ (22,000 $gal^{1/2}/min^{3/2}\ ft^{3/4}$ in dimensional form). This would definitely require either a very special impeller as used in condensate pumps or an "inducer" as used in the rocket pump field.

Attention must now be called to the fact (first pointed out in Section 3.1.2) that high suction specific speeds require a different impeller inlet design than do moderate suction specific speeds. When a pump that is designed for high suction specific speed is used at a much lower suction specific speed (say, at cruise conditions), it may not operate completely free of cavitation whereas a good pump designed for that lower suction specific speed (say, $S = 0.4$) may do so. Furthermore, some sacrifices in efficiency are also entailed when a pump designed for high suction specific speeds is operated at very low suction specific speeds.

The foregoing argument can be given more definite form in terms of the design flow coefficient $V_{m_i}/U_i$ by using Figure 15.

For $S = 0.407$, the optimum design flow coefficient is 0.37 (for a small inlet hub diameter ratio). For $S = 0.936$, the optimum design flow coefficient is 0.19 and for $S = 1.282$, it is 0.145.

Of course one does not have to use exactly the optimum flow coefficient. When designing for $S_c = 0.407$ and $S_1 = 0.936$, one may obtain acceptable performance when designing for and operating at an intermediate flow coefficient, say, $V_{m_i}/U_i = 0.25$. It is much more problematical whether such a compromise design will still be acceptable with $S_c = 0.407$ and $S_1 = 1.282$ in view of the fact that (as already indicated in Section 3.1.2) high suction specific speeds require thin leading vane edges.

One answer to this problem would be to select lower values for both suction specific speeds $S_c$ and $S_1$, for example, for $S_c$ the value 0.25 (4300 $gal^{1/2}/min^{3/2}\ ft^{3/4}$ in dimensional form) and, correspondingly, for $S_1 = 3.15 \cdot S_c = 0.788$ (13,530 $gal^{1/2}/min^{3/2}\ ft^{3/4}$ in dimensional form). This assumes that full speed of rotation is required or specified down to $V_1 = 0.10\ V_c$. Since the optimum flow coefficient for $S = 0.788$ is about $V_{m_i}/U_i = 0.23$, a compromise value of 0.30 would probably be quite acceptable. In this case one pays for specifying full rpm operation down to $V_1/V_c = 0.10$ by an increase in volume and weight of the rotating propulsion machinery approximately in the ratio 0.407/0.25 = 1.63, i.e., by a 60 percent increase in rotating machinery volume and weight. Although this estimate of the increase is quite crude, some increase is unavoidable, and, for the values used in this example, this increase is probably not negligible unless one is concerned with craft for very long ranges of travel where the entire weight of the propulsion plant may be negligible compared to the fuel weight (see Section 2.3).

It should be evident from Figure 23 that the relation between the cruising and low-speed conditions rapidly worsens as the absolute cruising speed is increased. The curves drawn for the 100-knot cruising

speed demonstrate this fact. The reason is obviously that the *fixed* part of the total inlet head, i.e., $h_{sv} - \Delta h_i$, has an effect *relative* to the cruise velocity head $V_c^2/2g_0$. This relative effect, therefore, decreases rapidly with increasing $V_c$. Thus the problems pointed out before increase rapidly with increasing cruise speed of travel.

Table 1 represents an attempt to summarize various conclusions from the preceding example. It includes some results for a 100-knot cruise speed; in this case, the calculations are based on a uniform *maximum* suction specific speed (at minimum velocity specified to use maximum speed of rotation) $S_1 = 1.00$ (17,170 $\text{gal}^{1/2}/\text{min}^{3/2}\ \text{ft}^{3/4}$ in dimensional form). In the opinion of the author, this value is close to the maximum suction specific speed that can be used without significantly compromising cruise performance at low suction specific speeds.

The Thoma cavitation number $\sigma_H = H_{sv}/H$ is first calculated for both cruising velocities according to Equation (3.35). The optimum design flow coefficient corresponding to an assumed maximum value of $S_i = 1.0$ is read from Figure 15 and listed for comparison purposes only since it is not expected to be used in the actual design.

The S-ratio curves in Figure 23, Equations (3.40) and (3.41) give the ratio of the assumed maximum suction specific speed $S_1 = 1.0$ (17,200 $\text{gal}^{1/2}/\text{min}^{3/2}\ \text{ft}^{3/4}$) to the suction specific speed at cruise conditions. This ratio leads to various cruise suction specific speeds $S_c$ under the assumption that $Q_1 = Q_c$ and $H_1 = H_c$ (also $n_1 = n_c$). This assumption of similar flow at cruise and low-speed conditions requires that the discharge opening be slightly adjustable. The optimum flow coefficients for these (lower) suction specific speeds are listed as read from Figure 15. A comparison of these flow coefficients with the optimum flow coefficient for $S_1 = 1.0$ ($V_{m_i}/U_i = 0.18$) permits compromise flow coefficients to be estimated for the various conditions listed. The compromise values are estimated from the corresponding suction head coefficients $2g_0H_{sv}/V_{m_i}^2$ as will be shown in Section 3.4. As mentioned before, the compromise flow coefficients determine the design as well as the operating conditions and so no "off-design" operation is implied. One merely does not design or operate according to the optimum conditions relative to cavitation since two widely differing conditions (suction specific speeds) have to be met.

Furthermore, according to Equation (3.36), the cruise values of the Thoma cavitation number $\sigma_H = H_{sv_c}/H$ and the cruise suction specific speeds permit the calculation of the basic specific speed which applies to the cruise as well as to the low-speed-of-travel condition because of the assumed similarity of flow in the pump. It thus determines, after certain "design choices," the design of the propulsion pump, as will be illustrated in Section 3.4.

Most of the specific speeds permit the use of single-stage, mixed-flow or radial-flow centrifugal pumps, with the exception of the 100-knot propulsion plant specified to permit full speed of rotation down to one-tenth of cruising speed of travel. The resulting low specific speed can still be met by a single-stage centrifugal pump but not without some sacrifices in efficiency (about 5 percent). The extent to which a two-stage arrangement would avoid this loss by virtue of a more favorable specific speed per stage is uncertain. The staging of radial-flow pumps also involves some losses in efficiency.

## TABLE 1 – PROPULSION SYSTEM CHARACTERISTICS AT TWO SHIP SPEEDS

(Assumptions: propulsion velocity ratio $\Delta V/V_c$ = 0.7 (Section 2.2); inlet and duct-loss coefficient $K$ = 0.40, $h_{sv}$ = 32 ft at free water surface; $\Delta h_i = \Delta h_j$ = 7 ft, single stage except where noted, single flow in parallel).

| Pump Characteristics | Cruise Speed of Travel | | | | Remarks |
|---|---|---|---|---|---|
| | 60 Knots | | 100 Knots | | |
| 1. Cavitation Number $H_{sv}/H$ | 0.324 | | 0.285 | | At cruise conditions |
| 2 Minimum Speed at Maximum Speed of Rotation $V_1/V_c$ | 0.4 | 0.1 | 0.4 | 0.1 | Section 2.1 and Figure 21 |
| 3 Suction Specific Speed Ratio $S_1/S_c$ | 2.273 | 3.16 | 2.99 | 5.84 | Equations 3.40 and 3.41 Figure 23 |
| 4 Assumed Maximum $S$ Value | 1.00 | 1.00 | 1.00 | 1.00 | 17,170 $gal^{1/2}/min^{3/2}$ $ft^{3/4}$ in dimensional form |
| 5 Optimum Flow Coefficient $V_{m_1}/U_1$ at Minimum Velocity of Travel | 0.18 | 0.18 | 0.18 | 0.18 | Figure 15 |
| 6. Cruise Suction Specific Speed $S_c$ | 0.440 | 0.3166 | 0.346 | 0.1713 | Lines 3 and 4 above |
| 7. Dimensional Value of $S_c$ | 7,640 | 5,445 | 5,950 | 1,947 | Equation (3.18) |
| 8 Optimum Flow Coefficient $V_{m_1}/U_1$ | 0.35 | 0.42 | 0.40 | >0.50 | Figure 15 |
| 9. Compromise Flow Coefficient | 0.22 | 0.23 | 0.23 | doubtful | See Section 3.4 |
| 10 Basic Specific Speed $n_s$ | 0.1888 | 0.1356 | 0.1351 | 0.0668 | Equation (3.36) Lines 1 and 6 |
| 11. Dimensional Value of $n_s$ | 3,248 | 2,335 | 2,312 | 1,149 | |
| 12 Design Conclusion | 1 St. Mix.* | 1 St. Rad.** | 1 St. Rad.** | *** | Equation (3.16) and Figure 13 |
| 13 Volume and Weight Ratio $V_1/V_c$ = 0.1 versus 0.4 | $\frac{n_s(0.4)}{n_s(0.1)} = 1.39$ | | $\frac{n_s(0.4)}{n_s(0.1)} = 2.02$ | | |

* Single stage mixed-flow (could be two or three stage axial flow, see Figure 19).

** Single stage radial flow (could be three or four stage axial flow, see Figure 19).

*** Single- or two stage radial flow or multistage axial flow

Finally, the increase in volume and weight of the directly coupled rotating machinery is estimated for the step from 0.4 to 0.1 for the speed ratio specified to be achievable at full speed of rotation. It is seen that this increase is quite considerable for the 100-knot cruising speed.

Thus it should be apparent that after certain "design choices" have been made the operating conditions of a propulsion pump are sufficient to determine its basic specific speed and therefore its design. (The design choices and the design process will be discussed in the next section.) To determine the specific speed, it is necessary to select a maximum suction specific speed for the minimum speed of travel for which full speed of rotation is required. The maximum suction specific speed that is usable for this application is limited because the same pump has to operate at high suction specific speeds temporarily and at low suction specific speeds for extended periods of time. These two conditions become incompatible if the particular maximum suction specific speed exceeds certain limits. The lower the minimum speed of travel for which operation at maximum speed of rotation is specified, the more severe is this conflict.

## 3.4 PROPULSION PUMP DESIGN, SINGLE SUCTION

With the specific speed of the propulsion pump determined according to Section 3.3 and Table 1, one is now in a position to determine the design of the pump according to Section 3.1, in particular Equations (3.16) and (3.22). The basic specific speed is

$$n_s = \frac{n\,Q^{1/2}}{(g_0 H)^{3/4}} = \frac{1}{2^{1/4}\,\pi^{1/2}} \left(\frac{U_0^2}{2g_0 H}\right)^{3/4} \left(\frac{V_{m_i}}{U_i}\right)^{1/2} \left(\frac{D_i}{D_0}\right)^{3/2} \left(1 - \frac{D_h^2}{D_i^2}\right)^{1/2} \tag{3.16}$$

and the suction specific speed is

$$S = \frac{n\,Q^{1/2}}{(g_0 H_{sv})^{3/4}} = \frac{1}{2^{1/4}\,\pi^{1/2}} \left(\frac{V_{m_i}^2}{2g_0 H_{sv}}\right)^{3/4} \left(\frac{U_i}{V_{m_i}}\right)\left(1 - \frac{D_h^2}{D_i^2}\right)^{1/2} \tag{3.22}$$

Other equivalent relations between the specific speeds and various design parameters will be used and derived later in this section.

The design process will be illustrated by means of the example given in Table 1, particularly the values in the second and third column: 60 knots with $V_1/V_c = 0.1$ and 100 knots with $V_1/V_c = 0.4$. Accordingly, the maximum suction specific speed is assumed to be $S_1 = 1.0$ (17,170 $\text{gal}^{1/2}/\text{min}^{3/2}\ \text{ft}^{3/4}$) and the basic specific speed $n_s = 0.135$ which is the same for cruise and low-speed conditions.

The estimated compromise flow coefficient $V_{m_i}/U_i$ is determined from the maximum suction specific speed $S_i = 1.0$ according to Equation (3.22). The suction head coefficient $2g_0 H_{sv}/V_{m_i}^2$ is calculated for a

number of estimated flow coefficients. Assuming $D_h/D_i = 0.3$, so that $1 - D_h^2/D_i^2 = 0.91$, one finds the following values for $2g_0H_{sv}/V_{m_i}^2$ and $V_{m_i}/U_i$.

| $V_{m_i}/U_i$ | $2g_0H_{sv}/V_{m_i}^2$ |
|---|---|
| 0.27 | 1.99 |
| 0.25 | 2.205 |
| 0.23 | 2.464 |
| 0.22 | 2.610 |
| 0.18 | 3.44 |

From these results, $V_{m_i}/U_i = 0.23$ was selected as the design flow coefficient. This coefficient should be as high as possible in order to have acceptable performance at cruise speed. Yet at low speed $2g_0H_{sv}/V_{m_i}^2$ cannot be so low as to render questionable the required maximum suction specific speed. *There is no exact way to make this selection, and its adequacy must ultimately be verified or refuted by cavitation tests.*

For a basic specific speed of 0.135 (2320 $gal^{1/2}/min^{3/2}$ $ft^{3/4}$ in dimensional form), a head coefficient $2g_0H/U_0^2 = 1.0$ should lead to good efficiency; this is an empirical fact that cannot be substantiated theoretically. With this value and $V_{m_i}/U_i = 0.23$, $D_h/D_i = 0.3$, Equation (3.16) gives $D_0/D_i = 1.37$.

Since the maximum suction specific speed is fairly high and the selected flow coefficient correspondingly low, it is well to check the resulting retardation of the relative flow along the outer shroud of the impeller (see Section 3.1.3). To simplify this calculation, the retardation will be judged by the retardation of the peripheral component of the relative velocity inasmuch as the exact lower limit for the retardation ratio $w_2/w_1$ is unknown.

For zero rotation of the absolute flow at the impeller inlet, the peripheral component of the relative inlet velocity is $w_{u_i} = -U_i$. At the discharge, this component is:

$$w_{u_0} = V_{u_0} - U_0 = U_0 (V_{u_0}/U_0 - 1)$$

For zero rotation at the inlet, $2g_0H/U_0^2 = 2\eta_h V_{u_0}/U_0$ (according to the Euler equation (3.9)). Assuming $\eta_h = 0.92$ and using $2g_0H/U_0^2 = 1$, one finds $V_{u_0}/U_0 = 0.544$ and $w_{u_0} = U_0 (0.544 - 1) = -0.456\ U_0$. Hence

$$\frac{w_{u_0}}{w_{u_i}} = \frac{0.456\ U_0}{U_i} = 0.456\ \frac{D_0}{D_i} = 0.456 \text{ x } 1.37 = 0.624$$

This may be considered as dangerously low because existing knowledge on radial- or mixed-flow impellers is inferior to that on axial-flow impellers. With radial impellers therefore, it is prudent to use more conservative (i.e., higher) values for $w_{u_0}/w_{u_i}$ than the suggested minimum of 0.60.

The impeller diameter at the *outer* shroud may well be selected to be larger than the minimum outside diameter $D_0$. Assuming $D_{0_{max}} = 1.45\ D_i$, one finds by the same reasoning as used above that $w_{u_0}/w_{u_i} = 0.746$. This appears to be safe. (In checking this calculation, consider that $2g_0H/U_{0_{max}}^2 = 0.893$ and that $V_{u_0}/U_0$ at the outer shroud is 0.485.)

In this connection it is well to determine the number of impeller vanes from the vane lift coefficient ($C_L$) according to Equation (3.31). For zero prerotation, this equation has the form:

$$C_L = 2\ \frac{V_{u_0}}{w_\infty}\ \frac{t_0}{\ell} = 2\ \frac{V_{u_0}}{w_\infty}\ \frac{\pi D_0}{N\ell}$$

where $N$ is the number of vanes and $w_\infty$ is the *mean* relative velocity. (Subscript 0 refers to the outside diameter and replaces subscript 2 in Equation (3.31).)

Assuming $C_L = 1$, $V_{u_0}/w_\infty = 2/3$, $\ell = D_0/2$, one finds $N = 8\pi/3 = 8.37$; this means that the number of vanes should not be less than 8, nor does it need to be larger than 9. The assumption of $C_L = 1.2$ would lead to $N = 7$.

The axial width $b_0$ of the impeller at its outer periphery can be determined by the condition of continuity:

$$V_{m_0} \times \pi D_0 b_0 = V_{m_i}\ \frac{\pi D_i^2}{4}\ \left(1 - \frac{D_h^2}{D_i^2}\right)$$

$$\frac{b_0}{D_0} = \frac{V_{m_i}}{V_{m_0}}\ \frac{D_i^2}{4D_0^2}\ \left(1 - \frac{D_h^2}{D_i^2}\right)$$

It is common practice with radial-flow pump impellers to retard the meridional flow so that $V_{m_0} < V_{m_i}$. Assuming $V_{m_0}/V_{m_i} = 0.667$, then

$$\frac{b_0}{D_0} = \frac{1}{0.667} \times \frac{1}{4 \times 1.876} \times 0.91 = 0.182$$

The ratios $D_{0_{min}}/D_i = 1.37$, $D_{0_{max}}/D_i = 1.45$, $b_0/D_{0_{min}} = 0.182$ and the assumed hub ratio $D_h/D_i = 0.3$ determine the impeller profile so far as the suction specific speed and the basic specific speed permit this determination. Beyond that, the impeller profile depends on the direction in which the flow is to be guided after it leaves the impeller.

The "design decision" to be made for propulsion pumps at this point is the direction of the propelling jet in relation to the direction of the axis of rotation. If the propelling jet is to have the same direction as and be coaxial with the axis of rotation, the most natural design is that shown in Figure 24. Furthermore,

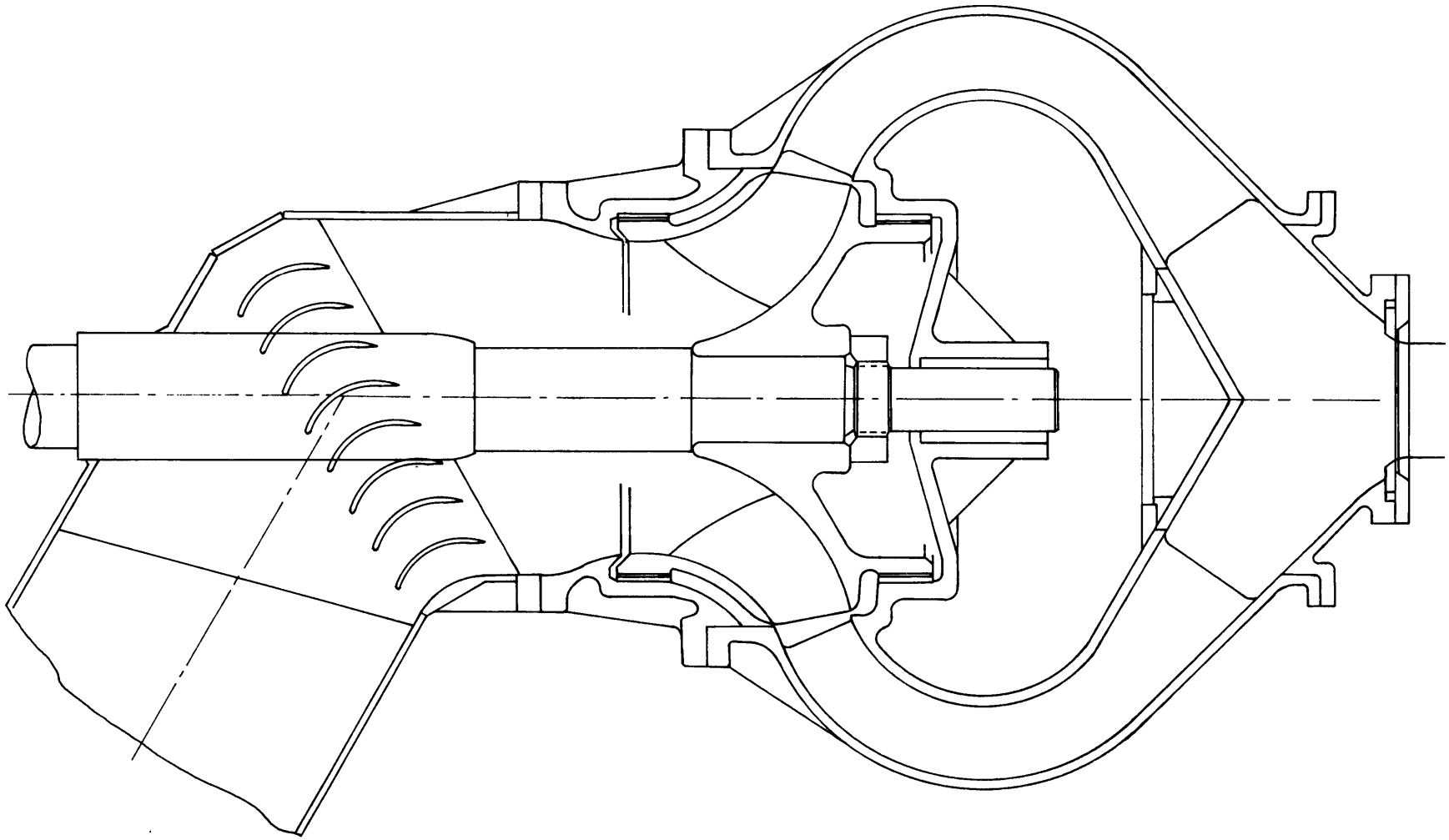

Figure 24 – Radial-Flow Propulsion Pump with Axial Discharge

the direction of the jet is to be the same as that of the flow entering the impeller. This arrangement is familiar from common aircraft jet engine practice. In this case the driving shaft must enter through the inlet passages of the pump. The passage leading from the impeller to the discharge nozzle is a multipassage vane or duct system arranged in an axially symmetric fashion. The inlet passage must have changing directions, usually S-shaped, in order to avoid interference with the axially concentric driver in front of the pump inlet. Note that with this arrangement, the flow leaving the impeller does not need to be retarded in the passages leading to the discharge nozzle. In this respect a propulsion pump of this arrangement is quite different from standard pumps intended to generate a pressure increase. The propulsion pump should thereby have an efficiency advantage over standard pumps since retardation of the flow is usually connected with losses. However, attention must be paid to the length and curvature of the passages between the impeller and the discharge nozzle in order to minimize head losses in these passages.

A different arrangement is indicated when a so-called "volute" casing is used at the impeller discharge as shown in Figure 18 and on the left side of Figure 19. In this case the preferred direction of discharge would be at right angles to the axis of rotation, preserving to some extent the circumferential component of the flow leaving the impeller. Figure 25 shows this arrangement for the propulsion pump considered here. The maximum radial cross section of the volute, sometimes called the "throat" area $A_{th}$, is calculated as follows: Evidently

$$V_{th} \times A_{th} = V_{m_i} \frac{D_i^2}{4} \left(1 - \frac{D_h^2}{D_i^2}\right) \tag{3.42}$$

where $V_{th}$ is the average fluid velocity in the throat. By the law of constant angular momentum, $V_{th} = V_{u_0} \times D_0/D_{th}$. Here $D_{th}$ is twice the average distance of the throat area from the axis of rotation. Hence:

$$A_{th} \frac{V_{u_0}}{U_0} \frac{D_0}{D_{th}} = \frac{V_{m_i}}{U_0} \frac{D_i^2 \pi}{4} \left(1 - \frac{D_h^2}{D_i^2}\right) \tag{3.43}$$

However for zero rotation of the absolute flow at the impeller inlet, one finds from the Euler equation (3.9):

$$\frac{V_{u_0}}{U_0} = \frac{1}{2\eta_h} \frac{2g_0H}{U_0^2} \tag{3.44}$$

Substituting this, with $U_i/U_0 = D_i/D_0$, into Equation (3.43):

$$\frac{A_{th}}{D_i^2 \pi/4} = \frac{D_{th}}{D_0} 2\eta_h \frac{U_0^2}{2g_0H} \frac{V_{m_i}}{U_i} \times \frac{D_i}{D_0} \left(1 - \frac{D_h^2}{D^2}\right) \tag{3.45}$$

With $\eta_h = 0.92$, $2g_0H/U_0^2 = 1$, $V_{m_i}/U_i = 0.23$, $D_0/D_i = 1.37$, and $D_h/D_i = 0.3$, one obtains:

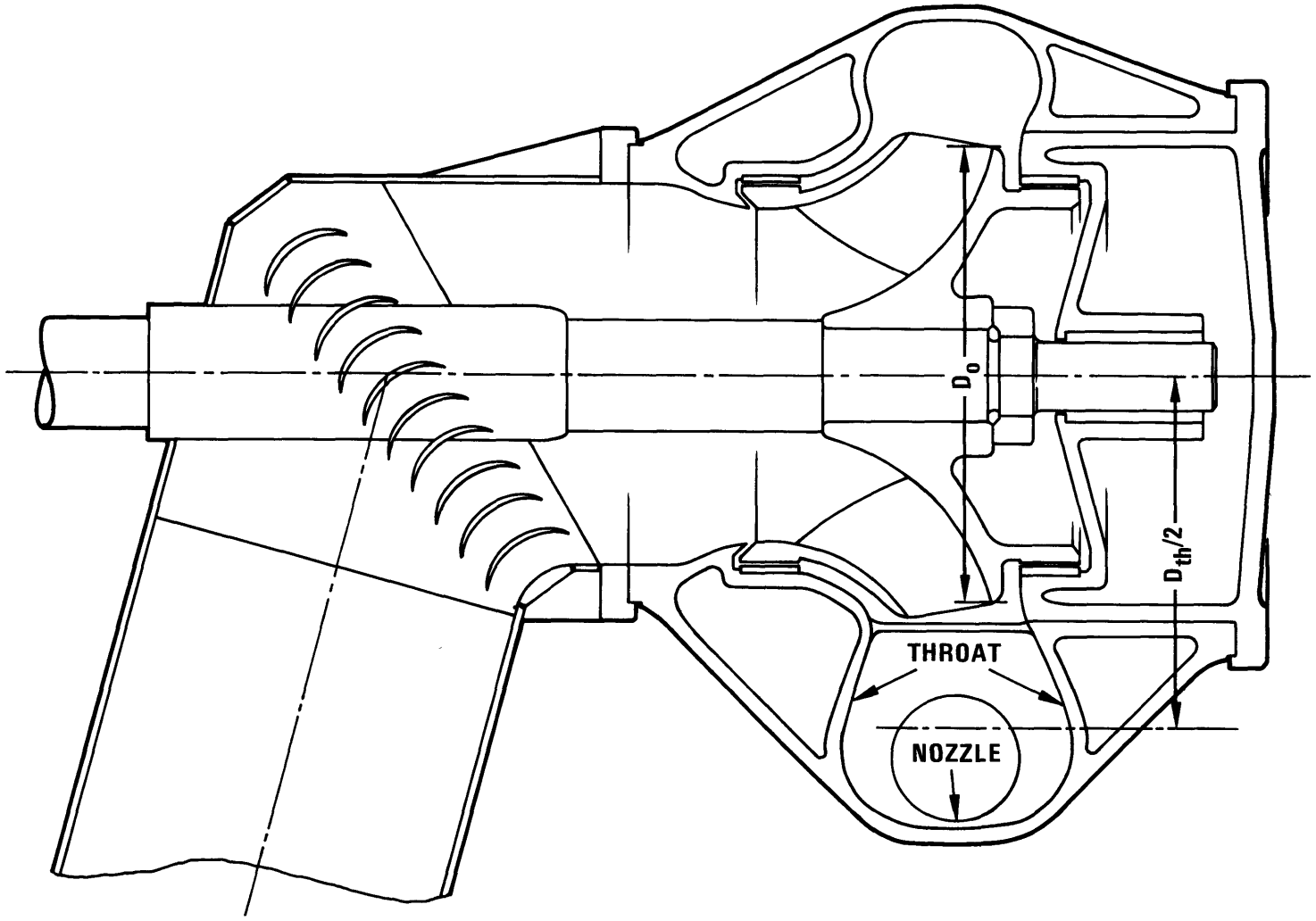


Figure 25 – Volute Propulsion Pump

$$\frac{A_{th}}{D_i^2\,\pi/4} = \frac{D_{th}}{D_0} \times 1.84 \times \frac{0.23}{1.37} \times 0.91 = \frac{D_{th}}{D_0} \times 0.281$$

From preliminary studies, assume $D_{th}/D_0 = 1.55$, so that $A_{th}/(D_i^2\,\pi/4) = 0.436$. This value was used in Figure 25 which confirms the foregoing assumption $D_{th}/D_0 = 1.55$.

To complete the outline of the propulsion unit, one must also determine the discharge jet area $A_j$. Evidently:

$$A_j \times V_j = V_{m_i} \frac{D_i^2\,\pi}{4} \left(1 - \frac{D_h^2}{D_i^2}\right) \tag{3.46}$$

where the jet velocity $V_j = V_0 + \Delta V = V_0\,(1 + \Delta V/V_0)$. According to Equation (3.33a),

$$\frac{2g_0H}{V_0^2} = 2\,\frac{\Delta V}{V_0} + \frac{\Delta V^2}{V_0^2} + K + \frac{2g_0\Delta h_j}{V_0^2} \tag{3.47}$$

With $V_0$ = 60 knots = 101.4 ft/sec, $\Delta h_j$ = 7 ft, $\Delta V/V = 0.7$, and $k = 0.4$:

$$\frac{2g_0H}{V_0^2} = 1.4 + 0.49 + 0.4 + 0.05 = 2.34$$

Referring to the minimum impeller discharge diameter:

$$\frac{2g_0H}{U_0^2} = 1 = \frac{2g_0H}{V_0^2}\,\frac{V_0^2}{U_0^2} = 2.34\,\frac{V_0^2}{U_0^2}$$

Hence $U_0/V_0 = \sqrt{2.34} = 1.53$. Furthermore, $V_j/V_0 = 1 + \Delta V/V_0 = 1.7$. From Equation (3.46):

$$\frac{A_j}{D_i^2\,\pi/4} = \frac{V_{m_i}}{U_i}\,\frac{U_i}{U_0}\,\frac{U_0}{V_0}\,\frac{V_0}{V_j}\left(1 - \frac{D_h^2}{D_i^2}\right)$$

$$\frac{A_j}{D_i^2\,\pi/4} = \frac{0.23}{1.37} \times \frac{1.53}{1.7} \times 0.91 = 0.1375$$

$$\frac{D_j}{D_i} = 0.1375^{1/2} = 0.371$$

Evidently the jet area $A_j$ is smaller than the throat area of a (single) volute, and $A_j/A_{th} = 0.1375/0.436 = 0.315$.

Volute pumps are very frequently used in the commercial field as well as in the field of rocket pumps. They pose a problem of arrangement in the propulsion field because their natural direction of discharge is normal to the axis of rotation. If this axis is parallel to the direction of travel, it is necessary to turn the flow by 90 deg after discharge from the pump casing. This is acceptable only if the velocity of flow at this turn does not represent a significant percentage of the total jet energy. Even a well-designed turn involves a loss of about 20 percent of the velocity head and much more with standard elbows (see Chapter 4). Thus one loses the aforementioned potential advantage of avoiding substantial retardation after discharge from the impeller.

To avoid a turn after discharge from a volute casing, it would be necessary to locate the shaft at right angles to the direction of travel, i.e., the shaft has to run either crosswise in a horizontal plane or be vertical. Figures 26 and 27 show two horizontal arrangements and Figure 28 a vertical-shaft arrangement. The vertical-shaft arrangement permits steering with the jet by rotation of the volute casing about the vertical pump axis over a large range of angles (larger than 180 deg).

With an open volute casing (volute without stationary vanes) as shown in Figure 25, the entire pump casing, perhaps including the driving gear box, would have to be rotated; this calls for a rotatable, watertight joint at the inlet end of the pump. For mechanical reasons, rotating only the volute around a stationary casing would require a fixed guide-vane system outside of the impeller, as shown diagrammatically in Figure 29. This would probably involve some losses in efficiency and would expose the rotatable joints between the volute and the stationary casing to (nearly) the discharge pressure of the pump. To avoid an angle drive, a vertical pump should be driven by a vertical-shaft, free-power turbine and a vertical-shaft reduction gear; the vertical turbine exhaust would have an efficiency advantage. The hot gas generator would retain its conventional, horizontal-shaft arrangement, and the admission of the power gas stream to the free turbine would take place through a volute casing; this arrangement is familiar from the field of hydraulic turbines.

There is one other important arrangement to be considered for single-suction pumps, namely, a multistage axial-flow pump as shown in Figure 30. This design will be described under the assumption that all operating conditions and the inlet flow conditions are exactly the same as for the single-stage, radial-flow machine previously described. All outside diameters of the axial-flow stages are the same as the impeller *inlet* diameter of the radial-flow pump. The first-stage impeller inlet has the same hub-to-tip diameter ratio as assumed previously ($D_h/D_i = D_h/D_0 = 0.3$). The first-stage impeller discharge hub-to-tip ratio $D_{h_2}/D_0$ is the same as for the remaining axial stages. The first task is to determine this increased hub-to-tip diameter ratio and the number of stages.

The hub-to-tip diameter ratio will first be estimated under the assumption that $V_{m_2}/U_0 = 0.5$; the subscript 2 applies to the discharge of the first stage and inlet as well as the discharge of all following vane systems.

Evidently, by continuity,

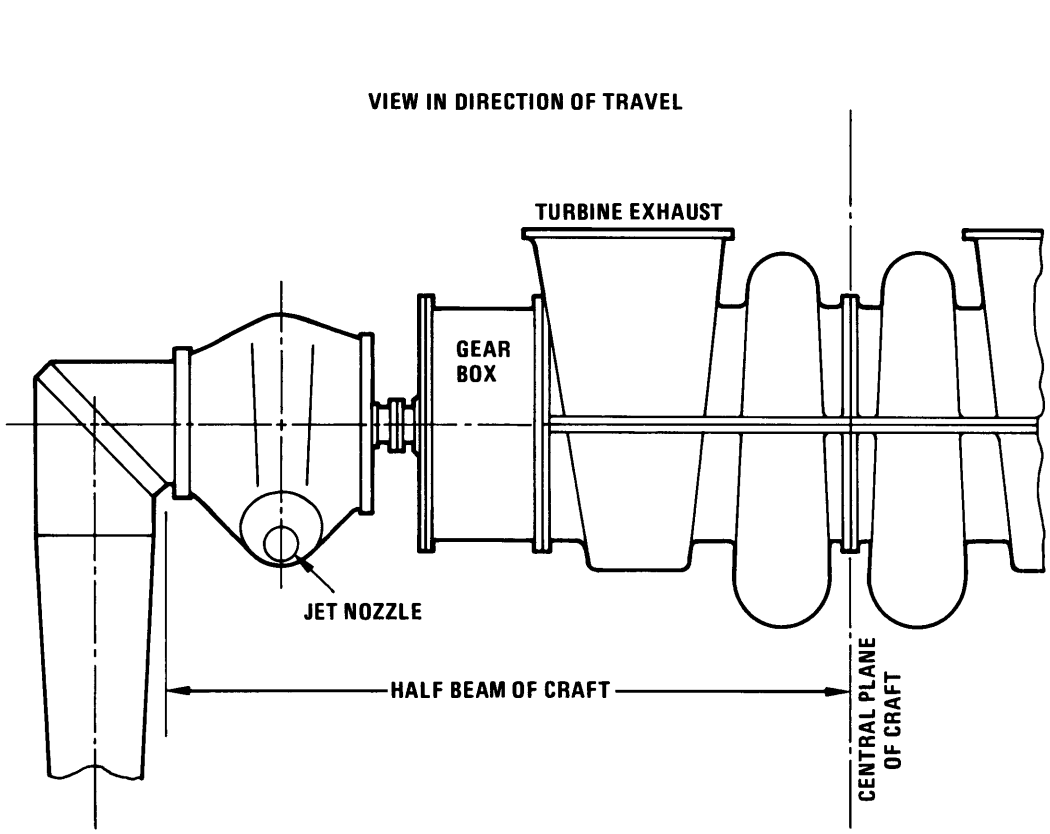


Figure 26 – Horizontal Arrangement of Volute Propulsion Pump, Scheme 1

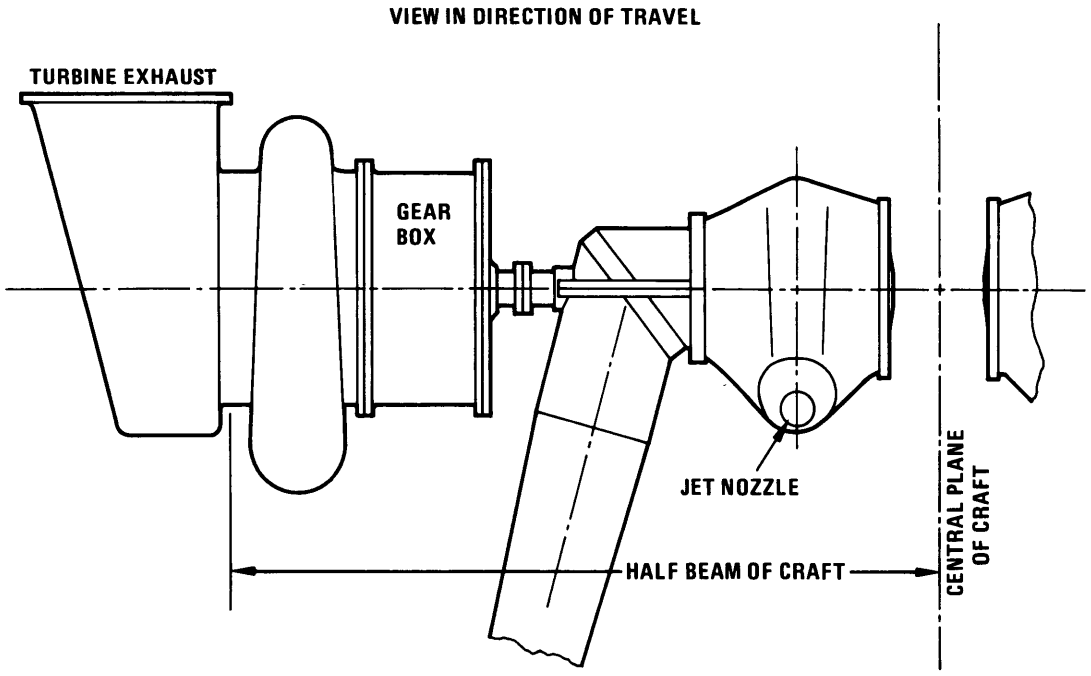


Figure 27 – Horizontal Arrangement of Volute Propulsion Pump, Scheme 2

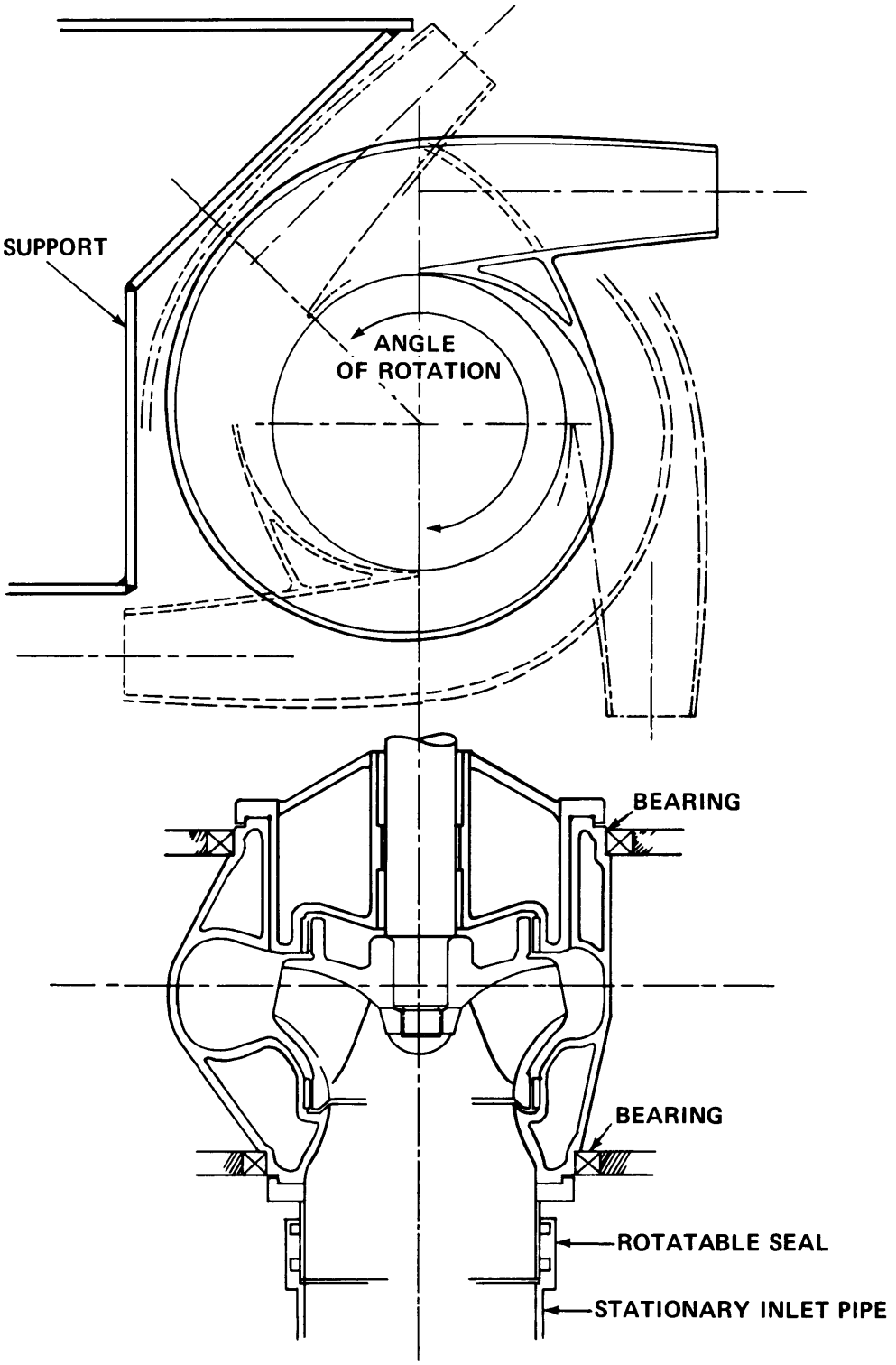


Figure 28 – Vertical Arrangement of Volute Propulsion Pump

(Pump, casing and discharge nozzle rotatable)

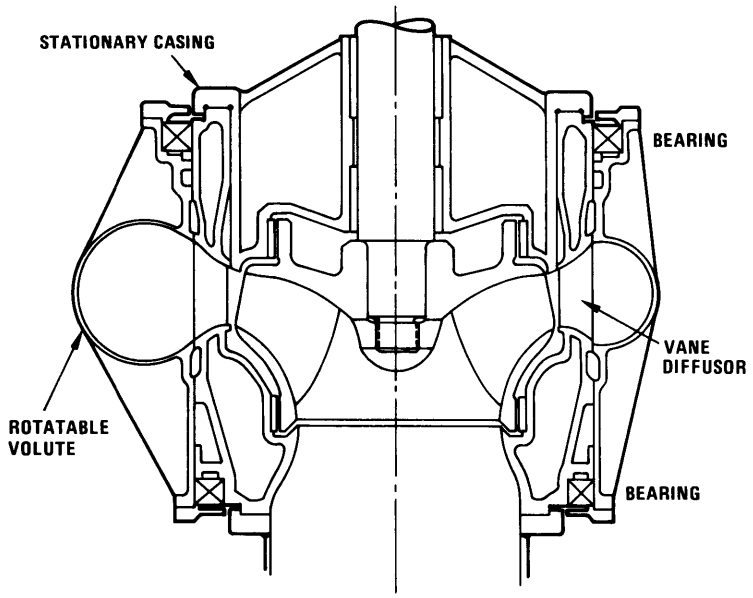


Figure 29 – Vertical Propulsion Pump with Rotatable Volute and Stationary Casing

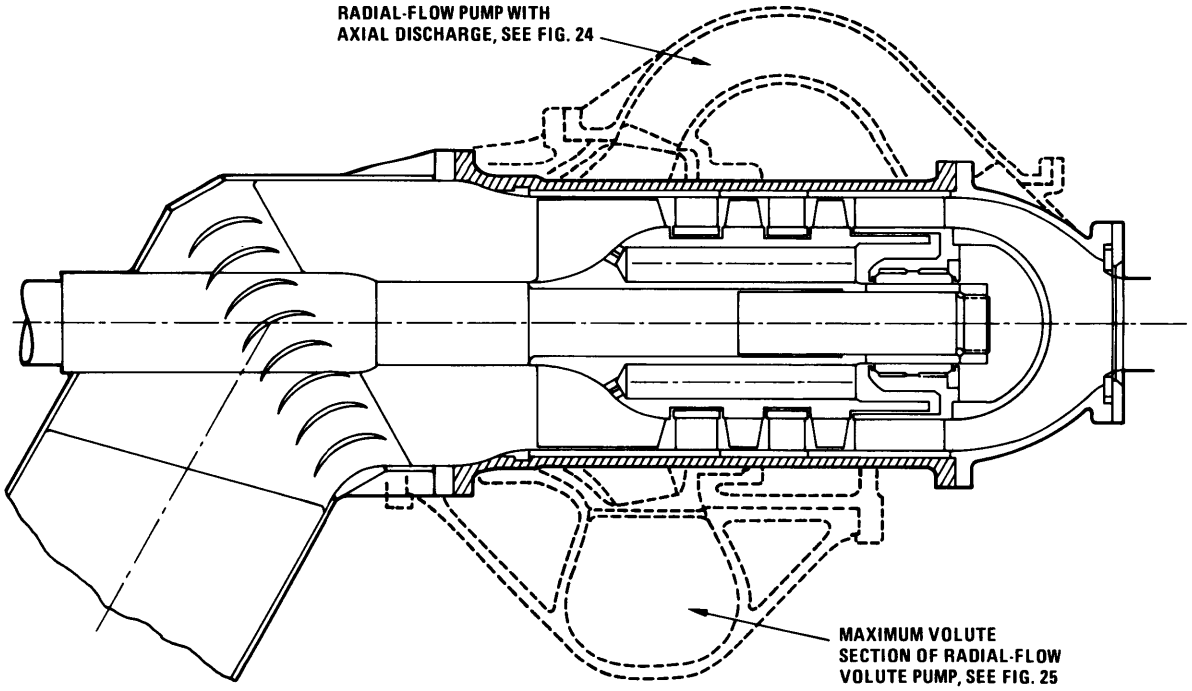


Figure 30 – Comparison of Axial-Flow and Radial-Flow Pumps

$$V_{m_i} \times \frac{D_i^2 \pi}{4} \left(1 - \frac{D_{h_i}^2}{D_0^2}\right) = V_{m_2} \frac{D_i^2 \pi}{4} \left(1 - \frac{D_{h_2}^2}{D_0^2}\right)$$

where it must be recognized that $D_0 = D_i$ = constant and $U_0 = U_i$ = constant. With $V_{m_i}/U_i = 0.23$ (as before) and $V_{m_2}/U_0 = 0.50$, $V_{m_i}/V_{m_2} = 0.23/0.50 = 0.46 = (1 - D_{h_2}^2/D_0^2)/(1 - D_{h_i}^2/D_0^2)$. Then $D_{h_i}^2/D_0^2 = 0.3^2 = 0.09$ and $1 - D_{h_i}^2/D_0^2 = 0.91$, and hence, $1 - D_{h_2}^2/D_0^2 = 0.4185$ and $D_{h_2}/D_0 = 0.762$.

If the number of stages is designated by $N$, the head per stage is obviously $H_1 = H/N$. It will now be assumed that the head coefficient $\psi = 2g_0H_1/U^2$ has the same value (i.e., 1.0) as assumed previously for the radial-flow impeller at its minimum outside diameter, provided $\psi$ is evaluated at the root diameter of the impeller discharge, i.e.,

$$\psi_{2,h} = \frac{2g_0H/N}{U_{2_h}^2} = 1.0$$

Hence

$$\left(\frac{2g_0H}{U_{0_{rad}}^2}\right) = \left(\frac{2g_0H/N}{U_{2_h}^2}\right)$$

The subscript rad refers to the previously described radial-flow pmp. Consider that $U_{i_{rad}} = U_{0_{axial}}$ therefore

$$N = \frac{U_{0_{rad}}^2}{U_{2_h}^2} = \left[\frac{U_{0_{rad}}}{U_{i_{rad}}} \frac{U_{0_{ax}}}{U_{2_h}}\right]^2 = \left[\frac{1.37}{0.7625}\right]^2 = 3.23$$

Assuming $N = 3$, the head coefficient $\psi$ at the discharge root diameter of the axial stages would be

$$\psi_h = \frac{2g_0H/N}{U_{2_h}^2} = \frac{2g_0H}{U_{0_{rad}}^2} \frac{U_{0_{rad}}^2}{U_{2_h}^2} \frac{1}{N} = \frac{3.23}{3} = 1.076$$

However, $(2g_0H/N\ U_{2_h}^2) = 1.076 = 2\ \eta_h\ (\Delta V_{u_{2_h}}/U_{2_h})$. Assuming $\eta_h = 0.90$,

$$\frac{\Delta V_{u_{2_h}}}{U_{2_h}} = \frac{1.076}{1.8} = 0.598$$

This value, together with $V_{m_2}/U_0 = 0.5$ or $V_{m_2}/U_{2_h} = (V_{m_2}/U_0) \times (U_0/U_{h_2}) = 0.656$, determines the root velocity diagram as shown in Figure 31 under the assumption of zero rotation of the absolute flow at the runner inlet. This diagram shows that the retardation ratio of the relative flow through the runner is $w_{2_h}/w_{1_h} = 0.642$ at the root section (subscript $h$) which is acceptable. The retardation in the stator vane system (returning flow to the axial direction) is $V_{m_2}/V_{2_h} = 0.747$ which is more conservative. The foregoing assumption of the flow coefficient $V_{m_2}/U_0 = 0.50$ with the resulting hub-to-tip diameter ratio of 0.7625 (except at the inlet to the first stage) and three stages has therefore lead to a satisfactory result. Of course, these assumptions can be altered. For example, a hub-to-tip diameter ratio slightly larger than 0.7625 would reduce the head coefficient $\psi$ and thereby $\Delta V_{u_{2_h}}/U_{2_h}$. This would give a more conservative retardation of the flow. Alternately a "symmetrical" velocity diagram as shown in Figure 32 could have been selected. This would also lead to a (slightly) more conservative retardation ratio (0.661). Retardation in the stator would also be 0.661.

The outlines of the radial-flow pumps previously calculated and shown in Figures 24 and 25 are indicated on Figure 30 by dashed lines. It is fairly evident that without being longer than the radial-flow pump with axial discharge, the three-stage, axial-flow pump is considerably smaller in diameter than the radial-flow machines designed for the same operating conditions. Thus the multistage, axial-flow pump is probably lighter than corresponding radial-flow machines, and this may be of considerable value in the propulsion field. This advantage would be lost to a large extent if discharge is desired at a right angle to the shaft. Furthermore, one cannot assume that the smaller axial-flow pump would be less expensive than radial-flow machines because the former requires a much larger number of blades, and these must be machined or otherwise manufactured to a high degree of precision. On the other hand, the advantage of useful operating ranges usually claimed for the radial-flow machine (at constant speed of rotation) is probably less important in the marine propulsion field than in other fields since propulsion pumps usually do not have to operate very far away from their design conditions. It does appear that the multistage axial-flow pump requires serious consideration (1) because of its lower weight and size (for the same performance and specific speed), (2) because of the relative simplicity and resulting reliability of its casing construction, and (3) because existing knowledge on axial-flow machines is more dependable than the predominantly empirical knowledge in the radial-flow field. However, this better knowledge exists primarily in the aerospace industry rather than in the commercial pump field.

Axial-flow pumps may also be used with a vertical shaft although this arrangement does not appear to be as natural as the vertical shaft arrangement of volute pumps. In this case one might use a (rotatable) 90 deg vane elbow at the discharge end of the pump, and have the drive shaft pass through this elbow. Alternately, the discharge from the last stage could be collected in a (rotatable) volute casing which would be fairly large, thus negating much of the size advantage of axial-flow pumps.

The foregoing design considerations have been carried out largely on the basis of one particular specific speed required for the propulsion pump. It is hoped that these considerations are sufficiently broad

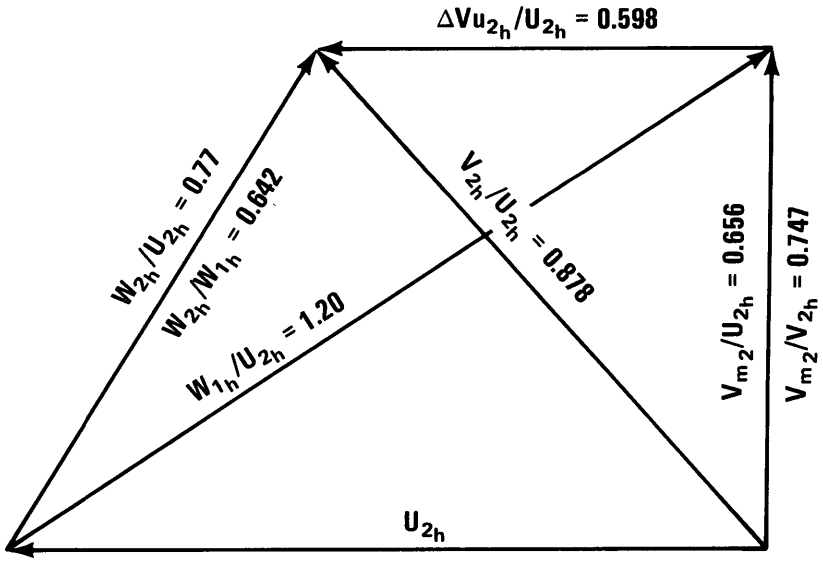


Figure 31 – Root Velocity Diagram of Axial-Flow Stages Except First

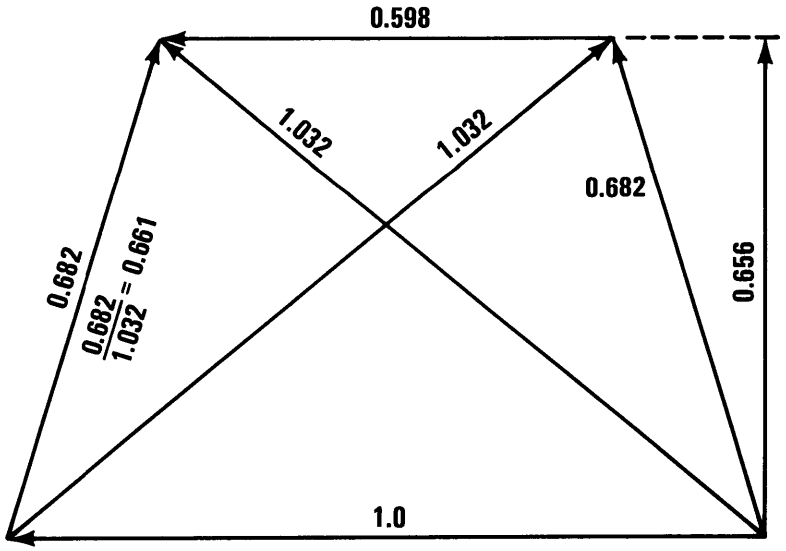


Figure 32 – Symmetrical Root Velocity Diagram of Axial-Flow Stages

to permit the design of propulsion pumps of different specific speeds so long as the specific speed does not depart too radically from the range covered by this presentation. It is therefore appropriate to investigate briefly the *range of specific speeds* that are likely to be encountered in the marine propulsion field.

The primary variable appears to be the Thoma parameter:

$$\sigma_H = \frac{H_{sv}}{H} = \frac{1 - K + \dfrac{2g_0}{V_0^2}\,(h_{sv} - \Delta h_j)}{2\,\dfrac{\Delta V}{V_0} + \left(\dfrac{\Delta V}{V_0}\right)^2 + K + \dfrac{2g_0\,\Delta h_j}{V_0^2}} \tag{3.35}$$

Recall that according to Chapter 2 (Figures 4 and 5), $\Delta V/V_0$ and $K$ are very closely related for optimum conditions and that $h_{sv} - \Delta h_j$ and $\Delta h_j$ (elevation of inlet and discharge of the propulsion pump) change very little compared with $V_0^2/2g_0$. Thus it should be possible to represent $\sigma_H$ as a function of $\Delta V/V_0$ and $V_0$ (the speed of travel). This evaluation of Equation (3.35) was carried out (see Figure 33) for an intake drag coefficient of $K_T$ = 0.05 and the following assumption about the relationship between $\Delta V/V_0$ and $K$ (based on Figure 5 in Section 2.2:

| $\Delta V/V_0$ | $K$ |
|---|---|
| 0.5 | 0.1 |
| 0.6 | 0.2 |
| 0.7 | 0.3 |
| 0.8 | 0.4 |
| 0.9 | 0.5 |
| 1.0 | 0.6 |

The relationship between $\sigma_H$ and the specific speed is given by Equation (3.36):

$$n_s = S_c \times {\sigma_H}_c^{3/4} = S_1\,{\sigma_H}_1^{3/4} \tag{3.36}$$

The relation between $S_c$ and $S_1$ was discussed in Section 3.3 and presented by Equations (3.40) and (3.41) as well as Figure 23. For a low-speed to cruise-speed ratio $V_1/V_c$ of one-tenth the suction specific speed ratio, $S_1/S_c$ ranges from 3 (at slightly less than 60 knots) to 6 (at slightly over 100 knots). At a speed ratio $V_1/V_c$ = 0.4, the ratio $S_1/S_c$ ranges from 2 to 3 with varying speed of travel. Thus the total range of $S_1/S_c$ to be considered is from 2 to 6; however, the most probable range of this variable is much smaller. A range from 2.5 to 5 was assumed, with a mean value of 3.5.

For the maximum suction specific speed $S_1$, the same value of 1 (17,170 $gal^{1/2}/min^{3/2}$ $ft^{3/4}$ in dimensional form) was assumed as before. A different value can easily be taken into account since the resulting specific speed is proportional to the value assumed for $S_1$. With the aforementioned range of the suction specific speed ratios $S_1/S_c$, the range for $S_c$ is from 0.2 to 0.4, with a mean value of 0.286. Equation (3.36) then determines the basic specific speed $n_s$.

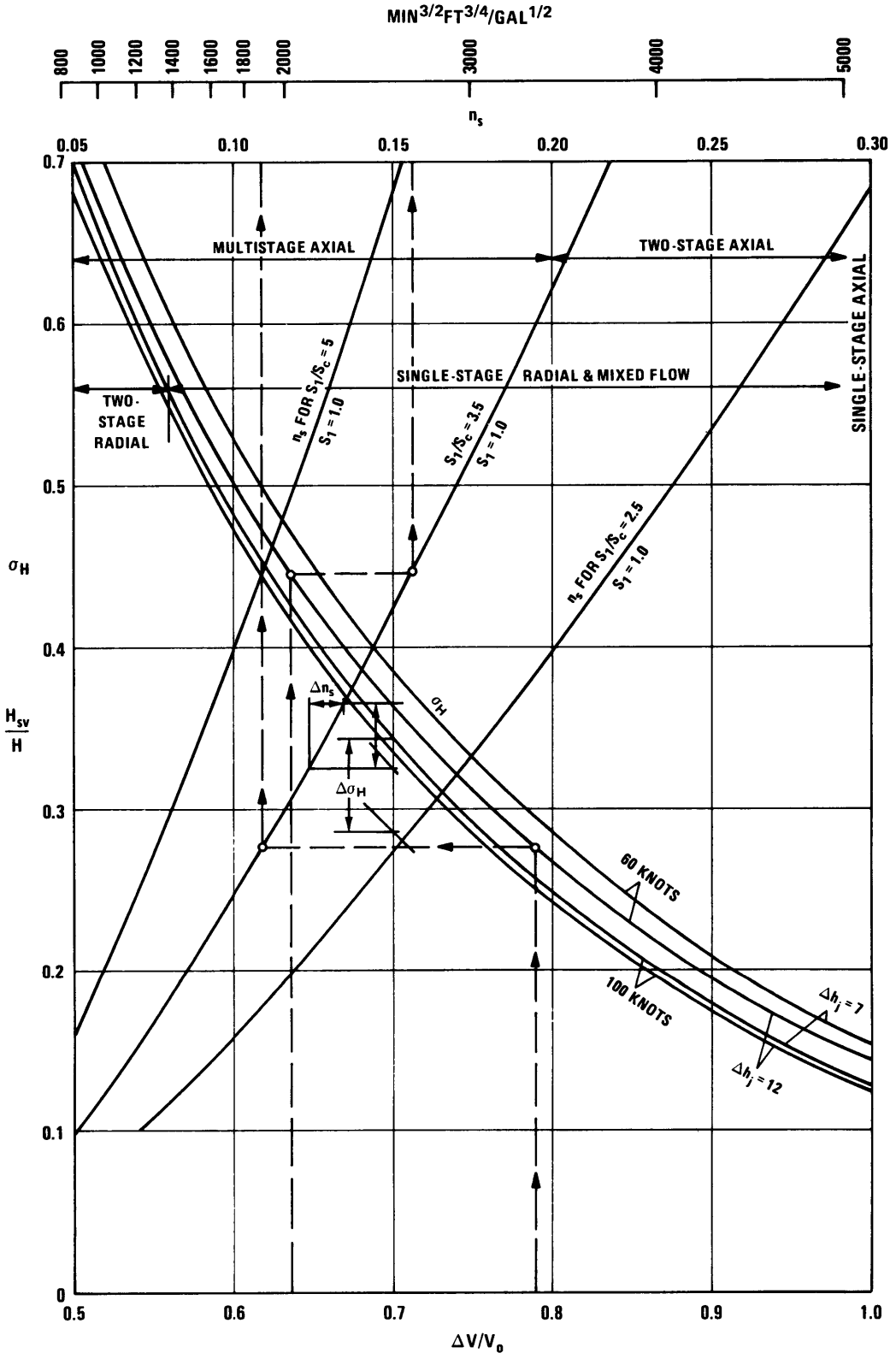


Figure 33 – Basic Specific Speed as a Function of $\Delta V/V_0$

The basic specific speeds so obtained are also plotted in Figure 33 as a function of $\sigma_H = H_{sv}/H$. However, it is not necessary to read the $\sigma_H$ value since one can go directly from the $\Delta V/V_0$ versus the $\sigma_H$ curves to the $S_1/S_c$ versus $n_s$ curves as indicated. Thus one can directly relate the range of $\Delta V/V_0$ to a corresponding range in basic specific speed. Although extreme conditions have been excluded, it is nevertheless evident that the resulting range in basic specific speed is quite considerable. At the high specific-speed end, it approaches the area of single-stage, axial-flow machines with high hub-to-tip diameter ratios at the discharge side, similar to the first stage of the pump shown in Figure 30. At the low-speed end ($n_s$ = 0.05), it touches the area of multistage, axial-flow pumps, or single- to two-stage, radial-flow pumps, or a combination of axial stages with one radial stage. The intermediate range of basic specific speeds is covered by Figures 24, 25, and 30.

It must be remembered that Figure 33 does not by any means cover all possible design conditions. This will be illustrated by comparison with the design examples given in Table 1. In that table the propulsor velocity ratio $\Delta V/V_0 = 0.7$ was coupled with a duct-loss coefficient $K = 0.4$ whereas in Figure 33 the ratio $\Delta V/V_0 = 0.7$ was coupled with $K = 0.3$. Both assumptions are justifiable, but the difference in the results derived under these two assumptions is not entirely negligible. As noted in Figure 33, $\Delta\sigma_H$ is the difference in $\sigma_H$ between results for $K = 0.3$ and 0.4 (the lower $\sigma_H$ applies to $K = 0.4$). The corresponding difference in basic specific speed $\Delta n_s$ is about 100 $\text{gal}^{1/2}/\text{min}^{3/2}\ \text{ft}^{3/4}$ in dimensional form; this is not major but neither is it completely negligible. Other variations should be considered; the most important is a variation in the maximum suction specific speed $S_1$. Higher values than $S_1 = 1.0$ (17,170 $\text{gal}^{1/2}/\text{min}^{3/2}\ \text{ft}^{3/4}$) should certainly be considered and may be found feasible. All basic specific speeds could then be increased proportionally to $S_1$. On the other hand, lower values may be found desirable to ensure long life relative to cavitation damage. A maximum suction specific speed of $S_1 = 1.0$ is merely a convenient and plausible reference value which the author believes is not too far from a practical maximum.

The last consideration to be briefly discussed in this section is the relation between the speed of rotation (or specific speed) and the volume and weight of a pump. This relation is essential in order to justify the contention that the specific speed should be chosen as high as possible for reasons of weight (and volume). In this consideration, weight and volume will be treated as proportional to each other; mass density, including that of the fluid, will be assumed constant although the actual relation between weight and volume must be pressure dependent.

It has been shown[3] that for dimensional reasons, the weight $W$ of a rotating machine is in first approximation proportional to the shaft torque $M$, i.e.,

$$W = \text{constant } M \tag{3.48}$$

where the constant of proportionality has the dimension: weight per unit volume divided by stress $[(F/L^3)(F/L^2) = 1/L]$, which renders Equation (3.48) dimensionally (and physically) consistent. It is realized that such consistency alone does not prove general validity, but it *is* sufficient for the following comparisons.

Consider the case of a rotating and torque-transmitting shaft of diameter $D$ and length $L$. Its volume is obviously proportional to $D^2L$, and its weight $W$ = constant $w\,D^2L$, where $w$ is the weight per unit volume. The torque is $M$ = constant $\tau\,D^3$, where $\tau$ is the shear stress.

Assuming geometric similarity, so that $L$ = constant x $D$, then, $W$ = constant, $w\,D^3$. With $M$ = constant x $\tau$ x $D^3$, one finds

$$W = \text{constant } (w/\tau)\, M \tag{3.49}$$

which agrees with Equation (3.48).

If, on the other hand, one assumes $L$ = constant (changes in diameter only), then:

$$W = \text{constant } M^{2/3} \tag{3.50}$$

where the constant of proportionality is dimensionally quite complex.

Since for the same power $M$ x $n$ = constant ($n$ is the speed of rotation), one derives from Equations (3.48) and (3.49):

$$W = \frac{\text{constant}}{n} \tag{3.51}$$

whereas from Equation (3.50):

$$W = \frac{\text{constant}}{n^{2/3}} \tag{3.52}$$

In the case of radial-flow pumps, it is evident that for the same head and the same peripheral velocity ($U_0$), the impeller diameter is $D$ = constant/$n$. However, the overall pump diameter $D_p$ is not proportional to the impeller diameter since the passages outside the impeller have approximately constant dimensions ($\Delta D$ and axial width $b$). The volume and weight of the pump is $W$ = constant $(D + \Delta D)^2 b$ where $b$ and $\Delta D$ are constants. Hence:

$$\frac{W}{W_0} = \frac{(D + \Delta D)^2}{(D_0 + \Delta D)^2} = \left[\frac{D}{D_0 + \Delta D} + \frac{\Delta D}{D_0 + \Delta D}\right]^2$$

where the subscript 0 denotes a reference case with which other cases can be compared. Let this reference case be characterized by $D_0 = \Delta D$, i.e., the case where the casing has about twice the diameter of the impeller. This case will be the definition of $W_0$, approximately represented by Figure 25 where $n_s$ = 0.135. With $D_0 = \Delta D$, the above expression for the weight ratio assumes the form:

$$\frac{W}{W_0} = \left(\frac{D}{2D_0} + \frac{1}{2}\right)^2 = \frac{1}{4}\left(\frac{D}{D_0} + 1\right)^2$$

For the same head and capacity; $D/D_0 = n_{s_0}/n_s$. Hence

$$\frac{W}{W_0} = \frac{1}{4}\left[\frac{n_{s_0}}{n_s} + 1\right]^2 \tag{3.53}$$

The evaluation of this equation is presented in Figure 34.

For purposes of comparison, Figure 34 also shows in broken lines the similarity relation $W$ = constant/$n_s$ corresponding to Equations (3.48) and (3.51). Note that the law derived here for radial-flow pumps (Equation (3.53)) agrees with the simple similarity relation from $n_s/n_{s_0}$ = 0.5 to 2 about as closely as the assumed law (or any other law) can possibly be expected to agree with reality. The assumed relation for radial-flow pumps, Equation (3.53) and Figure 34, is therefore considered as a confirmation of the similarity relation $W$ = constant/$n_s$.

The last approximation to be considered is the effect of speed of rotation on weight, *assuming that the variation in speed of rotation or specific speed is achieved by a change in the number of stages.* This consideration obviously applies to pumps of the type shown in Figure 30. The weight of the pump is divided into two parts: (1) $W_a$ proportional to the number of stages $N$, i.e., $W_a$ = constant $N$, and (2) $W_b$ the inlet and discharge part which is independent of the revolutions per second and the number of stages. The reference condition, described by subscript 0 and depicted approximately in Figure 30, is characterized by $W_{a_0} = W_b$. In other words, at this specific speed ($n_{s_0}$), the head and the part of the weight ($W_b$) that is independent of the number of stages is equal to the speed and the part of the weight ($W_a = N\,W_1$) that is dependent on the number of stages. With $N$ stages, $W = N \times W_1 + W_b$ where $W_1$ and $W_b$ are constants. However, for the same diameter and stage-head coefficient ($\psi_1 = 2g_0H_1/U^2$), $N \times n^2$ = constant x $H$ = constant. Hence $N$ = constant/$n^2$ and $W_a$ = constant/$n^2$.

Thus, with respect to the reference weight $W_0$:

$$\frac{W}{W_0} = \frac{W_a}{W_{a_0}}\frac{(1 + W_b/W_a)}{(1 + W_b/W_{a_0})} = \frac{n_0^2}{n^2}\,\frac{1}{2}\left(1 + \frac{W_b}{W_{a_0}}\frac{W_{a_0}}{W_a}\right) = \frac{n_0^2}{n^2}\,\frac{1}{2}\left(1 + \frac{n^2}{n_0^2}\right)$$

where $W_b = W_{a_0}$, and $W_{a_0}/W_a = n^2/n_0^2$ was used. Hence:

$$\frac{W}{W_0} = \frac{1}{2}\left(\frac{n_0^2}{n^2} + 1\right) = \frac{1}{2}\left(\frac{n_{s_0}^2}{n_s^2} + 1\right) \tag{3.54}$$

This curve is also plotted in Figure 34; there it departs somewhat more (but in the same direction) from the similarity curve $W$ = constant/$n_s$ than the curve previously derived for radial-flow pumps.

It may thus be concluded that for moderate steps in speed, the similarity relation

$$W = \frac{\text{constant}_1}{n} = \frac{\text{constant}_2}{n_s}$$

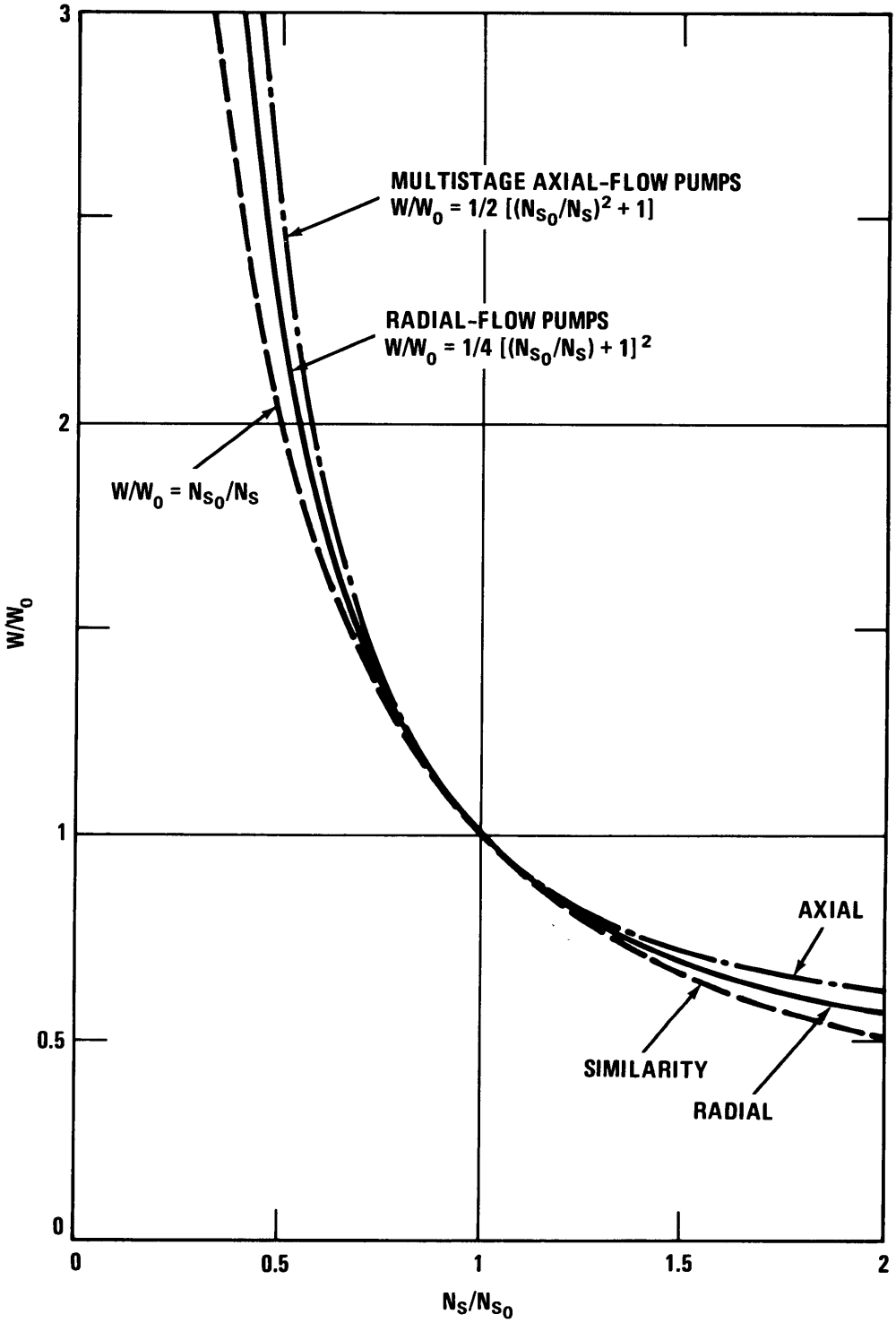


Figure 34 – Pump Weight as a Function of Basic Specific Speed

[$\eta_{s_0}$ *approximately* 0.135 (2300)]

gives a fair approximation of the pump weight as a function of the speed of rotation (or specific speed) and is within the limits of accuracy obtainable on *general* grounds. Relative to the reference specific speed $n_{s_0}$ (defined by $\Delta D = D$ and $W_a = W_b$, respectively), the weight does not diminish as fast as $1/n_s$ for an increase in specific speed ($n_s > n_{s_0}$) whereas it increases faster than $1/n_s$ for a decrease in specific speed ($n_s < n_{s_0}$). It must be repeated that the specific speed is a criterion of weight or size only for one type of pump. The comparison between Figures 24, 25, and 30 clearly shows that a step to the axial-flow type brings a saving in size and weight as great or greater than achievable by any practical increase in basic specific speed.

Note that practically all design considerations presented in this section as well as elsewhere in this report are carried out in a dimensionless fashion. This is natural and proper since operating conditions such as $\Delta V/V_0$ are used in dimensionless form. Yet somewhere the step must be taken to a dimensionally determined design.

Quite intentionally, most dimensions of the propulsion pump were related directly or indirectly to the impeller *inlet* diameter $D_i$. By using the relation $T = \rho_f Q \Delta V$, it is relatively easy to refer this diameter to the absolute operating conditions prescribed, namely, the thrust $T$, the cruise speed of travel $V_0$, and the rate of volume flow $Q$. The impeller inlet diameter $D_i$ is derived from the condition of continuity: $Q = V_{m_i} D_i^2 \pi/4 \times (1 - D_h^2/D_i^2)$. The meridional impeller inlet velocity $V_{m_i}$ is best related to the total inlet head $H_{sv}$ (NPSH) by the ratio $2g_0 H_{sv}/V_{m_i}^2$ which does not vary over very wide limits (say, from 2 to 4) and does appear in the dimensionless calculations.

It would have been equally possible to make the design dimensionless by a different dimension, say, the discharge jet diameter $D_j$. A relationship for $D_j$ very similar to that for $D_i$ could be derived, but this will be left to the reader. $D_j$ may be a very useful reference diameter for the discharge duct system, but it would not be as convenient as $D_i$ for the pump and the inlet duct system.

## 3.5 PROPULSION PUMPS IN PARALLEL, INCLUDING DOUBLE-SUCTION PUMPS

The effect of operating several pumps in *parallel* was briefly mentioned in Section 3.1.2 with particular reference to the suction characteristics of pumps. The considerations mentioned there for single-suction pumps apply immediately to pumps with several ($N$) inlets in parallel if the rate of volume flow $Q$ is defined as the rate of volume flow *per inlet*. The resulting fundamental relations have already been outlined in Section 3.1.2; they apply not only to the suction specific speed but also to the basic specific speed.

The principal practical design problem for pumps with multiple inlets to the impeller(s) is one of *arrangement*, and that topic will therefore consistute a major part of this section. In addition, some elementary similarity considerations are in order regarding the weight of several pumps in parallel compared to a single pump with the same total capacity as the pump-aggregate.

Let $W_1$ be the weight for every pump of an aggregate of $N$ pumps *in parallel*. The total weight $W_0$ of the aggregate is obviously $W_0 = N\, W_1$.

Rather than $N$ pumps in parallel, consider one larger pump with the capacity $Q = N\,Q_1$, where $Q_1$ is the capacity of one pump of the aggregate of $N$ pumps in parallel. Let $D$ be a representative linear dimension of the single large pump and $D_1$ the corresponding dimension of every one of the $N$ pumps in parallel. Since the pump head and suction head must be the same for all pumps compared, the velocities are also the same, so that:

$$N = \frac{Q}{Q_1} = \frac{D^2}{D_1^2} \tag{3.55}$$

However, for completely similar pumps:

$$\frac{W}{W_1} = \frac{D^3}{D_1^3} \tag{3.56}$$

where $W$ is the weight of the single pump with the total capacity $Q$. Comparing this with the weight of $N$ pumps in parallel, one finds:

$$\frac{W}{N\,W_1} = \frac{D^3}{ND_1^3} = \frac{D_1^2}{D^2}\,\frac{D^3}{D_1^3} = \frac{D}{D_1} = N^{1/2} \tag{3.57}$$

which merely confirms the well-known fact that a single large pump is heavier than several pumps in parallel according to the familiar "square-cube law."

Evidently the speed of rotation of $N$ pumps in parallel is higher than that of a single pump according to $N \times D = N_1\,D_1$, or

$$\frac{n_1}{n} = \frac{D}{D_1} = N^{1/2} \tag{3.58}$$

In accordance with the preceding section, assume that the weight of any directly coupled driver or transmission is inversely proportional to the speed of rotation. Comparison with Equation (3.57) indicates that the weight of any directly coupled driver or transmission is reduced in the same ratio as the weight of the pumps, i.e., inversely proportional to $N^{1/2}$.

The foregoing consideration is based on the assumption that the individual pumps of an aggregate of $N$ pumps in parallel are completely similar to a single pump having the total capacity of the aggregate. This assumption is rarely justified.

For several pumps on the *same* shaft, the shaft diameter *relative to the pump* is larger than for a single pump; this is a disadvantage that lessens the weight advantage of $N$ pumps in parallel. Furthermore, the inlet (and discharge) duct system for several pumps in parallel is more complex than for a single pump, and that also reduces the advantage of pumps in parallel.

On the other hand, it is quite possible to place several parallel pumps into *one* casing. This is standard practice with two pumps in parallel in the form of the well-established "double-suction" design shown in Figure 35 in comparison with a single-suction pump. The weight advantage of placing two back-to-back impellers into one casing should be obvious.

Figures 36 and 37 show three double-suction pumps, i.e., six pump-halves in parallel placed into one casing. This is a new design and would require a special development effort. The aforementioned complex inlet and discharge duct system is incorporated into the casing in an attempt to minimize this disadvantage of pumps in parallel. In this case the diameter (and speed) advantage of the "multistream" pump is $\sqrt{6}$ = 2.45 under the assumption of the same hub-to-inlet diameter ratio for both pumps compared. The new design is compared in Figure 36 to a single-suction radial-flow pump (broken lines) with the same basic specific speed (and suction specific speed) as each half of the impellers of the multistream pump.

With double suction and multistreams, one will be tempted to use a somewhat lower suction specific speed for every "stream" than with one single-suction ("single-stream") pump. For this reason Figures 35-37 show a somewhat lower basic specific speed (and suction specific speed) for every stream than was considered in the preceding sections for single-suction pumps. However, the specific speeds of the single-suction pumps shown in Figures 35 and 36 are the same here as for every stream of the double-suction and the multistream pumps in order to achieve a clear comparison of size.

It is, of course, not necessary to combine a multistream arrangement into *one* casing. Two more or less *separate* double-section pumps in parallel have been used successfully in (at least) one important project. In such cases, the external multistream ducting must be considered in weight and efficiency comparisons. The required arrangements will be discussed in Chapter 4.

The comparisons shown in Figures 35 and 36 between single-stream and double-stream or multistream pumps must be a little disappointing to the reader, as indeed it was to the author. The comparison will be limited here to the pumps alone. The advantage of a directly coupled driver or transmission (gear box) was covered previously by the speed or torque ratio, insofar as general principles permitted.

It is somewhat difficult to estimate the weight advantage of the double-suction pump over the single-suction pump shown at the same scale in Figure 35. It is expected that (for the same head and rate of flow) the weight of the slower running single-suction pump will be greater than that of the equivalent double-suction pump. However, detailed studies of both forms of design are necessary in order to determine whether or not this weight advantage conforms to the ratio of $\sqrt{2}$ previously derived by very simple similarity considerations.

One might hope that a clearer answer can be obtained from a more drastic step such as depicted in Figures 36 and 37. To achieve such a comparison, the lengths and average diameters are shown. The average diameter $D_{av}$ of the single-suction, single-impeller pump is about 1.5 times that of the multistream pump. On the other hand, the length of the pump alone (not counting the discharge nozzle which is the same for both types of pumps) for the single-suction, single-impeller pump is only 0.8 times that of the multistream pump.

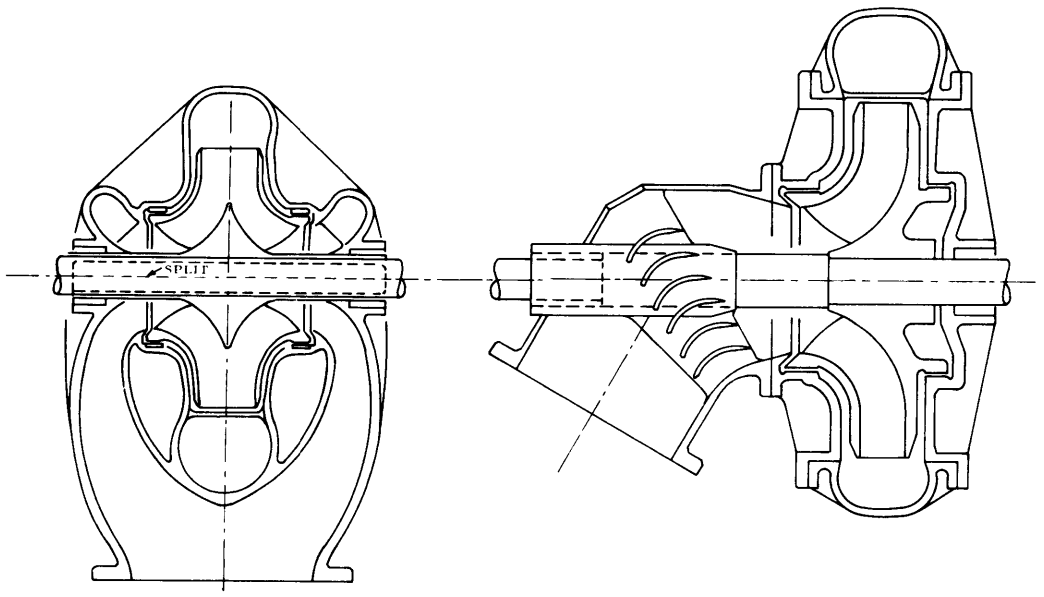


Figure 35 – Comparison of Single-Suction and Double-Suction Pumps

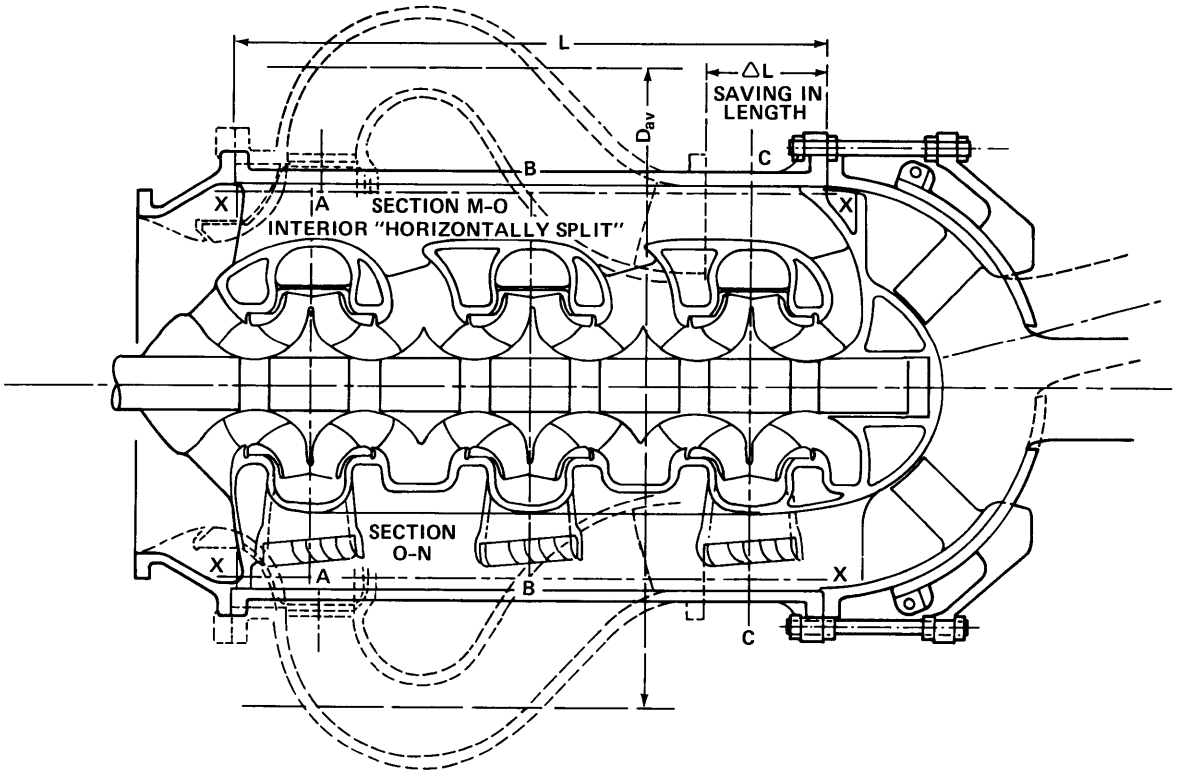


Figure 36 – Three Double-Suction Pumps in Parallel in One Casing

(See Figure 37 for Sections A-A, C-C, and X-X. The dashed lines are for a single-suction radial-flow pump with the same basic and suction specific speeds as each half of the impellers of the multistream pump)

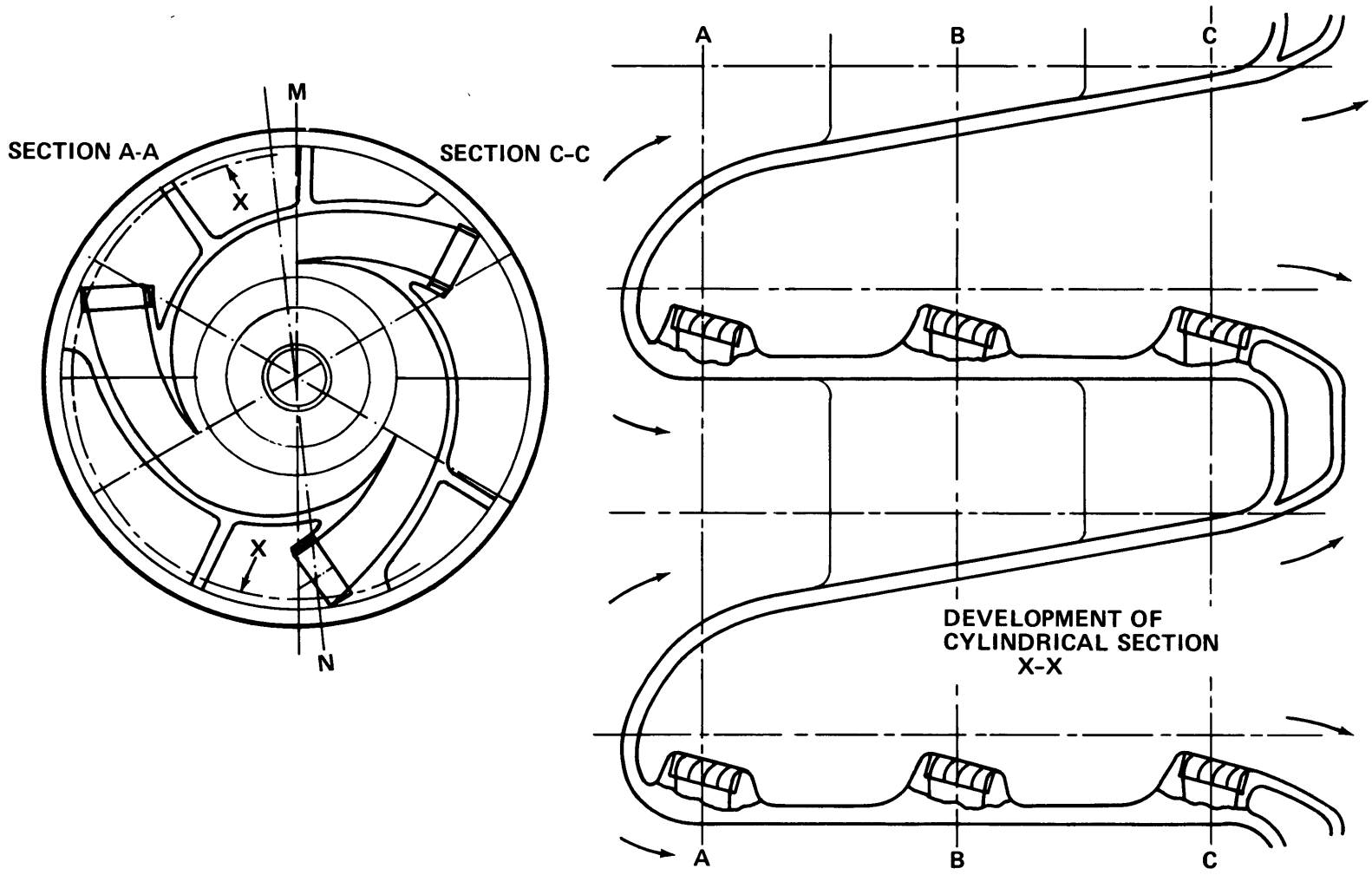


Figure 37 – Sections A-A, C-C, and X-X for the Double-Suction Pumps of Figure 36

Hence the weight of the single-suction, single-impeller pump may be estimated to be 0.8 x $1.5^2$ = 1.8 times that of the multistream pump. This estimate falls short of the estimate based on similarity considerations which, according to Equation (3.57), gives a ratio of $\sqrt{6}$ = 2.45.

One must conclude that the complex ducting (necessary with any double or multistream arrangement) is responsible for the fact that the weight savings for double-suction or multistream pumps is not as great as predicted on theoretical grounds. This ducting was incorporated into the pump casing for the examples presented in Figures 35-37 and should minimize the weight penalty. As will be discussed in Chapter 4, the weight of the external ducting must, of course, also count against the weight advantage of pumps in parallel.

It is indeed doubtful whether a 45-percent reduction in pump weight is sufficient to justify the complication of the multistream arrangement shown in Figures 36 and 37. One should also include in this comparison the multistage, axial-flow design form discussed in Section 3.4 (Figure 30). The single-stream, multistage, axial-flow pump would probably not be heavier than the multistream, radial-flow pump shown in Figure 36. Several multistage, axial-flow pumps *in parallel* might show a weight advantage over one pump of this type. In any event, it seems doubtful whether the weight savings achievable by using pumps or pump streams in parallel justify the resulting complications unless the weight saved by driver(s) or transmission(s) turns out to be very significant.

The multistream pump presented in Figure 36 is shown in connection with a discharge nozzle that is adjustable over a total range of 30 deg in direction (plus and minus 15 deg). However, this feature has nothing to do with the multistream arrangement of this pump, and would also be applicable to the single-suction pump shown in Figure 24 or by the dashed lines in Figure 36. Similarly, the adjustment of the discharge nozzle *area* shown in Figure 24 would also be applicable to any other propulsion pump, for example, that indicated in Figure 30.

A *combination* of adjustability of the jet *direction* (Figure 36) and adjustability of the nozzle *area* (Figure 24) might be unreasonably complicated unless adjustability of jet *direction* is achieved by rotation of the pump or pump casing as indicated in Figures 28 and 29.

## 3.6 EFFECT OF CONSTANT DISCHARGE NOZZLE AREA ON OPERATION AT GREATLY REDUCED SPEEDS OF TRAVEL

It has been mentioned repeatedly that the propulsor thrust versus speed-of-travel curves in Figures 21 and 22, together with Equation (3.38) from which these curves were calculated, are based on the assumption that for the given pump and speed of rotation, the rate of flow $Q$ and the pump head $H$ are the same at cruising speed of travel (subscript $c$) and at any reduced speed of travel (subscript 1), i.e., that

$$Q_1 = Q_c, H_1 = H_c, \text{ at } n_1 = n_c \tag{3.59}$$

This set of equations obviously specifies similar flow conditions in the same propulsion pump in the usual sense of these words.

It was also stated that Equations (3.59) can be satisfied only if the discharge nozzle area is (slightly) adjustable.

It is the purpose of this section to show how $Q$ and $H$ will change (at constant speed of rotation $n$) from cruising speed to reduced speed of travel for a *fixed* discharge jet nozzle area $A_j$. The answer is obtained here by a process of successive approximations although a more elegant, closed solution may be possible.

As a first approximation, assume that $H_1 = H_c$ and determine the relation between $Q_1$ and $Q_c$ on the basis of the condition of continuity with a constant nozzle discharge area $A_j$, i.e.:

$$\frac{Q_1}{V_{j_1}} = \frac{Q_c}{V_{j_c}} = A_j = \text{constant} \tag{3.60}$$

Under the assumption of constant pump head, the jet velocity:

$$V_j = V_0 + \Delta V = V_0 \left(1 + \frac{\Delta V}{V_0}\right) \tag{3.61}$$

can be calculated from Equation (3.38); $\Delta V/V_0$ can be assumed to be given for the cruising conditions by Figures 4 or 5. From Equation (3.38) one obtains:

$$2\left(\frac{\Delta V}{V_0}\right)_1 + \left(\frac{\Delta V}{V_0}\right)_1^2 = \frac{V_c^2}{V_1^2}\left[2\left(\frac{\Delta V}{V_0}\right)_c + \left(\frac{\Delta V}{V_0}\right)_c^2 + K_c\right] - K_1 \tag{3.62}$$

which can be solved for $(\Delta V/V_0)_1$ if an assumption is made for the duct-loss coefficient $K_1$, for example, that $K_1 = K_c$. (Recall that $K_c$ had to be assumed or estimated from the duct geometry in order to determine $(\Delta V/V_0)_c$ from Figures 4 or 5).

The approximation of $(\Delta V/V_0)_1$ obtained from Equation (3.62) for the low speed-of-travel condition can be used to determine the corresponding rate of flow $Q_1$ from the condition of continuity for the discharge jet nozzle according to Equation (3.60) with the notation $V_1 = V_{0_1}$, $V_c = V_{0_c}$, $(\Delta V/V_0)_1 = \Delta V_1/V_{0_1}$, and $(\Delta V/V_0)_c = \Delta V_c/V_{0_c}$. Thus,

$$Q_1 = Q_c \frac{V_1 + \Delta V_1}{V_c + \Delta V_c} = Q_c \frac{1 + (\Delta V/V_0)_1}{1 + (\Delta V/V_0)_c} \times \frac{V_1}{V_c} \tag{3.63}$$

and from this, a first approximation for the thrust at reduced speed is:

$$T_1 = \rho Q_1 \Delta V_1 \tag{3.64}$$

and

$$\frac{T_1}{T_c} = \frac{Q_1}{Q_c} \times \frac{\Delta V_1}{\Delta V_c} \tag{3.65}$$

where

$$\frac{Q_1}{Q_c} = \frac{1 + (\Delta V/V_0)_1}{1 + (\Delta V/V_0)_c} \times \frac{V_1}{V_c} \tag{3.66}$$

and

$$\frac{\Delta V_1}{\Delta V_c} = \left(\frac{\Delta V}{V_0}\right)_1 \times \left(\frac{V_0}{\Delta V}\right)_c \times \frac{V_1}{V_c} \tag{3.67}$$

$\frac{\Delta V}{V_0}_1$ can be determined from Equation (3.62).

To obtain a better approximation than that based on $H_1 = H_c$, now calculate the change in pump head resulting from a change in rate of flow from $Q_c$ to $Q_1$. If it is assumed that in this small range of flow rate, the pump operates near its point of best efficiency, any change in efficiency can be disregarded.

Figure 38 shows typical impeller discharge velocity diagrams of a centrifugal pump that may be used for propulsion. These diagrams are shown for rates of flow at cruising and at reduced speed of travel. The change in the meridional velocity $V_m$ corresponding to the change from $Q_c$ to $Q_1$ is

$$\Delta V_m = V_{m_c} - V_{m_1} \tag{3.68}$$

and the corresponding change in the peripheral fluid velocity $V_u$ is

$$\Delta V_u = V_{u_c} - V_{u_1} = w_{u_1} - w_{u_c} \tag{3.69}$$

Since the direction of the relative discharge velocity can be assumed to be constant as shown in Figure 38, it follows that:

$$-\frac{\Delta V_u}{\Delta V_m} = \frac{w_u}{V_m} = \frac{U - V_u}{V_m}\ ;\ \frac{\Delta V_u}{U - V_u} = -\frac{\Delta V_m}{V_m} \tag{3.70}$$

$$\frac{\Delta V_m}{V_m} = -\frac{\Delta V_u}{V_u}\frac{1}{\frac{U}{V_u} - 1}$$

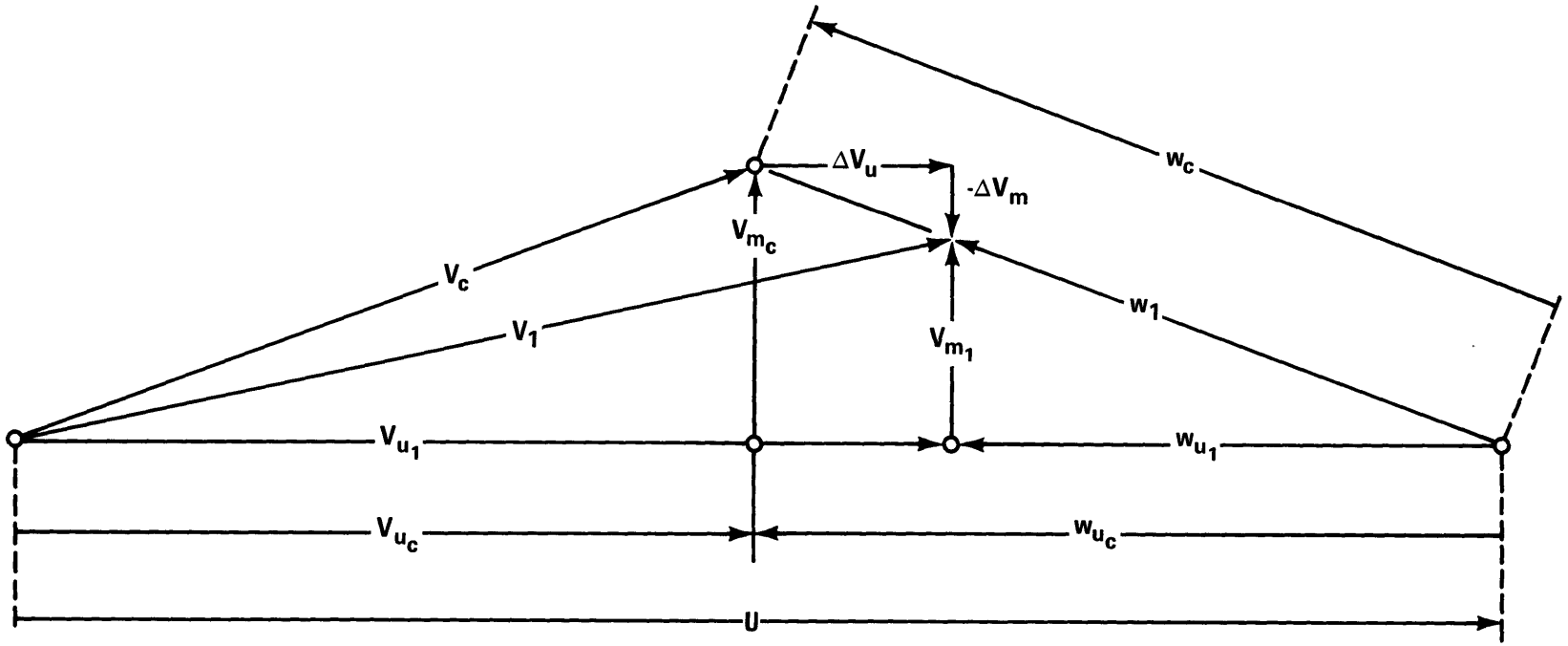


Figure 38 – Impeller Discharge Velocity Diagram for Cruising (c) and for Reduced-Speed (1) Rate of Flow

which applies to both subscripts 1 and $c$.

According to the Euler turbomachinery equation (3.9), for zero rotation of the absolute flow at the inlet side of the impeller, i.e., for $V_{u_i} = 0$:

$$g_0 H = \eta_h V_u U; \text{ or } \frac{g_0 H}{\eta_h U^2} = \frac{V_u}{U} \tag{3.71}$$

Hence Equation (3.70) can be written in the form:

$$\frac{\Delta V_m}{V_{m_c}} = - \frac{\Delta V_u}{V_{u_c}} \frac{1}{\frac{\eta_h U^2}{g_0 H} - 1} \tag{3.72}$$

According to Equations (3.69) and (3.71), one can write with $\eta_h$ = constant, and $U_1 = U_c = U$:

$$\frac{\Delta V_u}{V_{u_c}} = \frac{V_{u_c} - V_{u_1}}{V_{u_c}} = 1 - \frac{V_{u_1}}{V_{u_c}} = 1 - \frac{H_1}{H_c} \tag{3.73}$$

Furthermore the meridional velocity is obviously proportional to the rate of flow, so that

$$\frac{\Delta V_m}{V_{m_c}} = \frac{V_{m_c} - V_{m_1}}{V_{m_c}} = 1 - \frac{V_{m_1}}{V_{m_c}} = 1 - \frac{Q_1}{Q_c} \tag{3.74}$$

Substituting Equations (3.73) and (3.74) into Equation (3.72) leads to:

$$\left( \frac{\eta_h U^2}{g_0 H} - 1 \right) \left( 1 - \frac{Q_1}{Q_c} \right) = - \left( 1 - \frac{H_1}{H_c} \right) = \frac{H_1}{H_c} - 1 \tag{3.75}$$

thus permitting $H_1/H_c$ to be calculated as a function of $Q_1/Q_c$ and of the head coefficient $g_0 H/U^2$. This head coefficient and the "hydraulic efficiency" $\eta_h$ are given or can be estimated from the type and design of the pump. It is a fair approximation for standard centrifugal pumps to assume that $\eta_h U^2/g_0 H = 2$ for an average discharge diameter of the impeller; this can be said to determine the slope of the head-capacity curve. With this approximation, Equation (3.75) reduces to the simple relation:

$$\left( 1 - \frac{Q_1}{Q_c} \right) = \frac{H_1}{H_c} - 1 \tag{3.76}$$

The approximation for $Q_1/Q_c$ obtained under the assumption $H_1 = H_c$ (Equation (3.66)) can now be used to obtain a corresponding approximation for $H_1/H_c$. This ratio permits a second approximation to be made for $Q_1/Q_c$ and accordingly, for the thrust ratio $T_1/T_c$ (see Equation (3.65)) in the following manner.

According to Equation (3.37):

$$\frac{H_1 - \Delta h_j}{H_c - \Delta h_j} = \frac{\dfrac{H_1}{H_c} - \dfrac{\Delta h_j}{H_c}}{1 - \dfrac{\Delta h_j}{H_c}} = \frac{V_1^2}{V_c^2} \frac{2\left(\dfrac{\Delta V}{V_0}\right)_1 + \left(\dfrac{\Delta V}{V_0}\right)_1^2 + K_1}{2\left(\dfrac{\Delta V}{V_0}\right)_c + \left(\dfrac{\Delta V}{V_0}\right)_c^2 + K_c} \tag{3.77}$$

which can be solved for $(\Delta V/V)_1$ since $H_1/H_c$ is known from the approximation expressed by Equation (3.75) or (3.76) and all other variables are given from the initial design conditions. However, the result is not as general as obtained under the first approximation because the ratio $\Delta h_j/H_c$ depends on the absolute velocity of travel.

The new value of $(\Delta V/V_0)_1$ can now be used in Equation (3.66) to obtain a second approximation for the rate-of-flow ratio $Q_1/Q_c$ which, by Equations (3.67) and (3.65), leads to a second approximation for the thrust ratio $T_1/T_c$.

The second approximation for $Q_1/Q_c$ may be used in Equation (3.75) or (3.76) to obtain a third approximation for $H_1/H_c$. This, in turn, may be substituted into Equation (3.77) to find a better approximation for $(\Delta V/V_0)_1$ and thereby (by Equation (3.66)) for $Q_1/Q_c$, and so on.

The process described above will now be illustrated by calculating successive approximations of the thrust versus speed-of-travel curves for the design example discussed in Section 3.3 and presented in Table 1. Specifically, the following design values will be used:

Propulsion velocity ratio $(\Delta V/V_0)_c = 0.7$

Inlet and duct loss coefficient $K = 0.4$; $K_1 = K_c$

Elevation of the jet $\Delta h_j = 7$ ft

Velocity of travel (when needed) $V_0 = 60$ knots = 101.4 ft/sec

The calculations will be carried out for $V_1/V_c$ values of 0.1, 0.2, 0.4, and 0.6.

With $(\Delta V/V_0)_c = 0.7$ and $K_c = 0.4$, the following expression in Equations (3.62) and (3.77) assumes the constant value:

$$2\left(\frac{\Delta V}{V_0}\right)_c + \left(\frac{\Delta V}{V_0}\right)_c^2 + K_c = 2.29$$

Hence from Equation (3.37):

$$H_c = \frac{V_0^2}{2g_0} \quad 2.29 + 7 = 366 + 7 = 373 \text{ ft},$$

$$\frac{\Delta h_j}{H_c} = \frac{7}{373} = 0.019, \text{ i.e., the effect of } \Delta h_j \text{ is very small, and}$$

$$1 - \Delta h_j/H_c = 0.981.$$

The actual calculations are carried out according to Table 2, and the results are plotted in Figure 39 as functions of the speed-of-travel ratio $V_1/V_c$. It should be noted that in this figure, the ratios $H_1/H_c$ and $Q_1/Q_c$ are plotted at twice the scale of the thrust ratio $F_1/F_c$.

TABLE 2 – SUCCESSIVE APPROXIMATIONS OF THRUST VERSUS SPEED-OF-TRAVEL CURVES FOR THE DESIGN EXAMPLE GIVEN IN TABLE 1

**Adjustable Discharge Nozzle**

a. $H_1 = H_c : Q_1 = Q_c$

b. $2\left(\frac{\Delta V}{V_0}\right)_1 + \left(\frac{\Delta V}{V_0}\right)_1^2 = 2.29\ \frac{V_c^2}{V_1^2} \quad 0.4$

c. $\left(\frac{\Delta V}{V_0}\right)_1 = \sqrt{\left[2.29\ \frac{V_c^2}{V_1^2} \quad 0.4\right] + 1} \quad 1$

d. $\frac{\Delta V_1}{\Delta V_c} = \left(\frac{\Delta V}{V_0}\right)_1 \times \frac{1}{0.7} \times \frac{V_1}{V_c}$

$\frac{F_1}{F_c} = \frac{\Delta V_1}{\Delta V_c}$

**Fixed Nozzle, First Approximation**

a. $H_1 = H_c$

e. $\frac{Q_1}{Q_c} = \frac{1 + (\Delta V/V_0)_1}{1.7} \times \frac{V_1}{V_c}$

f. $\frac{F_1}{F_c} = \frac{Q_1}{Q_c}\ \frac{\Delta V_1}{\Delta V_c}$

**Fixed Nozzle, Second Approximation**

a. $H_1/H_c = (1 \quad Q_1/Q_c) + 1$

$(H_1/H_c \quad 0.019)/0.981 = HC$

b. $2\left(\frac{\Delta V}{V_0}\right)_1 + \left(\frac{\Delta V}{V_0}\right)_1^2 = 2.29\ HC\ \frac{V_c^2}{V_1^2} \quad 0.4$

c. $\left(\frac{\Delta V}{V_0}\right)_1 = \sqrt{\left[2.29\ HC\ (V_c/V_1)^2 \quad 0.4\right] + 1} \quad 1$

d. $\Delta V_1/\Delta V_c = \frac{(\Delta V/V_0)_1}{0.7} \times \frac{V_1}{V_c}$

e. $Q_1/Q_c = \frac{1 + (\Delta V/V_0)_1}{1.7} \times \frac{V_1}{V_c}$

f. $F_1/F_c = (Q_1/Q_c)\ (\Delta V_1/\Delta V_c)$

**Fixed Nozzle, Third Approximation**

a. $H_1/H_c = (1 \quad Q_1/Q_c) + 1$

$(H_1/H_c = 0.019)/0.981 = HC$

b. $2\left(\frac{\Delta V}{V_0}\right)_1 + \left(\frac{\Delta V}{V_0}\right)_1^2 = 2.29\ HC\ \frac{V_c^2}{V_1^{2\cdot}} \quad 0.4$

c. $\left(\frac{\Delta V}{V_0}\right)_1 = \sqrt{\left[2.29\ HC\ (V_c/V_1)^2 \quad 0.4\right] + 1} \quad 1$

d. $\Delta V_1/\Delta V_c = \frac{(\Delta V/V_0)_1}{0.7} \times \frac{V_1}{V_c}$

e. $Q_1/Q_c = \frac{1 + (\Delta V/V_0)_1}{1.7} \times \frac{V_1}{V_c}$

f. $F_1/F_c = (Q_1/Q_c)\ (\Delta V_1/\Delta V_c)$

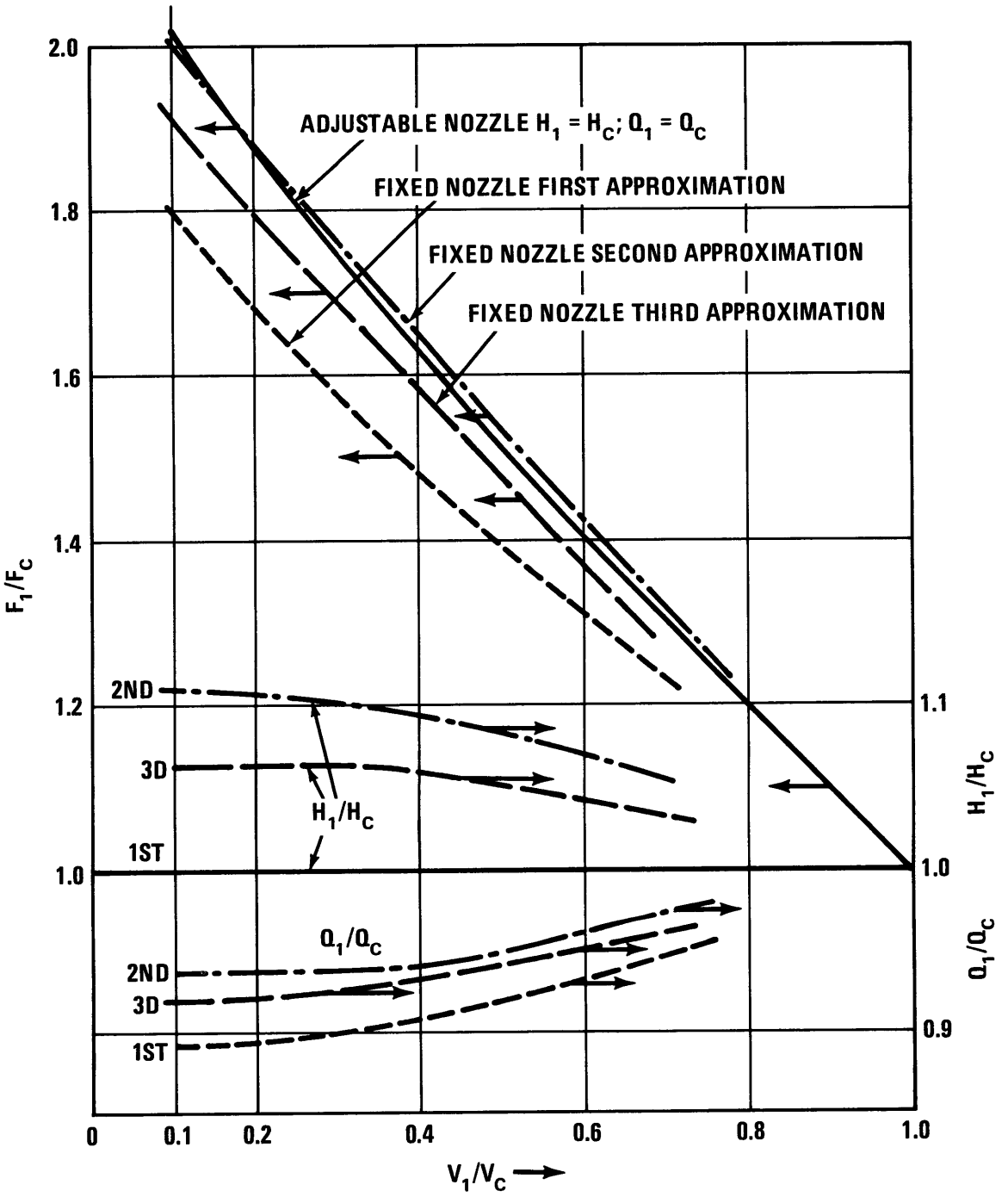


Figure 39 – Thrust versus Speed-of-Travel Ratios for $(\Delta V/V_0)_c = 0.7$

Figure 39 shows that the first and second approximations are quite inadequate for constant area ("fixed") nozzle operation. The final answer must be expected to lie between the second and third approximations, but is probably closer to the third. This means that the use of a constant-area jet nozzle reduces the thrust *increase* from cruise to reduced speed of travel by less than 10 percent, probably between 5 and 10 percent. (The reduction in total thrust at reduced speed lies between 2 and 5 percent). It is therefore questionable whether the complication of an adjustable area of the discharge nozzle can ever be justified. (Note that adjustability of the *intake* opening can hardly ever be avoided.)

## 3.7 IMPROVEMENTS GAINED BY DEPARTING FROM CONVENTIONAL PROPULSION PUMP PRACTICES

It is now necessary to consider whether major departures from more or less established practices in the field of propulsion pumps can be expected to lead to significant improvements in overall performance. The major sources of efficiency losses must be examined in order to focus attention on the areas where improvements should be sought.

With existing practices, the propulsion pump can be expected to have a pump efficiency between 85 and 90 percent. The highest pump efficiencies ever reported are between 92 and 93 percent. No methods are known whereby efficiencies can be obtained that exceed these values substantially. Improvements in the propulsion pump can therefore be expected to yield an increase in overall efficiency in the neighborhood of 4 percent. This small achievement is costly in that (assuming optimum design) it requires substantial reductions in internal surface imperfections compared with the *best* commercial pump practice.

Practically all sketches of propulsion pumps and their arrangements presented in this report show a very short *discharge* duct. This feature implies that discharge duct losses can be reduced by proper overall arrangement to not much more than 1 percent inasmuch as the flow can be accelerated in at least major portions of the discharge duct. (One arrangement where this is *not* possible will be mentioned in Chapter 4.) Improvements over the best discharge duct arrangements now known are therefore not to be expected.

It has already been indicated that the most significant losses in efficiency of systems with the propulsion pump above the free water surface (Figure 2) are connected with the intake structure and the ducting from the intake to the propulsion pump. These losses are mostly internal duct losses and can easily amount to 30 percent or more. Furthermore, the external drag of the inlet structure (nacelle) and of the duct that pierces the free water surface can easily amount to 10 percent or more, except possibly the "flush" intakes used in connection with the side skirts of "captured bubble craft."

The intake and inlet duct problem will be described in Chapter 4 and possible solutions will be indicated there. The particular objectives of the present section will be to describe *what contribution, if any, the pump designer can make to the reduction of the inlet duct problem.*

One contribution of this type has already been mentioned and to some extent described in Section 3.4 in connection with Figures 28 and 29, i.e., a vertical-shaft arrangement of the propulsion pump. To the best knowledge of the author this arrangement was first suggested in principle by M. Huppert (then associated

with the Rocketdyne Division of the North American Rockwell Corporation). Figure 28 shows the advantage of this arrangement for changes in the direction of the discharging jet. It should be obvious that the vertical-shaft arrangement can also lead to a reduction in the length of the inlet duct. Furthermore the two approximately 45 deg elbows needed for a propulsion pump with (approximately) horizontal shaft (see Figure 2) are replaced for a pump with vertical shaft by one 90-deg change in the direction of the incoming flow. This concept can be generalized to pumps with their shafts inclined against the horizontal and vertical direction by an intermediate angle, say, 45-deg, thus reducing the change in the direction of the incoming flow to a single change by about 45 deg. This possibility will be considered further later in this section and more particularly in Chapter 4 since it is concerned with the overall arrangement of the propulsion machinery rather than with the characteristics of the propulsion pump as such.

One characteristic of the inlet duct directly connected with the pump is *retardation of the incoming flow* from the external intake to the inlet to the pump impeller. This problem exists of course only at velocities of travel close to the cruising or maximum travel speed.

The required retardation will now be estimated under the assumption that the speed of travel is 60 knots. According to Equation (3.34)

$$\frac{2g_0 H_{sv}}{V_0^2} = 1 - K + \frac{(h_{sv} - \Delta h_i) 2g_0}{V_0^2} \tag{3.78}$$

and, for $K = 0.4$ (as assumed before) and $h_{sv} - \Delta h_i = 25$ ft,

$$\frac{2g_0 H_{sv}}{V_0^2} = 0.6 + (25/159) = 0.757 \tag{3.79}$$

It is customary to design centrifugal pumps for values of the ratio $2g_0 H_{sv}/V_{m_i}^2$ between 3 and 4, where $V_{m_i}$ is the meridional fluid velocity entering the impeller. With $2g_0 H_{sv}/V_{m_i}^2 = 3.5$, one obtains by comparison with Equation (3.79):

$$\frac{V_0}{V_{m_i}} = \sqrt{\frac{3.5}{0.757}} = 2.15 \tag{3.80}$$

i.e., the intake velocity must be retarded by a factor of about 2 before the stream enters the impeller. If the familiar "included cone angle" of 7 deg is assumed, this means that the length of a conical inlet diffusor will be about twice the diameter of the intake. Actually this length has to be somewhat greater to accommodate changes in direction and in the shape of the cross section. On this basis the required length of the inlet diffusor does not constitute a problem. However the total ratio of retardation is a problem since it may lead to a rather nonuniform velocity distribution at the impeller inlet, with possibly detrimental effects on cavitation performance and efficiency.

The situation becomes truly serious when cavitation performance at greatly reduced velocities of travel is taken into account. Consider the foregoing example which corresponds to the conditions investigated in Section 3.3 (Table 1):

At a cruising speed $V_0$ of 60 knots = 101.4 ft/sec and $V_c^2/2g_0$ = 160 ft, consider first $V_1/V_c$ = 0.4, so that $V_1$ = 24 knots = 40.55 ft/sec and $V_1^2/2g_0$ = 25.6 ft. Hence, at reduced speed, $H_{sv}$ = 0.6 x 25.6 + 25 = 40.36 ft. Assuming (according to Section 3.6, Figure 39) that $Q_1$ = 0.925 $Q_c$, one can derive from Equation (3.80) with $V_0 = V_c$:

$$V_{m_i} = \frac{0.925 \text{ x } 101.4}{2.15} = 43.6 \text{ ft/sec}$$

and

$$V_{m_i}^2/2g_0 = 29.6 \text{ ft}$$

so that

$$\frac{2g_0 H_{sv_1}}{V_{m_i}^2} = 1.363$$

It is obvious from Figure 15 that this ratio is not acceptable; it would lead to a very low suction specific speed for given impeller blade characteristics as expressed by the coefficient $\sigma_p$ in that figure. It can be estimated that a value as low as 1.363 for $2g_0H_{sv}/V_{m_i}^2$ would lead to a reduction in suction specific speed by a factor of 2 or more. Evidently the situation would be even worse if the speed-of-travel ratio were less than 0.4, say, 0.1 as investigated in Section 3.3. The matter will therefore be explored here only for $V_1/V_c$ = 0.4.

To correct the unacceptable ratio $2g_0H_{sv}/V_{m_i}^2$ = 1.363 to a higher value, it is necessary to reduce the impeller inlet velocity $V_{m_i}$. Assume that the ratio $2g_0H_{sv}/V_{m_i}^2$ at reduced speed of travel ($V_1$ = 0.4 $V_c$) has the value of 3.5 (as assumed previously for the cruising-speed conditions). This means that the meridional impeller inlet velocity of flow should be reduced by the ratio $\sqrt{1.363/3.5}$ = 0.624. This changes the velocity reduction ratio given by Equation (3.80) from 2.15 to 2.15/0.624 = 3.45 (and leads to an increase of the impeller inlet diameter by a factor of $\sqrt{1/0.624}$ = 1.266).

The old velocity reduction ratio of $V_{m_i}/V_0$ = 1/2.15 at cruising speed was previously described as serious with respect to the impeller inlet velocity distribution. Accordingly, a velocity reduction ratio of 1/3.45 may be considered as unacceptable; further, an increase in inlet duct length would be required to achieve this velocity reduction in a reasonable fashion. One contribution the pump designer can make to alleviate this part of the inlet duct problem is to permit a lower value of $2g_0H_{sv}/V_{m_i}^2$ than is conventional for reduced speeds of travel, where the cavitation requirements are most severe.

Assume that at reduced speed of travel, the ratio $2g_0H_{sv}/V_{m_i}^2$ were reduced from the previously assumed value of 3.5 to 2. Figure 15 shows that this will reduce the suction specific speed from its optimum value at about $2g_0H_{sv}/V_{m_i}^2 = 3.5$ by a factor between 0.85 and 0.9 for the same impeller blade cavitation number $\sigma_p$. Possibly this reduction in suction specific speed is acceptable, particularly since the resulting increase in $V_{m_i}/U_i$ (see Figure 15) and decrease in impeller inlet diameter are likely to have a beneficial effect on pump efficiency (because of the amelioration of the retardation of the relative flow through the impeller).

For the above example, the result would be as follows: The meridional impeller inlet velocity of flow would be reduced from the conditions leading to $2g_0H_{sv}/V_{m_i}^2 = 1.363$ by a $\sqrt{1.363/2}$ ratio of 0.826 instead of the 0.624 previously calculated for $2g_0H_{sv}/V_{m_i}^2 = 3.5$ at $V_1/V_c = 0.4$. At cruising speed, the new ratio 0.826 leads to a retardation from intake to impeller inlet by a factor of 0.826/2.15 = 1/2.6. Although this is still a severe retardation, it is a great deal less severe than the factor of 1/3.45 previously calculated on the basis of $2g_0H_{sv}/V_{m_i}^2 = 3.5$. It can therefore be concluded that *a reduction in the ratio* $2g_0H_{sv}/V_{m_i}^2$ *below its optimum value at reduced speed is an effective way for the pump designer to help ease the inlet-duct retardation problem.*

It should be noted that under the same assumptions used above and a speed-of-travel reduction ratio of $V_1/V_c = 0.1$, one arrives at a required inlet flow velocity reduction at cruise speed of $V_{m_i}/V_0 = 1/3.16$; this assumes that at the reduced speed, $2g_0H_{sv}/V_{m_i}^2 = 2$. This is a very severe velocity reduction for the inlet duct and may not be achievable with acceptable overall efficiencies. Hence *the resulting required retardation of the incoming flow at cruise speed-of-travel is an additional reason why the minimum speed of travel specified to use full speed of rotation (and power) should not be lower than truly necessary*. This speed is usually dictated by the "hump" in the drag versus speed-of-travel curve of the vehicle.

An additional way in which the pump designer can help to alleviate the problem of inlet flow retardation at cruise conditions is by adding to the meridional impeller inlet velocity $V_{m_i}$ a circumferential velocity component $V_{u_i}$ in the direction of the impeller rotation.

Intuitively one is inclined to overestimate the effectiveness of this step because positive "prerotation" $V_{u_i}$ reduces the inlet velocity $W_i$ relative to the impeller vanes. For this reason it is necessary to derive briefly the effect of (positive) "prerotation" on the suction specific speed and to present some practical results of this derivation.

With

$$V_i^2 = V_{m_i}^2 + V_{u_i}^2 \text{ and } W_i^2 = V_{m_i}^2 + W_{u_i}^2 = V_{m_i}^2 + (U_i - V_{u_i})^2 \quad ,$$

one can derive from Equation (3.24)

$$2g_0H_{sv} = C_1\, V_{m_i}^2 + C_1\, V_{u_i}^2 + \sigma_p\, V_{m_i}^2 + \sigma_p\, U_i^2 - 2\sigma_p\, U_i\, V_{u_i} + \sigma_p\, V_{u_i}^2$$

and

$$\frac{2g_0H_{sv}}{V_{m_i}^2} = C_1 + \sigma_p + \frac{V_{u_i}^2}{V_{m_i}^2}\left[C_1 - \sigma_p\left(2\frac{U_i}{V_{u_i}} - 1\right)\right] + \sigma_p\frac{U_i^2}{V_{m_i}^2} \tag{3.81}$$

Substitution into Equation (3.22) leads to

$$S = \frac{U_i/V_{m_i}\,(1 - D_h^2/D_i^2)^{1/2}}{2^{1/4}\pi^{1/2}\left[C_1 + \sigma_p + \frac{V_{u_i}^2}{V_{m_i}^2}\left[C_1 - \sigma_p\left(2\frac{U_i}{V_{m_i}}\frac{V_{m_i}}{V_{u_i}} - 1\right)\right] + \sigma_p\frac{U_i^2}{V_{m_i}^2}\right]^{3/4}} \tag{3.82}$$

The dimensionless evaluation of the last equation is shown in Figure 40, where $S_0$ denotes the corresponding suction specific speed for zero prerotation ($V_{u_i} = 0$). The relation between $S/S_0$ and the prerotation ratio $V_{u_i}/V_{m_i}$ is shown for three different considerations:

1. The upper, solid curve is for cruise conditions.
2. The middle, broken curve is for reduced speed (moderately high $S$).
3. The lower dash and dot curve is for still lower speed (high $S$) and $2g_0H_{sv}/V_{m_i}^2 = 2$ (as suggested by the preceding considerations on how to reduce the retardation in the inlet duct).

The first two curves indicate the possibility that a prerotation ratio $V_{u_i}/V_{m_i}$ as high as 1 could be used. This would increase the resultant impeller inlet velocity $V_i$ by a factor of $\sqrt{2}$, which would be quite considerable. However the final curve (prerotation combined with an increase in the *meridional* impeller inlet velocity, as discussed before) restricts prerotation to about $V_{u_i}/V_{m_i} = 0.5$. This would increase the resultant impeller inlet velocity over its meridional component by no more than about 12 percent. Such a reduction in retardation is not negligible, but it does not constitute a *major* improvement.

Recent investigations have shown that the increase in suction specific speed obtainable by positive prerotation is about twice as great as predicted by the foregoing considerations, if one considers the effect of "solid-body" prerotation on the meridional inlet velocity distribution (see Chapter 26 of Reference 2). The same consideration shows that the range of $V_{u_i}/V_{m_i}$ is about 50 percent greater than shown in Figure 40 before the suction specific speed drops below its value at zero prerotation. Therefore positive prerotation may be of somewhat greater practical value than indicated before.

Recall that retardation in the inlet duct is severe only at cruising speed and that high suction specific speeds are required only at reduced speeds of travel. These facts suggest the use of a variable ratio of prerotation by means of an automatically adjustable inlet guide vane system in front of the impeller inlet. The amount of this adjustment could not be great (in view of the resultant change in the angle of attack at

the inlet edges of the impeller vanes) yet it might be sufficient to constitute a significant advantage in overall performance. Presumably the fixed part of the inlet duct would be designed for the maximum prerotation desired under cruise conditions, and the adjustable guide vanes would reduce this prerotation at low speeds of travel. As this is a duct design problem, it will be considered further in Chapter 4.

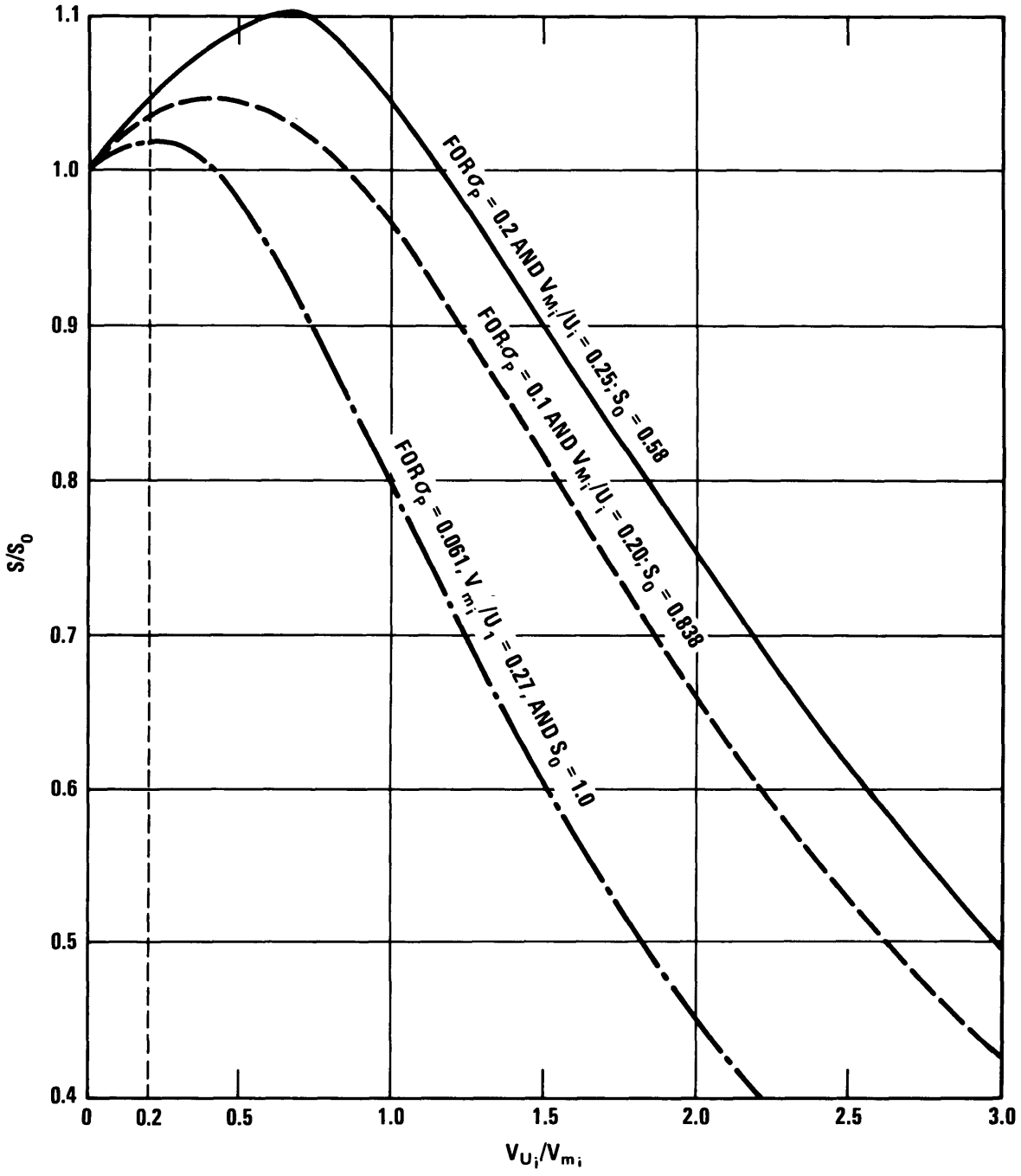


Figure 40 – Suction Specific Speed Ratio as a Function of Prerotation Ratio

Even with all improvements of the inlet duct discussed here and in Chapters 4 and 5, this study would be incomplete without considering whether it is truly necessary to locate the propulsion pump above the free water surface.

Perhaps the most significant contribution the pump engineer could make to the propulsion of high-speed surface vehicles would be to arrange the pump in such a fashion that it could be placed below the water surface but be easy to drive from a power plant above that surface. However, recall that the mechanical complication of an angle drive was largely responsible for placing the propulsion pump above the water surface in the first place. It follows that the principal reason for such placement would probably be eliminated by a propulsion pump with its impeller shaft approximately at right angles to the direction of the flow through the pump.

Since a marine propeller with this characteristic is available, it is natural to ask whether the principle of the Schneider-Voith propeller could not be used for pumps. The author is not aware of any promising attempt to do so. It should also be possible for a pump to have flow at right angles to the rotor shaft without need for the complex rotor blade movement employed with the Schneider-Voith propeller. However, an extensive design and experimental development process would be required to determine whether such a configuration can achieve the high efficiency required for a propulsion pump. This possibility must therefore be regarded as hypothetical, and will not be pursued further here.

Fortunately a well-established type of centrifugal pump with proven efficiencies up to 90 percent is available and can be adapted to meet the goal of the main through-flow at right angles to the rotor shaft. This is the familiar "double-suction pump" e.g., as shown in Figure 18. In order to use a double-suction pump for propulsion under water, the pump inlet passage would have to be of the "bottom suction" type (Figure 18), and the volume would have to be turned to direct the discharging flow into the same direction as the incoming flow but on the opposite side of the impeller. Furthermore, a determined effort would have to be made to minimize casing dimensions normal to the direction of the incoming and discharging casing flow.

Figure 41 shows how a double-suction pump could be incorporated into a streamline nacelle in an attempt to meet the aforementioned requirement of a reasonably small "frontal area." It is evident that an extensive redesign of existing double-suction pump casings would be required, together with an experimental development program. Nevertheless there is no reason why this arrangement of a submerged propulsion pump cannot be successfully executed essentially on the basis of existing knowledge.

As for all propulsion pumps with vertical shafts, some design development would be necessary to ensure that the arrangement of the driver and its reduction gear is in proper relation to the pump and its shaft. As already mentioned in connection with vertical-shaft pumps above the water surface (Section 3.4), the "free" power turbine and its reduction gear would have to have vertical shafts which would have an efficiency advantage regarding the turbine exhaust through a vertical stack. The hot gas generator would retain its conventional horizontal-shaft position, and the admission of the power gas stream to the free

Figure 41 – Submerged Propulsion Pump with Vertical Shaft

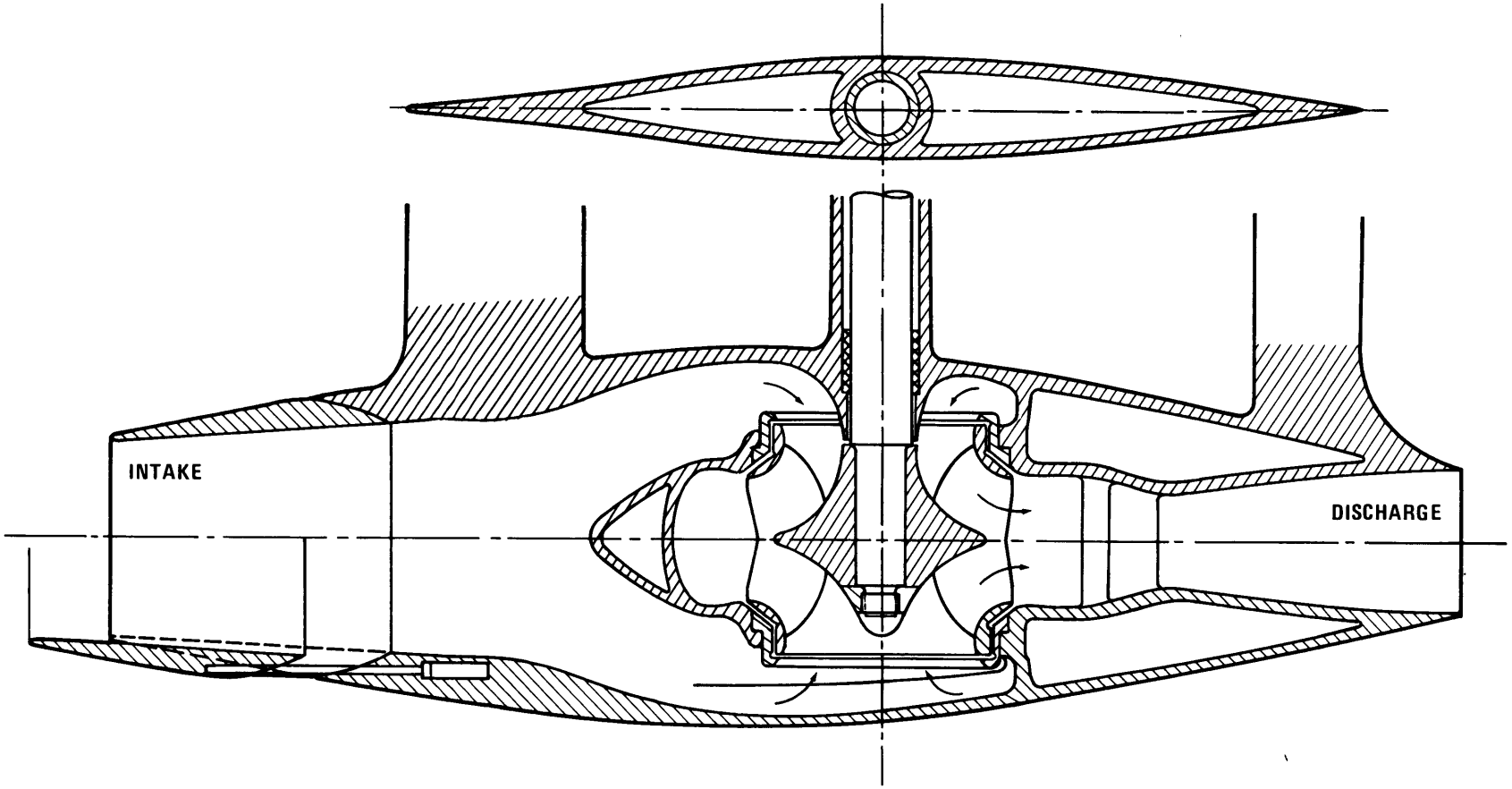


Figure 41a – Vertical Section

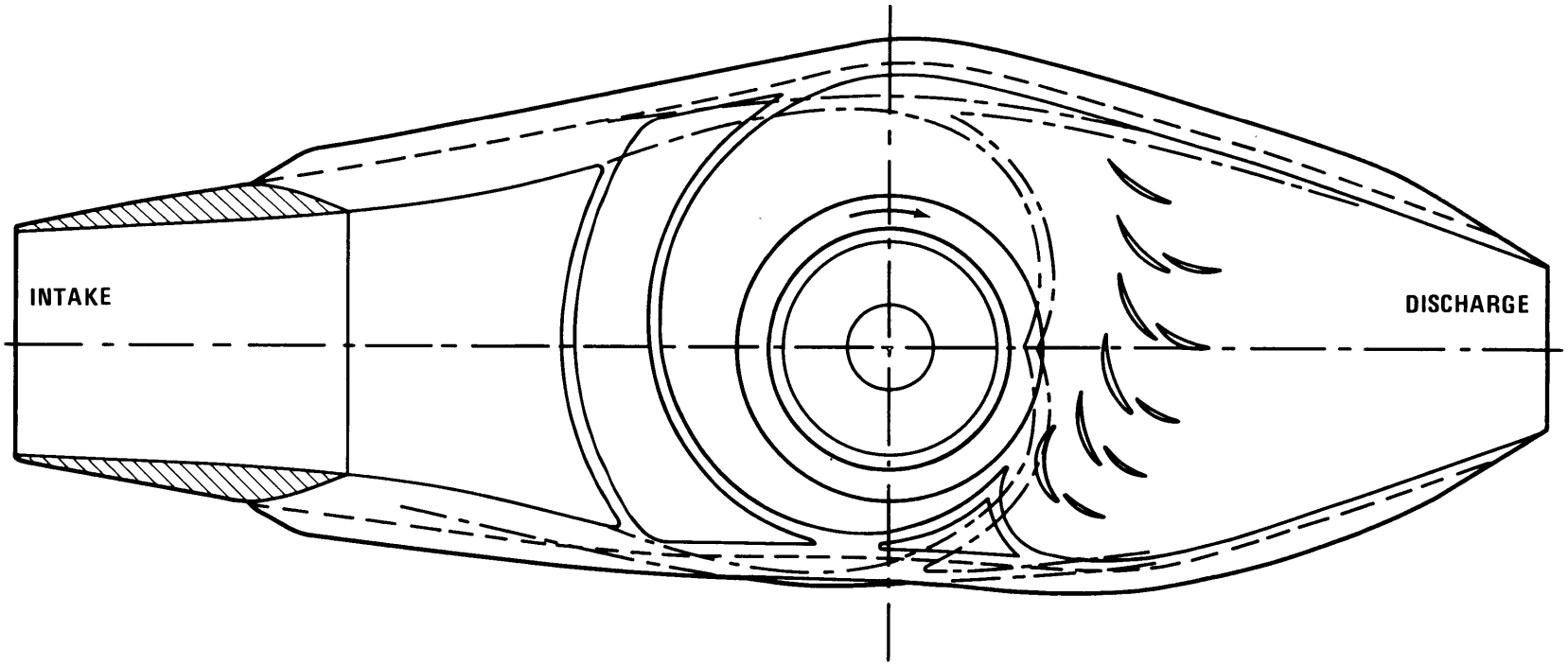


Figure 41b -- Horizontal Split

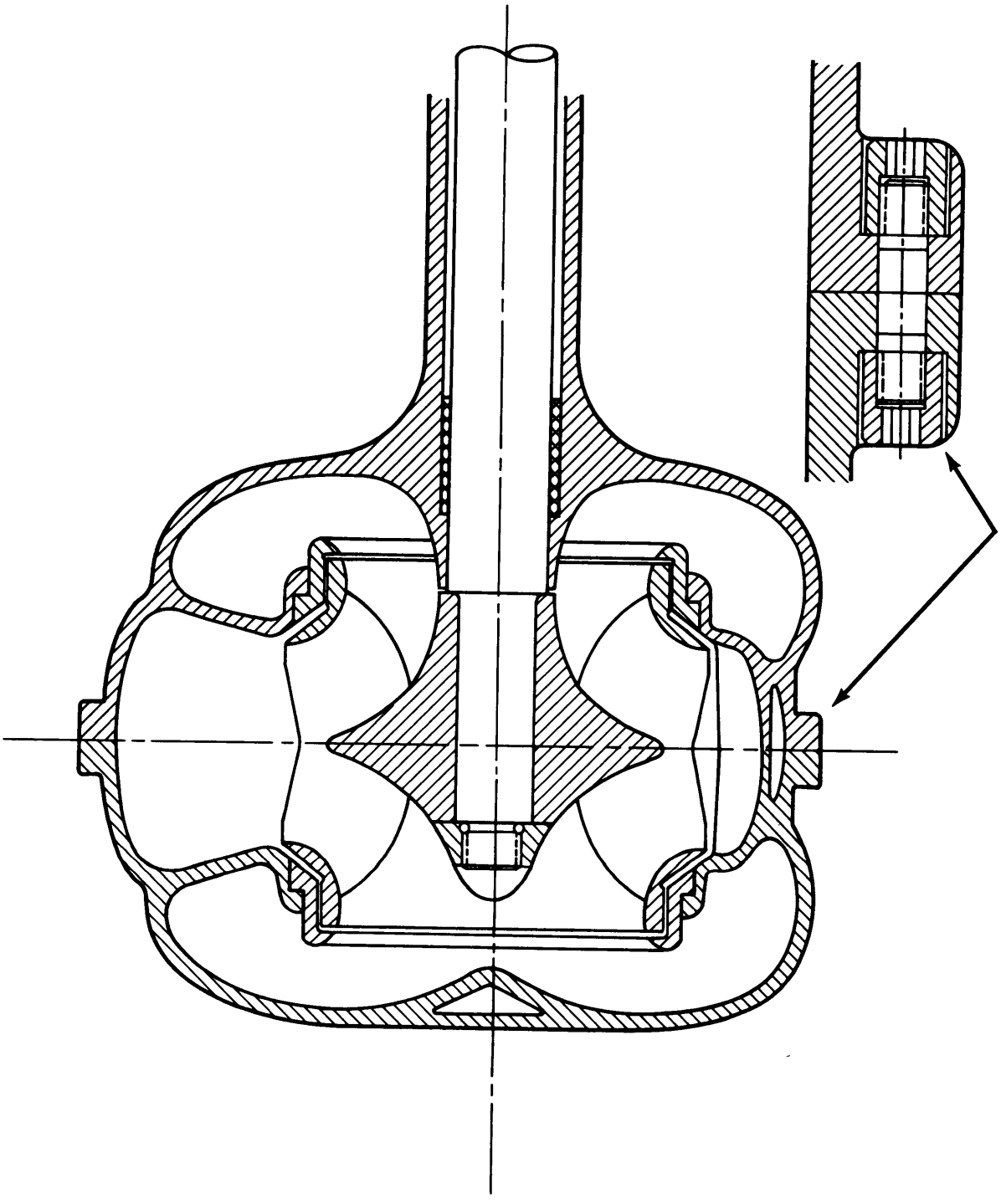

Figure 41c – Cross Section

power turbine would take place through a volute casing, preserving as much of the kinetic energy of the gas stream as desired for admission to the turbine. This arrangement can be highly efficient, as is well known from the field of hydraulic turbines.

Depending on the type of craft, steering as well as backing can be accomplished in many cases by turning the propulsion unit with its supporting streamlined strut about the vertical axis of the shaft. The turning mechanism could be located well above the free water surface.

Of course the use of a vertical shaft for the propulsion pump and its driver raises the question of whether a suitably *inclined* direction of the pump shaft may not have even greater advantages. This possibility has already been mentioned with respect to propulsion pumps above the water surface, and will be further explored in Chapter 4. Figure 42 shows a submerged single-suction propulsion pump with its shaft inclined by 45 deg against the horizontal and vertical direction. The frontal area of the nacelle would be about the same as for the double-suction pump shown in Figure 41. The "ram efficiency" of the incoming stream might be a little better for the single-suction pump with inclined shaft. However the design for the diffusor casing behind the impeller would be quite complex because in no sense is axial symmetry connected with this casing. Every vane and vane passage of the diffusor would have to be designed individually. Nevertheless a competent pump design engineer should come up with a good solution to this problem which is as challenging as it is interesting.

The greatest unsolved problem for a submerged propulsion pump with inclined shaft seems to be that of steering with the jet, in particular reversing the thrust. Jet deflectors that are usable above water are probably not usable below water, and so a separate reversed thrust unit may have to be employed.

Finally, some estimate is needed of the improvements in efficiency that may be expected from this arrangement compared with the conventional "waterjet" configuration with the pump above the water surface.

Although submerged pumps require a somewhat greater design effort, the author feels that there is no reason to assume a difference in pump efficiency for the two arrangements. It should be sufficient to compare their jet efficiencies corrected for duct losses and external drag, as given by Figure 5.

For a duct-loss coefficient $K = 0.4$, the "waterjet" arrangement with the pump above the water surface has a corrected jet efficiency (at optimum $\Delta V/V_0$) of 61.5 percent) for zero intake drag and an efficiency of 57 percent for an intake and strut drag coefficient $K_T = 0.1$.

For a nacelle and strut drag coefficient $K_T = 0.1$, the submerged propulsion pump has a corrected jet efficiency of 64.5 percent for a duct-loss coefficient $K = 0$ and an efficiency of 62 percent for $K = 0.05$. The difference in $K_T$ compared with that for the above-surface pump results from the fact that this coefficient is referred to the area of the intake *opening*, and thus its magnitude reflects the increased *total* frontal area of the submerged pump. In either case, $K_T$ represents only the *increase* in drag due to the presence of the propulsor.

Thus it is seen that submerging the propulsion pump may lead to an improvement of three to five points on the corrected jet efficiency scale, i.e., an improvement of 5 to 8 percent. However, if an improved

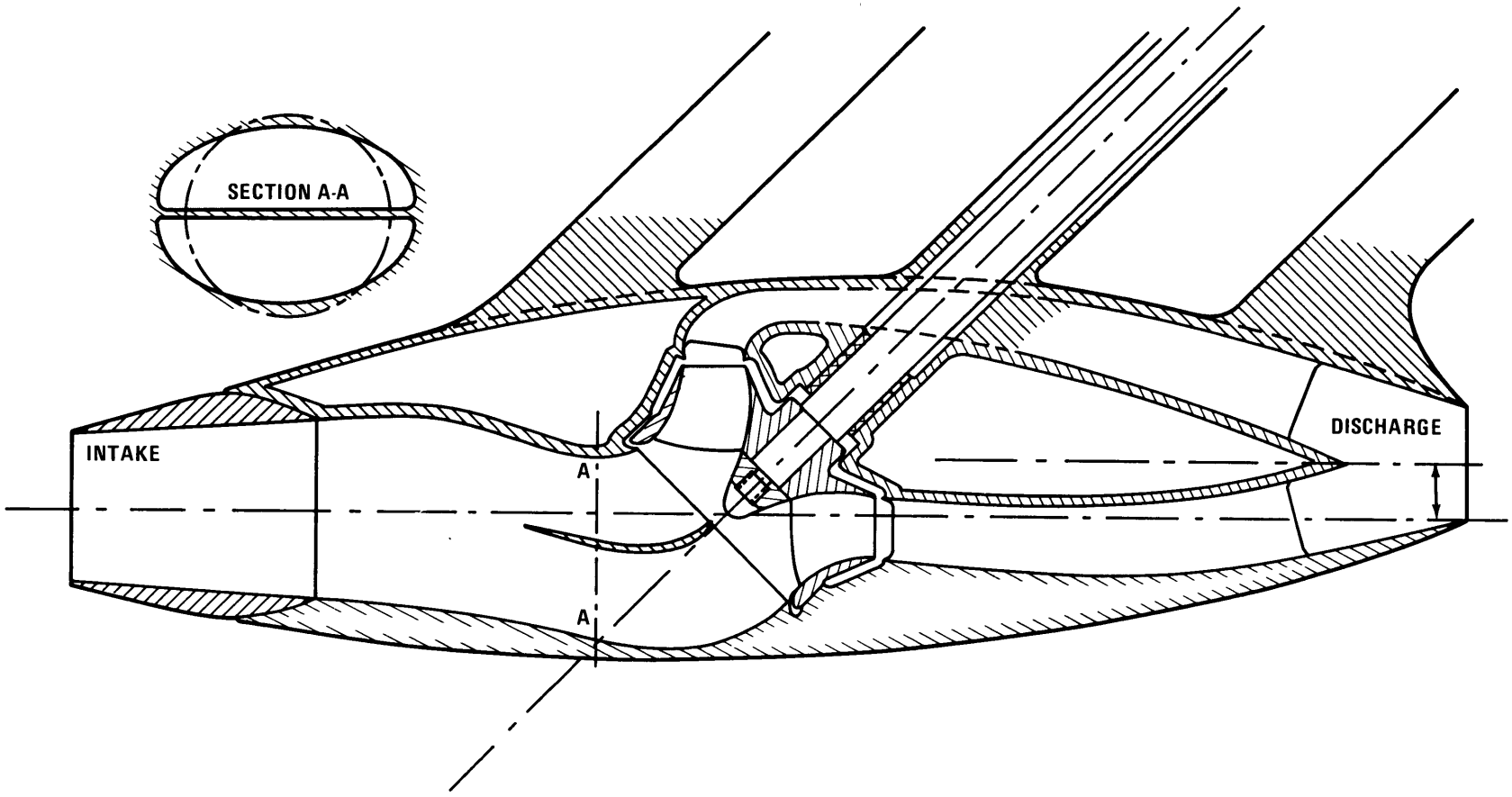


Figure 42 – Submerged Propulsion Pump with Inclined Shaft

inlet duct (see Chapter 4) can reduce the duct-loss coefficient $K$ (for the pump above the water surface) from 0.4 to, say, 0.3, the corrected jet efficiency would be 64.8 percent for $K_T = 0$ and 59.4 percent for $K_T = 0.1$, approximately matching the submerged pump arrangement. Duct-loss coefficients of less than $K = 0.3$ give the propulsion pump above the water surface a definite advantage.

## 3.8 SUMMARY OF PROPULSION PUMP DESIGN CONSIDERATIONS

The most important considerations presented in Chapter 3 for propulsion pump design may be summed up as follows:

1. Definite relationships exist between the operating conditions of hydrodynamic pumps and a number of important design parameters or characteristics of the pumps. The operating conditions are expressed in dimensionless form by the specific speeds. The relation between the basic specific speed $n_s$ and design parameters is given (for example) by Equation (3.16), and the relation between the suction specific speed $S$ and design parameters by Equation (3.22) and Figure 15.
2. Definite relationships exist between the operating conditions of a hydrodynamic propulsor and the usual operating conditions of a hydrodynamic pump:

   a. For propulsor thrust $T$, rate of flow $Q$, and change in velocity generated by the propulsor ($\Delta V = V_j - V_0$), this relation (Equation (3.32)) is:

$$T = \rho Q \Delta V$$

   b. For the pump head $H$ and the inlet and discharge fluid velocities $V_0$ and $V_j$ of the propulsor, this relation (Equations (3.33) and (3.37)) is:

$$H = \frac{V_j^2 - V_0^2}{2g_0} + K\,\frac{V_0^2}{2g_0} + \Delta h_j = \frac{V_0^2}{2g_0}\left[2\,\frac{\Delta V}{V_0} + \left(\frac{\Delta V}{V_0}\right)^2 + K\right] + \Delta h_j$$

   c. For the total inlet head of the pump ($H_{sv}$ = NPSH) and an intake velocity that equals the negative of the velocity of travel $V_0$, this relation (Equation (3.34)) is:

$$H_{sv} = (1 - K)\,\frac{V_0^2}{2g_0} + h_{sv} - \Delta h_j$$

   d. The variables $Q$, $H$, and $H_{sv}$ together with the speed of rotation $n$ determine the basic specific speed and the suction specific speed (or vice versa) and thereby the design of the propulsion pump, subject to certain design decisions (see Figure 33).
3. The thrust required to propel a water surface craft does not change with the square of the speed of travel, i.e., it does not follow dynamic similarity relations. Hence the pump design is based on two speeds of travel:

a. The maximum or cruise speed (subscript $c$) determines the jet efficiency and velocity increase ratio $\Delta V/V_0$ (see Figures 4 and 5).

b. The minimum speed of travel at which the pump is expected to operate at full speed of rotation (subscript 1) determines the cavitation characteristics of the pump (see Figure 23). The "minimum speed ratio" $V_1/V_0$ should be chosen as high as possible (see Figure 21) because a very low $V_1/V_c$ ratio necessarily leads to a less favorable propulsor design than a higher ratio (see Table 1).

4. Design variations of propulsion pumps for essentially the same specific speed (Section 3.4) include the following:

a. Single-stage, mixed-flow diffusor pump with jet coaxial with the pump shaft (Figure 24).

b. Single-stage, mixed- (or radial-) flow volute pump with the jet normal to the direction of the shaft. Possible arrangements include (1) a horizontal shaft crosswise to the direction of travel (Figures 25-27) and (2) vertical shaft (Figures 28 and 29) that permits changes in direction of the jet over a wide angle (steering and backing).

c. Multistage, axial-flow pump with jet coaxial to the pump shaft (Figure 30). This type of pump constitutes a saving in weight and size compared with a single-stage, mixed- (or radial-) flow pump of the same specific speed.

5. Variations in specific speed and pump form as a function of the jet velocity increase ratio $\Delta V/V_0$ (see Figure 33).

6. The use of several pumps in parallel instead of a single, larger pump should result in an increase in speed of rotation and a reduction in the weight of the pump and the directly coupled driver according to the square root of the number of parallel streams. Because of the complexity of the ducting connected with pumps in parallel, the weight saving is less than stated above on the basis of simple similarity considerations (see Figures 35-37).

7. The simplest relation between propulsor thrust and speed of travel is obtained with a slightly adjustable discharge nozzle area so that (for constant speed of rotation), $Q$ = constant and $H$ = constant (see Figure 22). A fixed discharge nozzle area reduces the thrust *increase* from full to reduced speed of travel ($T_1 - T_c$) by only about 10 percent and the total low speed thrust by less than 5 percent (see Figure 39).

8. Retardation of the inlet duct flow is serious at full (cruising) speed because of the cavitation design requirements at low speed of travel. This problem can be alleviated by:

a. Reduction of the impeller inlet coefficient $2g_0H_{sv}/V_{m_i}^2$ at low speed of travel from its (cavitation-wise) optimum value between 3 and 4 to a (practical) minimum of about 2, i.e., by designing for a higher meridional impeller inlet velocity than the optimum at low speed of travel.

b. By keeping the minimum speed of travel ratio $V_1/V_0$ required at full speed of rotation as high as possible.

9. Retardation of the inlet duct flow can be reduced by adding a circumferential component $V_{u_i}$ to the flow entering the impeller. This "prerotation" is limited to values of $V_{u_i}/V_{m_i}$ between 0.5 and 1.0 by its

detrimental effect on cavitation performance as shown in Figure 40. At full speed, retardation is at a maximum and contains conditions at a minimum whereas at low speed, there is little if any retardation but the most severe cavitation conditions exist. Accordingly, prerotation should be adjustable; it should be higher than the above-stated limits at full speed but not exceed these limits at low speed.

10. It is possible to eliminate the inlet duct losses almost completely by placing the propulsion pump into a nacelle below the water surface.

a. An undesirable angle drive can be avoided by selecting a double-suction pump arranged so that it fits into a nacelle with its shaft normal to the direction of the flow entering and leaving the casing (see Figure 41).

b. Steering and backing can be achieved in many cases by rotating the entire unit with its strut about the vertical axis of its shaft.

c. An alternate arrangement (Figure 42) is to place into a submerged nacelle a single-suction pump with its shaft inclined against the vertical and horizontal directions.

d. The geometric and mechanical feasibility of submerged propulsion pumps as shown in Figures 41 and 42 can hardly be questioned. The hydrodynamic feasibility depends on the flow (duct and drag) losses external to the pump. At a duct-loss factor $K = 0.4$ for the pump above the water surfaces, the submerged pump has an efficiency advantage of about 5 to 8 percent. If it were possible to reduce the duct losses to $K = 0.3$, the above-surface pump and the submerged-pump arrangement should be about equal in efficiency. At $K < 0.3$, the above-surface pump should have an advantage in overall efficiency.

# CHAPTER 4. DUCT DESIGN AND OVERALL ARRANGEMENT OF PROPULSION PUMPS

## 4.1 INTRODUCTION

This chapter briefly reviews the most important *arrangement problems* of waterjet propulsion. It attempts to pinpoint those problems that are judged to fall within the general scope of the report and suggests solutions.

Internal duct flow losses and the external drag of the intake structure and of the submerged and surface-piercing parts of the ducting are the principal reasons why waterjet propulsion is relatively less efficient than completely submerged propulsors used in connection with displacement surface craft and submerged vessels. This was pointed out in Chapter 2 and demonstrated by Figures 4 and 5. Chapter 3 discussed the design of the propulsion pump and the variations in pump design that may be important for improving the overall propulsion plant.

The present chapter discusses the ducting and intake structures insofar as these fall within the scope of this report. In other words, the discussion is primarily concerned with the *internal* flow problems of intake and ducting; the external drag of intake and ducting systems is considered outside the scope of this report. Therefore, the control of external cavitation or ventilation and the reduction of friction drag, wave drag, and induced drag of submerged and surface-piercing parts connected with the pump flow will *not* be discussed here. Their effects are of major importance and have been included in the thrust increase $\Delta T$ that can be attributed to the propulsion plant (see Chapter 2).

The necessity of an adjustable intake for any hydrodynamic propulsor intended for use with hydrofoil and captured air-cushion craft constitutes a major practical problem primarily because of the *reliability* aspects of the adjusting mechanism. The solution of this problem will be discussed here only in pricinple and from a hydrodynamic point of view. An adequate presentation of the entire subject of intake adjustment (like that of external drag) is a major undertaking. It certainly could not be covered in a report whose primary concern is with the propulsion pump.

Other major problems are internal duct losses and the associated maldistribution of the flow entering the pump. These will be attacked mainly by considering the location or arrangement of the pump relative to the intake. Evidently any change in the direction of the flow will lead to losses and often cause maldistributions of velocity. These can be reduced most effectively by reducing the number of turns (elbows) and the angles of turning. One turn shortly after (or as part of) the intake is unavoidable for pumps located above the waterline. However, the angle of this change in the direction of flow can and should be minimized. Beyond that, additional changes in the direction and the velocity of the flow must be reduced as much as possible.

## 4.2 AN EXISTING, SUCCESSFUL PROPULSION PLANT ARRANGEMENT AND SUGGESTIONS FOR ITS IMPROVEMENT

Figure 43 shows the existing propulsion plant arrangement of the hydrofoil boat TUCUMCARI. To the best knowledge of the author, this arrangement accomplished the purpose of its development and should therefore be considered successful. Whether this particular arrangement can be considered as *optimum in principle* is an entirely different matter.

The TUCUMCARI uses a single turbine placed along the central plane of symmetry of the craft. Its shaft is approximately horizontal and in line with two double-suction propulsion pumps.

The two water intakes are located on both sides of the craft in the center of two pairs of hydrofoils. Close to each intake, a long-radius elbow deflects the propulsion stream into approximately the vertical direction through the support struts of the hydrofoils. At the elevation of the hull, the propulsion stream is deflected by 90 deg toward the central plane of the craft; each stream enters one of the two propulsion pumps in an essentially horizontal direction normal to the pump shaft. Each stream is divided into two parts; one enters the pump impeller from the front and one from behind in the axial direction, in conformance with the standard arrangement for double-suction pumps.

The propulsion stream leaves the pump volute casing at right angles to the pump shaft and to the direction of travel. It must therefore be deflected once more by 90 deg toward the aft end of the craft. Outside the pump casing, the stream therefore changes its direction three times by approximately 90 deg. In addition the stream changes its direction once more inside the pump casing before it enters the impeller in the axial direction. This last turn is unavoidable with double-suction pumps, and its losses are included in computing their efficiency. These losses are apparently small since the efficiencies of double-suction pumps are known to be no more than 1 or 2 percent lower than those of single-suction pumps with otherwise the same general characteristics and qualities.

Undoubtedly, some practical design restrictions existed for TUCUMCARI. Could some of the changes in the direction of the propulsion stream have been eliminated or reduced in angle? Figure 44 shows the result of one such attempt.

Because of their high potential qualities, double-suction pumps were retained for this attempt, with a so-called "bottom-suction" casing inclined against the vertical direction by about 30 deg. (Bottom-suction, double-suction pumps are well known in the commercial pump field.)

In order to avoid a change in direction after the flow leaves the pump casing, the direction of the shaft of the pump and its driver was changed to be normal to the direction of travel (as described in Chapter 3 in connection with Figure 26). This change enables the propulsion pumps to be placed into the vertical planes of their respective intakes on the two sides of the craft, thereby avoiding another change in the direction of the flow (i.e., the elbows on top of the hydrofoil support the struts of TUCUMCARI).

Of course the proposed change requires the separation of the power turbine from the hot gas generator (this has already been discussed in Chapter 3). The cost and time required for such a development

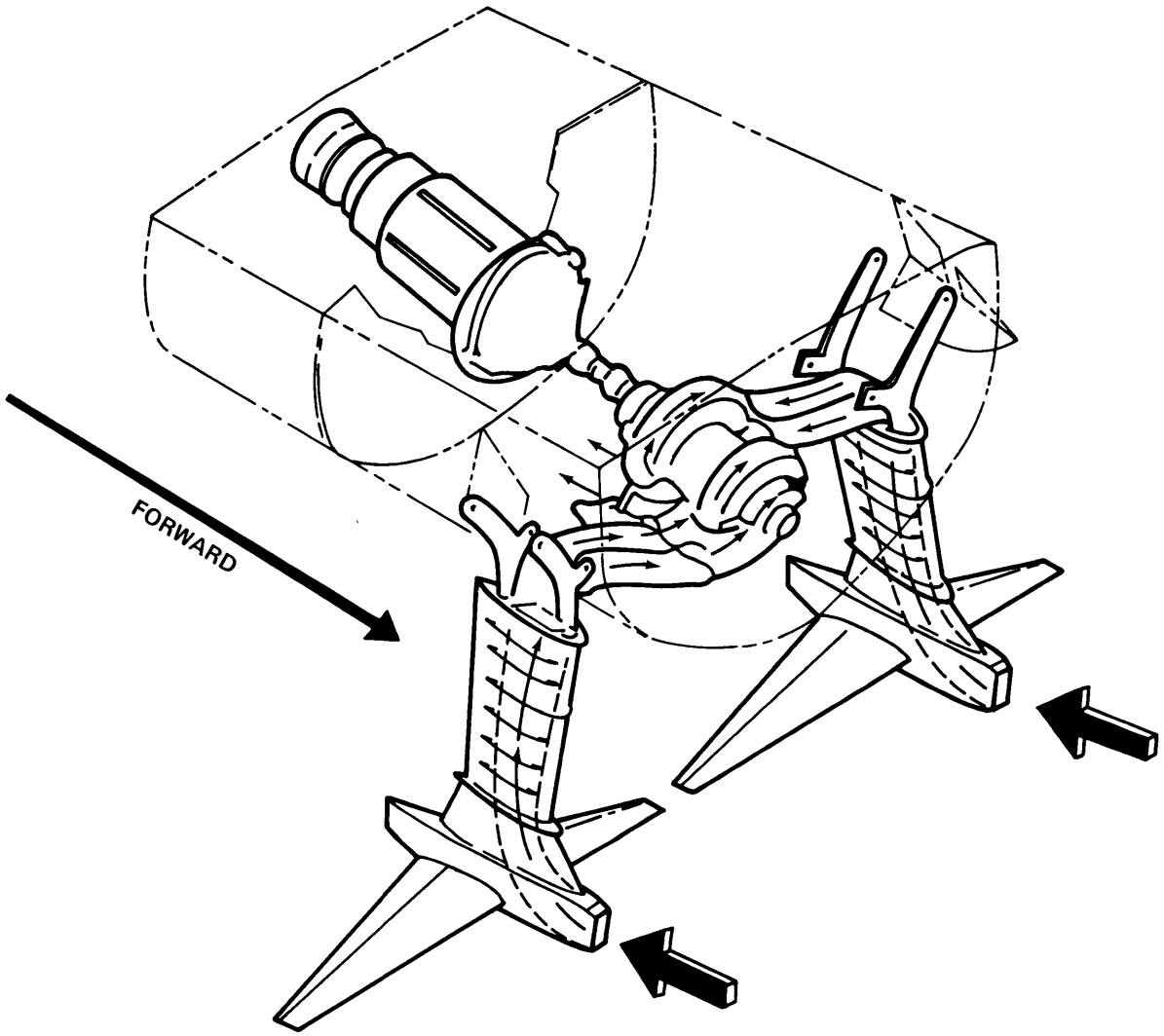


Figure 43 – Propulsion System for TUCUMCARI

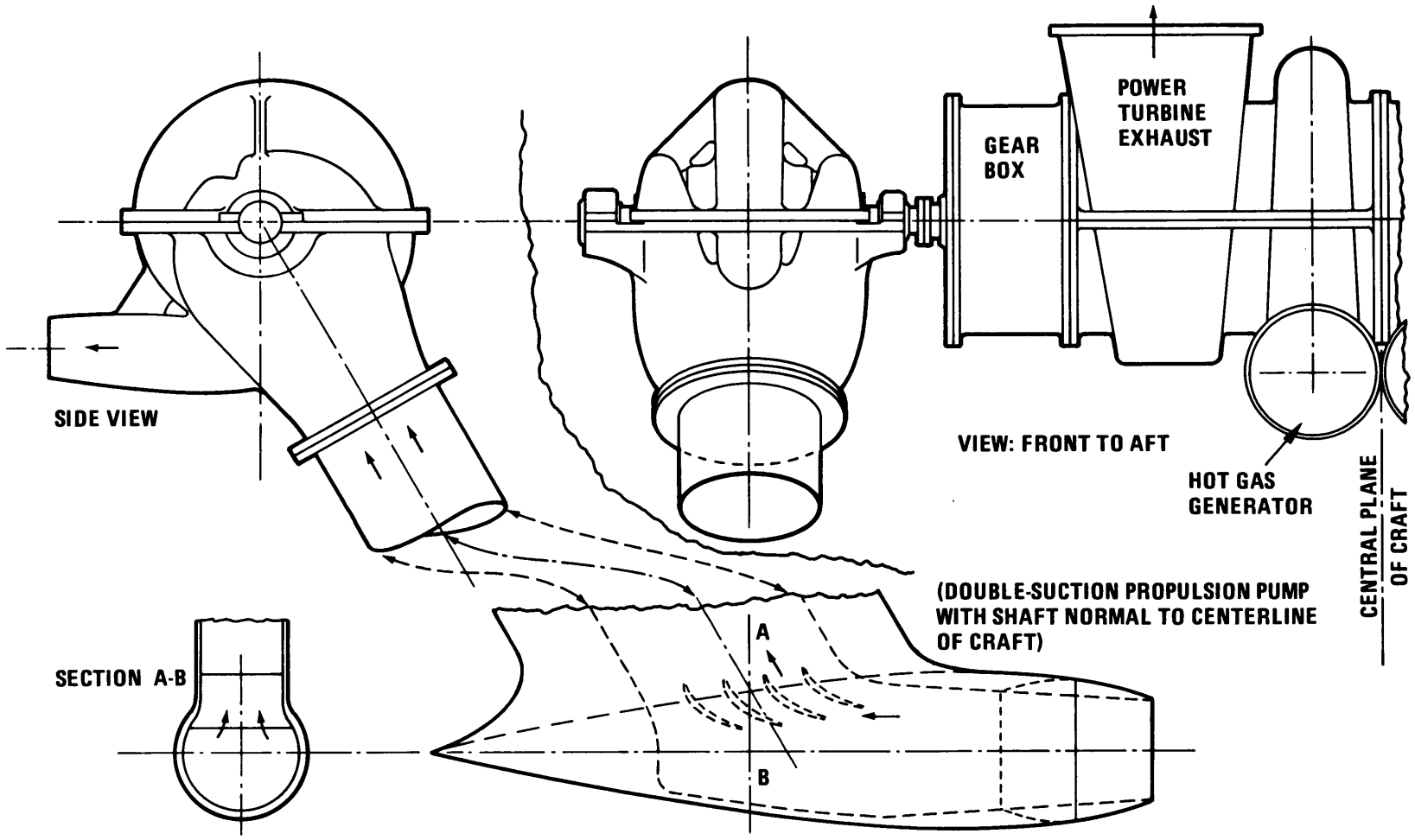


Figure 44 – Suggested Improvement in TUCUMCARI Propulsion Plant

was probably not available for TUCUMCARI. However these must be made available if significant improvements are to be achieved in the efficiency of waterjet propulsion.

Figure 44 shows two driving gas turbines. If these two turbines are coupled, this arrangement avoids the familiar risk of relying on a single-engine craft. With one turbine out of service, the propulsion power would, of course, be cut to less than one-half (because of the aerodynamic drag of the idling turbine), but operation in the drag-trough after the "hump" (Figures 3 and 21) may still be possible. If the single-turbine arrangement is desired, there is, of course, no difficulty in retaining it. A double-ended power turbine would be used in the center of the craft with two gear boxes to drive the two pumps.

With the arrangement shown in Figure 44, there is only one change in the direction of the propulsion stream external to the pump casing, i.e., the unavoidable change in direction after the submerged intake. Its angle of deflection has been reduced from about 90 to 60 deg and could conceivably be reduced still more. The losses in this elbow can be further reduced by retarding the flow before it reaches the elbow and by using a carefully designed turning vane system. The velocity of flow through such a system can be approximately constant, and the losses can be quite low if the development is aided by appropriate experimental investigations.

The elimination of two of the three changes in direction, the reduction in turning angle of the remaining turn, and the reduction in duct length resulting from this change in arrangement is expected to lead to a major reduction of the duct-loss coefficient $K$ (Figures 4 and 5) perhaps by as much as a factor of 4. This should certainly give a very significant improvement in overall efficiency.

## 4.3 DUCT AND INTAKE DESIGN FOR VERTICAL PROPULSION PUMPS

In connection with a study on surface effect vehicles (SEV's) conducted by the Institute of Defense Analysis (IDA) in the summer of 1969, the writer had occasion to examine possible improvement in ducting to be used with vertical propulsion pumps. This examination resulted in the sketches reproduced as Figures 45a-45d.

A few months prior to the IDA study, the use of vertical propulsion pumps had been suggested by M. Huppert who was then associated with the Rocketdyne Division of North American Rockwell. (The disclosure of this arrangement of a propulsion pump during the IDA study was authorized by Rocketdyne.) To the best knowledge of the author, Figures 45a-45d were the first sketches ever made of a vertical propulsion pump. They represent this writer's interpretation of Mr. Huppert's suggestion and include provision for changing the direction of the propulsion jet by rotating the discharge part of the pump casing about the vertical axis (in this case, together with the reduction gear).

Other studies had indicated that a "flush" intake might be the best form of intake for SEV's, specifically for captured air-cushion craft where such an intake can advantageously be arranged in the side skirts of the craft.

Figure 45 – Vertical Propulsion Pump with Axial Inlet Volute (IDA Study)

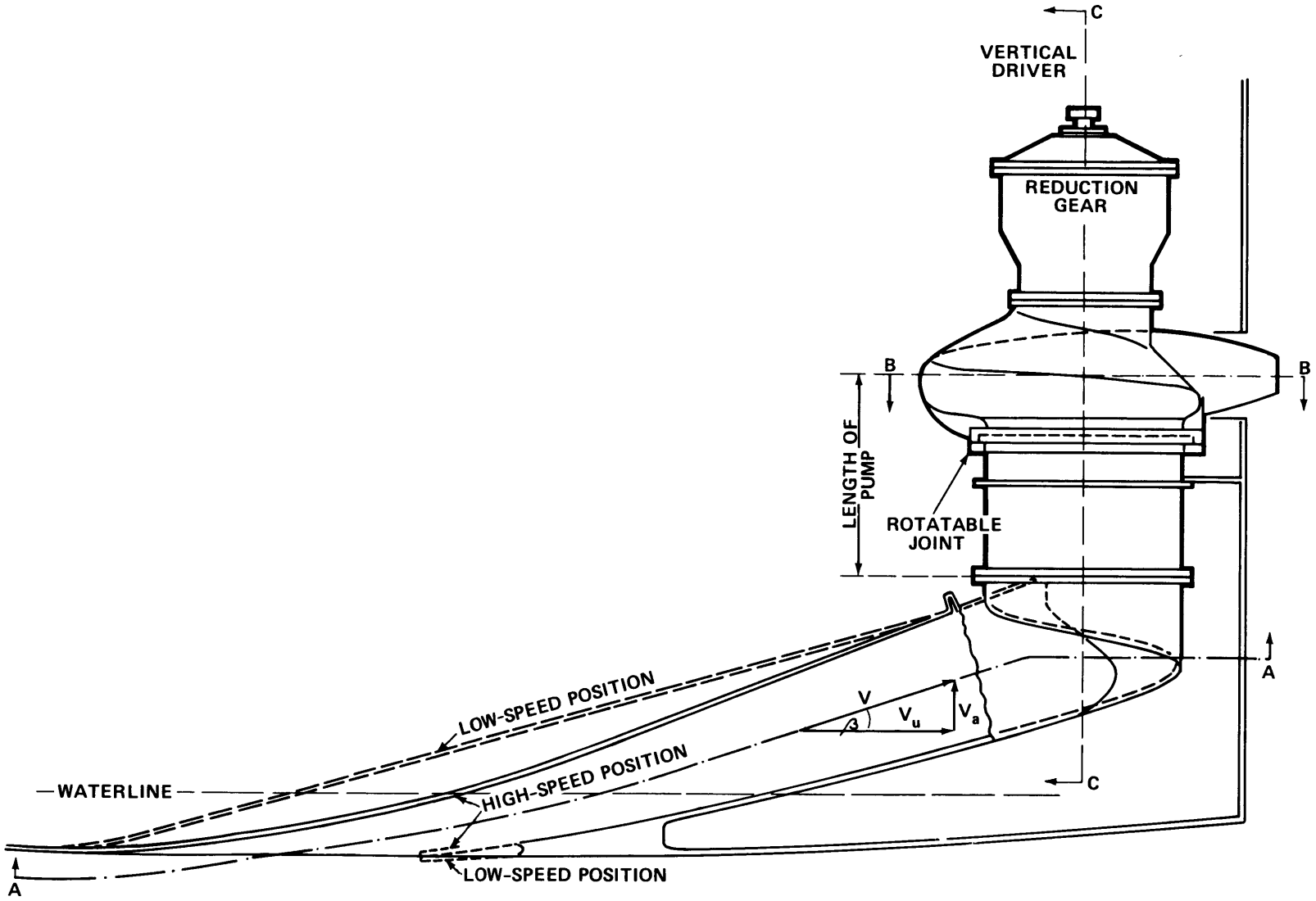


Figure 45a – General Configuration

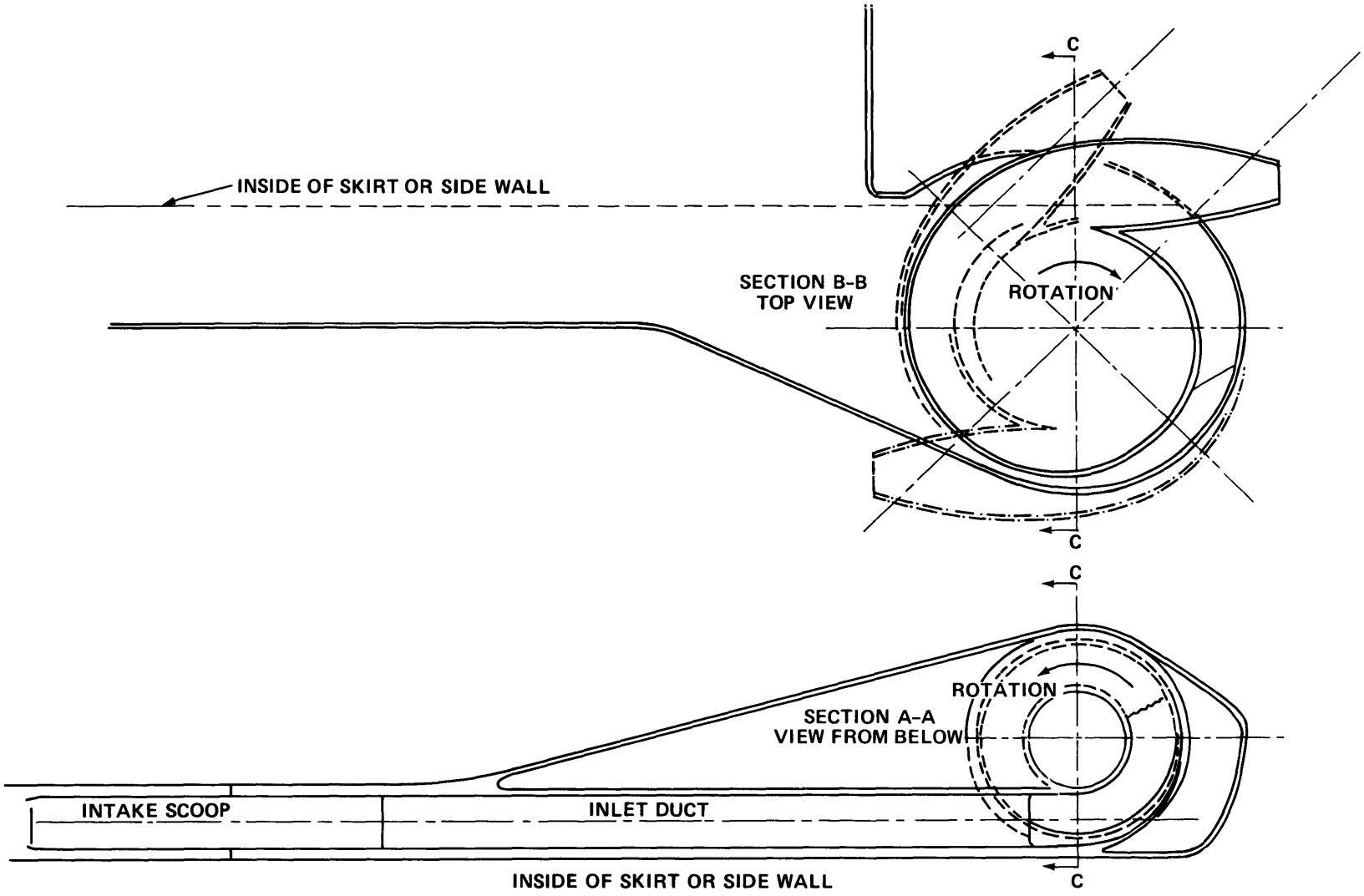


Figure 45b – Approximately Horizontal Sections A-A and B-B

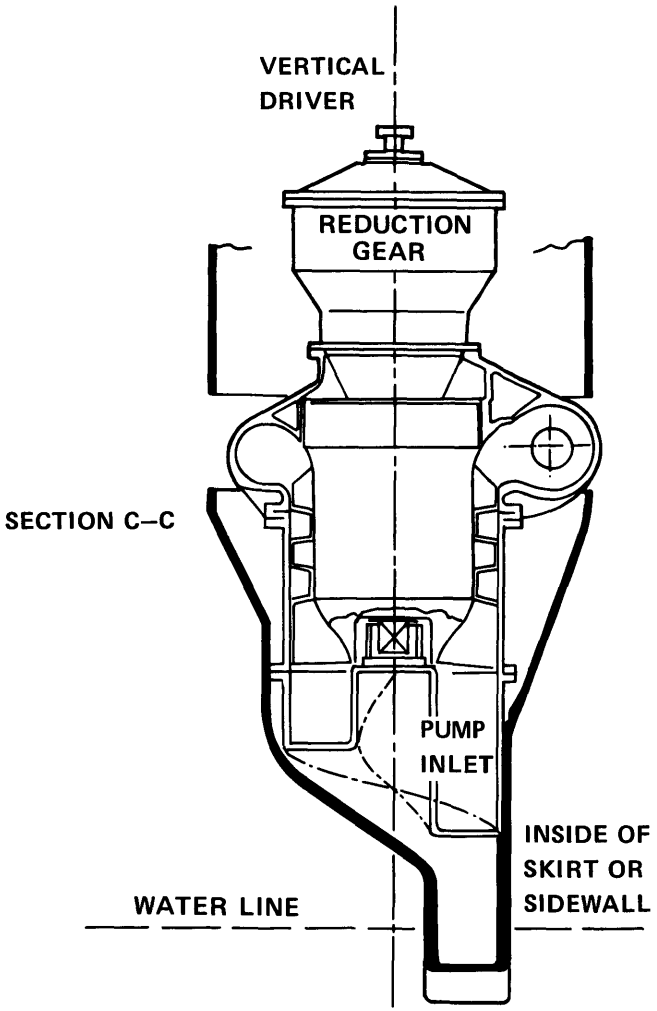


Figure 45c – Axial-Flow Vertical Propulsion Pump with Axial Inlet Volute

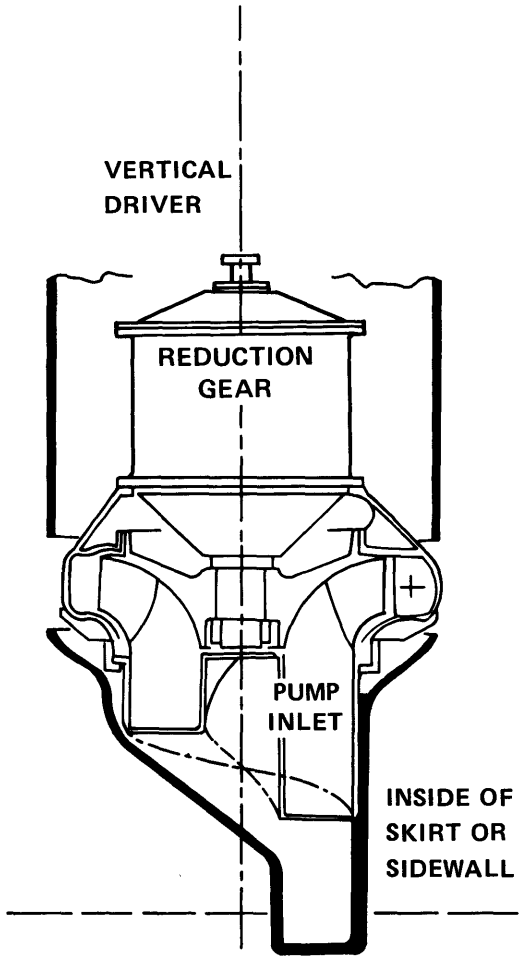


Figure 45d – Radial-Flow Vertical Propulsion Pump with Axial Inlet Volute

Furthermore, the problem of retarding the incoming flow to the highest allowable axial inlet velocity of the pump impeller was well recognized at the time of this study. A temporary departure of the intake from the water is followed by sudden reentry and causes a slug of water to hit the empty pump impeller at very high velocities. There was justifiable concern about the mechanical hazards involved. As a consequence of the foregoing considerations, the vertical pump and duct sketches were prepared under the following assumptions:

1. A flush, adjustable intake with a small inclination of the inlet duct against the horizontal direction.
2. An "axial volute" at the pump inlet that retains a fairly large circumferential component of the inlet flow in the direction of the rotor motion in addition to the prescribed fairly low axial (vertical) component of the flow. It was reasonable to assume that this arrangement would reduce the damaging effects of a high-velocity slug of water after the intake has left and reentered the water surface. (Measures to reduce the resulting high positive prerotation—which according to Figure 40 reduces the achievable suction specific speed—will be discussed later in this section.)

Figure 45a shows that the flush inlet involves only a small change in the direction of the flow. Thus without further deflection, the flow proceeds toward the pump inlet at a fairly small angle $\beta$ against the horizontal direction. It was and is felt that the resulting low elevation of the pump inlet can best be accomplished by using a vertical pump.

The required adjustment of the intake (Figure 45a) is accomplished primarily by forming the upper wall of the intake and duct from a strong, flexible sheet whose position can be controlled by a number of jacks (similar to the adjusting mechanism used with the nozzles of some supersonic wind tunnels). This design ensures minimum and continuously changing wall curvature in all positions of the wall. This is essential for preventing or minimizing cavitation inside the duct. The variation in the intake area and the resistance against cavitation are further increased by making the "lip" of the intake slightly adjustable as shown.

The form of adjustment of a flush intake shown in Figure 45a is, of course, not the only way in which such adjustment can be achieved. Figure 46 shows an alternate solution of this problem, namely, an adjustable vane system in the intake. The vane shape indicates the high degree of attention that must be paid to the cavitation characteristics of such a system. On the assumption that it is possible to avoid the admission of atmospheric air ("ventilation"), the cavitation number $(2(p\text{-}p_v)/\rho V_0^2)$ of the system (or of the intake shown in Figure 45a) would be about 0.2 at 60 knots and about 0.1 at 85 knots. The latter condition can probably not be met without permitting some local cavitation. In any event, the intake development will require the most careful theoretical and experimental work to achieve a reasonably successful solution, and intake cavitation may well be found to set an upper limit for the speed of travel.

The pump inlet configuration shown in Figures 45a-45d uses a high degree of (positive) prerotation at the impeller inlet in order to avoid excessive flow retardation from the external intake to the pump inlet. Otherwise retardation would be very severe at full speed of travel, as discussed in Chapter 3. Specifically,

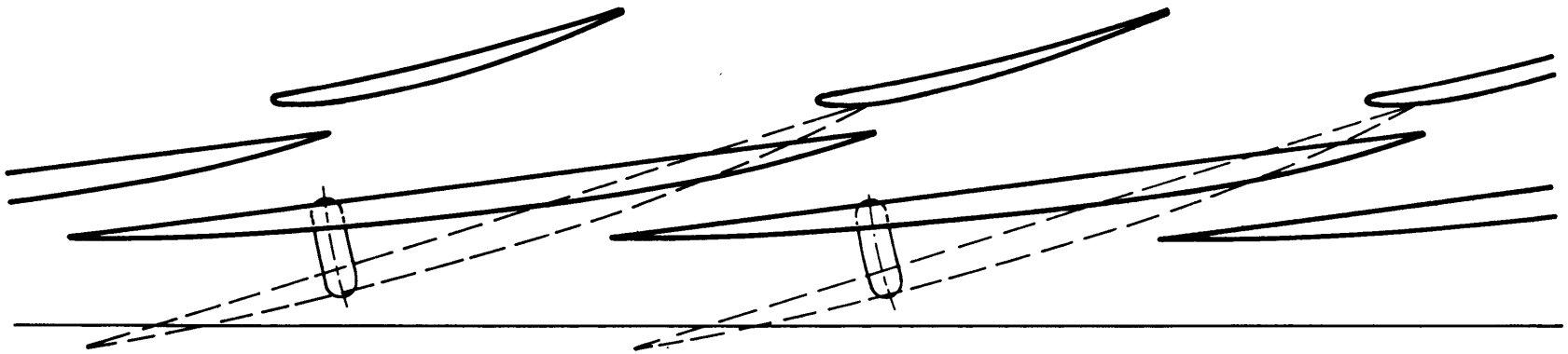

Figure 46 – Adjustable Vane System in a Flush Intake

Figure 45a indicates a ratio of prerotation of $V_{u_i}/V_{m_i} = V_u/V_a = 3$ (approximately) which, according to Figure 40 would reduce the suction specific speed to less than one-half of what it would be with zero prerotation, even if the impeller inlet were designed for this prerotation. Such a reduction in suction specific speed is unacceptable, particularly at the most critical conditions for reduced speeds of travel ("hump" conditions).

Figure 47 shows an adjustable, axial-flow vane system between an axial flow volute and the pump. This is intended to reduce the circumferential component of prerotation by a factor of slightly over 0.5. It would change the effect of prerotation (according to Figure 40) to factors between 0.6 and 0.9, which will be acceptable in its higher ranges. It is generally not necessary to make this vane system adjustable (and thus avoid some reliability risks) except for the previously mentioned aspect of intermittent flow and the unknown aspects of inlet flow variations and control of pump performance at variable speed of rotation. In any event, the development of such a vane system will require careful theoretical and experimental investigation. It is particularly important to experimentally determine the flow that leaves the axial volute in front of this vane system because it may depart substantially from the frictionless flow pattern, i.e., from the flow of radially constant angular momentum.

Figure 48 shows a right-angle discharge from a vertical, axial-flow pump. The elbow shown is suitable for very little rotation of the flow that leaves the last stage. (In this case, the volute casing shown in Figures 45a, 45b, and 45c would become unreasonably large or entirely unusable.) The velocity of flow leaving the axial-flow pump in Figure 48 may be comparatively low and the flow in the elbow strongly accelerated. Thus assuming a good design, the flow energy losses may be quite low. In this design (Figure 48), the discharge jet, the discharge elbow, and the pump are rotated together without rotating the driving gear box. A flexible coupling takes care of minor misalignments between the pump and the gear box caused by the rotation of the pump.

## 4.4 INCLINED PROPULSION PUMP ARRANGEMENT

Except for the submerged pump with inclined shaft shown in Figure 42, only propulsion pumps with horizontal and vertical shafts have been considered so far. However, an inclined shaft may also have distinct advantages for waterjet propulsion pumps and their drivers both located above the water surface. Figure 49 shows such an arrangement.

The intake is similar to that indicated in Figure 44. However, an inclined pump and duct system is also usable in connection with a flush intake. The pump and its discharge elbow are similar to that shown in Figure 48 except that the elbow has a much smaller angle of deflection, a factor which should provide an advantage in efficiency. Steering is accomplished by rotating the pump and its elbow by fairly small angles (say, 30 deg). This causes a slight change in the inclination of the jet against the horizontal direction. Thrust reversal requires a rotation of pump and elbow by about 120 deg in order to direct the jet against a deflector located on the side of the craft.

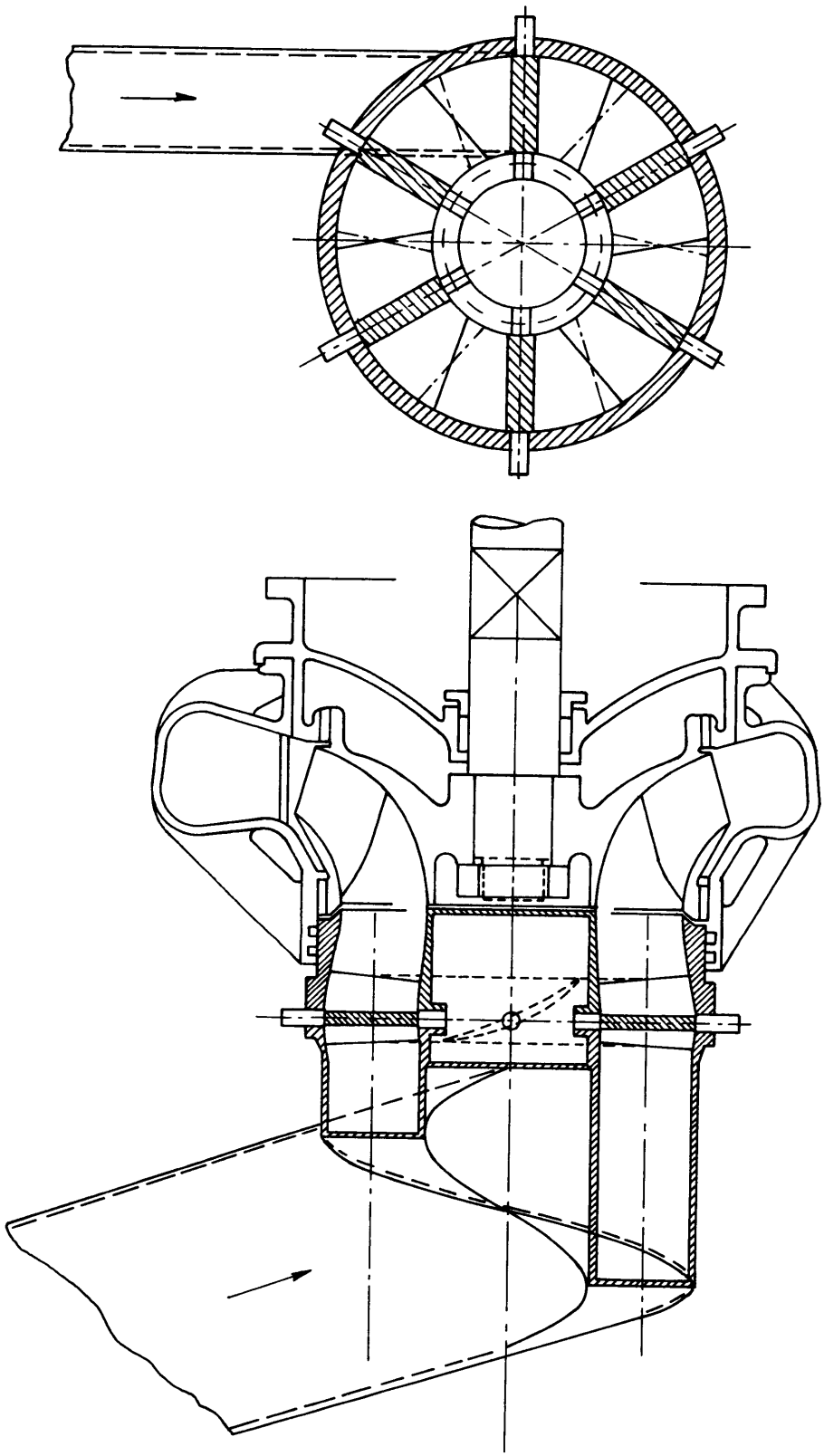

Figure 47 – Prerotation Vane System with Axial Inlet Volute

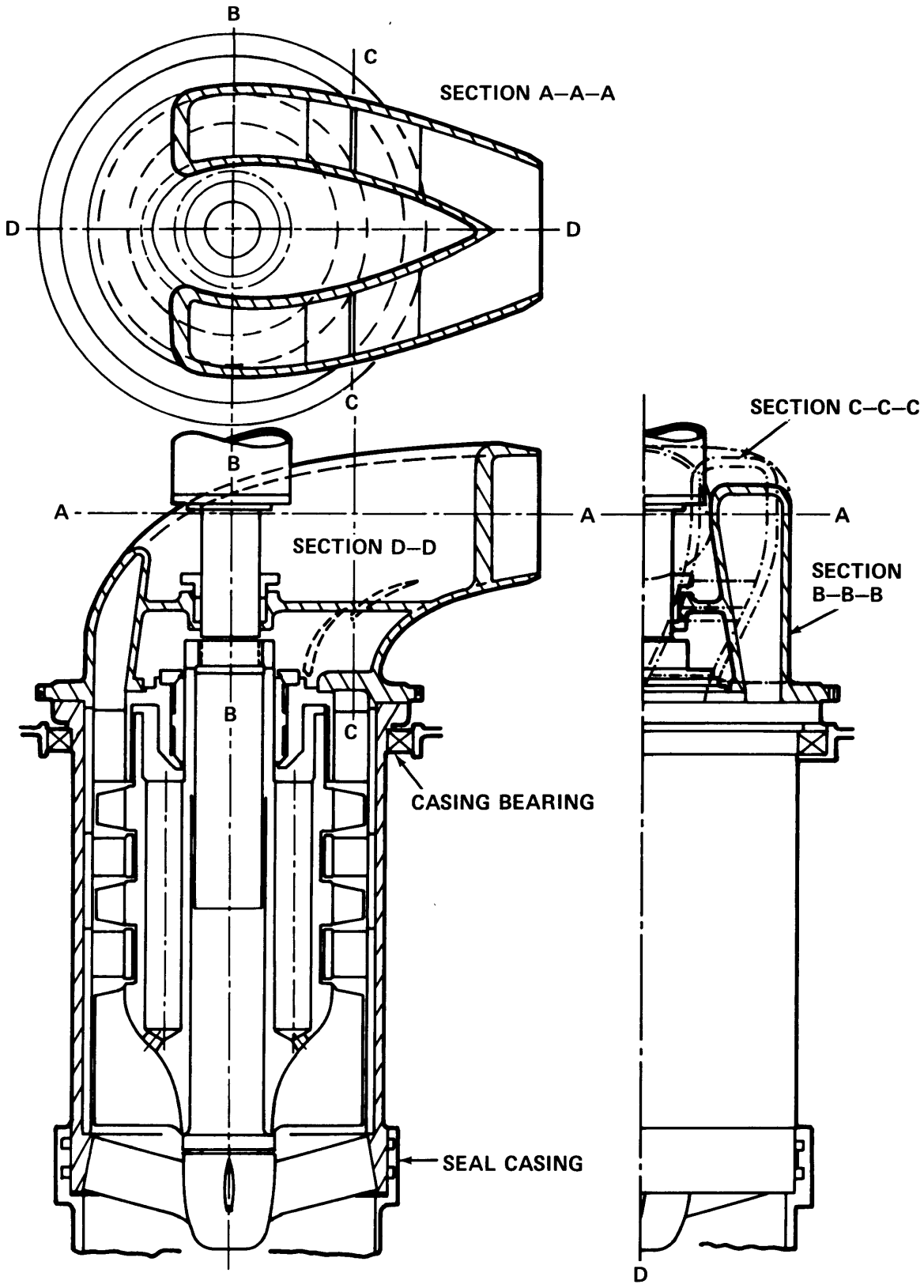


Figure 48 – Vertical Axial-Flow Propulsion Pump

The inclined position of the shaft also has advantages with respect to the gas inlet to the hot gas generator and the gas discharge from the power turbine. Changes in the direction of the gas streams are quite small or zero.

It should be recognized that an inclined position of the pump shaft is by no means limited to axial-flow pumps. On the contrary, a single-stage, mixed-flow pump whose specific speed lies in the center of the specific speed range (see Figure 33) can be used advantageously with a discharge volute developed about a 45 deg conical surface (assuming the angle of inclination $\alpha$ is 45 deg so that its discharge is inclined against the axis of rotation as shown in Figure 49. Such a pump would be larger in diameter and shorter in length than an axial-flow pump. For equal quality in design, the efficiencies should be about the same (close to 90 percent).

It thus appears that an inclined position of the pump and its driver gives the design engineer additional freedom of arrangement which should enable him to reduce duct losses substantially.

## 4.5 REDUCTION OF FLOW DISTORTIONS AT THE PUMP INLET

Flow distortions are departures from the uniform velocity distributions that are usually assumed. Axially symmetric, i.e., radial, nonuniformities of the velocity distribution can be taken into account in designing an axially symmetric vane system such as a rotating or stationary vane system of a turbomachine. Circumferential nonuniformities can never be incorporated in the design of rotating vane systems.

Obviously, any departures from the velocity distribution assumed in the design prevents a vane system from optimal operation. At a pump inlet, such departures will lead to local cavitation and other disturbances which should be expected to reduce the efficiency. The latter effect is not well established. Some highly efficient centrifugal pumps have been found to have an amazingly flat efficiency curve over a substantial range of flow rate at constant speed of rotation. Therefore, in this case, substantial changes in the angle of attack at the impeller inlet have only minor effects on efficiency. Furthermore, standard double-suction pumps are known to have substantial circumferential flow distortions at the impeller inlet, yet efficiencies approaching 90 percent have been achieved with this type of pump.

On the other hand, it has been established conclusively that local cavitation is strongly dependent on the angle of attack at the leading edges of impeller vanes. At the fluid velocities encountered in the propulsion pumps of hydrofoil and captured air-cushion craft, even local cavitation might lead to severe cavitation damage under prolonged operation at full speed. This suggests that flow distortions at the inlet to propulsion pumps may cause unacceptable cavitation damage even if they do not seem to have significant effects on efficiency.

Whenever the direction of the flow in the ducts leading to the pump must be changed, one of the most effective ways to minimize flow distortions is the use of vane elbows. For this reason, all inlet duct elbows shown in this report are of the vane type (see Figures 24, 25, 30, 44, and 49). This is particularly important ahead of the retarding portion of the inlet duct (Figures 44 and 49) because flow distortions are

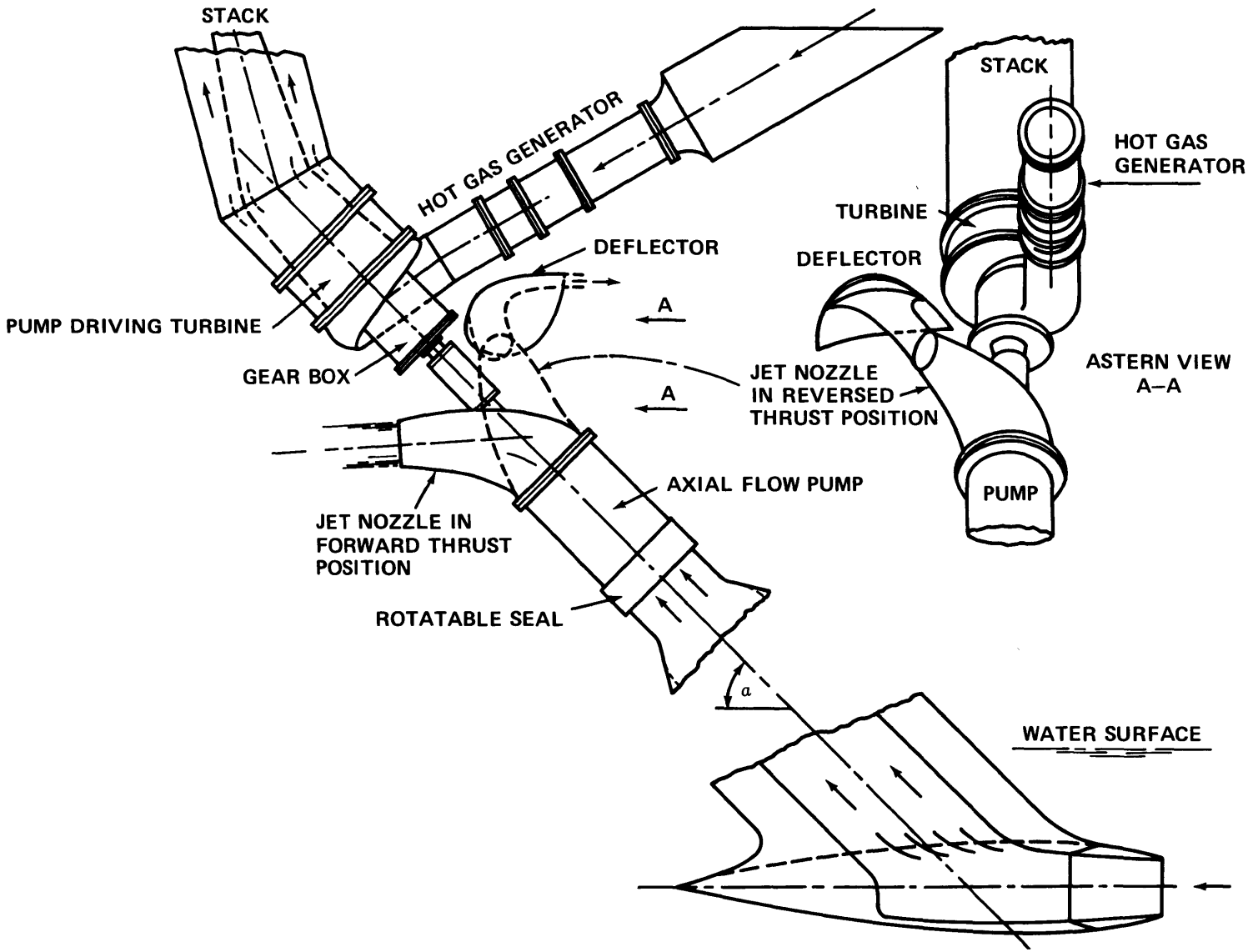


Figure 49 – Inclined Propulsion Plant to Minimize Changes in Direction of Flow

rapidly increased in a retarded flow. After a retarding duct section, a vane elbow may have a slight equalizing effect on a flow with nonuniform velocity distribution. In any event, a vane elbow does not generate the large secondary motions which are characteristic of elbows without vanes in a stream with non-uniform velocities.

The vanes of vane elbows do not need to be expensive (see Figures 24, 25, and 30), but they should be carefully designed according to the principles of cascade design. In particular, the vanes must turn through a slightly larger angle than that through which the direction of the mean flow is to be changed.

Because of the required retardation of the incoming flow, vane elbows may or may not be sufficient to avoid major flow distortions at the pump inlet. This fact can be established only by experimental investigations of the intake and duct before their design is definitely established (experimentation in air at a reasonably large scale is usually sufficient, except for the intake cavitation problem which requires testing in a water tunnel).

If, despite a carefully developed intake and inlet duct, the flow distortion at the pump inlet is still judged to be excessive, it may be necessary to use a rotating flow velocity equalizer as shown in Figure 50. The idling rotor has straight, helical vanes with a symmetrical, streamlined cross section. The stator vanes are axial. Both vane systems have a solidity (ratio of vane length to circumferential vane spacing) of approximately unity. In the low energy regions of the oncoming flow, the rotor acts as a pump, and in the high energy regions, it acts as a turbine. The duct cross section normal to the axis of rotation should be approximately constant through the device with proper allowance for the blockage effect of the vanes. This writer has no information on the effectiveness of this device, but it should be helpful if carefully designed.

## 4.6 SUMMARY AND CONCLUSIONS

1. The most conventional waterjet propulsion arrangement is probably that shown in Figure 2 with pumps as shown in Figures 24 and 30 and perhaps Figure 36 also. The intake should probably be of the nacelle type with a vane system as shown in Figure 44.

2. The volute pump is the most efficient type of centrifugal pump (90 percent efficiency or more). To avoid an elbow in the discharge line, the volute pump requires a fairly large angle (45 to 90 deg) between the direction of the shaft and the direction of travel:

a. Volute pumps with horizontal shaft normal to direction of travel. For single suction, see Figures 25-27; for double suction, see Figure 44.

b. Volute pumps with vertical shaft (see Figures 28, 29, 45, and 47).

c. Volute mixed-flow pump with inclined shaft, e.g., see arrangement similar to that shown in Figure 49.

3. All arrangements with the shaft *not* approximately in line with the direction of travel require a departure from the conventional gas turbine configuration, i.e., they require a free power turbine with its shaft

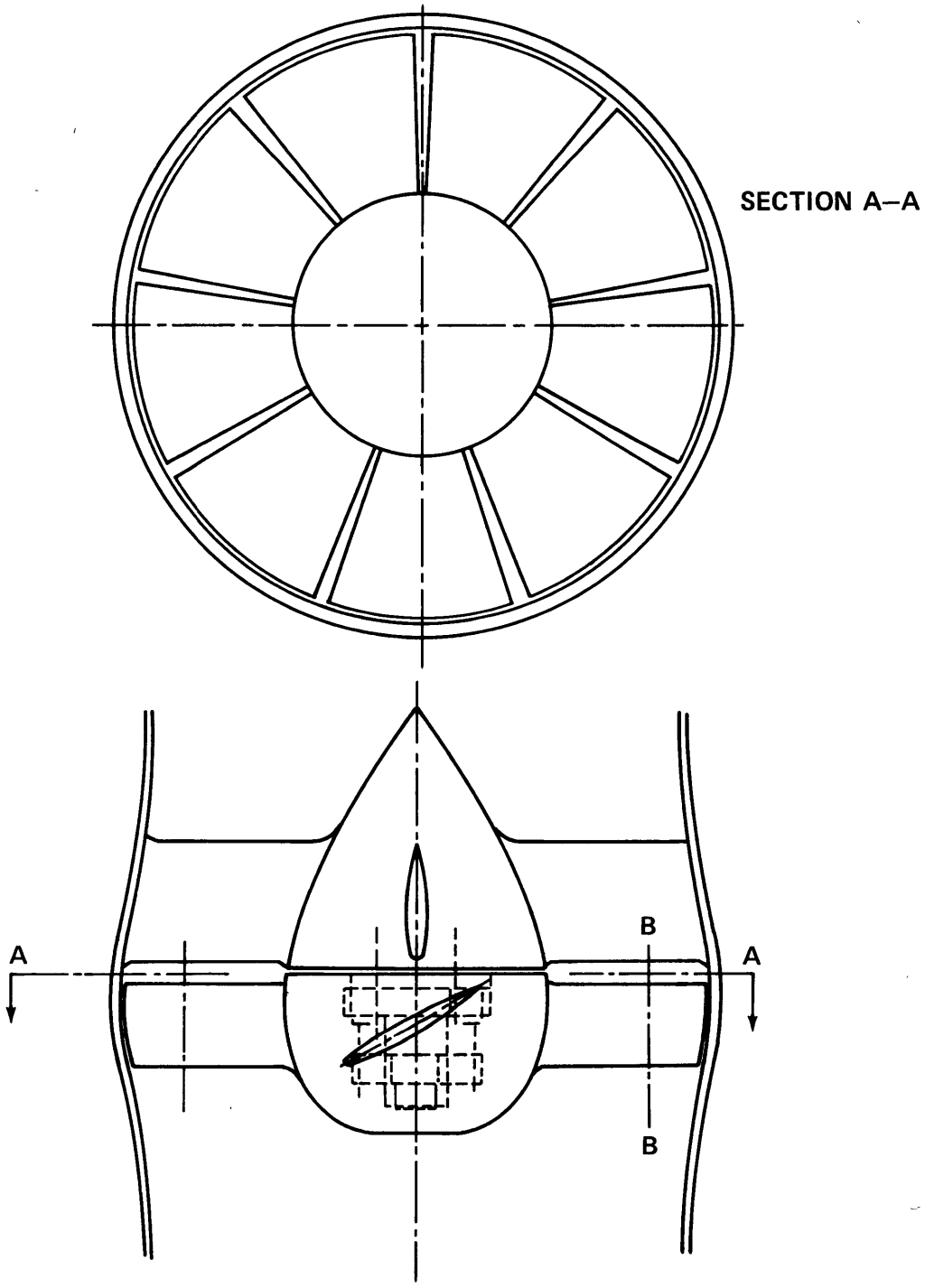


Figure 50 – Rotating Flow Velocity Equalizer

approximately at right angles to the shaft of the hot gas generator. Admission of the hot gas stream to the power turbine by a volute can be highly efficient, at least as efficient as the conventional in-line arrangement. Its development is recommended in order to free the design engineer from the limitation imposed by the "conventional" arrangement (Item 1 above) or by the inefficient TUCUMCARI arrangement.

4. Axial-flow propulsion pumps can be used in an in-line configuration (Item 1 and Figure 30), in vertical position (Figures 45a-45c and Figure 48), and in an inclined position (Figure 49). They are smaller and lighter than other pumps (including the water contents), but they are probably more costly to produce than single-stage, radial- or mixed-flow pumps. Their efficiency approaches that of the best centrifugal pumps (90 percent). They probably have the lowest amplitude of discharge pressure pulsations because of the large number of vanes. The energy in the stream leaving an axial-flow multistage pump is quite low compared with the head of the machine; therefore, a well-designed discharge elbow as indicated diagrammatically in Figures 48 and 49 should have very small losses.

5. Flow distortions at the pump inlet may be serious from the viewpoint of cavitation damage. Vane elbows and other good design principles of the inlet ducting may help to minimize flow distortions. If good design of stationary duct parts is not sufficient to meet this challenge, a rotating flow-velocity equalizer (Figure 50) may give significant improvements.

6. Inclined pump and ducting may offer the possibility for substantial reduction of duct losses (Figure 49).

# CHAPTER 5. PRELIMINARY DESIGN OF THE HYDRODYNAMIC PROPULSION PLANT FOR A HYDROFOIL BOAT

## 5.1 DESIGN SPECIFICATIONS

The prescribed specifications and assumptions for the design example to be presented in this chapter are as follows:

Ship configuration (see Figure 51) and weight (403,200 lb)

Lift/drag curve (see Figure 52)

Design speed (optimum cruise) = 40 knots

Specific fuel consumption (SFC) = 0.5 (constant at 40 knots)

Takeoff speed = 25 knots or less. Thrust margin at takeoff must be at least 20 percent to account for extra drag which occurs in rough water.

Maximum speed = 48 knots

Negligible variation in strut drag with duct size, i.e., constant $L/D$ curve

Weight of prime mover with gear box installed = 1.2 lb/hp

Weight of fuel plus propulsion system weight = 134,400 lb

The prescribed lift/drag characteristic given in Figure 52 was converted to a drag/lift curve as used in this report (Figures 3 and 21). It is shown in Figure 53 together with two approximate propulsor thrust curves at two constant speeds of rotation. One curve is required for 40 knots and the other for 48 knots (see Figures 21 and 22). The curve through the 40-knot point does not quite meet the 20 percent thrust margin requirement whereas that through the 48-knot point exceeds this requirement confortably.

The thrust curves shown in Figure 53 have been drawn first under the assumption that $\Delta V/V_0 = 0.65$. It will be seen that $\Delta V/V_0 = 0.75$ was finally chosen. This leads to the somewhat flatter thrust curves indicated by the dash- and dot-curves of the figure. The substantial thrust margin at the speed of rotation corresponding to 48 knots over the 20 percent requirement is certainly sufficient to meet the pump cavitation problem connected with speeds of rotation higher than that required at the 40-knot point. An exact answer to the cavitation problem can be obtained only by cavitation testing the propulsion pump.

Furthermore, it is rather comforting to observe on Figure 53 that the drag increase from 40 to 48 knots is somewhat less than by the square of the speed of travel. The two "thrust parabolas" shown are drawn under the assumption that the *speed of rotation increases proportionally to the speed of travel.* If this is done in going from 40 to 48 knots, the thrust will increase faster than the drag. In other words, to balance the increasing drag, the speed of rotation can be increased slightly less than the speed of travel (disregarding the extra thrust required to accelerate the craft).

Finally, the case considered here is favorable because the minimum speed at which a relatively high thrust is required ("hump" condition) is just about one-half of the cruising speed (40 knots) and about 40 percent of the maximum speed of travel. These comparatively high ratios ease the cavitation problem at

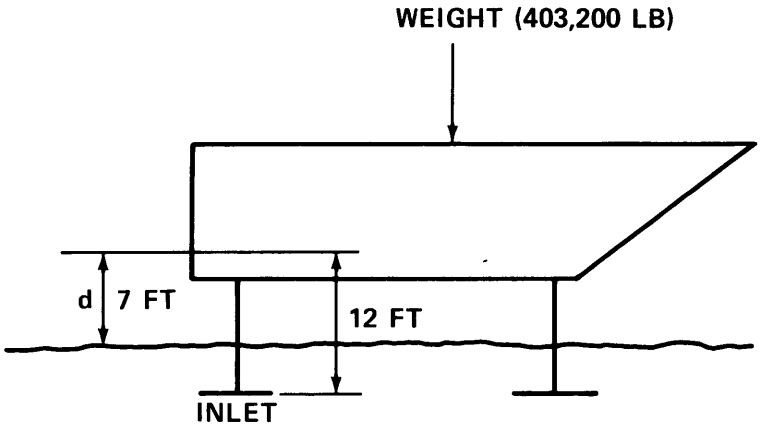


Figure 51 – Ship Configuration for the Design Example

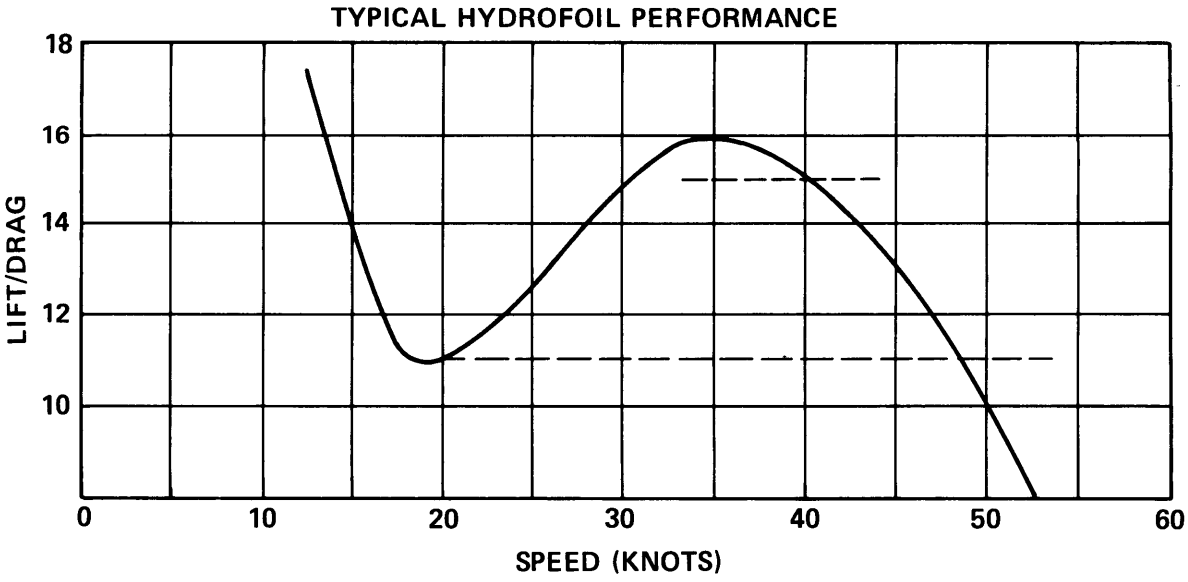


Figure 52 – Prescribed Lift/Drag Characteristic for the Design Example

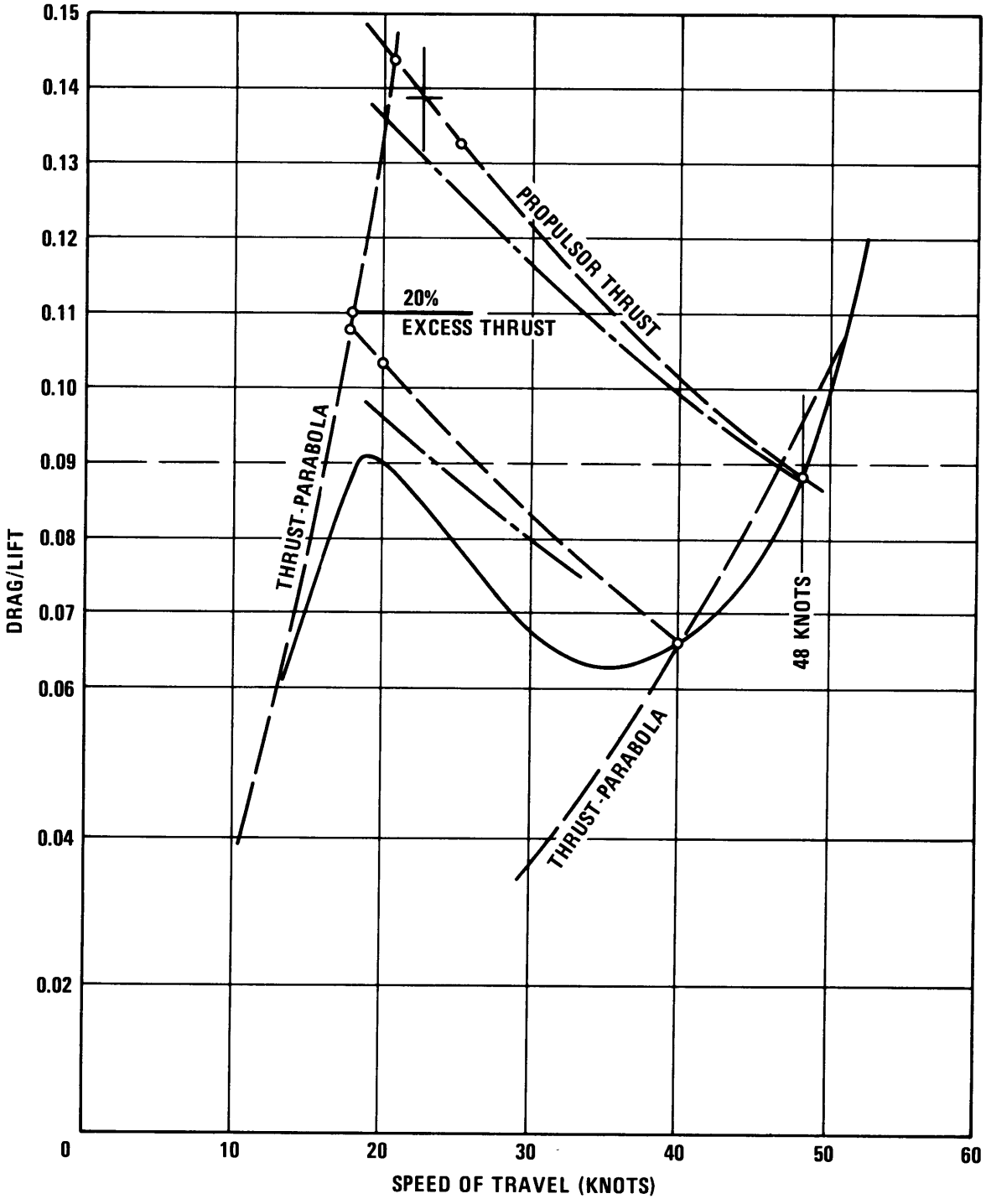


Figure 53 – Prescribed Drag/Lift Curve and Propulsor Thrust Characteristics for the Design Example

low speed (20 knots) and make it unnecessary to design for extremely high suction specific speeds at low speed of travel. This will avoid or minimize the need to compromise the design in favor of the low-speed-of-travel condition. In this connection, the fairly conservative maximum speed of travel is also an advantage. Figure 23 shows that the suction specific speed at 20 knots does not need to be greater than twice the suction specific speed at cruising and maximum speed of travel.

Before turning to specific aspects of the design example to be discussed, it seems prudent to call attention to the limits set by the general scope and practical extent of this report.

The design of the propulsion plant for a hydrofoil boat as described in the specifications is a *major* undertaking. It exceeds the intended scope of this report by several orders of magnitude. This is particularly true because the propulsion of *new* types of vehicles, such as hydrofoil craft, requires the development of *new* forms of machinery and mechanisms in order to obtain favorable results. In this light, the original engineering effort applied to a craft as described in the specifications should be expected to be much greater than that connected with a new, but more conventional, ship with a tonnage a hundred times that specified here. It must also be considered that the 200-ton craft considered here may be the "model" for between 100 and 1000 vehicles of its type. From this point of view, the development of new forms of machinery, structures, and mechanisms must receive the same attention as that given to the development of a *new type* of aircraft or spacecraft.

In view of these facts, the question arises as to what the present very modest effort can be expected to accomplish. The answer is twofold. It can and must demonstrate the application of the principles outlined in the previous chapters to a particular design example. It must also demonstrate that the answers so obtained do not involve obvious contradictions or impossibilities. Therefore, the design forms suggested in the following cannot be expected to present *proven* possibilities. At best they suggest ways in which the design problems presented *can* be solved. The intent is to stimulate the design engineer to think about as yet untried solutions of the design problems that confront him. Details of the designs suggested are included only to demonstrate the *existence* of the problems rather than their most useful solutions. The term "preliminary design" is probably too optimistic. "*pre*-preliminary design" may be more appropriate for something which suggests a direction in which preliminary design studies should be conducted. Yet it is hoped to point out that many design details deserve serious consideration in the earliest phases of design. General design forms are chosen in these very early phases, and it is then that either fatal mistakes or constructive and fruitful decisions are formulated which later, necessary refinements can neither correct nor improve fundamentally.

## 5.2 CHOICE OF THE GENERAL FORM AND ARRANGEMENT OF THE PROPULSION PLANT

The specified, very general arrangement suggested by Figure 51 indicates two *vertical* inlet ducts on the two sides of the craft similar to those used on TUCUMCARI (Figure 43). The shortcomings of the

TUCUMCARI arrangement and its possible improvements have been described in Section 4.2 and will not be repeated here. This description leads to the conclusion that the propulsion pumps should be placed on top of each of the vertical foil-supporting struts. Three possible propulsion pump arrangements and forms have been shown in Figures 2, 24, and 30 with the pump shaft approximately *in* the direction of travel and in Figures 26, 25, 44, 28, and 48 with the pump shaft at right angles to the direction of travel. All arrangements shown in these illustrations place the propulsion pump close to the top of the hydrofoil support strut and vertical suction duct, and they avoid a change in the direction of the flow after the propulsion pump. Only the vertical shaft arrangements (Figures 28 and 48) avoid a change in the direction of the suction flow between the vertical suction duct and the pump impeller inlet.

The cross-shaft arrangements shown in Figures 26, 25, and 44 have the reliability advantage that two driving gas turbines make it possible to maintain symmetrical propulsion with one driving turbine in case the other foils. Whether it would be possible to maintain the craft *on the foils* with one turbine can be estimated by means of the curves in Figure 53.

The effective propulsion power is obviously the drag (or resistance) times the speed of travel. The minimum foilborne power requirement is near the trough of the drag versus speed-of-travel curve at 35 knots; it is proportional to 2.19 knots (i.e., 0.0625 x 35 knots). The maximum power requirement is obviously at the maximum speed of 48 knots at drag/lift = 0.088; it is proportional to 4.22 knots (i.e., 0.088 x 48 knots). Hence if the driving turbines develop their maximum power at 48 knots, one turbine will not be able to propel the craft at 35 knots even under the favorable assumption of the same efficiency of propulsion under both operating conditions considered. Actually, the power available from one turbine is less than one-half the power of two turbines on the same shaft because of the windage losses of the idling turbine. This makes it very dubious whether foilborne operation would be possible with one turbine incapacitated even at a still lower speed, say, 29 knots. The power required would be only about 5 percent less than one-half the power at 48 knots whereas the windage losses may well be considerably more than 5 percent.

Whether hullborne operation with less than one-half power, or the installation of turbines with more power than required for 48 knots, would justify the use of the cross-shaft arrangements shown in Figures 26 and 44 cannot be decided on the basis of the technical specifications given. In any event, the cross-shaft arrangement must be given serious consideration; this includes the problem of how in this case to deflect the jets for steering and reversing of the thrust.

*For the present study it was decided to use a vertical-shaft unit on top of each of the vertical struts of the rear foils. The craft is steered and thrust reversed by rotation of the pump casing as shown in Figure* 28. Since the jet velocity is unaffected by changes in the direction of the jet, single-engine operation may indeed be possible with this arrangement by deflecting the jet so that its thrust passes through the center of the resistance of the craft with one engine not operating. It must be considered that the vertical foil struts (enlarged because they also serve as inlet ducts) can sustain a substantial side force. The practical feasibility of this form of operation can be proven or disproven only by model and full-scale experiments.

In addition to the advantage of vertical-shaft units for steering and reversing, the elimination of one change in direction of flow on top of the vertical suction duct should result in a reduction of the inlet duct losses; these have been shown to be of major importance. The foregoing decision on arrangement will therefore be accepted without further investigation. A more detailed evaluation can be conducted only on the basis of fairly extensive design studies of various arrangements which fall outside of the scope of this report.

## 5.3 DIMENSIONLESS DESIGN OF THE INTAKE NACELLE AND DUCTING AND ESTIMATE OF THEIR LOSSES

The intake structure will be assumed to be a nacelle of the general type shown in Figure 44 connected with a duct which externally must be streamlined so as to minimize its skin friction and form drag in the submerged regions as well as to minimize the wave drag where this strut passes through the open water surface. The external shape of nacelle and strut has been given only qualitative consideration since external flow problems are not part of this study.

For the reasons given in Section 5.2 (Figure 53), flow conditions at 48 knots can safely be regarded as similar to those at 40 knots and will therefore not be given separate consideration. The only flow conditions considered will be those at 40 knots and at 20 knots, except for power and some cavitation considerations.

Figure 54 shows the nacelle design which will be developed in the following. Dimensions in feet will be derived in the following section and are to be disregarded for the present. Only the dimensions given in terms of the intake diameter $D_1$ are considered in the present section.

From the specifications and Figure 52, one can derive the following data:

| Speed of Travel | | Drag/Lift | Drag |
|---|---|---|---|
| knots | ft/sec | | lb |
| 20 | 33.8 | 0.0909 | 36,600 |
| 40 | 67.6 | 0.0665 | 26,800 |

The ratio of "prediffusion," i.e., the velocity at the intake cross section with diameter $D_1$ divided by the velocity of travel (approach), will be assumed to be 0.85 at 40 knots. This is conservative with respect to cavitation on the outside of the nacelle. A lower ratio would have been more efficient internally but might involve external cavitation problems.

The velocity in the intake (diameter $D_1$) at 40 knots is therefore:

$$V_1 = 0.85\ V_0 = 0.85 \times 67.6 \text{ ft/sec} = 57.46 \text{ ft/sec} \qquad (5.1)$$

At 20 knots, the intake nozzle must be opened up in order to avoid excessive acceleration and internal cavitation of the incoming flow. Two ways to do this are indicated diagrammatically in Figure 54. It

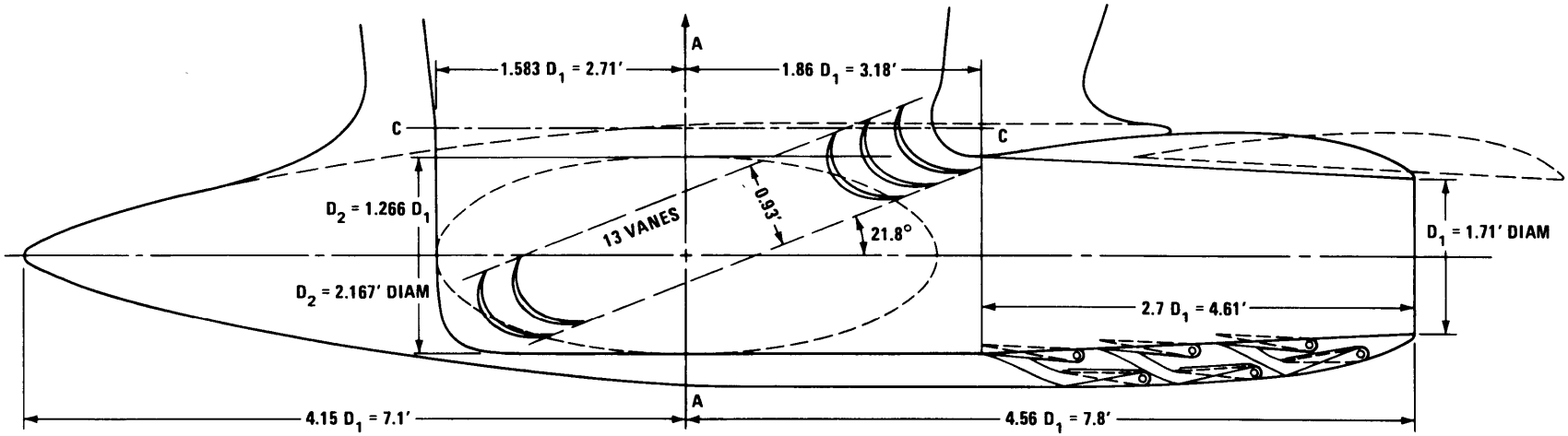


Vertical Section through Nacelle

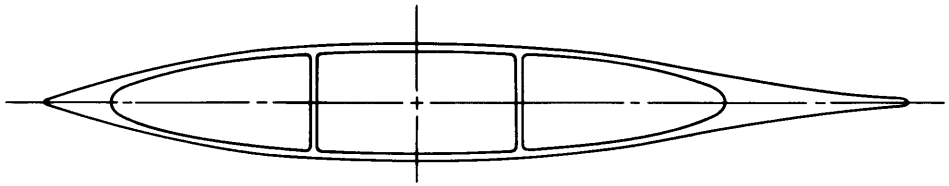

Horizontal Section D-D
(Section at Free Water Surface; see Figure 57)

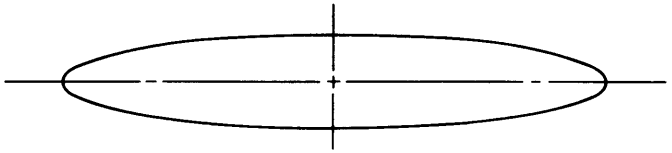

Horizontal Section C-C

Figure 54 – Vertical Section through Nacelle and Two Horizontal Sections through Vertical Duct

will be assumed that at 20 knots the incoming flow is neither accelerated nor retarded before reaching the internal cross section with diameter $D_2$ immediately in front of the vane system that turns the flow vertically upward. This means that the velocity in this cross section is 33.8 ft/sec at 20 knots.

For a fixed discharge nozzle area (as will be assumed here), the rate of flow $Q_{20}$ at 20 knots is (according to Figure 39) approximately:

$$Q_{20} = 0.945\ Q_{40} \tag{5.2}$$

where $Q_{40}$ is the rate of flow at the cruise velocity of 40 knots. Hence:

$$\frac{D_2^2\,\pi}{4} \text{ x } 33.8 \text{ ft/sec} = 0.945\ Q_{40} = 0.945\ \frac{D_1^2\,\pi}{4} \text{ x } 57.46 \text{ ft/sec}$$

$$\frac{D_2}{D_1} = \sqrt{\frac{0.945 \text{ x } 57.45}{33.8}} = 1.267 \tag{5.3}$$

as given in Figure 54.

The length of the conical diffusor from $D_1$ to $D_2$, which is 2.7 $D_1$, implies an included diffusor angle arc tan 0.267/2.7 = 5.6 deg, and this is quite reasonable.

After the turning vane system, the velocity will be the same as in front of the system, but the cross section must fit into a fairly long and thin support strut of the nacelle and the hydrofoil(s) connected therewith. After a process of trial and error, it was decided to place the vane system at an angle of 21.8 deg against the horizontal axis of the nacelle, with tan 21.8 deg = 0.4, which is geometrically convenient. The horizontal, elliptic flow section above the vane system has a major axis:

$$a = D_2/0.4 = 3.168\ D_1$$

and a minor axis

$$b = \frac{D_2^2}{a} = 0.4\ D_2 = 0.5 \text{ x } D_1$$

In order to account for the boundary layers, the minor axis was actually made 10 percent larger, i.e., 1.1 $b$ = 0.55 $D_1$. This elliptic flow section is shown as Section C-C in Figure 54.

The design of the vane system, and elements of its development are shown in Figure 55. A first approximation was obtained by the "mean streamline" method described in Chapters 27 and 29 of Reference 2. By successive approximations one arrives at the dimensionless "design" vane pressure distribution shown on the right side of Figure 55a. This assumed pressure distribution is plotted against the normal extent of the "mean streamline" derived from this pressure distribution rather than against the

normal extent of the vane itself, meaning "normal" to the vane-to-vane direction of the system. The figures given in parentheses next to the dimensionless pressure difference are these pressure differences multiplied by the local, traverse channel-width. This product determines the velocity change in the vane-to-vane direction of the system. The vane shape derived from this pressure distribution by means of the "mean streamline" is shown by a *broken-line* contour on the left side of Figure 55a.

The vane shape so obtained is found to have an unreasonably low, normal distance $d_2$ between successive vanes at the discharge side of the system. A correction of this defect leads approximately to the vane shape shown in solid lines.

The channel width normal to the vane shape is also shown in Figure 55a. It is needed to carry out the aforementioned operations of the mean streamline method. The determination of the mean velocity vectors within the system takes the variations of this width into account in a one-dimensional manner. The traverse passage width is shown for the maximum width at the fore and aft center of the system. The angle of convergence of the lateral walls of the system is therefore reduced near the forward and aft ends of the turning vane system.

The lift coefficient of the vanes obtained by integration of the dimensionless vane pressure diagram is $C_{L_1} = 0.8092$ with reference to the inlet velocity $V_2$ of the system. With reference to the vectorial mean relative velocity $V_\infty$, the lift coefficient $C_{L_\infty}$ is 1.6. This is still acceptable inasmuch as there is practically no static pressure rise from inlet to discharge of this system.

The ratio of vane length to spacing $t$ ("solidity") can be calculated from the familiar expression for the lift coefficient:

$$C_{L_\infty} = 2 \frac{\Delta V_u}{V_\infty} \frac{t}{\ell}$$

or

$$\frac{\ell}{t} = \frac{2}{C_{L_\infty}} \frac{\Delta V_u}{V_\infty}$$

where $\Delta V_u$ is the change of the fluid velocity parallel to the vane system, and $V_\infty$ is the vectorial mean between the inlet and discharge velocity $V_2$ to and from the vane system. The solidity is found to be $\ell/t = 2.3$ This determines the vane spacing $t$ for a given vane length $\ell$ .

The vane pressure difference on which the mean streamline solution was based should guarantee with some degree of approximation that there are no *major* local peaks of the vane pressure difference and therefore no major negative peaks of pressure on the low-pressure side of the vane. The correction of the vane shape from that connected with the mean streamline method should tend to reduce the pressure differences over the trailing parts of the vanes. According to the mean streamline method, the minimum pressure coefficient with reference to the system inlet velocity $V_2$ is about 0.45. This should prevent significant cavitation under the most unfavorable flow conditions present at 20 knots.

Figure 55 – Nacelle Turning Vane System

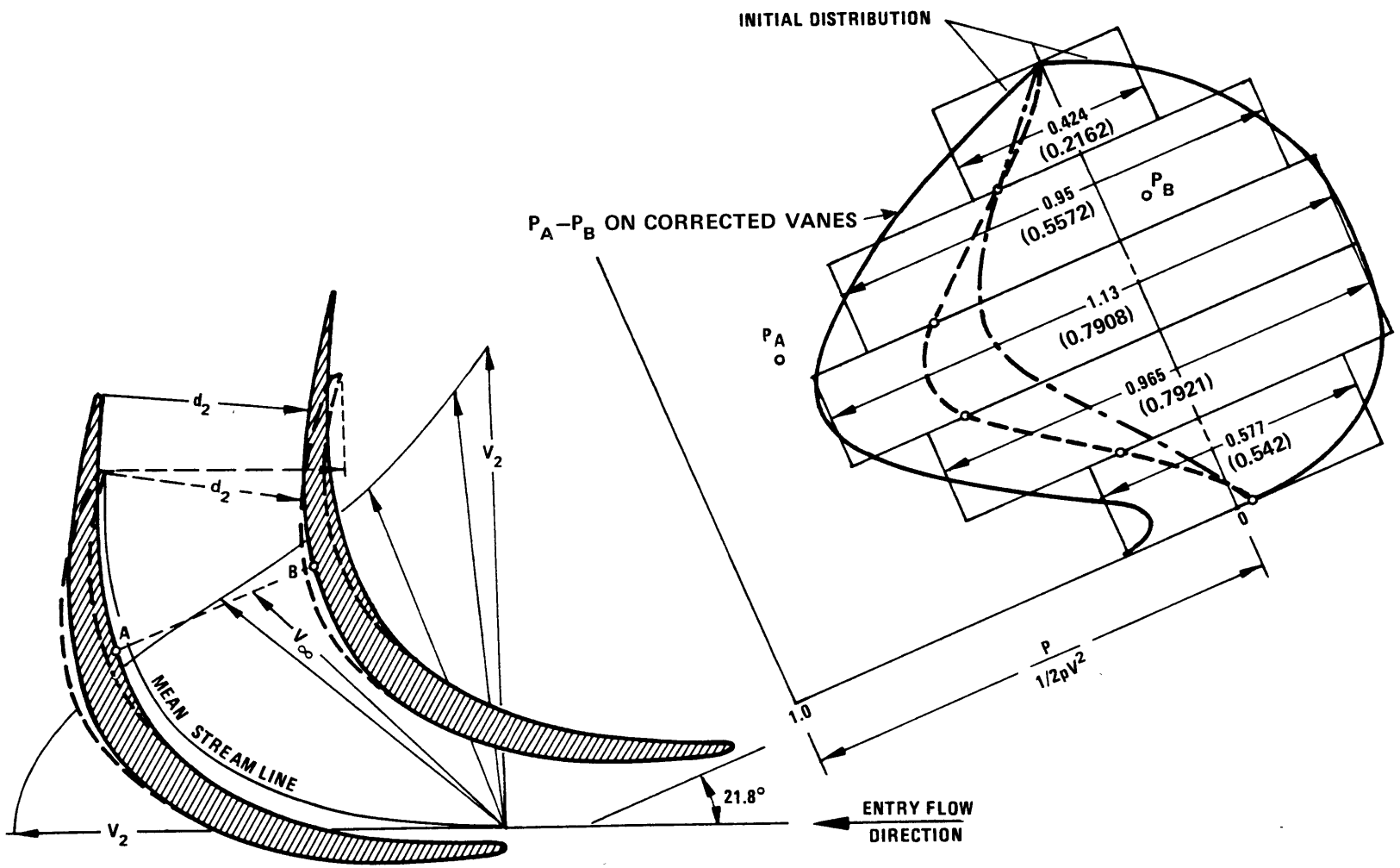


Figure 55a – Layout and Design Pressure Distribution

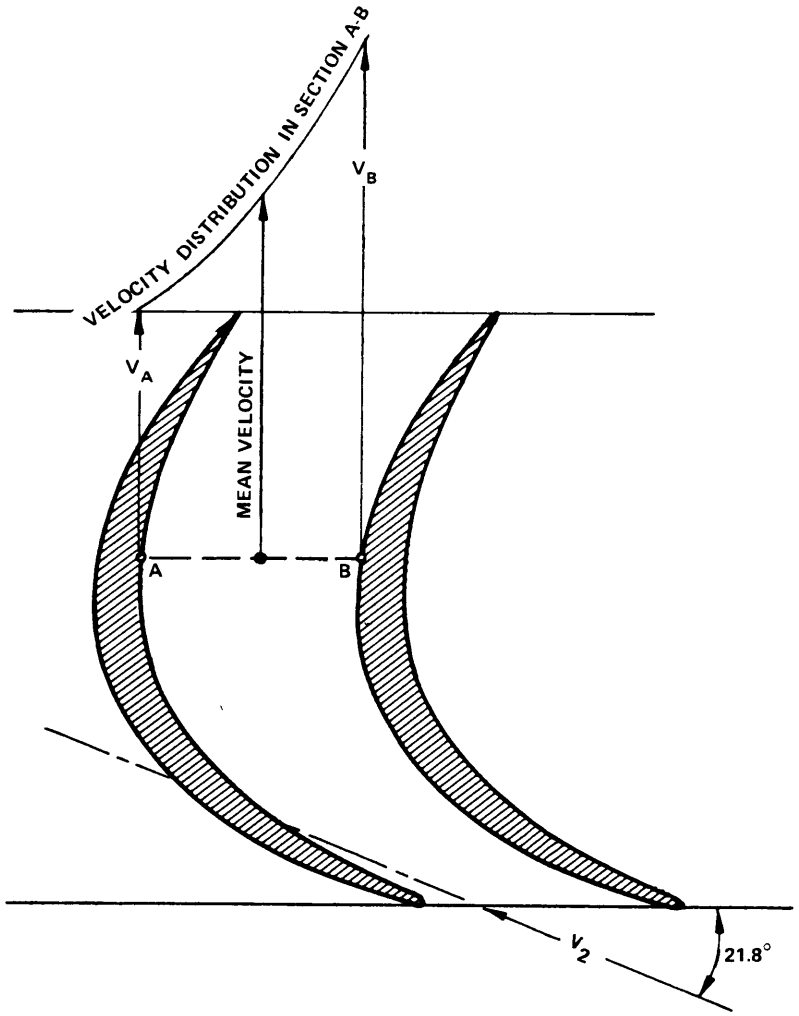


Figure 55b – Velocity Distribution over Flow Cross Section

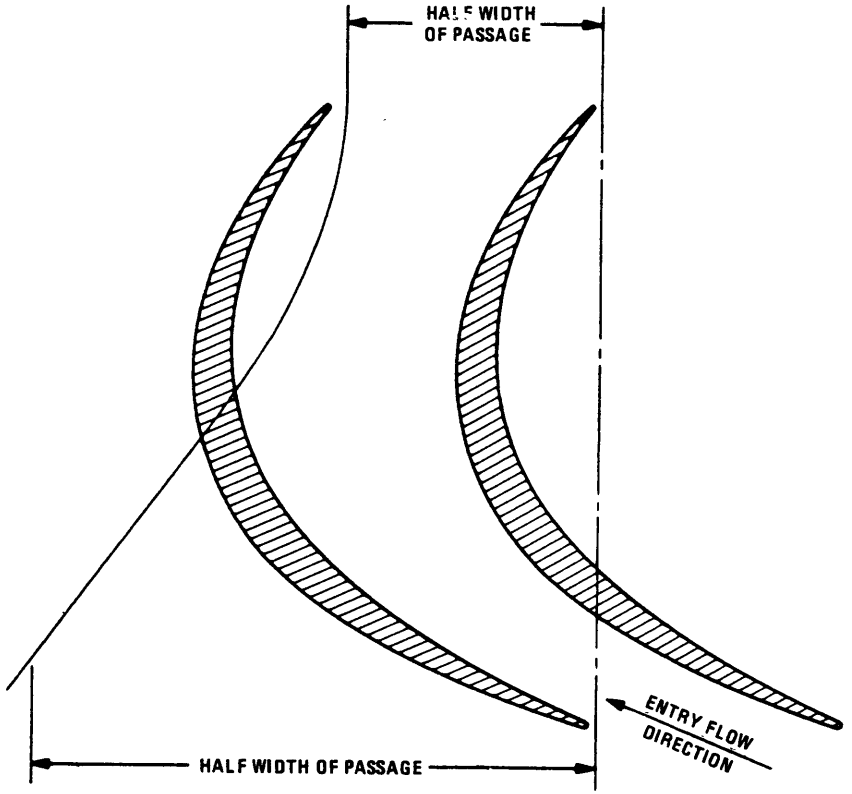


Figure 55c – Passage Transverse-Width Distribution

In view of the change in vane shape from the broken to the solid-line contour shown in Figure 55a, it is desirable to have an independent check on the expected performance of the revised vane shape. This check is accomplished approximately by an analysis of the velocity distribution in the vane section A-B shown in Figure 55b. The slope of the velocity distribution curve is determined from the radius of curvature $R$ of the streamlines on the basis of the relation for irrotational, plane flow:

$$\frac{dV}{dn} + \frac{V}{R} = 0$$

where $n$ is the coordinate across and normal to the flow. Starting from the mean velocity in cross section A-B (determined from the condition of continuity) the above equation was used to obtain the tangents for the velocity distribution curve shown in Figure 55b.

The vane pressures corresponding to the velocities so determined at Points A and B are indicated on Figure 55a as $p_A$ and $p_B$. They are higher than the vane pressures originally assumed. Since the *mean* pressures derived by the Bernoulli equation from the mean velocities shown in Figure 55a are also higher than those originally assumed, this departure from the design pressure distribution is quite reasonable. Recall also that the vane curvature was considerably reduced over the aft ends of the vanes and that the overall vane length was increased.

If the 10-percent allowance for boundary layer displacement is disregarded, the vertical discharge velocity from the vane system in the nacelle should be the same as the vane system inlet velocity $V_2$. This gives 33.8 ft/sec at 20 knots, and about 33.8 ft/sec x $Q_{40}/Q_{20}$ = 35.8 ft/sec at 40 knots.

The inlet velocity to the pump impeller can best be calculated from the ratio $2gH_{sv}/V_{m_i}^2$, where $V_{m_i}$ is the meridional or axial inlet velocity to the impeller. According to Figure 15, the ratio $2gH_{sv}/V_{m_i}^2$ should lie between 3 and 4. It should be as low as possible to avoid unnecessary retardation of the incoming flow. Therefore a value $2gH_{sv}/V_{m_i}^2 = 3$ will be assumed here for the 20-knot condition which is known to be the more severe with respect to cavitation.

The total inlet head of the pump impeller $H_{sv}$ may be estimated according to Equation (3.34):

$$H_{sv} = (1 - K)\ \frac{V_0^2}{2g} + h_{sv} - \Delta h_i \qquad (3.34)$$

The duct loss coefficient $K$ will be calculated below to be about 0.42 at 20 knots. The static intake head $h_{sv}$ is about 31 ft in sea water, and according to Figure 51, $\Delta h_i$ may be assumed to be not over 6 ft. At 20 knots, $V_0^2/2g_0$ = 17.8 ft. Hence:

$$H_{sv} = 0.58 \text{ x } 17.8 \text{ ft} + 25 \text{ ft} = 35.3 \text{ ft} \qquad (5.4)$$

and with $2g_0H_{sv}/V_{m_i}^2 = 3$,

$$V_{m_i} = \sqrt{2g_0 H_{sv}/3} = 27.5 \text{ ft/sec} \tag{5.5}$$

Therefore, there is only a slight retardation from $V_2$ = 33.8 ft/sec to the impeller inlet. It will be seen later that one will probably first retard to a lower velocity than 27.5 ft/sec and then reaccelerate to the impeller inlet. This will give a reasonably uniform inlet velocity distribution despite the change from the long cross-sectional shape inside the strut to the circular cross section at the impeller inlet.

Now estimate the head drop from intake to the pump impeller inlet for the 20-knot condition:

Approximate the intake passage as a straight pipe with a length-to-diameter ratio of 3. With a pipe friction coefficient of 0.02 (corresponding to a roughness-to-diameter ratio of about 0.001 to account for other irregularities, the intake head drop is $h_{L_1} = 0.06\ V_0^2/2g$. For well-designed turning vane systems such as considered here, a head loss $h_{L_2} = 0.16\ V_2^2/2g$ has been measured, where for the 20-knot condition $V_2 = V_0$.

Preliminary studies indicate that it is reasonable to assume a length-to-diameter ratio of 10 for the vertical, diffusing suction duct. By using the same pipe friction coefficient of $f = 0.02$, as before, and estimating the head loss in a diffusing passage by the velocity head at its inlet, the head loss in the vertical suction duct may be estimated to be:

$$h_{L_3} = 10 \times 0.02\ V_2^2/2g = 0.2\ V_0^2/2g$$

Hence, at 20 knots, the total head loss from intake to pump impeller inlet may be estimated to be

$$h_{L_{20}} = (0.06 + 0.16 + 0.2)\ V_0^2/2g$$

$$= 0.42\ V_0^2/2g \tag{5.6}$$

The factor 0.42 is obviously the duct-loss coefficient $K$ as appearing in Figures 4 and 5 (application to the 20-knot condition only).

The essential characteristics of the propulsion plant must be derived on the basis of the *cruise* condition (40 knots) because it is at that speed that optimum efficiency is required. Under these conditions, the entire flow enters through the front nacelle opening with diameter $D_1$. The velocity in the cross section with diameter $D_2$ (after the intake diffusor but in front of the turning vane system) is

$$V_2 = V_1 \frac{D_1^2}{D_2^2} = \frac{57.45 \text{ ft/sec}}{1.266^2} = 35.82 \text{ ft/sec} \tag{5.7}$$

The total head loss from the intake to the pump impeller inlet may now be estimated as follows by using the same coefficients as before except 0.2 for the vane system loss:

$$h_{L_1} = 0.06\ V_1^2/2g = 0.06\ V_0^2/2g\ (V_1^2/V_0^2)$$

$$h_{L_2} = 0.20\ V_2^2/2g = 0.20\ V_0^2/2g\ (V_2^2/V_0^2)$$

$$h_{L_3} = 0.20\ V_2^2/2g = 0.20\ V_0^2/2g\ (V_2^2/V_0^2)$$

The loss coefficient 0.2 for the vane system accounts for the nonuniformity in $V_2$ distribution at its inlet (a result of the diffusion in front of its inlet).

Since $V_1^2/V_0^2 = 0.85^2 = 0.724$ and $V_2^2/V_0^2 = (35.8/67.6)^2 = 0.2808$, one obtains for the total head loss from intake to pump:

$$h_L = (0.04345 + 2 \times 0.05616)\ V_0^2/2g = 0.156\ V_0^2/2g \tag{5.8}$$

i.e., the $K$ factor in Figures 4 and 5 is 0.156 at 40 knots and $V_1/V_0 = 0.85$.

## 5.4 SELECTION OF THE JET VELOCITY RATIO $\Delta V/V_0$ AND DETERMINATION OF THE RATE OF FLOW, PUMP HEAD, AND DIMENSIONS

According to Equation (2.15), the duct-loss coefficient $K$ (determined at the end of Section 5.3 for 40 knots), the jet elevation $\Delta h_j = 7$ ft (according to Figure 51), and the nacelle drag coefficient $K_T$ (yet to be determined) establish the jet efficiency $\eta_{j_4}$ as a function of the jet velocity ratio $\Delta V/V_0 = (V_j - V_0)/V_0$. In this determination one can use Figure 5 and replace $K$ in that figure by $K + 2g_0\,\Delta h_j/V_0^2$. It can be immediately read from Figure 7 that at 40 knots, $2g_0\,\Delta h_j/V_0^2 = 0.1$. On the other hand, the nacelle drag coefficient $K_T$ can only be estimated from experience with other submerged bodies. Here it will be assumed to be 0.10. (This coefficient is used to express only the excess in external drag over what would exist if the vertical struts were to serve solely as supports for the hydrofoils.)

With the before-stated values and assumptions, and with $K + 2g_0\Delta h_j/V_0^2 = 0.256$, Equation (2.15) assumes the form:

$$\eta_{j_4} = \frac{1 - 0.1\ V_0/2\,\Delta V}{1 + \dfrac{\Delta V}{2V_0} + 0.256\ \dfrac{V_0}{2\,\Delta V}} \tag{5.9}$$

which, of course, does not include pump and gear box losses. The evaluation of this equation is shown in Figure 56 as a broken line marked 0.256. The figure also includes other $\eta_{j_4}$ curves for nearby values of $K + 2g_0\,\Delta h_j/V_0^2$. This diagram is obviously an enlarged view of part of Figure 5 for $K_T = 0.10$.

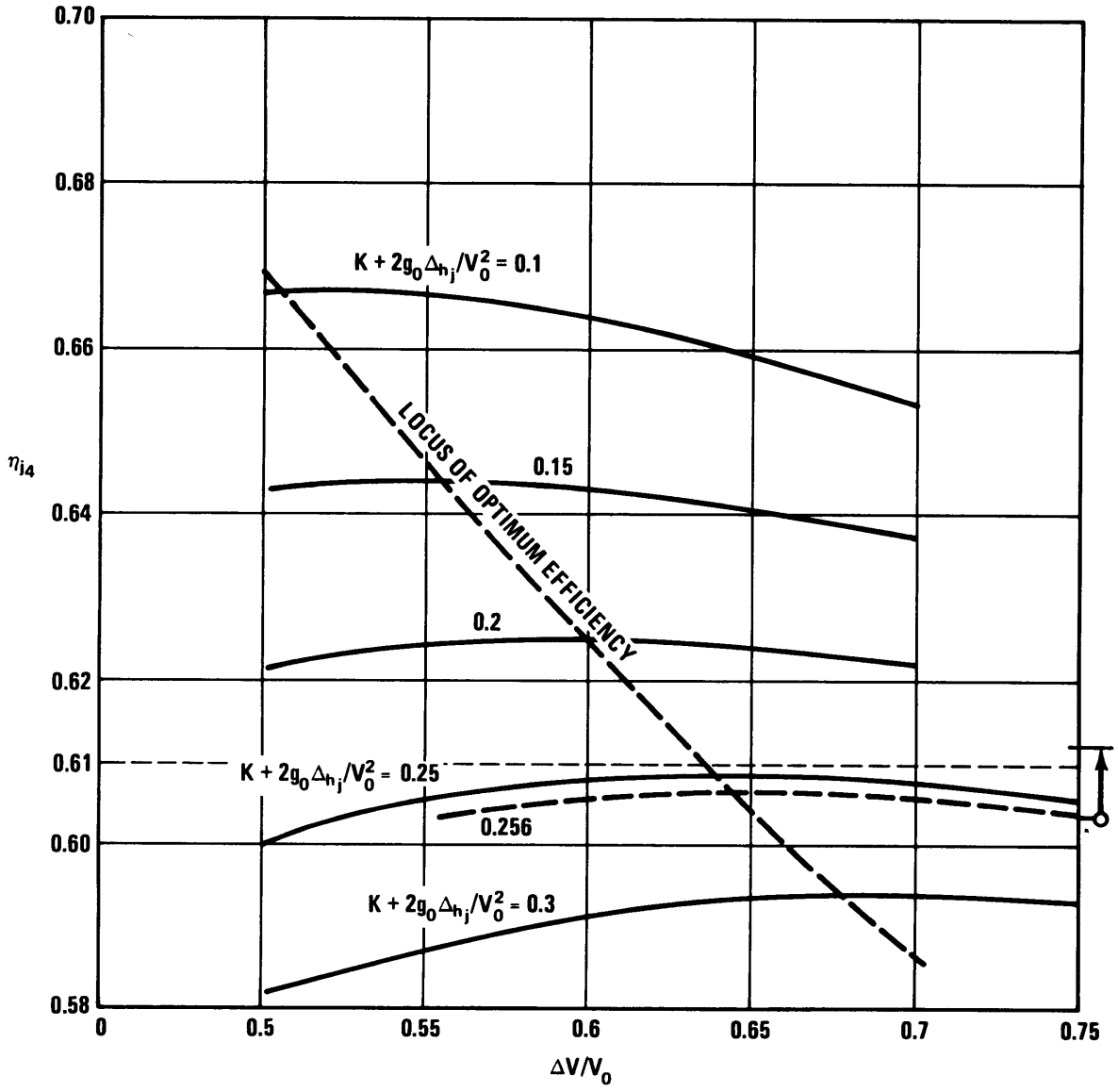


Figure 56 – Jet Efficiencies for Drag Coefficient $K_T$ = 0.1

The maximum value for $\eta_{j_4}$ occurs with $K + 2g_0 \Delta h_j / V_0^2 = 0.256$, evidently at slightly less than $\Delta V/V_0 = 0.65$. At first glance, this appears to be a good choice for this ratio, and it was used in preliminary calculations. However, the fact that $\eta_{j_4}$ varies between $\Delta V/V_0 = 0.57$ and $\Delta V/V_0 = 0.75$ only from 0.604 to 0.6065 indicates that the maximum of such a flat curve alone is a fairly poor criterion for choosing a value of $\Delta V/V_0$. To overcome this difficulty, it is necessary to violate for a moment the specifications that there must be negligible variation in strut drag with duct size (i.e., constant $L/D$ curve). Over the $\Delta V/V_0$ range just mentioned, the changes in $\eta_{j_4}$ for constant $K_T$ may well be smaller than changes that result in $K_T$ because of the fairly large changes in $\Delta V/V_0$ considered.

For the rate of flow calculated with $\Delta V/V_0 = 0.65$, the submerged strut surface area (one strut) was estimated to be approximately 60 $ft^2$ and the surface area of one nacelle about 130 $ft^2$, for a total of about 190 $ft^2$. The minimum strut area required to merely *support* the hydrofoils was estimated to be about 70 $ft^2$ for one strut (7-ft length x 5-ft depth x 2). When the strut is also used as intake nacelle and duct, the area increase is therefore about 120 $ft^2$ for $\Delta V/V_0 = 0.65$.

To maintain a desired thrust, the rate of flow is inversely proportional to $\Delta V/V_0$ (at constant speed of travel). The *strut* area changes for similar cross-sectional shape with the square root of the rate of flow. This is so because the depth of submergence is constant whereas the nacelle surface area changes proportionally to the rate of flow (constant diameter-to-length ratio).

For a step from $\Delta V/V_0 = 0.65$ to $\Delta V/V_0 = 0.75$, the strut surface area changes to 60 $ft^2$ x $(0.65/0.75)^{1/2}$ = 55.8 $ft^2$; the nacelle surface area also changes to 130 $ft^2$ x 0.65/0.75 = 112.7 $ft^2$. This gives a total of 168.5 $ft^2$ or an excess of approximately 100 $ft^2$ over the minimum strut area (70 $ft^2$).

For similar flow cross sections, the surface area of the strut is proportional to its frontal area. This may well be assumed to be proportional to the wave drag at the free surface. Thus the total drag follows the same law as the skin-friction drag. Therefore, the drag coefficient $C_T$ may be expected to be reduced proportionally to the "excess" surface area, i.e., in the ratio 100 to 120. Since a 0.1 difference in drag coefficient $C_T$ changes the efficiency $\eta_{j_4}$ by about 0.05 of its scale (see Figure 5), a change in $C_T$ by the ratio of 100/120 = 0.833 should increase $\eta_{j_4}$ by 0.84 percent points of its scale, for example, from 60.4 to 61.2 percent at $\Delta V/V_0 = 0.75$, as shown by the arrow in Figure 56. This implies that the actual jet efficiency would be higher at $\Delta V/V_0 = 0.75$ than at 0.65. In fact, there is no reason to assume that $\Delta V/V_0 = 0.75$ would lead to an optimum in $\eta_{j_4}$ since even higher values of $\Delta V/V_0$ might give better efficiencies. However, in agreement with the aforementioned specification, there is no reason to assume that the above simple reasoning would apply to larger changes in $\Delta V/V_0$.

In view of the foregoing considerations, it is reasonable to conclude that $\Delta V/V_0 = 0.65$ does *not* constitute a true optimum value of this ratio, and that $\Delta V/V_0 = 0.75$ is closer to such an optimum. As a consequence, $\Delta V/V_0 = 0.75$ was selected as the jet velocity increase ratio to be used in this study without further justification.

Here it must be considered that the increase in $\Delta V/V_0$, specifically the resulting reduction in the rate of pump flow, will reduce the pump, gear box, and duct weight including the weight of the water contained

in parts located above the free water surface. On the other hand, the duct friction losses might increase because the ratio of duct length to the "hydraulic diameter" increases with $\Delta V/V_0$, and the present value of this ratio appears to be sufficient for effective retardation of the duct flow. A tradeoff study of the overall ship characteristics will generally give a higher optimum $\Delta V/V_0$ ratio than will hydrodynamic considerations alone.

This type of optimization can be carried out only on the basis of a number of design studies for various values of $\Delta V/V_0$. This clearly exceeds the scope of the present investigation. This is probably the reason why a constant $L/D$ curve was included in the specifications. Suffice it to say that the hydrodynamic principles, which are the primary objective of the present study, would not be affected fundamentally if overall investigations showed that a different (presumably still higher) ratio than $\Delta V/V_0 = 0.75$ is more advantageous.

With $\Delta V/V_0 = 0.75$ at 40 knots established, it is possible to calculate definite values for the rate of flow, for the pump head and for various critical dimensions of the hydrodynamic propulsion system.

The rate of flow and pump head will be calculated for the cruise condition of $V_0$ = 40 knots = 67.6 ft/sec. Therefore, with $\Delta V/V_0 = 0.75$, $\Delta V$ = 50.7 ft/sec and according to Equations (1.1) and (3.32), and the data derived from the specifications (see page 183),

$$Q_{tot_{40}} = \frac{26{,}800}{2 \text{ x } 50.7 \text{ ft}^3/\text{sec}} = 264.2 \text{ ft}^3/\text{sec} \tag{5.10}$$

where $\rho$ = 2 slugs/ft$^3$ is the standard value used in this report for the mass per cubic foot of sea water.

The volume flow per intake or per pump is

$$Q_{tot_{40}}/2 = Q_{40} = 132.1 \text{ ft}^3/\text{sec} \tag{5.11}$$

From Equation (3.33a) as the pump head is calculated

$$H = \frac{V_0^2}{2g_0} \left[ 2 \frac{\Delta V}{V_0} + \left( \frac{\Delta V}{V_0} \right)^2 + K + 2g_0 \Delta h_j / V_0^2 \right]$$

At 40 knots, $V_0^2/2g$ = 71.1 ft and $2g_0 \Delta h_j/V_0^2 = 0.10$ according to Figure 51 and Figure 7. Section 5.3 gave the duct-loss coefficient $K$ as 0.156. Hence:

$$H = 71.1 \text{ ft } [1.5 + 0.563 + 0.156 + 0.10] = 164.9 \text{ ft} \tag{5.12}$$

Finally, the intake diameter $D_1$ in Figure 54 can now be determined for 40 knots as:

$$\frac{D_1^2 \pi}{4} \text{ x } V_1 = Q_{40}; \text{ or } \frac{D_1^2 \pi}{4} = \frac{132.1 \text{ ft}^2}{57.45} = 2.3 \text{ ft}^2$$

and

$$D_1 = \left(\frac{4}{\pi} \text{ x } 2.3 \text{ ft}^2\right)^{1/2} = 1.71 \text{ ft} \tag{5.13}$$

as shown in Figure 54. All other dimensions in that figure can be derived from $D_1$.

It will be assumed that the propulsion pump has a fixed discharge nozzle area. As a consequence, the rate of flow at 20 knots ($Q_{20}$) is not the same as at 40 knots, neither is the pump head at 20 knots ($H_{20}$) the same as at 40 knots. The new values $Q_{20}$ and $H_{20}$ can be calculated by successive approximations as described in Section 3.6. However, for the present very preliminary design considerations, it is sufficient to read $Q_{20}$ and $H_{20}$ from the $Q_1/Q_c$ and $H_1/H_c$ curves in Figure 39. The method of calculation is approximate only and the difference between $\Delta V/V_0 = 0.7$, as used in that figure, and $\Delta V/V_0 = 0.75$, as employed in this example, can hardly be very significant.

From Figure 39 and with $V_{0_{20}}/V_{0_{40}} = 0.50$, $Q_{20}/Q_{40} = 0.945$ and $H_{20}/H_{40} = 1.060$. Therefore, $Q_{20} = 0.945$ x 132.1 ft$^3$/sec = 124.8 ft$^3$/sec, and $H_{20} = 1.060$ x 164.5 ft = 174.4 ft.

## 5.5 DESIGN OF THE DUCT FROM THE NACELLE TO THE PROPULSION PUMP

The vertical discharge velocity from the nacelle was made equal to the inlet velocity $V_2$ to the vane system in the nacelle. The definition of $V_2$ at the vertical discharge included the 10-percent increase in cross section from inlet to discharge of this vane system to account for the growth of boundary layers in the system.

The inlet and discharge velocities of the vane system are $V_{2_{20}} = 33.8$ ft/sec at 20 knots (33.8 ft/sec = 20 knots) and 33.8/0.945 = 35.8 ft/sec at 40 knots. The inlet cross section to the vane system is $D_2^2\pi/4$ = 124.8 ft$^3$/sec/33.8 ft/sec = 3.692 ft$^2$, and $D_2 = 2.165$ ft = 1.266 $D_1$. (Evidently the same result must be obtained with the rate of flow and velocity at 40 knots.)

The discharge cross section from the turning vane system is evidently 1.1 x 3.692 = 4.06 ft$^2$. This is formed by an ellipse with (according to Section 5.3) a major axis 3.166 $D_1$ = 3.166 x 1.71 ft = 5.414 ft and a minor axis 0.55 $D_1$ = 0.55 x 1.71 ft = 0.94 ft.

The upper end of the vertical inlet duct is obviously the inlet to the pump impeller. Its area is determined mainly by cavitation considerations, and the cavitation requirements are known to be most severe under the 20-knot operating condition. The 20-knot condition therefore determines the impeller inlet.

The inlet conditions to the impeller were determined in Section 5.3 under the assumption that $2g_0H_{sv}/V_{m_i}^2 = 3$. The data derived there for 20 knots are listed here for convenience:

Total head drop from intake to pump: $h_{L_{20}} = 0.42\ V_0^2/2g$

Total pump inlet head at 20 knots (according to Equation (3.34) and Figure 51): $H_{sv_{20}} = 35.3$ ft

Meridional (axial) inlet velocity to the pump impeller: $V_{m_{i_{20}}} \sqrt{2g_0 H_{sv_{20}}/3} = 27.5$ ft/sec.

According to the last value, the impeller inlet area is $D_i^2\pi/4 = 124.7$ ft$^3$/sec/27.5 ft/sec = 4.535 ft$^2$ and the inlet diameter is $D_i = 2.4$ ft.

From these and the foregoing figures, it is evident that the retardation of flow from the nacelle to the pump is not severe. In fact, in the transition from the elliptic cross section inside the strut to the circular inlet to the impeller, it is probably advisable to retard the flow to a lower velocity than $V_{m_i}$ and to reaccelerate to $V_{m_i} = 27.5$ ft/sec.

If the chosen minimum velocity in the inlet duct is assumed to be 22 ft/sec at 20 knots (which is the average over the maximum elliptic cross section), then

$$\left(\frac{a \times b \times \pi}{4}\right)_{max} = \frac{124.7 \text{ ft}^3}{22 \text{ ft/sec}} = 5.67 \text{ ft}^2$$

To judge the rate of diffusion, it is customary to convert the actual diffusor into a diffusor with circular cross sections, to use the actual cross sections and length, and to calculate the "enclosed" diffusor angle.

The *minimum* cross section of the diffusing inlet duct is 4.06 ft$^2$, and the corresponding diameter $\sqrt{4.06 \text{ ft}^2 \times 4/\pi} = 2.274$ ft. The *maximum* equivalent diffusor diameter is $\sqrt{5.67 \text{ ft}^2 \times 4/\pi} = 2.687$ ft.

According to Figure 57 (prepared according to Figures 51 and 54), the vertical distance between these two cross sections is 6.6 ft. Thus the tangent of the enclosed diffusor angle is $(2.687 - 2.274)/6.6 = 0.413/6.6 = 0.0626$, and the enclosed diffusor angle is 3.6 deg. This is quite conservative and certainly acceptable.

The cross section at the free water level outside the strut is of particular interest because it determines the strut section that is responsible for the wave drag of the strut. If the cross section increase along the duct is linear, this cross section should be 4.94 ft$^2$. The actual area of Section D-D in Figures 54 and 57 is 4.835 ft$^2$. This is slightly less than the cross section given by a linear increase, which favors (reduces) the cross section at the most critical position, i.e., the free water level.

The vertical duct requires at least two longitudinal internal ribs in order to strengthen the duct against the internal pressure which is larger than the external pressure by the diffusion from the free-stream velocity $V_0$ to the duct velocity. This pressure increase must be calculated for the maximum velocity of travel (48 knots) and is approximately $(81.1^2 - 28^2)$ ft$^2$/sec$^2$ $\rho/2 = 5800$ psf = 40 psi.

The wall can be considered as a uniformly loaded, continuous beam. The span to wall thickness ratio is shown in Figure 54 to be about $s/t = 30$, and the stress-to-pressure ratio is

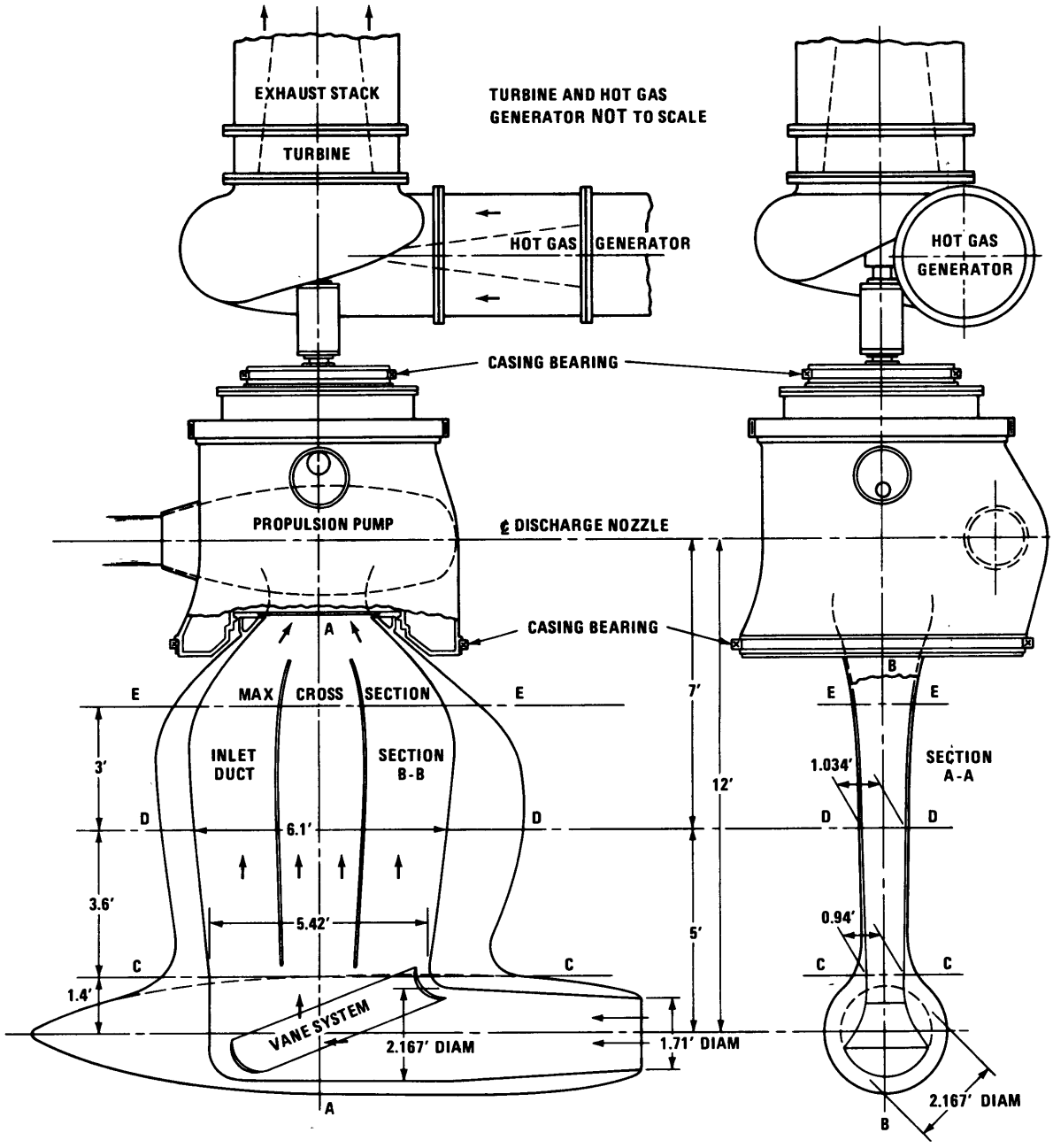


Figure 57 – Inlet Duct System and Overall Arrangement of One Propulsion Unit

$$\frac{\sigma}{p} = \frac{1}{2}\frac{s^2}{t^2} = 450$$

With the above figure of $p$ = 40 psi, this gives a bending stress of 18,000 psi. This value must be considered in the selection of the strut material.

Figure 54 shows the strut cross section D-D at the free water level. Its external shape is merely an estimate, indicating that the leading edge must probably be thin and slender to minimize the external wave drag. The external Froude number is, of course, extremely high and will require a very high-speed towing channel for proper experimentation and design development.

The transition from the elliptic duct section E-E to the circular inlet to the impeller is shown in Figure 57 under the assumption that this transition begins somewhat below the maximum cross section E-E The elliptic section E-E has therefore a slightly larger ratio of minor to major axis than sections C-C, D-D, and the sections in between.

It should be understood that a successful development of the vertical inlet duct as well as of the nacelle cannot be accomplished without careful and detailed experimental investigations of the internal as well as the external flow. However, every detail of the initial layout described here should receive the most careful consideration in order to keep the time required for the overall development within reasonable limits.

## 5.6 DESIGN OF THE PROPULSION PUMP IMPELLER

The impeller inlet diameter was determined in Section 5.5 as $D_i$ = 2.4 ft which is also the discharge diameter of the vertical inlet duct. This diameter was calculated from $V_{m_{i_{20}}}$ = 27.5 ft/sec, derived by $2g_0 H_{sv}/V_{m_i}^2 = 3$, and $Q_{20}$ = 124.7 ft$^3$/sec. The rate of flow $Q_{20}$ and $V_{m_{i_{20}}}$ apply to the 20-knot condition which is critical with respect to cavitation.

The NPSH was established as $H_{sv}$ = 35.3 ft at 20 knots, and (at the end of Section 5.4) the pump head was found to be $H_{20}$ = 174.3 ft at the same velocity of travel. Therefore, the Thoma cavitation parameter is:

$$\sigma_H = \frac{H_{sv}}{H} = \frac{35.3}{174.3} = 0.2026$$

Somewhat arbitrarily, the maximum suction specific speed at 20 knots will be assumed to be 0.70 (in contrast to the value $S$ = 1.0 assumed in Chapter 3). This lower value should be sufficient for the conservative operating conditions assumed here. Thus, the basic specific speed is:

$$n_S = S \times \sigma^{3/4} = 0.70 \times 0.2026^{3/4} = 0.2106 \qquad (5.14)$$

According to the first part of Chapter 3:

$$n_S = \frac{1}{2.106} \left( \frac{U_{0_{min}}^2}{2g_0 H} \right)^{3/4} \left( \frac{V_{m_i}}{U_i} \right)^{1/2} \left( \frac{D_i}{D_{0_{min}}} \right)^{3/2} \tag{5.15}$$

for zero hub diameter ($D_h/D_i = 0$). This is a reasonable assumption for an overhung, single-suction impeller.

According to Figure 15, $V_{m_i}/U_i = 0.29$ for $S = 0.7$ and $2g_0 H_{sv}/V_{m_i}^2 = 3$. Furthermore, it is reasonable to assume for radial- or mixed-flow pumps that $2g_0 H/U_{0_{min}}^2 = 1.0$. With $n_S = 0.2106$ and the foregoing values and assumptions, Equation (5.15) assumes the numerical form:

$$n_S = 0.2106 = \frac{0.5385}{2.106} \left( \frac{D_i}{D_{0_{min}}} \right)^{3/2}$$

$$\frac{D_{0_{min}}}{D_i} = 1.214^{2/3} = 1.138 \tag{5.16}$$

The maximum impeller diameter which receives the stream surface along the outer shroud of the impeller (beginning at the "eye" diameter $D_i$) must be determined in such a manner that the retardation along this surface is not excessive. It will be assumed conservatively that the ratio of relative velocity retardation along this stream surface is:

$$w_{u_2}/w_{u_1} = 0.75 \tag{5.17}$$

Furthermore, considering that $w_{u_1} = -U_i$ and $-w_{u_2} = U_{0_{max}} - V_{u_0}$, as well as

$$2g_0 H/U_{0_{max}}^2 = (2g_0 H/U_{0_{min}}^2) \frac{D_{0_{min}}^2}{D_{0_{max}}^2} = 2\eta_h \frac{V_{u_0}}{U_{0_{max}}} \tag{5.18}$$

where $\eta_h$ is the "hydraulic efficiency" (not including increases in torque by fluid and seal plus bearing friction), it follows that:

$$\frac{w_{u_2}}{w_{u_1}} = 0.75 = \frac{D_{0_{max}}}{D_{0_{min}}} \times \frac{D_{0_{min}}}{D_i} \left( 1 - \frac{V_{u_0}}{U_{0_{max}}} \right) = \frac{D_{0_{max}}}{D_{0_{min}}} \times 1.138 \left( 1 - \frac{V_{u_0}}{U_{0_{max}}} \right) \tag{5.19}$$

Assuming $\eta_h = 0.9$ and using $2g_0 H/U_{0_{min}}{}^2 = 1$, one obtains:

$$\frac{V_{u_0}}{U_{0_{max}}} = \frac{D_{0_{min}}{}^2}{D_{0_{max}}{}^2} \times \frac{1}{1.8}$$

and therefore Equation (5.19) appears in the form:

$$0.75 = 1.138 \left[ \frac{D_{0_{max}}}{D_{0_{min}}} - \frac{D_{0_{min}}}{D_{0_{max}}} \frac{1}{1.8} \right] \tag{5.20}$$

This quadratic equation has the solution:

$$\frac{D_{0_{max}}}{D_{0_{min}}} = 1.144 \tag{5.21}$$

and therefore:

$$\frac{D_{0_{max}}}{D_i} = \frac{D_{0_{max}}}{D_{0_{min}}} \times \frac{D_{0_{min}}}{D_i} = 1.144 \times 1.138 = 1.302 \tag{5.22}$$

Furthermore, it will be assumed (after some process of trial and error) that the axial width of the impeller between shrouds is

$$b_0 = \frac{D_i}{3} \tag{5.23}$$

which, by the condition of continuity, leads to

$$\frac{V_{m_0}}{V_{m_i}} = 0.578 \tag{5.24}$$

and with $V_{m_i}/U_i = 0.29$, as stated before:

$$\frac{V_{m_0}}{U_i} = \frac{V_{m_0}}{V_{m_i}} \frac{V_{m_i}}{U_i} = 0.578 \times 0.29 = 0.168 \tag{5.25}$$

Furthermore, it follows from $2g_0 H/U_{0_{min}}^2 = 1 = 2\,\eta_h\,(V_{u_0})/(U_{0_{min}})$ and $\eta_h = 0.9$ that at $D = D_{0_{min}}$:

$$\frac{V_{u_0}}{U_{0_{min}}} = \frac{1}{1.8} = 0.556 \tag{5.26}$$

and at $D = D_{0_{max}}$:

$$\frac{V_{u_0}}{U_{0_{max}}} = 0.556 \times \frac{D_{0_{min}}^2}{D_{0_{max}}^2} = 0.425 \tag{5.27}$$

Equations (5.16) and (5.21) through (5.27) permit the construction of the impeller profile and of the principal velocity diagrams as shown in Figure 58. The inlet and discharge velocity diagrams determine the vane shape on the basis of theoretical or empirical rules. Figure 59 presents a first approximation of this vane shape in the form of a conformal representation of three vane sections along three meridional stream surfaces. Two follow the front and back shroud surfaces and a third is halfway between. Note that the central portions of the vanes are somewhat steeper than the vane ends to allow for vane blockage and to obtain a reasonable vane pressure distribution. A radial section A-A through two successive vanes, derived from Figure 59, is shown in the upper, right corner of Figure 58. For manufacturing purposes, the vane shape is determined by a series of such sections and corresponding sections normal to the axis of rotation ("board sections," not shown).

The velocity diagrams as given in Figure 58 show the following velocities:

$$V_{m_{i_{20}}} = 27.5 \text{ ft/sec}; \; U_i = 27.5/0.29 = 94.8 \text{ ft/sec}$$

$$U_{0_{min}} = 1.138\, U_i = 107.9 \text{ ft/sec}$$

$$H_{20} = U_{0_{min}}^2/2g_0 = 180.6 \text{ ft at 20 knots}$$

$$H_{40} = H_{20}/1.06 = 170.4 \text{ ft at 40 knots}$$

The head values turn out to be slightly higher than originally derived. The discrepancy is attributed to minor numerical inaccuracies which are fortunately on the safe side, i.e., to meet the actual 20- and 40-knot requirements; the speed of rotation can be slightly less than assumed here. The most important impeller dimensions are:

Inlet diameter $D_i = 2.4$ ft

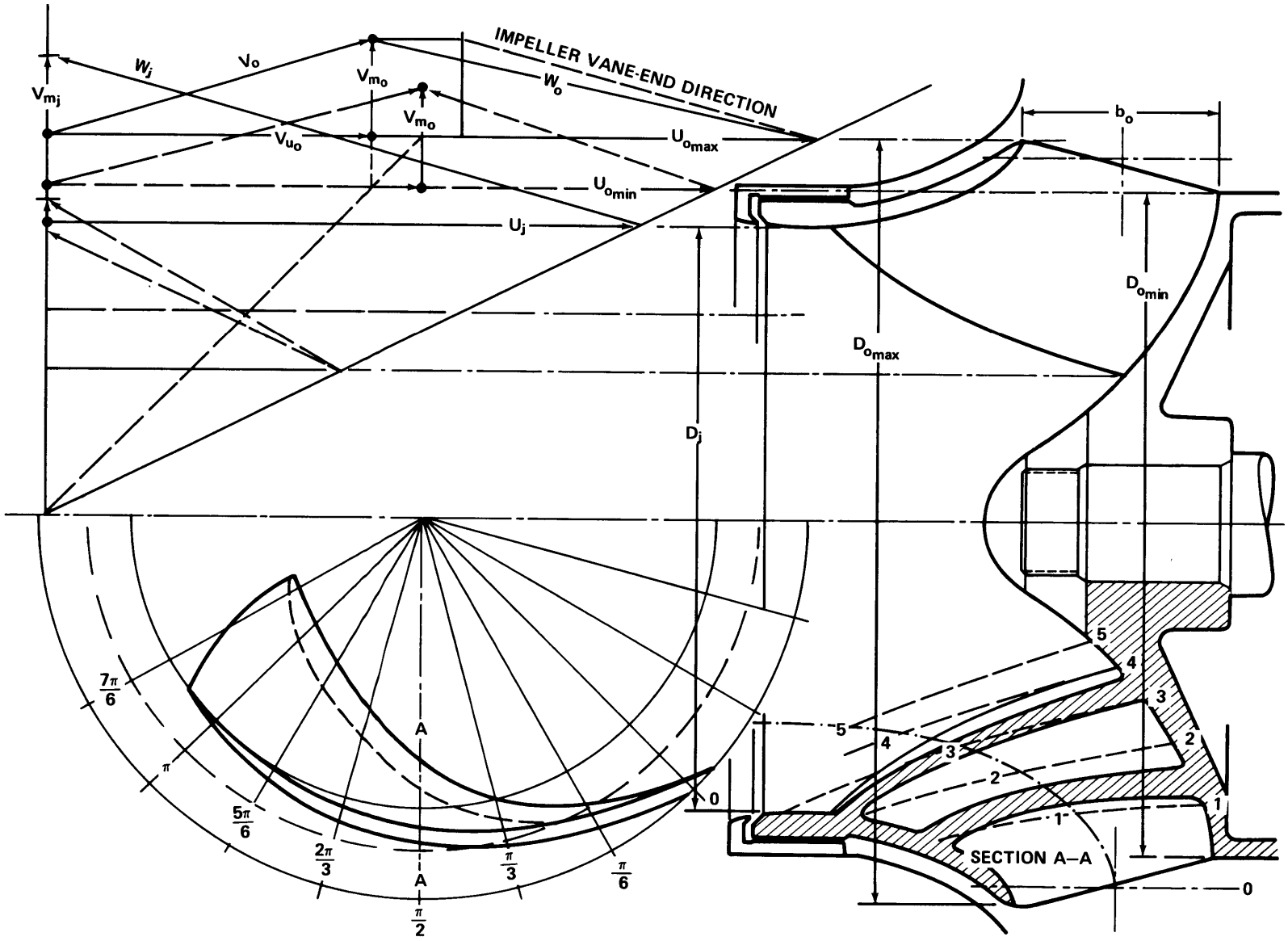


Figure 58 – Layout of Propulsion Pump Impeller, First Approximation

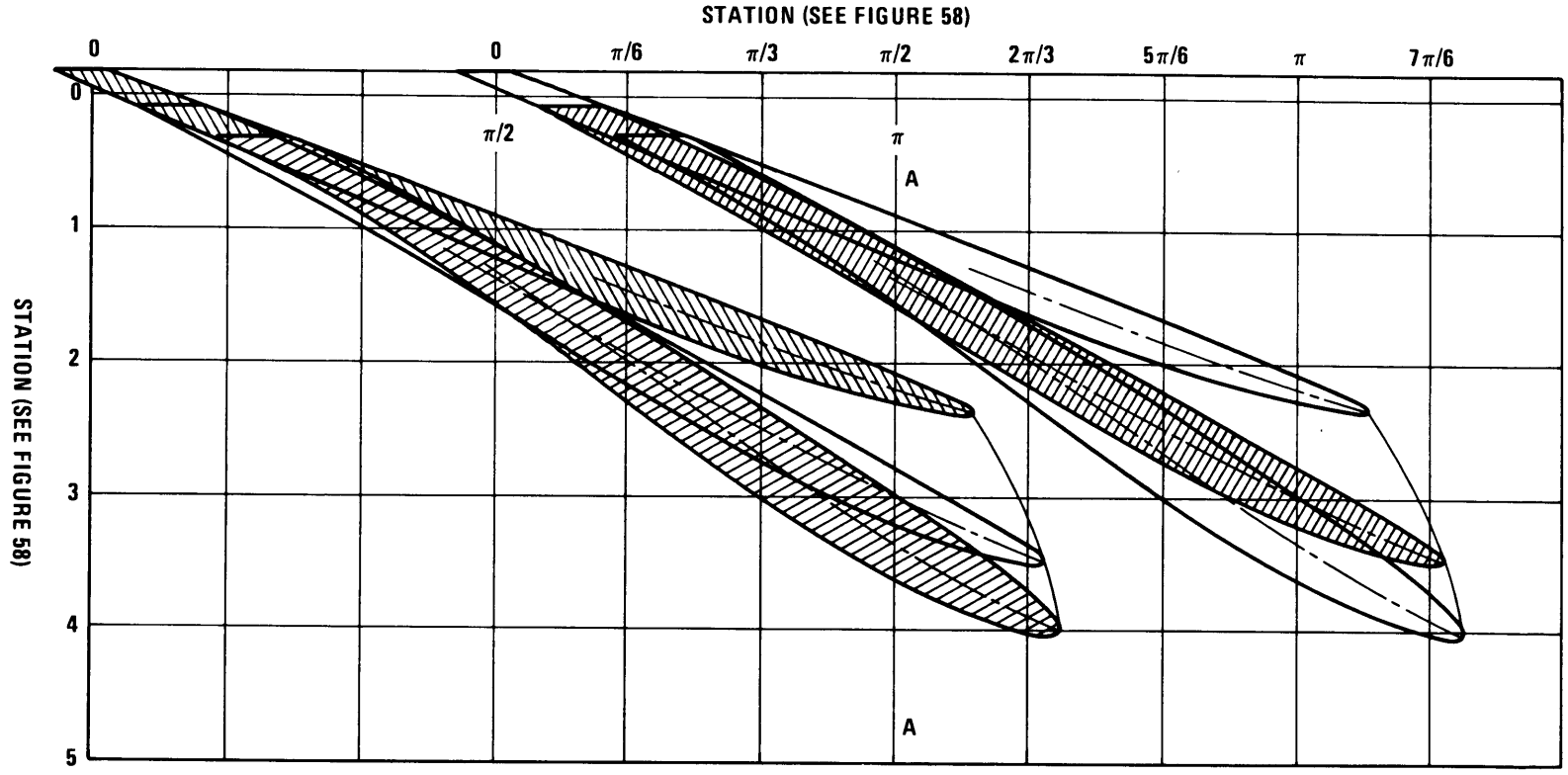


Figure 59 – Conformal Map of Impeller Vanes,
First Approximation

Minimum discharge diameter $D_{0_{min}} = 1.138\ D_i = 2.73$ ft

Maximum discharge diameter $D_{0_{max}} = 1.303\ D_i = 3.127$ ft

Discharge width $b_0 = D_i/3 = 0.80$ ft

## 5.7 DESIGN OF THE PROPULSION PUMP CASING

The propulsion pump casing is intended to be a volute casing without vanes as shown in Figure 28 because this form of casing must be expected to lead to the highest pump efficiency, particularly as the flow after the maximum radial section through the volute (adjacent to the "splitter" or "tongue") is accelerated.

So far as it is open toward the impeller, the flow in the volute must follow the law of radially uniform angular momentum to expose the impeller to a circumferentially uniform static pressure.

The radial volute section areas will be calculated for the cruise condition at 40 knots because maximum efficiency is desired under these conditions. According to the Euler turbomachinery equation (Equation (3.9)),

$$H_{40} = 170.4 \text{ ft} = \eta_h \times V_{u_0} \times U_0/g_0 \tag{5.28}$$

since it is assumed that the flow does not have a peripheral velocity component at the impeller inlet.

At $D_{0_{max}}$, $U_{0_{max}} = 1.303\ U_i = 123.5$ ft/sec. Hence

$$V_{u_0} = g_0 H/\eta_h\ U_{0_{max}} = 49.35 \text{ ft/sec} \tag{5.29}$$

By a process of trial and error, one can estimate the distance of the maximum volute area ("throat"), i.e., its center, from the axis of rotation to be $r_{th} = 1.8\ D_{0_{max}}/2$ so that, according to the law of constant angular momentum, the volute throat velocity is:

$$V_{th} = \frac{49.35 \text{ ft/sec}}{1.8} = 27.4 \text{ ft/sec} \tag{5.30}$$

Hence, with $Q_{40} = 132.25$ ft$^3$/sec, the volute throat area is $A_{th} = 132.25$ ft/sec/27.4 ft/sec = 4.82 ft$^2$.

The maximum volute section indicated in Figure 60 has approximately this area. The section is rather large compared with the impeller dimensions, but this is natural for a radial-flow pump of fairly high specific speed.

The mechanical construction of the casing follows the scheme shown in Figure 28. Thereby it avoids the large, horseshoe-shaped radial ribs which would otherwise be necessary to withstand the pressure inside the volute. Moreover this construction minimizes the maximum outside radius of the volute part of the casing. The maximum circumferential stress in the downward axial extension from the volute casing has been found to be no greater than 12,000 psi at 48 knots for the wall thicknesses shown in Figure 60.

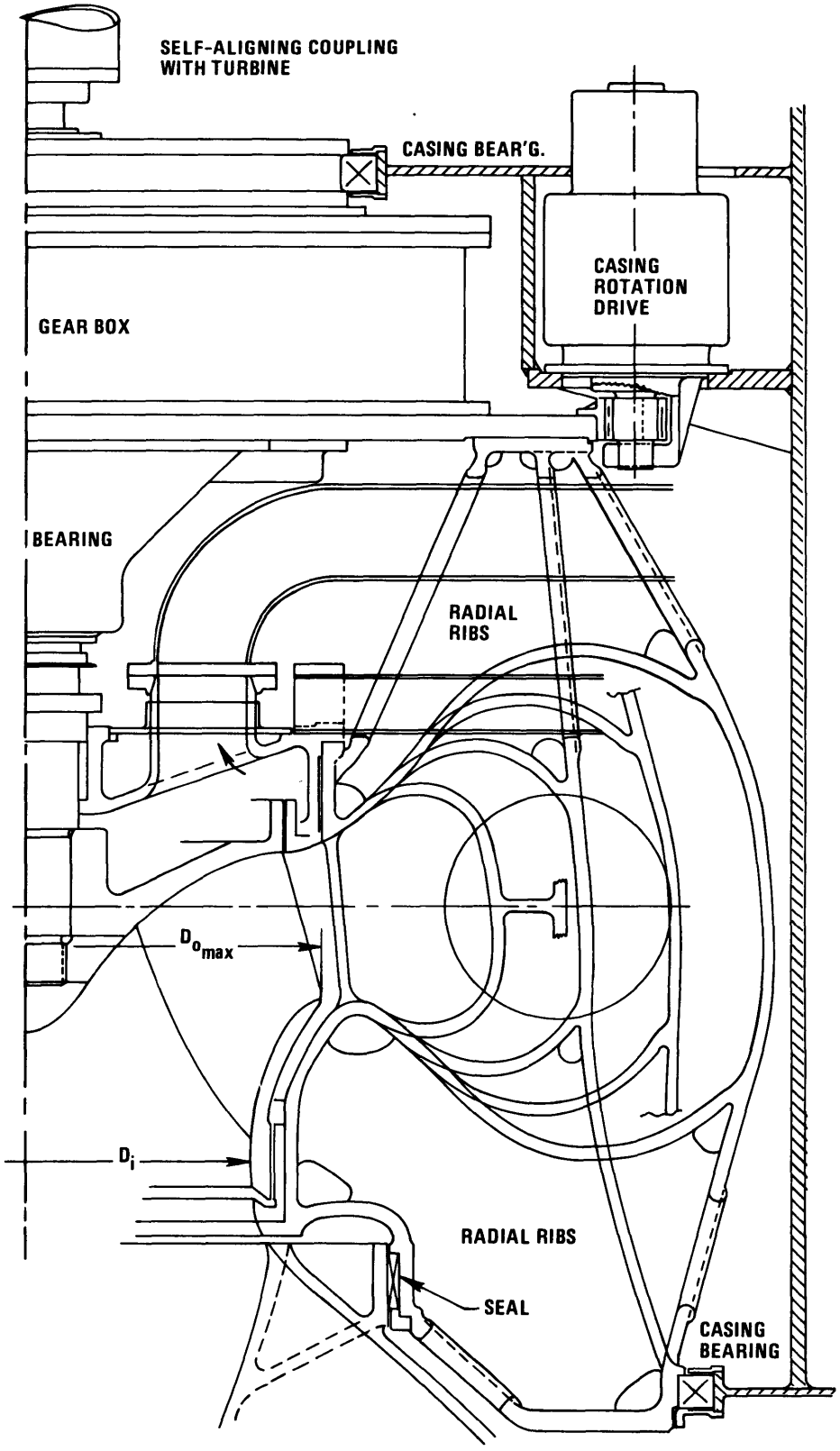


Figure 60 – Propulsion Pump with Rotatable Volute Casing

It is hoped that Figure 60 is reasonably self-explanatory with reference to Figures 28 and 57. The size and approximate location of the discharge nozzle are indicated by a circle in the volute cross sections. The jet velocity is $V_j = V_0 \left(1 + \frac{\Delta V}{V_0}\right) = 118.3$ ft/sec at 40 knots and about 142 ft/sec at 48 knots. The jet area is therefore

$$A_j = 132.1 \text{ ft}^3/\text{sec}/118.3 \text{ ft/sec} = 1.12 \text{ ft}^2$$

with a jet diameter of 1.194 ft.

At 40 knots, the jet thrust is $T_{40} = \rho Q_{40} V_{j_{40}} = 31{,}250$ lb. At 48 knots, it is $T_{48} = 45{,}200$ lb and must be counteracted by the casing turning unit. At best, the unit shown in Figure 60 satisfies this requirement only approximately.

The gear box shown in Figure 60 has not been analyzed in any way, except that it was assumed to house a double reduction gear set with coaxial input and output shafts. When the direction of the jet is changed, the gear box is rotated together with the pump casing.

## 5.8 POWER REQUIREMENTS

The power required will be calculated under the assumption that the efficiency of the pump is 89 percent and that of the gear is 98 percent.

The pump head required at 40 knots was originally calculated as $H_{40} = 164.9$ ft. This means that 40 knots is (probably) attained at a slightly lower speed of rotation than assumed for the impeller velocity diagrams derived in Section 5.6 and shown in Figure 58.

The hydrodynamic power at 40 knots is

$$H_{40} \text{ x } Q_{40} \text{ x } (64.4 \text{ lb/ft}^3) = 164.5 \text{ ft x } 132.1 \text{ ft}^3/\text{sec x } 64.4 \text{ lb/ft}^3 = 1{,}399{,}000 \text{ ft-lb/sec}$$

The power input to the gear box is therefore:

$$\frac{1{,}399{,}000 \text{ ft-lb/sec}}{0.89 \text{ x } 0.98} = 1{,}604{,}000 \text{ ft-lb/sec} = 2916 \text{ hp}$$

for each of two propulsion units.

Under the assumption of the same efficiencies, the power required at 48 knots is

$$2916 \text{ hp } \frac{48}{40} \text{ x } \frac{0.088}{0.066} = 4670 \text{ hp per unit}$$

It is, of course, desirable to install gas turbines with slightly greater power.

A tentative picture of the overall arrangement of one propulsion unit is shown in Figure 57 (see also Figure 28).

## 5.9 CONCLUDING REMARKS

As mentioned in Section 5.0, the study presented in this chapter at best merely lays the foundation for additional preliminary design studies.

It should be clear from Section 5.2 that the general arrangement selected for this study is by no means the only arrangement that deserves serious consideration. Moreover, significant alternatives are possible even within the present choice of general arrangement.

Perhaps the most important variation to be considered pertains to the specific speed of the propulsion pumps. As indicated in Section 5.6, this specific speed was directly dictated by the chosen maximum suction specific speed because the pump head and the pump inlet head above the vapor pressure are given primarily by the prescribed operating conditions and, to a lesser degree, by the duct and intake losses. The maximum suction specific speed was chosen to be substantially lower than the value previously considered in Chapter 3, yet, it was higher than the conventional suction specific speeds of stationary, commercial pumps. The resulting specific speed of the propulsion pumps turned out to be quite high for radial-flow pumps. Inspection of Figure 60 suggests that a somewhat lower specific speed might not increase the pump weight substantially. An increase in the diameter of the impeller discharge would tend to increase the fluid velocities in the volute, thus reducing the required volute section areas. This is not necessarily in conflict with Figure 34 since the basic specific speed $n_{s_0}$ considered here is substantially higher than that used in deriving the "radial" and "axial" curves in Figure 34. If in the present case, it were found that the pump weight does not increase significantly with decreasing specific speed, the only significant weight increase would come from the reduction gear. That increase should follow the similarity curve in Figure 34, i.e., the weight penalty for reduced specific speed might not be sufficient to justify the risk that is always connected with high suction specific speeds. An alternate study with a lower maximum suction specific speed, e.g., 0.6 instead of 0.7, therefore seems to be definitely indicated under the given operating conditions.

Another way to reduce the specific speed of the propulsion pump is, of course, to increase the propulsor velocity ratio $\Delta V/V_0$. In this case, a reduction in the basic specific speed at constant suction specific speed is accompanied by a reduction in the rate of flow and increase in the pump head of the propulsor. This will lead to a reduction in the volume and weight of the pump and the duct system as mentioned in Section 5.4. It will be recalled that the previously selected ratio $\Delta V/V_0 = 0.75$ was determined on the basis of hydrodynamic considerations only because these are the only considerations available within the scope of this report. It has already been stated that an extension of these considerations to include optimization with respect to overall weight will lead to higher $\Delta V/V_0$ values than 0.75. Even without going into details of weight considerations, an arbitrary increase in $\Delta V/V_0$ to values in the neighborhood of unity or more is therefore of distinct practical interest. The present study indicates that the resulting reduction in basic specific speed should not involve any difficulties.

The reader is encouraged to explore other variations in design that might give a near-optimum solution of this propulsion problem. The foregoing example is probably sufficient to illustrate the effects of design assumptions that had to be made in order to keep the present study within acceptable limits. Variations in these assumptions should serve to broaden the scope and significance of this investigation.

## INITIAL DISTRIBUTION

| Copies | |
|---|---|
| 2 | DDR&E |
| | 1 Library |
| 1 | ARPA/Lib |
| 1 | ASTSECNAV (R&D)/Smith |
| 1 | DNL |
| 11 | OP |
| | 1 OP 095 |
| | 1 OP 96 |
| | 1 Center for Naval Analyses |
| | 1 OP 962 |
| | 1 OP 971 |
| | 1 OP 098 |
| | 1 OP 098T |
| | 1 OP 982 |
| | 1 OP 982F |
| | 1 OP 983 |
| | 1 OP 32Z |
| 3 | CHONR |
| | 1 Code 438 |
| | 1 Code 438/R. Cooper |
| 4 | NAVMAT |
| | 1 MAT 03L |
| | 1 MAT 03L/J. Lawson |
| | 1 MAT 033/Bloomquist |
| | 1 MAT 0333/Vittucci |
| 1 | USNA Lib |
| 1 | NAVPGSCOL Lib |
| 1 | NROTC & NAVADMINU, MIT |
| 1 | NAVWARCOL |
| 7 | NAVSHIPS |
| | 1 SHIPS 2052 |
| | 1 SHIPS 03 |
| | 1 SHIPS 03Z |
| | 1 SHIPS 03Z2/Schuler |
| | 1 SHIPS 03Z22/Benen |
| | 1 SHIPS 031 |
| | 1 SHIPS 0341 |
| 5 | NAVSEC |
| | 1 SEC 6034B |
| | 1 SEC 6110 |
| | 1 SEC 6114/R. Johnson |
| | 1 SEC 6140 |
| | 1 SEC 6140B/Foncannon |

| Copies | |
|---|---|
| 12 | DDC |
| 1 | HQS COGARD OFF RES & DEV |
| 1 | LC/SCI & TECH DIV |
| 1 | MARAD/DIV SHIP DES |
| 1 | NASA STIF |
| 1 | NSF ENGR DIV LIB |
| 1 | Arizona State U/Lib |
| 1 | U Cal Berkeley/Dept NAME |
| 1 | U Cal NAME/Paulling |
| 3 | CIT |
| | 1 Aero Lib |
| | 1 Acosta |
| | 1 Wu |
| 1 | Catholic U Tech Lib |
| 2 | U Iowa |
| | 1 IHR/Lib |
| | 1 IHR/Landweber |
| 3 | MIT OCEAN ENGR |
| | 1 Lib |
| | 1 Leehey |
| | 1 Newman |
| 1 | U Michigan NAME Lib |
| 1 | U Minnesota SAFHL |
| 1 | State U Maritime Coll |
| 1 | Penn State U ARL Lib |
| 1 | SWRI Lib |
| 1 | Stanford U/Street |
| 1 | SIT Davidson Lab/Breslin |
| 1 | U Washington APL Lib |
| 1 | Webb Institute/Lib |
| 1 | NAS-NRC |
| 1 | SNAME |
| 3 | Aerojet-Gen |
| | 1 Beckwith |
| | 1 SES Tacoma |
| | 1 Harthower |
| 1 | Bell Aerospace |
| 1 | Boeing Adv Mar Sys Div/Ray |

| Copies | |
|---|---|
| 1 | Bolt Beranek and Newman Lib |
| 1 | Cornell Aero Lab Appl Mech |
| 1 | Eastern Res Group |
| 1 | Gen Dyn Elect Boat TIC |
| 1 | Grumman Aerospace/Palmer |
| 1 | Hydronautics Lib |
| 1 | Hydrospace-Challenger |
| 1 | Lockheed M&S Palo Alto |
| 1 | Oceanics/Kaplan |
| 1 | Rosenblatt & Son |
| 1 | UA/Hamilton Standard |

## CENTER DISTRIBUTION

| Copies | Code | |
|---|---|---|
| 1 | 00 | CAPT P.W. Nelson (C) |
| 1 | 1100 | William M. Ellsworth (C) |
| 1 | 1103 | Data Bank (C) |
| 1 | 1150 | Robert J. Johnston (C) |
| 1 | 1151 | William C. O'Neill (C) |
| 1 | 1154 | HYSTU (C) |
| 1 | 1158 | Dennis J. Clark (C) |
| 1 | 1159 | David P. Halper (C) |
| 1 | 1500 | William E. Cummins (C) |
| 1 | 1524 | High Perf Craft (L) |
| 1 | 1532 | Gabor F. Dobay (C) |
| 1 | 1556 | Daniel S. Cieslowski (C) |
| 1 | 1560 | Jacques B. Hadler (C) |
| 1 | 2700 | Leo Rubinowitz (Acting) (A) |
| 1 | 2707 | Henry W. Schab (A) |
| 1 | 2720 | Earl R. Quandt, Jr. (A) |
| 2 | 2721 | John G. Stricker (A) |
| 30 | 5614 | Reports Distribution (C) |
| 1 | 5641 | Main Library (C) |
| 1 | 5642 | Annapolis Library (A) |
| 1 | 9400 | Carl J. Boyd (C) |



☆U.S. GOVERNMENT PRINTING OFFICE:1974 542-170/225 1-3

UNCLASSIFIED
Security Classification

**DOCUMENT CONTROL DATA - R & D**

*(Security classification of title, body of abstract and indexing annotation must be entered when the overall report is classified)*

| 1 ORIGINATING ACTIVITY (Corporate author) | 2a. REPORT SECURITY CLASSIFICATION |
|---|---|
| Naval Ship Research & Development Center<br>Bethesda, Maryland 20034 | Unclassified |
| | 2b. GROUP |

3 REPORT TITLE

HYDRODYNAMIC DESIGN PRINCIPLES OF PUMPS AND DUCTING FOR WATERJET PROPULSION

4 DESCRIPTIVE NOTES (Type of report and inclusive dates)

5 AUTHOR(S) (First name, middle initial, last name)

George F. Wislicenus

| 6 REPORT DATE | 7a. TOTAL NO OF PAGES | 7b. NO OF REFS |
|---|---|---|
| June 1973 | 173 | 3 |
| 8a CONTRACT OR GRANT NO | 9a. ORIGINATOR'S REPORT NUMBER(S) | |
| b. PROJECT NO<br>Subproject S4606 | 3990 | |
| c.<br>Task 1722 | 9b. OTHER REPORT NO(S) (Any other numbers that may be assigned this report) | |
| d. | | |

10 DISTRIBUTION STATEMENT

APPROVED FOR PUBLIC RELEASE: DISTRIBUTION UNLIMITED.

| 11 SUPPLEMENTARY NOTES | 12 SPONSORING MILITARY ACTIVITY |
|---|---|
| Prepared under Contract 00014-70-C-0019 | NAVSHIPS |

13 ABSTRACT

The purpose of this report on the special form of hydrodynamic propulsion known as waterjet propulsion is to make the viewpoint of a pump designer known to the developers of waterjet devices. More specifically, it is concerned with the contribution that the pump designer can make in order to give the designer of the entire propulsion plant the greatest possible freedom to find and use the most favorable overall arrangement. There is no attempt to cover the entire field of waterjet propulsion. Moreover, only aspects of preliminary design are considered because it is in this stage of development that irreparable mistakes can be made.

The report assumes that the reader is familiar with the general characteristics of hydrofoil and captured air-cushion craft to which this type of propulsion mainly applies. Following an outline of the principal problems involved in the propulsion of high-speed surface craft, the design principles of hydrodynamic (centrifugal and axial flow) pumps are described and later applied to the design of waterjet propulsion pumps. The intake and duct problem is then described and designs are illustrated for a few typical overall arrangements. The report concludes with an example of propulsion pump and duct design for a particular set of specifications. This example can serve as the foundation for additional preliminary design studies.

| 14 KEY WORDS | LINK A | | LINK B | | LINK C | |
|---|---|---|---|---|---|---|
| | ROLE | WT | ROLE | WT | ROLE | WT |
| Hydrofoil propulsion | | | | | | |
| High speed ship propulsion | | | | | | |
| Waterjet design | | | | | | |
| Pump design | | | | | | |